Compensation grouting

experiments, field experiences and mechanisms

Adam Bezuijen

Compensation grouting was developed to compensate for settlement during underground construction. Tubes are installed prior to the underground construction work together with a monitoring system. Injection of grout into the soil at various locations between the underground construction work and the foundations of the building leads locally to heave that compensates the settlement.

This book reports on experimental research in sand about how the grout bodies made during injection depend on the grout properties, the density of the sand and the way the tubes are installed. The shape of the grout body affects the injection pressure and whether heave is localised to one injection point or distributed over a wider area. The evaluation of field measurements shows the influence of soil disturbance.

Compensation grouting

Adam Bezuijen

ISBN 978-90-8570-507-9

Compensation Grouting in Sand

Experiments, Field Experiences and Mechanisms

Compensation Grouting in Sand

Experiments, Field Experiences and Mechanisms

PROEFSCHRIFT

Ter verkrijging van de graad van doctor
aan de Technische Universiteit Delft,
op gezag van de Rector Magnificus, prof.ir. K.C.A.M. Luyben
voorzitter van het College van Promoties
in het openbaar te verdedigen op dinsdag 9 maart 2010 om 15:00 uur

door Adam BEZUIJEN

natuurkundig ingenieur
geboren te Ouddorp (Z-H)

Dit proefschrift is goedgekeurd door de promotoren:
Prof. ir. A.F. van Tol
Prof. ir. J.W. Bosch

Samenstelling promotiecommissie:

Rector Magnificus	Technische Universiteit Delft, voorzitter
Prof. ir. A.F. van Tol	Technische Universiteit Delft, promotor
Prof. ir. J.W. Bosch	Technische Universiteit Delft, promotor
Prof. dr. K. Soga	University of Cambridge
Prof. dr. M.A. Hicks	Technische Universiteit Delft
Prof. dr. ir. K. van Breugel	Technische Universiteit Delft
Prof. drs. ir. J.K. Vrijling	Technische Universiteit Delft
R.D. Essler	RD Geotech Ltd

Cover by: Arne Bezuijen
possible situation with (front) and without (back) compensation grouting

Printed by:
Wörmann Print Service
P.O. Box 92
2702 CZ Zutphen
Telephone: +31 575 58 53 00
E-mail: wps@wps.nl

ISBN 978-90-8570-507-9

Printed in the Netherlands

Summary

Compensation Grouting in Sand
Experiments, Field Experiences and Mechanisms

Compensation grouting was developed to compensate for settlement during underground construction. The successful deployment of the technique depends on being able to inject several times at the same injection point. This can be achieved with fracture grouting (the grout creates fractures in the soil so that not all grout remains around the injection point, where it would block further injections). This process has been successfully applied in clay and the results of full-scale field trials and a limited number of projects abroad have demonstrated that it is also possible in sand. However, our understanding of the actual process in sand is limited and so we lack theoretical models.

Compensation grouting will be used in Amsterdam during the construction of the North-South underground line, where compensation grouting is planned as a mitigation measure for possible settlement during tunnelling. A better understanding of the processes involved is needed to reduce the risks and evaluate the results.

The aim of this study was to improve our understanding of the process, and the relevant process parameters, of compensation grouting in sand. On that basis, we hope to establish a sounder theoretical basis for the description of compensation grouting in sand.

The mechanisms present during compensation grouting in sand have been investigated in laboratory experiments. Compensation grouting in sand differs from the same procedure in clay because, in sand, the water in the grout mixture can drain from the grout, something which is highly unlikely in clay, which is much more impermeable. Furthermore, the sand itself will behave in a drained way when fractured and the clay will behave in an undrained way. The models for fracture initiation and propagation developed in clay cannot therefore be used in sand. Without any fracturing in the sand, heave is very local and compaction of the sand may occur, impairing the efficiency of the process. At the other extreme, there could be very long, thin fractures, which make it difficult to create local heave. The ideal situation would therefore be some fracturing, but with fractures of limited length (a maximum of a few metres in field conditions).

The literature shows that it is difficult to achieve fractures in sand in a laboratory set-up when injecting a cement-bentonite grout, as in compensation grouting. However, excavations in the field have shown that fractures have been created by the injection of a cement-bentonite grout in sand.

Experiments and theory have demonstrated that the maximum injection pressure is given by the cavity expansion theory. Cavity expansion will lead to the symmetric expansion of the soil around the cavity during injection with grout. Fracturing of the soil may occur at a lower injection pressure. This study provides a qualitative description of a possible mechanism that leads to fracturing in sand, as well as a quantitative demonstration of a relation between the shape of a fracture and the injection pressure. Relatively low injection pressures may be associated with thin fractures. Higher injection pressures in sand will result in broader and shorter fractures. The shape of fractures occurring during compensation grouting is influenced by

the water that is pressed out of the grout into the soil during injection, a process known as "pressure filtration". A thin impermeable filter cake is needed between the injected grout and the sand to create a fracture in the sand. A filter cake that is too thick hampers fracture formation and only short fractures or no fractures at all will be formed.

Four series of grout injection experiments were performed involving a total of 34 tests. The grout properties, injection rate, confining pressure, relative density of the sand and the sand itself were varied. In three test series, the grout was injected directly into the sand. The fourth test series simulated the installation procedure used in the field.

We found, in agreement with the developed theory, that more cement in the grout results in a thicker filter cake and therefore to higher injection pressures and shorter and thicker fractures. We also found that, in the conditions prevailing during the test, a low cement concentration in the grout leads to pressure infiltration: the liquid and solid particles in the grout are pressed together into the grain skeleton without deformation of the soil skeleton.

The efficiency of the grouting process (the ratio between the volume of heave created and the volume of grout injected) proved to be dependent on the density of the sand. Low relative density of the sand results in low efficiency. Efficiency increases at higher relative densities of the sand and also when the grout used contains more solid material. When grout is injected in sand with a low relative density, there will be densification of the sand, compensating for the volume of grout injected. At very high relative densities, there may even be dilatancy of the sand during deformation, resulting in higher efficiencies. However, it was not possible to prove this on the basis of the results of the measurements, because only overall efficiency was measured, with the amount of heave always being much less than the volume of grout injected.

If the installation procedure of the grout injection tubes is taken into account, as in the fourth test series, lower injection pressures result. The process of pressure filtration is also present in the sleeve grout, reducing the load on the sand around the sleeve grout, and therefore the confining stresses in the sand directly around the sleeve grout. These lower confining stresses lead to lower injection pressures. As a consequence, there is less pressure filtration during the injection (the driving parameter for pressure filtration – the pressure – is lower). The limited pressure filtration in the fourth series leads to a thinner filter cake, and therefore thinner fractures. These tests showed that, comparable to what was found in the field at several locations, grout not only concentrates in fractures, it also concentrates around the sleeve grout and forms a thin cylinder around it. This can cause heave at quite some distance from the injection point. The results from the fourth and last test series showed that it is essential to take the influence of the installation procedure into account to simulate the compensation grouting process as it occurs in the field.

At the end of this study, the bearing capacity of the pile foundations under houses at the Vijzelgracht location, which had settled after a leak through a diaphragm wall, was restored using the compensation grouting technique. Although the technique is the same, this is not compensation grouting because compensation grouting is used before settling occurs. When used after settling, the technique is known as "corrective grouting". Analysing the measurements showed that, in this case, the achieved efficiency was only very low at less than 1.7%, while normal efficiency figures are in the range of 4 to 22% (Chambosse and Otterbein, 2001[b]). The corrective grouting resulted in a maximum heave of 10 mm in the buildings. After the end of the grouting campaign, there was settlement for a period of 5.5 months. During this time, most of the heave that had been achieved disappeared. This ongoing settlement was much higher than at

other locations in Amsterdam in "undisturbed" soil conditions. It was not caused by consolidation of the grout but probably by the consolidation of the soft soil layers overlying the bearing strata.

The consequences of this study for practice are that, for sand with a relative density higher than 60%, compaction or fracture grouting result in broadly similar efficiencies. Compaction grouting will result in more localised heave than fracturing. Efficiency is determined more by the amount of solids in the grout: the more solids, the higher the efficiency.

Grout and soil properties determine the length of the fracture during compensation grouting. This was modelled in an analytical calculation model. For a fracture with a plane shape, the ratio between the thickness of the fracture and its length can be calculated using the stiffness of the soil and the grout properties. The model showed that the injection rate, the effective stress, the permeability of the grout cake and the shear modulus of the soil determine the ratio between the thickness and length of the fracture. The results of the model concur with experiments for situations where the pressure infiltration of the grout during injection is negligible.

Adam Bezuijen.

Samenvatting

Compenserend Routen in Zand
Experimenten, Veldmetingen en Mechanismen

Compenserend grouten is een funderingstechniek die ontwikkeld is om zettingen tegen te gaan die kunnen ontstaan bij ondergronds bouwen. Om deze techniek toe te kunnen passen tijdens de bouw is het nodig dat er op één injectiepunt een aantal keren geïnjecteerd kan worden. Dit kan worden gerealiseerd met fracture grouting. Tijdens fracture grouting wordt de grout, een cement met een lage uiteindelijke sterkte, onder druk in de grond gebracht waardoor de grond scheurt. De grout loopt in de scheuren weg van het injectiepunt. Wanneer alle grout rondom het injectiepunt blijft, zou de uitgeharde grout verdere injecties blokkeren. Compenserend grouten is met succes toegepast in klei en moet op basis van het al voor deze studie uitgevoerde onderzoek en veldproeven ook mogelijk zijn in zand. Probleem is echter dat we het proces nog niet echt begrijpen en er daarom ook nog geen (theoretische) modellen zijn die beschrijven hoe dit proces verloopt.

Compenserend grouten zal worden toegepast in Amsterdam bij de bouw van de Noord-Zuid lijn met als doel om zo nodig zettingen te verminderen van een aantal gebouwen in de directe omgeving van de te boren tunnel. Wanneer de processen die optreden bij compenserend grouten beter worden begrepen, leidt dit tot kleinere risico's bij toepassing van deze techniek.

Doel van deze studie was om de processen bij compenserend grouten beter te begrijpen en te onderzoeken wat de relevante parameter zijn bij toepassing in zand.

De mechanismen die optreden bij het compenserend grouten in zand zijn onderzocht in laboratoriumexperimenten. Compenserend grouten in zand is anders dan in klei omdat in zand water uit het grout mengsel in het zand kan stromen en dit de grouteigenschappen sterk beïnvloedt. Daarbij zal de klei zich bij injectie ongedraineerd gedragen en bij injectie in zand zal het zand gedraineerd zijn, wat leidt tot een ander gedrag. Rekenmodellen die zijn ontwikkeld voor rots of voor klei zijn daarom niet toepasbaar voor compenserend grouten in zand. Wanneer er geen scheurvorming in het zand optreedt, zal alleen heel lokaal de grond omhoog komen wanneer er grout in de grond wordt gepompt. Dit gaat gepaard met grote drukken en dat kan verdichting van het zand tot gevolg hebben waardoor de efficiëntie van het proces afneemt (de efficiëntie is gedefinieerd als hoeveel de grond naar boven wordt gedrukt, uitgedrukt in een volume, gedeeld door de hoeveelheid grout die wordt ingepompt). Een ander extreem dat kan optreden zijn hele lange en dunne scheuren, die maken het weer lastig om bijvoorbeeld alleen onder een gebouw de zettingen te compenseren. Een ideale situatie zou zijn scheurvorming, maar scheuren van een beperkte lengte (maximaal een paar meter in het veld).

Vanuit de literatuur was het bekend dat het niet zo eenvoudig is om scheuren in zand te maken met een laboratoriumopstelling. Dit is wat tegenstrijdig met veldmetingen. Een enkele keer is een scheur die is gemaakt in het veld opgegraven en dan bleek dat waar in het laboratorium geen scheur optreedt, die in het veld vaak wel wordt gevonden. Dit bleek te maken te hebben met de manier waarop de injectiepunten worden geïnstalleerd in de grond. Deze invloed van de installatie was nog niet eerder beschreven.

Uit experimenten en theorie is gebleken dat de maximaal mogelijke druk bij het injectiepunt wordt beschreven door de zogenaamde cavity expansion theorie. Daarin wordt aangenomen dat het zand symmetrisch wordt weggedrukt van het injectiepunt. Wanneer er een scheur ontstaat, zal de injectiedruk lager zijn. Uit deze studie is gebleken dat er een relatie is tussen de injectiedruk en de vorm van de scheur. Lange en dunne scheuren worden gevormd met relatief lage injectiedrukken en voor korte en dikke scheuren is bij hetzelfde zand en dezelfde gronddruk een veel hogere injectiedruk nodig. De vorm van de scheuren hangt mede af van de hoeveelheid water die tijdens de injectie uit de grout wordt gedrukt. Doordat er tijdens de injectie water uit de grout wordt geperst, ontstaat er op de overgang tussen de grout en het zand een zogenaamde filter cake. Die filter cake bepaalt hoe dik de scheuren zijn, omdat elke scheur minimaal 2 keer dikker moet zijn dan de filter cake (de filter cake zit aan beide kanten van de scheur).

Voor dit onderzoek zijn vier series experimenten uitgevoerd, in totaal 34 proeven. In die proeven zijn grouteigenschappen, injectiedrukken, injectiesnelheid, gronddrukken en de relatieve dichtheid van het zand en het zand zelf gevarieerd. In de eerste drie series is het grout direct in het zand geïnjecteerd. In de vierde serie is het installatieproces gesimuleerd.

Een groutmengsel bevat meestal cement, bentoniet en water. De samenstelling van het mengsel wordt gegeven ten opzichte van de hoeveelheid water in het mengsel. Meer cement in de grout betekent dus dat de verhouding tussen water en cement (de water-cement factor) verandert en dit geldt op dezelfde manier voor de bentoniet. In overeenstemming met de ontwikkelde theorie bleek dat meer cement in de grout leidt tot een dikkere filter cake en dus tot dikkere en kortere scheuren in vergelijking met grout met maar weinig cement. Verder bleek dat bij hele lage cementconcentraties er voor de omstandigheden waarbij de proeven zijn uitgevoerd 'pressure infiltration' optreedt. Dan wordt niet alleen het water uit de grout in het zand geperst, maar ook het water en de fijne deeltjes in de grout. Dit heeft tot gevolg dat bij lage cement concentraties in de grout de efficiëntie van het compenserend grouten sterk afneemt. Het grout wordt dan in het korrelskelet geperst zonder dat dit vervormt.

De efficiëntie bleek ook afhankelijk van de relatieve dichtheid van het zand. Bij een lage relatieve dichtheid zal het zand eerst verdichten en wordt de efficiëntie minder. Bij hele hoge dichtheid kan er juist dilatantie optreden (het volume van het zand wordt groter) en dat levert dan een hogere efficiëntie op. Bij de metingen was overigens de efficiëntie altijd belangrijk kleiner dan één.

Wanneer het installatieproces van de injectiebuizen wordt nagebootst in de experimenten leidt dat tot lagere injectiedrukken. Bij het installeren van de injectiebuizen wordt gebruik gemaakt van 'sleeve grout' dat rondom de injectiebuis wordt aangebracht. Omdat deze grout ook water verliest, is er een ontspanning in de grond. Door de lagere grondspanning is ook een lagere injectiedruk mogelijk. Omdat er bij een lagere injectiedruk ook minder water uit de grout in het zand wordt gedrukt, is er een dunnere filter cake met als gevolg dat ook de scheuren dunner zijn. Bij de proeven van de 4de serie bleek dat de grout, in plaats van een scheur in het zand te maken, ook langs de injectiebuizen kan lopen. Er ontstaat dan een scheur, gevuld met grout tussen het zand en de sleeve grout. Dit is minder gewenst, omdat de grout zo zich over een behoorlijk grote afstand langs de injectiebuis kan lopen en dan dus kan komen op een plaats waar deze niet nodig is.
Tegen het einde van deze studie ontstond de schade aan de Vijzelgracht en was het mogelijk om aan de hand van de meetdata te onderzoeken in hoeverre de compenserend grouten techniek voor een dergelijke situatie, waar de fundering was verzakt door een gat in een diepwand, kon worden

toegepast. Omdat hier dus de zettingen niet zijn gecompenseerd, toen ze optraden, maar achteraf is geprobeerd om een klein deel van de opgetreden zettingen weer te corrigeren, wordt dit geen compenserend grouten genoemd, maar 'corrective grouting', hoewel de techniek dus precies hetzelfde is. In deze omstandigheden waarin de grondlagen verstoord zijn door de lekkage, is de efficiëntie van het grouten veel minder dan gebruikelijk (maar ongeveer 1.7% in plaats van de gebruikelijke 4 tot 22% (Chambosse and Otterbein, 2001[b])). Het bleek mogelijk om de verzakte gebouwen over de vooraf gewenste hoogte op te tillen (tot maximaal 10 mm). Wel bleken daarna langdurig alsnog zettingen op te treden. Deze zettingen waren veel hoger dan de zettingen die gevonden zijn in een ongestoorde situatie in Amsterdam waar ook compenserend grouten is toegepast. Waarschijnlijk worden de restzettingen veroorzaakt door consolidatie van de slappe lagen (veen en klei) boven de zandlagen.

Voor de praktijk is uit de studie gebleken dat bij een relatieve dichtheid van 60% of meer er minder verschil zit tussen compaction grouting en fracture grouting dan vooraf werd gedacht. Compaction grouting geeft geen scheuren en daardoor een meer gelokaliseerde vervorming, maar compaction grouting wordt uitgevoerd met een hoger percentage vaste stof in het grout en omdat juist het water in de grout weglekt in het zand is een hoog percentage vaste stof wenselijk om een goede efficiency te krijgen. Grout- en grondeigenschappen bepalen de lengte van een scheur bij compensation grouting. Hiervoor is een analytisch rekenmodel ontwikkeld. Voor een vlakke scheur kan de verhouding tussen de lengte en breedte van de scheur worden berekend uit de stijfheid van de grond, de gronddruk, de grouteigenschappen en de injectiedruk. Dit rekenmodel komt redelijk overeen met de meetresultaten voor situaties waar de pressure infiltration van de grout verwaarloosd kan worden, zoals meestal het geval is bij de in de praktijk toegepaste groutmengsels. Het model voorspelt te smalle scheuren wanneer pressure infiltration wel belangrijk is. Voor de praktijk is dit model van belang omdat uit gemeten drukken en grouteigenschappen geschat kan worden wat de maximale scheurlengte is.

Adam Bezuijen.

Table of contents

1 Introduction

1.1 Background to this study

One of the mitigating measures used during the construction of a new Amsterdam underground line, the "North-South line", is compensation grouting. The North-South line will be constructed using shield tunnelling through the old city centre of Amsterdam. At some locations the line will pass very close to important buildings and mitigating measures will be necessary to meet the settlement criteria imposed to avoid damage to these buildings. These measures include compensation grouting.

Littlejohn (2003) gives a definition of compensating grouting:
"In current practice compensation grouting is defined as the introduction of medium to high viscosity particulate suspensions into the ground between a subsurface excavation and a structure, in order to negate or reduce settlement of the structure due to ongoing excavation. To achieve this objective, appropriate grouts are injected at high pressures to displace the ground by localised hydraulic fracturing or compaction."

Compensation or corrective grouting has been used since the 1930s to compensate for soil settlement at various locations (see Section 1.3 for the history of compensation grouting). The technique was improved in the 1990s to compensate for the settlement of structures due to tunnelling (Mair 1992) and it has been applied successfully in various projects (Harris et al. 1994; Falk, 1997; Haimoni and Wright, 1999; Chambosse G. and Otterbein R. 2001[a,b]; Gens et al., 2005). Yet the situation in Amsterdam is unique because this will be the world's first application of the technique during tunnelling underneath pile foundations with soft soil layers above the sand layer in which the piles are founded.

Because of this unique situation, research projects have taken place to investigate the applicability of this technique in these circumstances. The influence of tunnelling on piles was investigated at the 2nd Heinenoord Tunnel (Kaalberg et al., 2005). A full-scale compensation grouting trial was performed in comparable conditions at the Sophia Rail Tunnel near Rotterdam (Haasnoot et al., 2002). Furthermore, it was decided to construct one of the compensating grouting shafts a few years before actual tunnel boring starts and to perform some tests on site. Alongside these tests, which can be considered to be applied research specifically for the situation in Amsterdam during the construction of the North-South line, it was decided to set up a more fundamental programme to enhance our knowledge of the mechanisms that are important during compensation grouting. This decision was based on the observation that there has been some fundamental research to describe compensation grouting in clay (Au, 2001), that some work on hydraulic fracturing (Murdoch, 1993[a,b]) can also be used to describe the processes during hydraulic fracturing in clay, but that there are hardly any studies that describe the mechanisms involved in hydraulic fracturing in sand.

The different applications, only a few of which are mentioned in Section 1.2, use empirical knowledge to define the layout of the grout injection tubes and the grout properties and the observational method to determine the amount of grout that has to be injected.

The aim of the study covered by this thesis was to enhance our knowledge of the mechanisms that are important for compensation grouting in sand in order to supplement the empirical knowledge available in compensation grout projects.

1.2 Compensation grouting and other grouting processes

Compensation grouting was developed to heave soil and the structures on top of the soil. In most cases, it is used to compensate for settlement that may occur due to tunnelling or other construction activities in the subsoil. The principle is quite simple. In Figure 1-1, the left-hand picture shows some settlement that is corrected in the right-hand picture. However, this is for the purposes of illustration only. The technique should prevent settlement, as in the case of Big Ben during the building of an underground station in the vicinity. The building was monitored during the construction of the station and compensation grouting was used to compensate for minor settlement (about 15 mm movement at the top).

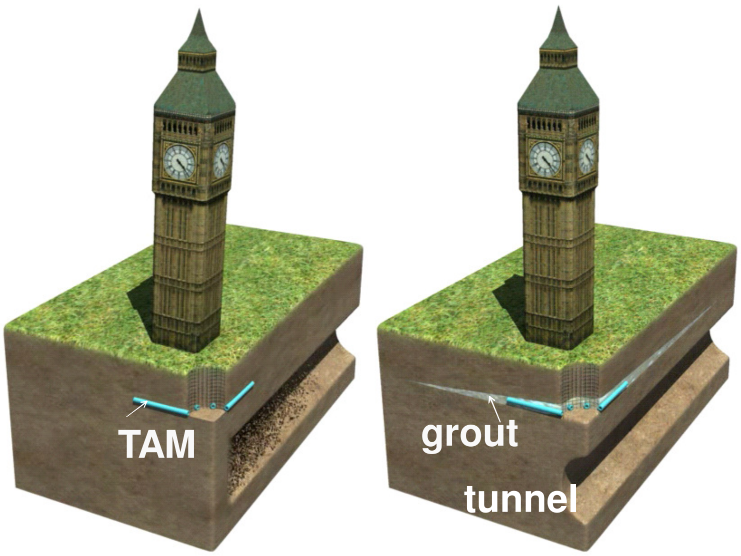

Figure 1-1: Principle of compensation grouting: grout is injected using TAMs to prevent settlement that may occur due to underground construction.

Using horizontal pipes with "tubes à manchettes[1]" (the "TAMs" in Figure 1-2), grout is injected into the soil. Grout is injected in one position at a time through a selected manchette using two rubber packers which select the part of the tube where the grout will be injected. See Figure 1-3.

Figure 1-2: TAMs waiting to be installed

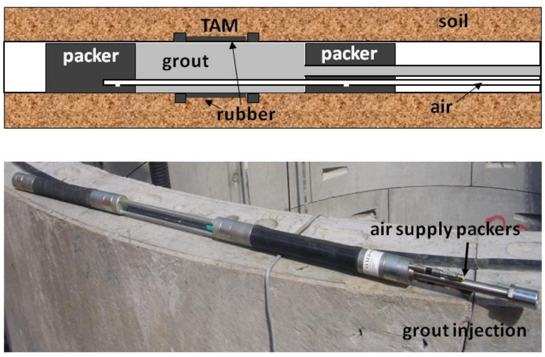

Figure 1-3: Packer to select injection hole

[1] Tubes à manchettes are steel tubes with rubber sleeves at regular distances. Grout can be injected from underneath the rubber sleeves and, when there is no injection, the sleeves prevent soil entering the tube.

The grout is injected at such a high pressure that the soil is deformed in a plastic manner, or is fractured. The grout replaces the soil in that location, resulting in heave of the soil. Normally the grout is injected in more than one injection. According to the usual description (Kummerer, 1993), the first batch of injections is applied to increase horizontal pressure (this process is known as pre-conditioning) and to increase the stiffness and density of the soil. A second batch is used to start the fracture process. However, since the horizontal pressure now exceeds the vertical pressure, the second injection creates a horizontal fracture. The fracture mechanism as described here is the theoretical fracture mechanism. In reality, the fracture mechanism is more complicated, as is also pointed out by Kummerer (1993), and fractures are not confined to the horizontal direction.

A key element of compensation grouting is monitoring (Mair, 1992). The heave generated by the injection of the grout is difficult to determine. So careful monitoring of the heave achieved is essential. The amount of grout injected and the injection pattern used depends on the measured heave. This makes it possible, during tunnelling operations for example, to compensate for settlement and prevent unwanted movement of houses or other objects. As soon as the soil or a structure starts to settle due to tunnelling, the initial settlement measured is compensated for, making it possible to control settlement and heave to within a few millimetres. However, it may be necessary to reduce the speed of the TBM process to allow for concurrent injection to compensate for settlement. Nowadays, drilling velocities are so high that immediate compensation of this kind may be difficult unless the tunnel excavation velocity is significantly reduced. Without a reduction in tunnel excavation velocity, it proved impossible to compensate for the settlement caused during the construction of the Sophia Rail Tunnel (to be discussed later) and during the construction of a metro line in Barcelona (Gens, 2005). The actual “speed” of the compensation grouting along a tunnel lining under construction depends on the efficiency of the grouting and the geometry of the TAMs. In another case in Perth (Kleinlugtenbelt, 2006), the soil conditions and/or the pre-conditioning before the tunnel passed proved to be adequate to limit settlement as the tunnel passed.

Compensation grouting is just one of the grouting processes that have been developed. Van der Stoel (2001) has given an overview of the various techniques developed for pile foundation improvement (in addition to compensation grouting). The primary aim of all grouting techniques (permeation grouting, jet grouting and compaction grouting) is to strengthen soil. Compaction grouting can also lead to some heave, but its prime aim is to densify the soil. The aim of compensation grouting is to heave the soil. Since the soil is fractured during the process the increase in soil density during fracture grouting will normally be limited. Compensation grouting can be repeated. Using the same TAM, it is possible to inject up to 80 times (Watt, 2002). This makes compensation grouting very suitable for the "observational method". After the injection of grout, the result (i.e. the heave) can be analysed and more grout can be injected depending on the result.

1.3 What’s in a name

1.3.1 Compensation grouting

The term "compensation grouting" for this technique is relatively recent. Mair (1992) claims that it was coined by David Hight. Mair does not mention a date but the context of this paper indicates that the term must have been coined towards the late 1980s or in the very early 1990s. Mair (2009) suggests limiting the term "compensation grouting" exclusively to situations in which compensation takes place at the same time settlement occurs. This means that the infrastructure for compensation grouting has to be in place before underground construction starts. A lot of the older applications of the technique do not conform with this definition, because the first applications of the technique were to correct settlement that had occurred previously. Mair suggests that the term "corrective grouting" should be used for this application of the grouting technique. Since the technique is exactly the same for both compensation grouting and corrective grouting, all grouting performed using this technique is often called compensation grouting. Furthermore, it is questionable whether, from a historical point of view, the term "compensation" can be limited to compensation during construction. Pleithner and Bernaztzik (1953) describe the same technique as “a method for compensating settlement” nearly 40 years before the term compensation grouting was used. In their article they describe compensation for prior settlement not caused by underground construction.

This means that Mair's suggestion that the term "compensation grouting" should be limited to correcting for settlement after it occurs is weakened by historical considerations. However, the suggestion has been followed by others (such as Schweiger et al., 2004) and the definitions have become more systematic as a result. Mair's definition has therefore been adopted in this study (except in the title, where "compensation grouting" is used because it is a term that will be more familiar to most people than "corrective grouting").

Littlejohn (2003) distinguishes between different types of compensation grouting: initial compensation grouting to stiffen the soil before any settlement (also known as "pre-conditioning"); concurrent compensation grouting during settlement; and corrective compensation grouting, which takes place after settlement has been noticed.

The above terms are linked to the outcome of the grouting process: correction of, or compensation for, settlement. Another way of distinguishing between various processes is to refer to the mechanism involved. This results in the terms "compaction grouting" and "fracture grouting". According to the European EN 12715 norm, these processes are both varieties of displacement grouting and the following definitions apply:

- Displacement grouting: injection of grout into a host medium in such a manner to deform, compress or displace the ground.
- Compaction grouting: a displacement grouting method which aims at forcing a mortar of high internal friction into the soil to compact it without fracturing it.
- Hydraulic fracturing: the fracturing of ground initiated by the injection of water or grout under a pressure in excess of the local tensile strength and confining pressure; also called hydrofracturing, hydrosplitting, hydrojacking or claquage.

In the EN 12715 norm, fracture grouting is not defined separately; it is covered by the hydraulic fracturing definition when grout is used as an injection liquid. According to the norm, compaction grouting and hydraulic fracturing are the two types of displacement grouting. The norm also deals with "grouting without displacement of the host material (permeation, fissure grouting, bulk filling)" but this is not covered in this study.

The definitions imply that compensation grouting and corrective grouting are two types of displacement grouting.

1.3.2 Other definitions

Other concepts of importance in this thesis are: pressure filtration, pressure infiltration and efficiency.

Pressure filtration is defined as the flow of water from the grout into the sand when the grout is pressed against the sand, reducing the porosity of the grout. The liquid grout loses its water and therefore becomes a solid material at the boundary of the granular material. The process is the same as consolidation in geotechnical engineering. It is different from ‘bleeding’, a term used in relation to grout and cement mixtures. Bleeding is also a flow of water from a grout or cement mixture, but it is caused by the weight of the mixture itself. In pressure filtration, extra pressure is applied.

Pressure infiltration is not a standard term in grouting operations. Generally, it is understood as a process in which gas or a liquid under pressure is forced into a matrix structure. By contrast with pressure filtration, then, it is not only the water from the grout that is pressed into the granular material, but also all of the grout. When viewed in this way, permeation grouting is pressure infiltration. However, in this thesis, the term is used slightly differently. The grout used in compensation or corrective grouting comprises different materials with quite different grain sizes. It would therefore seem more realistic to postulate that, during pressure infiltration, not all materials that compose the grout are pushed into the granular skeleton and that only the fine materials will leak off. For traditional grout composed of water, bentonite and cement, it is reasonable to assume that, when there is pressure infiltration, the water and bentonite will be pushed into the granular skeleton but the cement particles will remain at the boundary between the grout and the granular skeleton. The term is used in this way in this thesis: it is assumed that only fine particles and liquid in the grout are pressed into the soil. The mechanism in which only liquid is pressed into the soil will be referred to as pressure filtration. In an earlier publication (Bezuijen et al., 2009) pressure infiltration was termed "leak-off" but it emerged that, in the oil industry, the term "leakoff" is used as the pressure at which fluid starts to flow in a formation. This can be through the pore spaces or through cracks. In a leakoff test the leakoff is the pressure where the matrix flow changes to flow through cracks (Slumberger, 2010) and this is the mechanism at issue here.

The efficiency of the grouting process is the volume of heave created, divided by the volume of grout injected.

1.4 The history of compensation and displacement grouting

Littlejohn (2003) gives an interesting overview of the history of displacement grouting. Some historical remarks from his paper are presented here in order to place the work done for this thesis in a context that shows the ongoing developments in this field.

The first application mentioned by Littlejohn is highway maintenance in 1930 by the Iowa Highway department in the United States, which used the technique to raise and re-bed pavement slabs. At that time, grout with a water-solid ratio of 0.45 (a high amount of solids compared with current practice) was pumped into the soil using a hand pump. However, this was soon replaced by a gasoline pump. Injection pressures of up to 3.5 bar were attained. In the first season, nearly 3 km of highway was raised 75 to 380 mm.

The technique was used first to correct the settlement of a structure in 1934: a storage tank on a raft foundation was realigned after a settlement of 127 mm.

Littlejohn says that Pleithner and Bernatzik (1953) in Germany were the first to use the term “compensation” in relation to displacement grouting for controlled structural movement. They reported the raising of a coking plant furnace near Essen and a power station for the "Hessigheim am Neckar" dam. One corner of the coking plant was raised 90 mm and the maximum heave at the power station was even higher at 170 mm. The efficiency (the volume of heave created divided by the volume of grout injected) proved to be limited: 17% in the case of the power plant.

Compensation grouting associated with tunnelling was first seen in 1974 after the collapse of a 23-metre section of an old railway tunnel below a building belonging to the University of Kent at Canterbury in England. Compensation grouting was used to strengthen the soil in order to prevent further settlement. The first use of grouting to prevent settlement during tunnelling was in Baltimore in the United States during the construction of the Bolton Subway Tunnels (1977-1980).

Displacement grouting involving a pile foundation was first used in the Netherlands in 1969-1970 (Cambefort and Puglisi, 1971), when corrective grouting was used to re-level a refinery with a “fast-stiffening thick paste”. The injection holes were 20 to 25 m deep and the pile tips were 21 m below the surface. Injection pressures were 10 to 20 bar, which roughly corresponds with the CPT value at that location. The TAMs (injection pipes were installed next to and under the piles that settled) were located in different positions than those for the Amsterdam North-South underground line (horizontally below the pile foundation). The injection pipe layout for the Rotterdam refinery resembled the layout that is now common for compaction grouting (Stoel, 2001).

The history of displacement grouting shows that the method evolved from an experimental one to a well-established approach. Buildings below which compensation grouting has been used include city icons as the Big Ben in London (Haimoni and Wright, 1999) and the Central Station of Antwerp (Chambosse and Otterbein, 2001[a]). So this thesis has not been written because compensation grouting is still experimental. The reason is that we want to learn more about the mechanism involved. The ultimate aim is to avoid unpleasant surprises when the method is used in conditions that differ from the literature. The Amsterdam North-South line, where there are a lot of buildings on pile foundations and where compensation grouting will be used in sand rather than clay (the soil type in most other applications), is just such a project in which the conditions are different.

1.5 Focus of this study

Kaalberg (2006) suggests breaking down the mechanisms that occur during displacement grouting into three components:

1. The micro-level
   In which conditions will there be fracturing of the soil and what will be the shape of the fractures? What is the interaction between the fracture and the surrounding soil and, as a consequence, what will be the pattern of soil deformation close to the fracture?

2. The intermediate level
   What will be the pattern of soil deformation around the fracture and how will this affect the way the piles respond?
3. The macro-level
   The efficiency of the compensation grouting process and the compensation achieved for the building under which the compensation grouting is applied.

This study focuses on the mechanisms at the micro-level since there are many uncertainties about the mechanisms operating at this level, and the mechanisms at the intermediate and macro-levels can only be understood when we know what type of fracture can be expected and understand the interaction with the subsoil.

The aim of this study was to improve our understanding of the process and the relevant process parameters of compensation grouting in sand. To attain this aim, four series of laboratory tests were performed, field tests were evaluated and theory was developed. On that basis, it is hoped to establish a sounder theoretical foundation for the description of compensation grouting in sand. The main topics are the shape of the fractures, the injection pressures, pressure filtration, pressure infiltration and efficiency.

Information about the shape of the fractures is important in order to estimate the area over which heave is created with a grout injection and therefore how many injections will be necessary to produce homogeneous heave under the whole of a building. Grotenhuis (2004) developed an analytical model that includes the influence of pressure filtration and predicted long and thin fractures. This model was tested experimentally in the first phase of this study. The first tests showed that the fractures made during the experiments differ from the model of Grotenhuis and that fracturing did not always occur, but that pressure filtration and pressure infiltration determine the shape of the fracture and the injection pressure and influence the efficiency The conditions that lead to fracturing or that actually prevent fracturing were investigated. It is important to be able to create fractures because the efficiency of the grouting process is expected to improve when the soil is fractured rather than compacted.

1.6 Thesis structure

Chapter 2 presents a literature review. That chapter also covers the contributions of other research groups that have been working in this area during the study. The literature presented shows how the soil in which the fracture is created affects fracture shapes and it focuses mainly on laboratory experiments. Some calculation results from the literature are also presented.

Chapter 3 presents some field observations. A lot of field data are available showing how much heave is created or presenting compensation as a function of time. This chapter focuses on projects that present some more information about the fractures created or that included other issues important for this study.

Chapter 4 presents some theory about both fracture initiation and fracture propagation.

Chapter 5 focuses on the properties of the grout used and how these can be influenced by changing the cement and bentonite content in the grout.

Chapter 6 looks at the laboratory experiments performed and describes the results. Since the aim is to enhance our understanding of the fracturing mechanism and to develop a model for this mechanism in sand, this study had a large experimental component. Laboratory tests were performed with different sand densities and different grout mixtures.

Chapter 7 discusses the results and Chapter 8 presents conclusions and recommendations.

2 Literature review

2.1 Introduction to literature

This chapter focuses on the literature covering the mechanisms that occur during compensation grouting in sand. As described in Section 1.4, Littlejohn (2003) gives an extensive historical overview. Project descriptions do not usually help us to understand the mechanism, with some exceptions that will be included in this review. According to Eisa[2] (2008) more literature is available on compensation grouting in clay. Au (2001) and the literature review by Eisa (2008) look at compensation grouting in clay.

The amount of literature describing the mechanism of displacement grouting is relatively limited compared to the literature dealing with project descriptions. This can be explained by the fact that compensation grouting has developed as an empirical technique. An approach describing the possible mechanisms is more often found in the hydraulic fracturing literature describing hydraulic fractures created by the oil industry to enhance oil production in soils with a low permeability. However, the fracturing fluids used in the oil industry are very different from the grout used in compensation grouting.

Section 2.2 presents some literature on grout properties and how these influence the resulting fracture shapes. It also looks at the literature on pressure filtration. This part of the literature study is used in Chapter 5, which reviews the classification experiments on the grout.

Section 2.3 discusses the experiments described in the literature, which show how the fracture shape is influenced by the type of soil and the injection liquid. The number of experiments performed on sand using a cement-bentonite grout as the injection fluid is limited.

Section 2.4 deals with calculation methods. By contrast with rock and clay, there is no theory available describing the fracturing process in sand. The theory examined here describes analytical models based on cavity expansion theory. These describe the plastic deformation which is the basis for fracturing and one of the models describes how the confining stress directly around the injection point is influenced by unloading and loading the soil around that injection point. Furthermore, this section presents the results of the Finite Element Method (FEM) and Discrete Element Method (DEM) calculations. In Chapter 4 the analytical models will be used as the basis for deriving an analytical model that predicts the resulting shape of the fractures. The results of the DEM calculations are used to formulate the mechanism that leads to fracture initiation in sand, which is different from the fracture initiation mechanism when a hydraulic fracture is created in rock.

Sections 2.5 and 2.6 discuss fracture propagation and fracture direction. Fracture propagation is linked to fracture shape. The available literature is limited and this issue will therefore be examined in greater detail in Chapter 4.

[2] Eisa also uses the name Gafar. This thesis uses the name used by him in the original publication (mostly Gafar, Eisa in the case of his Ph.D. thesis).

Section 2.7 turns to the installation procedure, and chiefly concludes that there is a lack of literature on this topic.

Section 2.8 looks briefly at field observations. Chapter 3 looks at this area in more detail.

Section 2.9 presents a brief summary.

2.2 Grout properties

2.2.1 Importance of grout properties

The influence of grout properties on the types of fracture in sand have not been studied systematically for displacement grouting.

Greenwood and Hutchinson (1982) describe the stabilisation of soil around deep tunnels with what they call "squeeze grouting". They find that pressure filtration in the grout may lead to a filter cake that limits or prevents fractures. Harris et al. (1996) describe experiments in a compensation grouting campaign where different grouting mixtures were used: a "fluid" with a WCR (Water-Cement Ratio) of 4 and 6% bentonite, and a paste with a WCR of 10 and a Water-Fly Ash Ratio of 0.5 and again 6% bentonite. In London Clay the liquid grout resulted in lenses that were 1–2 mm thick; the paste grout produced shorter and thicker lenses than the liquid grout. The lenses produced by the paste were 10 mm thick. The injection pressures were higher for the paste grout. This means that, with the paste grout, the pressure loading on the tunnel was higher. This may damage the tunnel lining.
Chang (2004) demonstrated that the injection fluid affects the grout shape, but he did not use a cement-bentonite grout. Pater et al. (2003[b]) found that, in the case of hydraulic fracturing in sand, the fracture is also affected by the injection fluid, but he used x-linked (cross-linked) gel as the fracturing fluid instead of a cement-bentonite mixture. Eisa (2008) reports tests with different grout properties. His tests were performed in collaboration with this study and partly in the test facility that was developed for this study. Chapter 5 will look at the results of his test.

2.2.2 Pressure filtration properties

The literature describes the equipment and the theory used to determine grout properties. The important properties are the yield stress, the viscosity and the pressure filtration properties. The first two parameters are measured using a standard viscometer; the pressure filtration properties are normally measured using a consolidation cell. The cells used (McKinley, 1993; Gustin et al. 2007) are usually slightly larger than the standard oedometer test equipment because the permeability of the grout cake is normally higher than the permeability of the soft soils tested in an oedometer. See, for example, Figure 2-1.

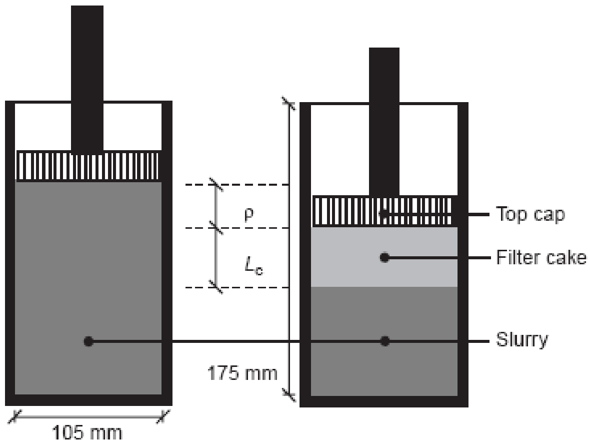

Figure 2-1: Sketch of set-up used for slurry filtration (after McKinley, 1993)

McKinley and Bolton (1999) describe a way of analysing these tests. They assume drainage at one side of the slurry sample (through the top cap in Figure 2-1). During the drainage of the water close to the top cap, a filter cake forms. The remaining water from the slurry has to pass through that filter cake, the thickness of which will increase during the test until all the slurry has lost its water. The idea is that the slurry has no effective stress at all and that, as soon as the grains in the slurry make contact, the formed filter cake reacts in a very stiff way. This analysis is different from the standard Terzaghi consolidation analysis and will also result in a different settlement curve for the plunger and different permeability. Permeability using the standard Terzaghi analysis is 1.5 times higher than the permeability based on the filtration analysis suggested by McKinley and Bolton using the same measurement data. Figure 2-2 shows the settlement curves using both analyses. The curves are reasonably comparable. McKinley and Bolton say that the measurement data should be between these 2 curves.

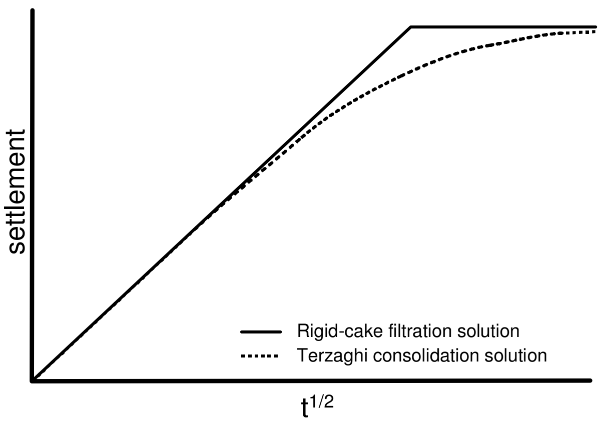

Figure 2-2: Sketch of archetypal settlement curves (after McKinley and Bolton, 1999, adapted)

Bezuijen and Talmon (2003) investigated the interaction between pressure filtration in the grout and the surrounding soil for tail void grout around a tunnel lining. They showed that it was possible to explain the reduction in measured grout pressures on the tunnel lining assuming volume loss due to pressure filtration.

2.3 Experimental research in the laboratory

2.3.1 Links to other work

The work done at Cambridge University (Eisa, 2008) links up to this study. Some of that work was performed using the set-up described in Chapter 6, when Eisa visited Delft, and some took place using a similar set-up built in Cambridge. The work in Cambridge by Eisa was based on earlier work by Au (2001) on compensation grouting in clay. Eisa and other researchers (Chang, 2004; Younes, 2008) showed that it was rather difficult to create fractures in a sandy subsoil, especially when the pressure conditions in the laboratory model are the same as the pressure conditions in the field. In most cases the grout injected resulted in an irregular grout body ("potato-shaped"), but not in fractures. See Figure 2-3 (upper right, and lower left and right). These results are different from the results of laboratory tests where epoxy was injected in kaolin clay that was normally consolidated to 140 kPa (Au et al., 2003). These tests found relatively thin fractures. See also Figure 2-3, upper left picture. The comparison is not fair, because Au et al. (2003) and Komiya et al. (2001) showed that, using a cement-bentonite grout, the shape of the fractures depends on the WCR ratio of the grout and the over-consolidation ratio (OCR) of the clay. See Figure 2-4. However, the result in Figure 2-3 is shown for the purposes of comparison, because these were the kind of fractures that were aimed for in sand at the beginning of this research.

2.3.2 Other laboratory tests from the literature

Chang (2004) investigated the influence of injection parameters, of scale, and of the kind and density of the soil. For example, Figure 2-5 shows the influence of the subsoil on the resulting fractures obtained in laboratory tests in a container with a diameter of 0.28 m and a height of 0.46 m using joint compound, a viscous paste of water and gypsum particles with a density of 1600 kg/m^3.The container had a fixed lateral boundary and the vertical confining stress used in these tests was 7 kPa. Remarkably high peak injection pressures were reported for these tests: 3300 kPa in sand, 1500 kPa in silt and 1400 kPa in clay, but the horizontal confining stress is probably much higher than the vertical stress due to the densification of the sand. This could also explain why the difference in injection pressure between a test in silica flour with a confining stress of 7 kPa and one with a confining stress of 76 kPa is only limited, although it is also possible that friction in the injection tube was high. It was found that, at similar injection volumes, the length and width of the fracture decreased (and therefore that thickness increased) with increasing vertical load. Furthermore, these tests showed that the shape of the grout body is more "fracture-like" when injecting in samples of silt and clay compared with the results of injections in a mixture of sand and silica flour. The mixed sand/silica flour samples respond differently: there are no thin fractures. Chang performed tests at different scales using containers with diameters of 0.15 and 0.28 m. An important conclusion of his work is that the “scale effect (within the range of the laboratory scales) is relatively insignificant”.

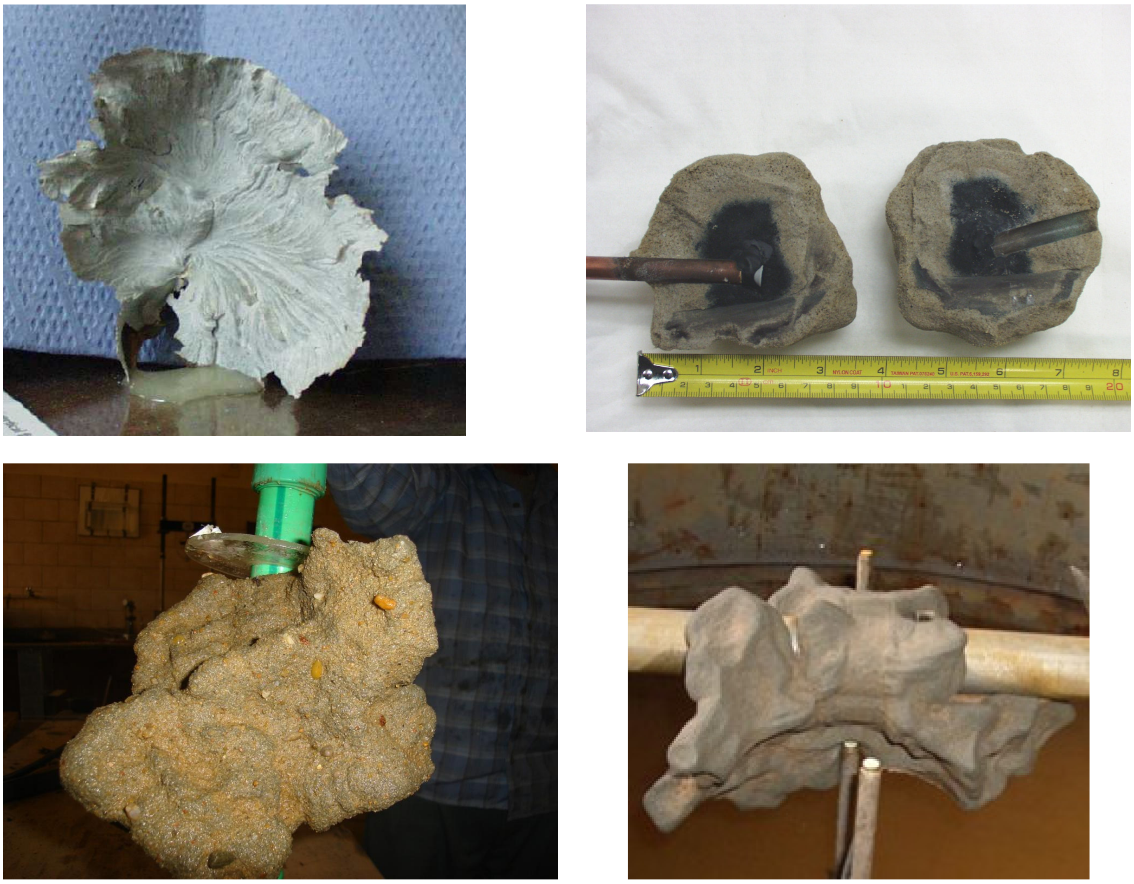

Figure 2-3: Various attempts to create fractures in sand or sand using grout with a water-cement ratio of 0.5 to 1. Top right: Gafar, 2003; bottom left: Younes 2009; bottom right: Kleinlugtenbelt, 2005. The top-left picture shows a result from Au (2001) of an injection of epoxy in clay and is provided for the purposes of comparison.

OCR=1

OCR=5

Figure 2-4: Results of Au et al. (2003). The injection of a cement-bentonite grout (5% bentonite with respect to the weight of the water and a WCR of 0.6) in kaolin clay for different OCR values. The confining stress was 140 kPa.

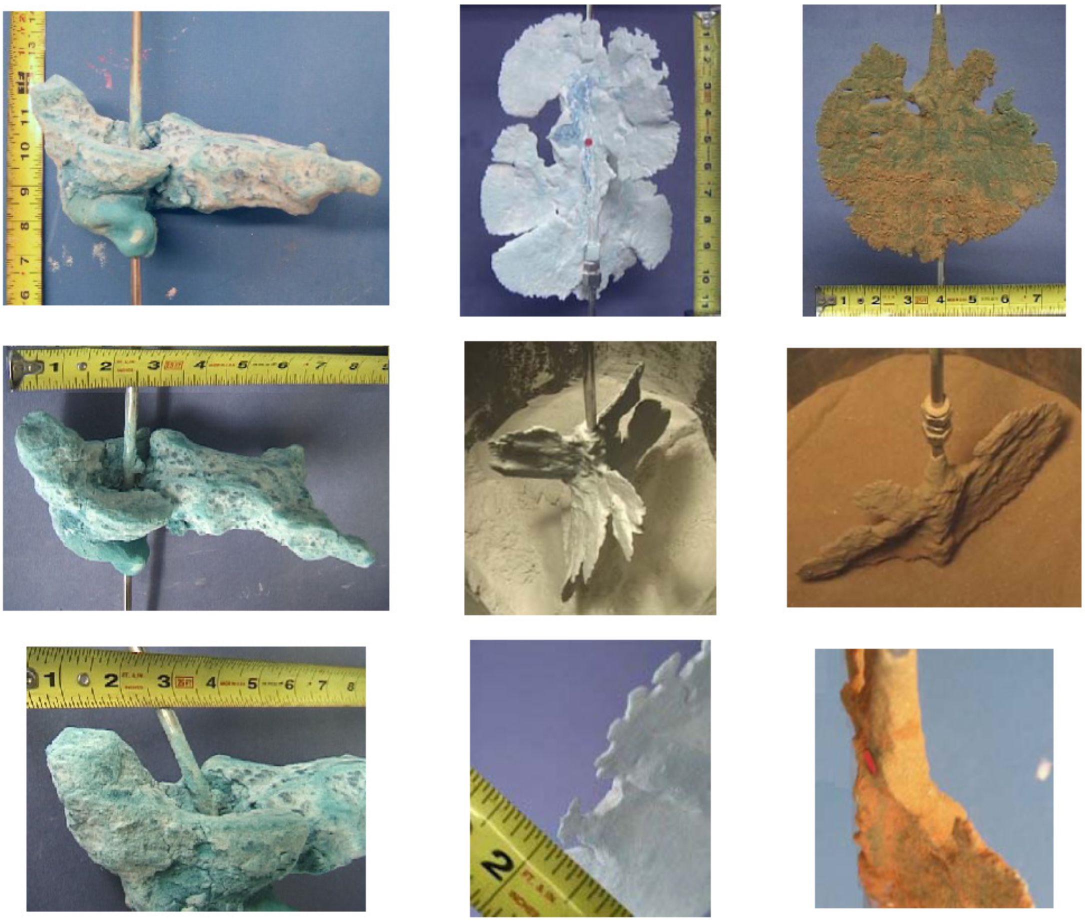

(a) test 2 (b) test 4 (c) test 3

Fractures in different types of particulate materials: (a) mixture of fine sand and silica flour, (b) silica flour, and (c) Georgia Red Clay.

Figure 2-5: Results of Chang (2004) based on laboratory tests using joint compound, a water-based, viscous paste of gypsum particles, as the injection fluid. The distances are presented in inches.

Cho (2009) performed comparable experiments. See Figure 2-6. His set-up was slightly different since the air in the injection system allowed him to perform more or less pressure-controlled experiments, although he questioned the efficiency of that part of the set-up. He also injected an epoxy raisin and not a cement-bentonite grout. He distinguishes between the shapes of grout bodies, breaking them down into "bulging", "intermediate" and "sheet" grout bodies. He found that coarse sand (600 µm) and high viscosity (2000 cp) lead to bulging, and that fine sand (75 µm) and low viscosity (500 cp) result in sheet-shaped grout bodies. A lower injection rate (0.15 ml/s) and a lower relative density lead to bulging and a high injection rate (1.25 ml/s) to sheet-shaped grout bodies. High relative density results in sheet-shaped grout bodies. The higher the injected volume, the higher the probability of bulging. In Cho's experiments, higher confining stress seems to result in more sheet-shaped grout bodies. These last results contradict those of Eisa (2008). The different results are probably caused by the different injection liquids. Cement-based grout bulges more at higher confining pressures in the experiments of Eisa due to the pressure filtration that occurs at higher pressures. Without pressure filtration, other mechanisms may dominate. The lower part of Figure 2-6 shows the set-up for electrical resistivity tomography to determine the shape of the grout bodies *in situ*. The results were never published outside the website and so no detailed information is known about these tests (injection pressures, injection rate, grain size, confining stress etc.).

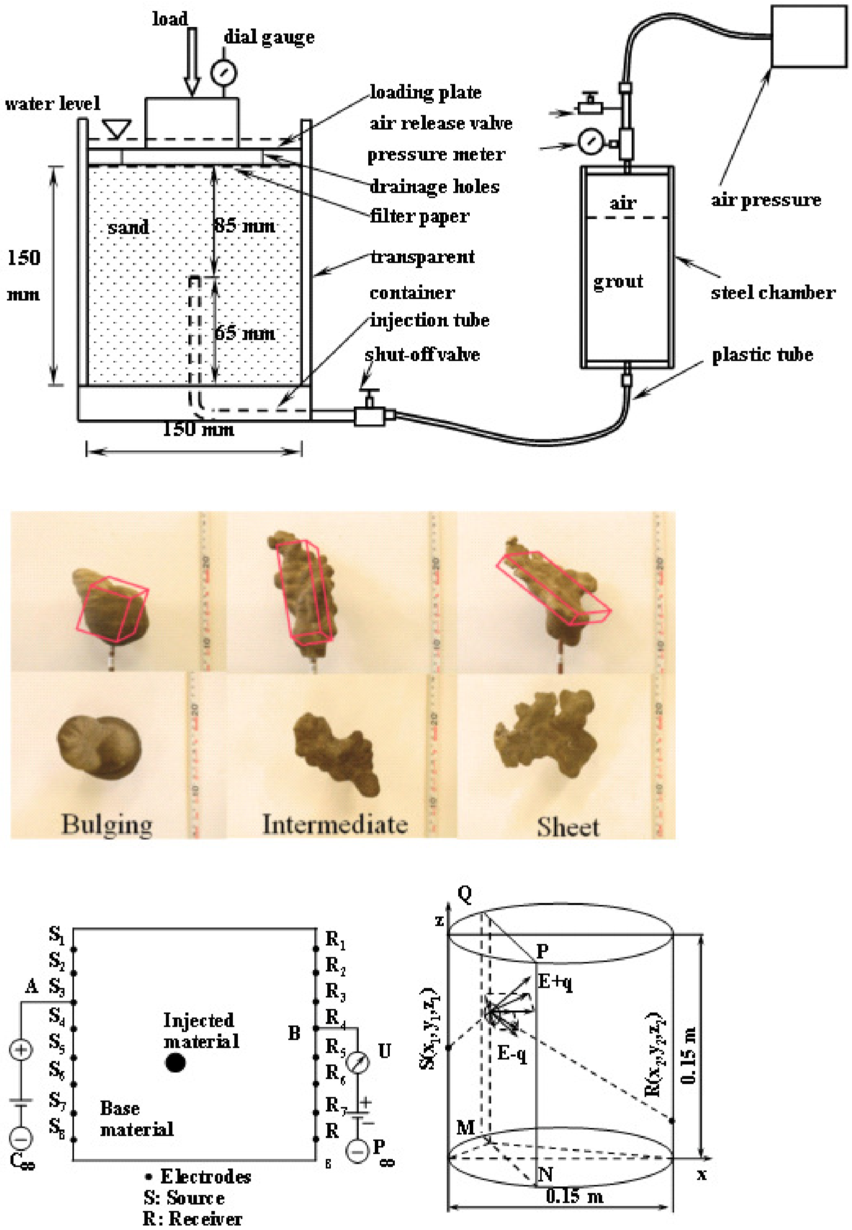

Figure 2-6: Set-up and results of experiments from Cho (2009)

The influence of the injection fluid and the mechanisms that are important in hydraulic fracturing were also investigated by the DELFRAC consortium at Delft University of Technology, which focuses on fracture research for the oil industry. It was found that a cake-building fluid was essential to create fractures in sandy soil. Cross-linked gel as produced by Slumberger, mixed with 0.5% of quartz flour to block the pores in the sand, resulted in long and slender fractures. See Figure 2-7 (Bohloli and Pater, 2006). Pure viscous fluids did not lead to any fractures.

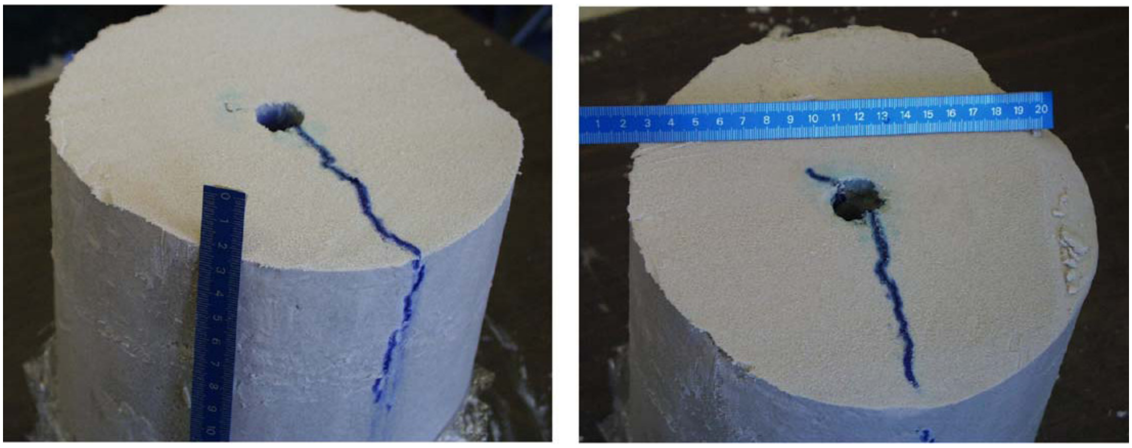

Figure 2-7: Long thin fracture obtained in sand using cross-linked gel with 0.5% quartz flour as the injection fluid

Dong and Pater (2008) showed that the tip of a fracture can have different shapes. This can be a "smooth tip" where the width gradually tails off to zero. However, when the fracturing fluid contains a lot of particles (as is the case with a cement-bentonite grout), these particles block the tip, resulting in a "blunt tip". The results of other tests showed the effect of non-homogeneous soil and confining pressure (Pater and Dong, 2009). Tests were performed at different scales in 0.15 and 0.4 m diameter containers, but no significant differences were found.

Some hydraulic fracturing tests using bentonite as the fracturing fluid were performed for the DELFRAC consortium (Bezuijen, 2003). These tests were performed using a set-up comparable to the test set-up for the compensation grouting experiments to be described in Chapter 6, but the diameter of the container was smaller (0.6 m). Figure 2-8 shows the principle and Figure 2-9 the set-up.

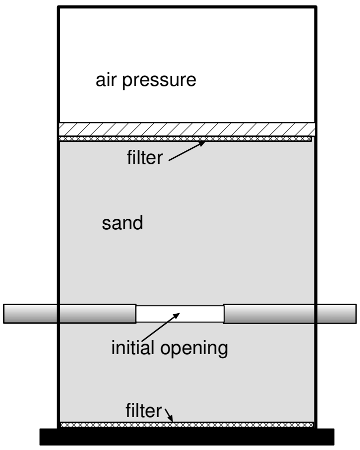

Figure 2-8: Schematic cross-section of test set-up

Figure 2-9: Picture of test-set-up

The pressure transducers used during the tests are shown in Figure 2-10.

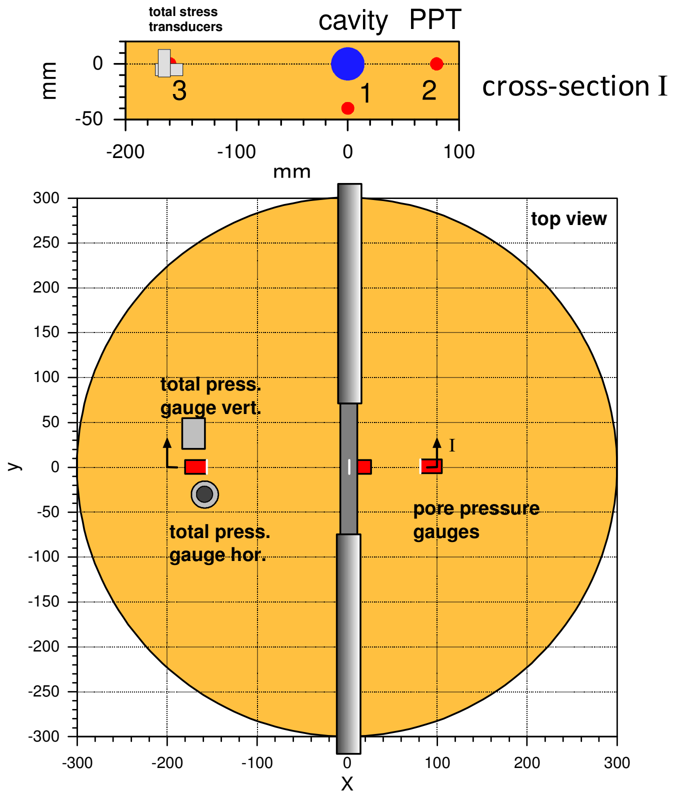

Figure 2-10: Top view, and detail from the side view, of the instrumentation used. The total pressure transducers are shown in grey, the pore pressure transducers in red. The blue circle in the upper plot is the injection tube.

A homogenous sand body was created and pressurised to the desired vertical effective stress (100 kPa). Pressurising and the experiments afterwards were performed under drained conditions. Pore water drained through the filter layers on the top and bottom of the sand sample. An injection opening of 0.15 m length and 0.02 m diameter was created in the centre of the container by removing an inner tube and applying enough pressure to the bentonite to prevent the collapse of the created opening. Hydraulic fracturing in the sand was initiated by injecting bentonite slurry using a plunger pump. Various injection velocities, bentonite slurries and sand densities were tested. The amount of bentonite in the slurry was varied from 80 to 180 gr/l. As shown in Figure 2-11, this variation in bentonite corresponds to a variation in the peak yield stress from 4 to 690 Pa.

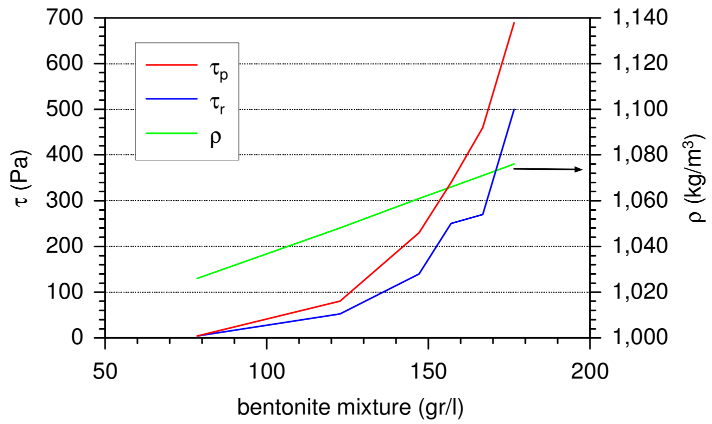

Figure 2-11: Bentonite slurry properties, peak yield strength (τ_p), residual yield strength (τ_r) and density (ρ) as a function of the bentonite concentration (Bezuijen, 2003)

Considerable pressure infiltration was found in all tests (Bezuijen, 2003). At a relative density of around 56% (measured using the void ratio) the injection pressure proved to be independent of the bentonite concentration. The injection pressure was between 2 to 4 times the vertical effective stress. Tests using various relative densities of the sand showed that the injection pressure varies significantly with the relative density.

At low bentonite concentrations, the injection pressure fluctuates significantly. See Figure 2-12. It was assumed that, just after the creation of a new fracture, there is the possibility of increased pressure infiltration because the area where pressure infiltration is possible is increased. With a constant injection rate (as in most of the experiments) extra pressure infiltration means a decrease in pressure. As a result, fracturing stops and pressure infiltration decreases. The reduction in pressure infiltration leads to an increase in injection pressure, which may initiate another fracture. This explanation could not be proved with a number of fractures that were found because the injections with low bentonite concentrations did not result in visible fractures. However, it was confirmed by comparing the measured pressure increase during injection with calculations assuming a Bingham liquid. The pore pressure transducer PPT 1 also shows the fluctuations, as measured in the injection pressure, because this PPT is in the pressure infiltration zone. See Figure 2-14.

Using slurry with 125 gr/l of bentonite and no cement reduced these fluctuations. See Figure 2-13. The slurry had a larger yield stress and therefore the rate at which pressure infiltration occurred is slower and this does not lead to a pressure drop in the injection pressure. Here, PPT 1 shows a steady increase, representing the pressure drop necessary to push the boundary of the pressure infiltration zone away from the injection point

The green and blue lines in Figure 2-13 show the injection pressure as measured at the pump (blue line) and at the other side of the container (green line). The difference between these two lines shows that the pressure drop in the injection system is only small.

Figure 2-14 shows the pressure infiltration and the fractures, as found after the tests, for both tests described above. Hardly any fracture was found afterwards in Test 202 with the 80 gr/l bentonite concentration. As mentioned above, it is assumed that there were fractures, but that these closed down at the end of the test. Test 205 showed a vertical fracture. This vertical fracture causes an increase in horizontal stress ("TST hor" in Figure 2-13). This increase is more than in Test 202, in which there was not such a clear fracture.

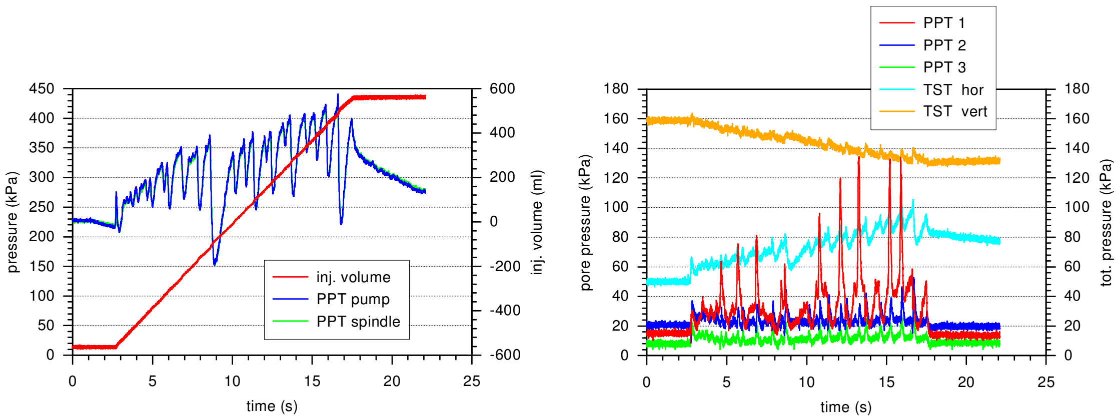

Figure 2-12: Results of Test 202. In this test the injection liquid was 80 gr/l bentonite slurry (Bezuijen, 2003).

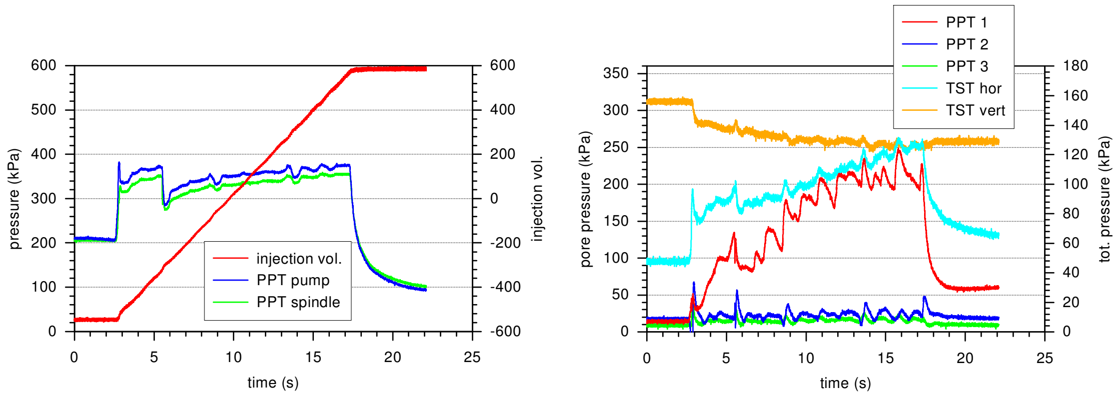

Figure 2-13: Results of Test 205. In this test the injection liquid was 125 gr/l bentonite slurry (Bezuijen, 2003).

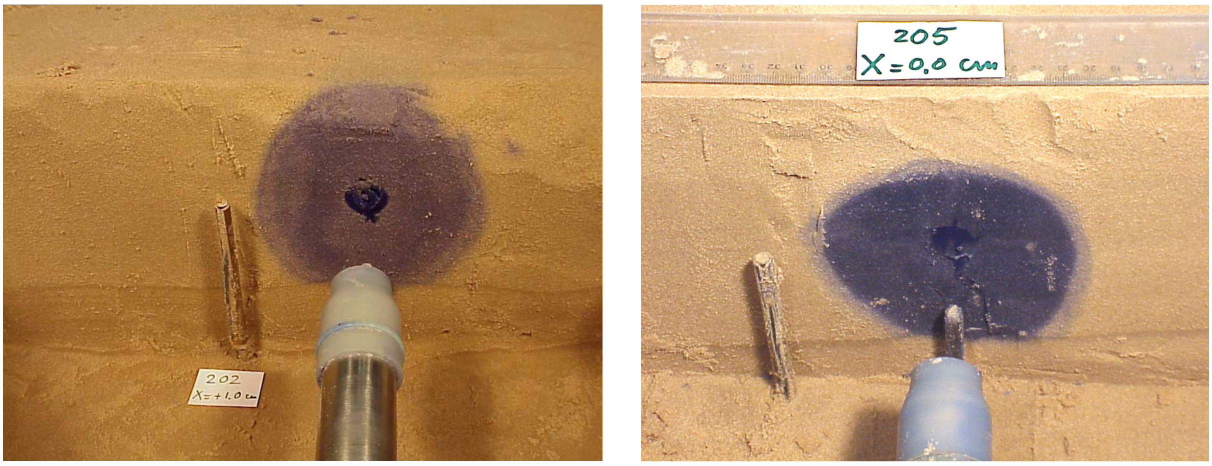

Figure 2-14: Fractures and pressure infiltration, Test 202 (left) and Test 205 (right) (Bezuijen, 2003)

2.3.3 Summary of laboratory research

Table 1 presents an overview of the recent experimental work on hydraulic fracturing or compensation grouting. Apart from the work of Au (2001), all the results were for injections in a sandy soil.

The literature used is only a selection of what is available and each experimental programme includes a number of tests with results that are sometimes quite different. The literature presented was used in this study and helped to shape ideas about the processes that occur during the injection of grout in sand. Showing only one test result for each experimental programme helps to provide an overview. The aim was to select a typical result.

The table shows that none of the researchers was able to create real fractures in sand with a bentonite slurry or a cement-bentonite slurry when the confining stress was 100 kPa or more. Eisa (2008) has shown that fracturing of sand with cement-bentonite slurry is possible when no confining stress is applied. When there is a confining stress, it proves difficult to create fractures. Since most of the studies described in the literature were based on hydraulic fracturing as performed for the oil industry, there is hardly any information about the efficiency of the process and no information about how efficiency relates to the fracture shape.

Table 1: Summary of tests and test results obtained from literature.

Researchers/Publication	Set-up	Main findings	Picture of result
Au (2001): Epoxy injection in clay	*Dimensions:* Ø1.4x1.6x0.75 m *soil:* Kaolin clay OCR 1 - *Injected material:* epoxy *pressures:* conf. 140 kPa injection: not presented	Fractures depend on injection rate and OCR. Clay consolidates after injection reducing the efficiency.	
Bezuijen (2003): Bentonite mixture injected in saturated sand	*dimensions:* Ø0.6x0.75m *soil:* sat. sand Rd 50-85%, *Injected material:* bentonite 8-20% *pressures:* conf. 100-200 kPa injection: 250 – 525 kPa	Large pressure infiltration and press. Fluctuations at low bentonite percentages. Short fractures.	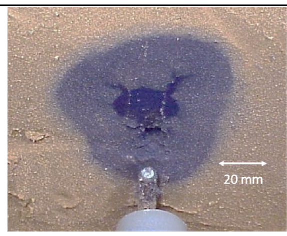
Chang (2004) : Small scale Epoxy and gypsum slurry injected in dry sand, dry silt and clay (picture from silt)	*dimensions:* Ø0.15x0.15m *soil:* silica flour Rd 95% dry *Injected material:* gypsum 15 ml, 4 ml/s *pressures:* conf. 7 kPa injection: 4300 kPa	Dense silica flour. High injection press.	
Chang (2004)[1]: Medium scale Epoxy and gypsum slurry injected in sand, silt and clay (picture from silt)	*Dimensions:* Ø0.28x0.34m *soil:* silica flour Rd 92% dry *Injected material:* gypsum 15 ml, 4 ml/s *pressure:* conf. 7 kPa injection: 4500 kPa	Comparable to small scale experiments.	
Younes (2008): Cement-bentonite grout injected in saturated and dry sand (picture dry sand)	*Dimensions:* 1.4x1.6x0.75 m *soil:* sand Rd 40 – 60%, *Injected material:* 5% bentonite WCR 0.5 -2 *pressures:* conf. 100-250 kPa injection: 10-16*σ_v	Compaction grouting. Rd increased from 40% to 80%	
Eisa (2008): (Cambridge tests) Cement-bentonite grout injected in saturated sand. Picture WCR 1, 3.3 l/min	*Dimensions:* Ø 0.85x0.375 m *soil:* sand Rd 70 – 93%, *Injected material:* 4-8% bentonite WCR 0.5 -1.8 *pressures:* conf. 100 kPa injection: 1350 kPa	Fracture shapes depend on WCR confinement and injection rate. Dynamic injection does not change the results. WCR has a large influence on injection press. for non-fracturing tests	

Cho (2009): Small-scale Epoxy resin in sand and clay	*Dimensions:* Ø 0.15x0.15 m *soil:* sand Rd 70 – 93%, clay *Injected material:* Epoxy raisin *pressures:* conf. 0-136 kPa injection: no values pres.	"Bulging", "intermediate" or sheet-shaped fractures could be obtained depending on injection conditions. Pictures show intermediate and sheet.	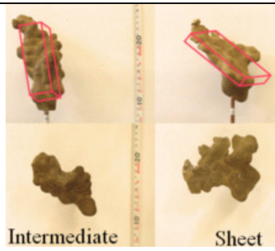

[1] The difference with the result shown in Figure 2-5 (test 4) is the relative density of the silica flour, which was 73% in test 4.

2.4 Calculations

2.4.1 Analytical calculations

Analytical fracture models are available to analyse fracture development in rock (for example, Aktkinson, 1989 and Dam, 1999). These models assume that the tension strength is exceeded at the tip, resulting in a fracture. A model of this kind is not available for fracturing in sand. Sand has no tensile strength, so the fracture mechanism will be different.

Analytical models used in research into compensation grouting are mostly cavity expansion models for calculating stresses around bore holes. Different models use different constitutive models. In simple soil models, an analytical solution is possible (Vesic, 1972 and Luger and Hergarden, 1988); more complicated constitutive models require a numerical solution (Salgado a Randolph, 2001). These cavity expansion models do not predict when a fracture occurs, but show what pressures are necessary for plastic deformation (plastic deformation is necessary before a fracture can occur). Keulen (2005) suggested that a minimum plastic deformation is necessary before a fracture can develop. More generally, these models generate an insight into soil behaviour around a pressurised cavity.

Most cavity expansion models are valid for the loading or unloading of the cavity. Wang and Dusseault (1994) present a model that is suitable for repeated loading and unloading. They assume the unloading of the cavity during excavation, which leads to an active plastic zone. When the pressure in the cavity is increased after construction, there will be a passive zone within the active zone. This plastic zone will occur at much lower stress conditions than in virgin soil when pressurised. Since the development of a passive plastic zone can be the start of a fracture, this means that unloading the sand to an extent that plastic deformation occurs before pressurising the sand may result in fracturing at lower injection pressures than in virgin soil.

The situation during displacement grouting can be compared with the situation of a cavity under repeated loading as analysed by Wang and Dusseault (1994). They used cavity expansion theory to calculate the stress distribution in the soil around a bore hole during unloading and reloading. In the case of compensation grouting, the removal of the casing will result in unloading and the reloading will occur during injection of the grout. Cavity contraction and expansion theory cannot state when a fracture will start, but it can be used to calculate the pressures that will lead to a plastic zone in the soil.

Parts of Wang and Dusseault's analyses will be presented here in a shortened and slightly adapted version to allow for the calculation of the influence of previous unloading on the loading pressure at which plastic deformation occurs. It is assumed that, after the installation of a TAM, there is a pressure release due to the removal of the casing, and that this leads to an active failure of the soil around the hole. This means that the radial stress σ_r is less than the tangential stress σ_θ. After installation, the radial pressure increases due to the injection process and passive yield will occur. In such a situation, σ_r exceeds the tangential stress σ_θ and a fracture can occur. In line with Wang and Dusseault's analyses, it is assumed that the fracture initiation pressure is related to the pressure that results in the passive failure of the cavity.

Assuming a Mohr-Coulomb failure criterion, the plastic stresses must fulfil the criterion:

$$\sigma'_\theta - N\sigma'_r + S = 0 \tag{2.1}$$

where the prime indicates the effective stress. The material parameters N and S are different for active and passive yield and can be written as:

$$\begin{aligned} N_a &= [1+\sin\phi]/[1-\sin\phi] \\ N_p &= [1-\sin\phi]/[1+\sin\phi] \end{aligned} \tag{2.2}$$

and

$$\begin{aligned} S_a &= -2c\cos\phi/[1-\sin\phi] \\ S_p &= 2c\cos\phi/[1+\sin\phi] \end{aligned} \tag{2.3}$$

Here, ϕ is the friction angle and c the cohesion of the soil material. (In their publication, Wang and Dusseault discriminate between the peak values and residual values of the friction angle. The calculations here use only one value.)

Active yield will occur when:

$$p_a < \frac{2\sigma'_0 + S_a}{1+N_a} \tag{2.4}$$

where p_a is the pressure at the boundary of the opening in the active state (assuming perfect plastering on this boundary, in other words assuming that the grout pressure is directly transferred to the grain stress at the boundary of the opening) and σ'_0 the initial effective stress around the opening. When the effective pressure around the TAM remains higher than the criterion mentioned in Equation (2.4), there will be no plastic deformation and the limit pressure for passive plastic deformation will remain the same as if there were no unloading of the soil. If the criterion of Equation (2.4) is fulfilled, there will be an active plastic zone. Increasing the pressure in the cavity afterwards will lead to the situation sketched in Figure 2-15. There will be an active plastic zone containing a passive plastic zone. When pressure is increased further, the active zone will disappear, but our interest is the pressure at which the passive zone starts.

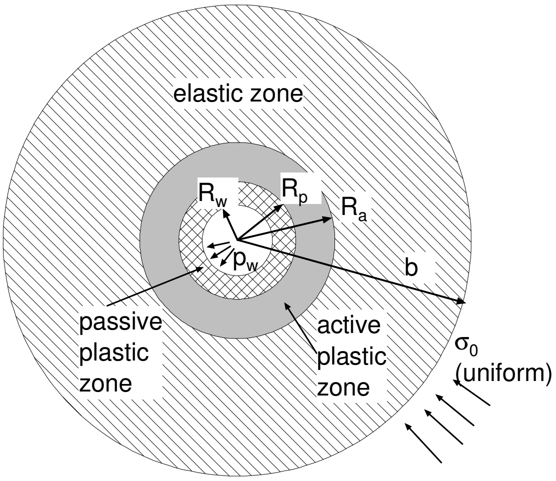

Figure 2-15: Definition sketch for the situation with active and passive soil around the cavity. See also text.

During unloading, when the active zone is formed, p_r, the pressure in the cavity based on the equations presented by Wang and Dusseault, can be expressed as a function of the thickness of the plastic zone R_a and other parameters (see also Figure 2-15):

$$p_r = \left[\sigma'_0 - H \frac{b^2 - R_a^2}{b^2 R_a^2} - S_a \right] \left(\frac{R_w}{R_a} \right)^{N_a} \tag{2.5}$$

where:

$$H = \frac{\sigma'_0 (N_a - 1) - S_a}{b^2 (N_a + 1) + (1 - N_a) R_a^2} R_a^2 b^2 \tag{2.6}$$

When the pressure is increased after active yield, the first soil will enter the passive plastic state when:

$$p_p > \frac{2 p_a + S_p - S_a}{1 + N_p} \tag{2.7}$$

Without active failure, this relation would read as follows:

$$p_p > \frac{2\sigma'_0 + S_p}{1 + N_p} \tag{2.8}$$

Table 2 presents the input parameters used for calculations using the formulae presented above. The results are shown in Figure 2-16. Without active plasticity the pressure at which passive plasticity starts is 157 kPa. These results make it clear that plastic deformation in the active state can considerably reduce the borehole pressure at which passive plastic deformation occurs. The pressure needed to achieve passive plastic deformation falls as the active plastic radius created by the low pressure before the pressure increase increases. This results in quantitative information for the statement already made by Wang and Dusseault: “Our study suggests that initial active formation damage reduces the pressure required to initiate such a fracture”.

Table 2. Input parameters used in calculation

Parameter	Value	Dim.
σ'_0 (original stress in sand)	100	kPa
ϕ (friction angle sand)	35	degr.
C (cohesion)	0	kPa
R_w (radius of tube. See Figure 2-15)	0.035	m
b (radius with constant press.)	5	m

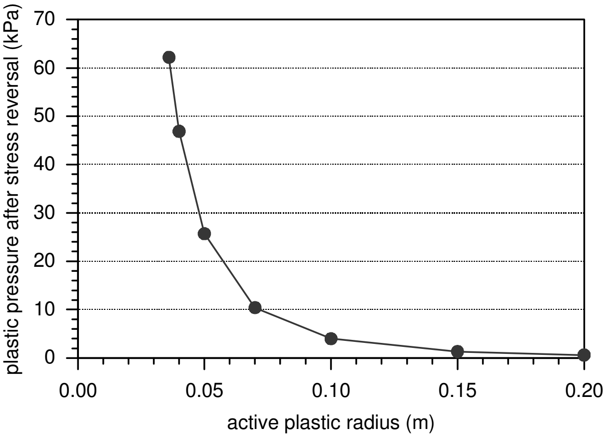

Figure 2-16. Pressure that is necessary to create passive plastic deformation following first active yield as a function of the original active plastic zone

Chang (2004) suggested two extreme ways of evaluating the injection pressure based on the cavity expansion theory. He described the first situation as “pile driving”. The plastic zone around the cavity is relatively limited and the soil is displaced (i.e. “pushed”) away from the advancing fracturing fluid. In the other extreme, the plastic zone is much bigger and the cavity expansion of an elliptic fracture is calculated. The “pile driving” calculation mode will lead to very high injection pressures. High injection pressures of this kind were found in Chang's study, but this is probably related to the closure of the injection tube before the test. This closure has to be removed and this resembles pile driving in some respects. On the basis of other results, it must be assumed that the "pile driving" mechanism results in much higher injection pressures than found in experiments.

2.4.2 DEM calculations

The DEM (Discrete Element Method) calculations performed by Pruiksma (2002) and summarised in Bezuijen et al. (2003) are important to understand the mechanism of hydraulic fracturing as it occurs during compensation grouting. Pruiksma used the commercial PFC code (Cundall, 2001) to perform distinct element calculations for a 2-D situation. He first simulated a biaxial test to fit the micro-mechanic parameters used in the code (friction between particles and elastic behaviour of the connection points between the particles) with the macroscopic parameters (friction angle, Young’s modulus and Poisson ratio). He used these results to simulate a hydraulic fracture. To do this, he incorporated the pressure distribution caused by the injection of the liquid into the DEM model. This method was developed by De Pater (Pater et al., 2003[a]). It is assumed that the injection pressure is present in a pore only when it is connected to the injection opening. When the pore space between "discs" (the two-dimensional representation of grains) is closed, the original pore pressure will apply. The force on the grains exerted by the injection liquid is calculated by assuming a uniform pressure perpendicular to the grain surface. See Figure 2-17.

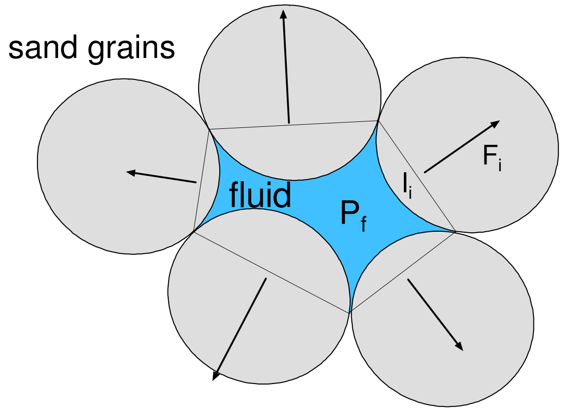

Figure 2-17: Forces on "grains" due to fluid pressure P_f. In the 2-D set-up of the PFC code the force on the grain exerted by the fluid is proportional to the length of the lines l_i.

Figure 2-18 shows the results of a calculation for a pressure increase in an opening between the discs. The black lines show the stresses between the discs: the thicker the line, the greater the stress. At the outset, there is a K_0=1 stress situation in the discs. The confining stress is 100 kPa and isotropic. Pressurising the injection opening leads to an increase in the radial stress around the injection opening and a decrease in the tangential stress around the injection hole. This can be seen from the black "stress lines", which concentrate around the injection hole. No fractures are present at the maximum injection pressure (result 2 in Figure 2-18) but further injection leads to an increase in the number of broken contacts between the discs and to the beginning of fractures (result 3 in Figure 2-18).

Pater et al. (2003[a]) performed comparable two-dimensional calculations with a larger number of particles and a higher effective confining stress of 10 MPa using the DEM code developed by Baars (1996). See Figure 2-19. Pater found the same results for sand as Pruiksma. In material with an unconfined strength of 17 MPa and, once again, an effective confining stress of 10 MPa, he found more distinct fractures and a significant decrease in injection pressure after the start of the fracture. Remarkably, the unconfined strength did not lead to a higher maximum in the injection pressure before fracturing starts. In both of Pater's simulations – with and without the unconfined strength of 17 MPa – the maximum pressure before fracturing is around 35 MPa.

These calculations are important to understand the mechanism of compensation grouting, as we will see later. The drawback of these calculations is that they are quite time-consuming and, although the results look like reality (discs that are displaced as grains in the soils), it is not certain to what extent the results are actually realistic because, if a mechanism such as cake building is not modelled, its impact on the results cannot be determined using the calculation method. This issue can only be investigated by comparing the results with the results of field tests or model tests.

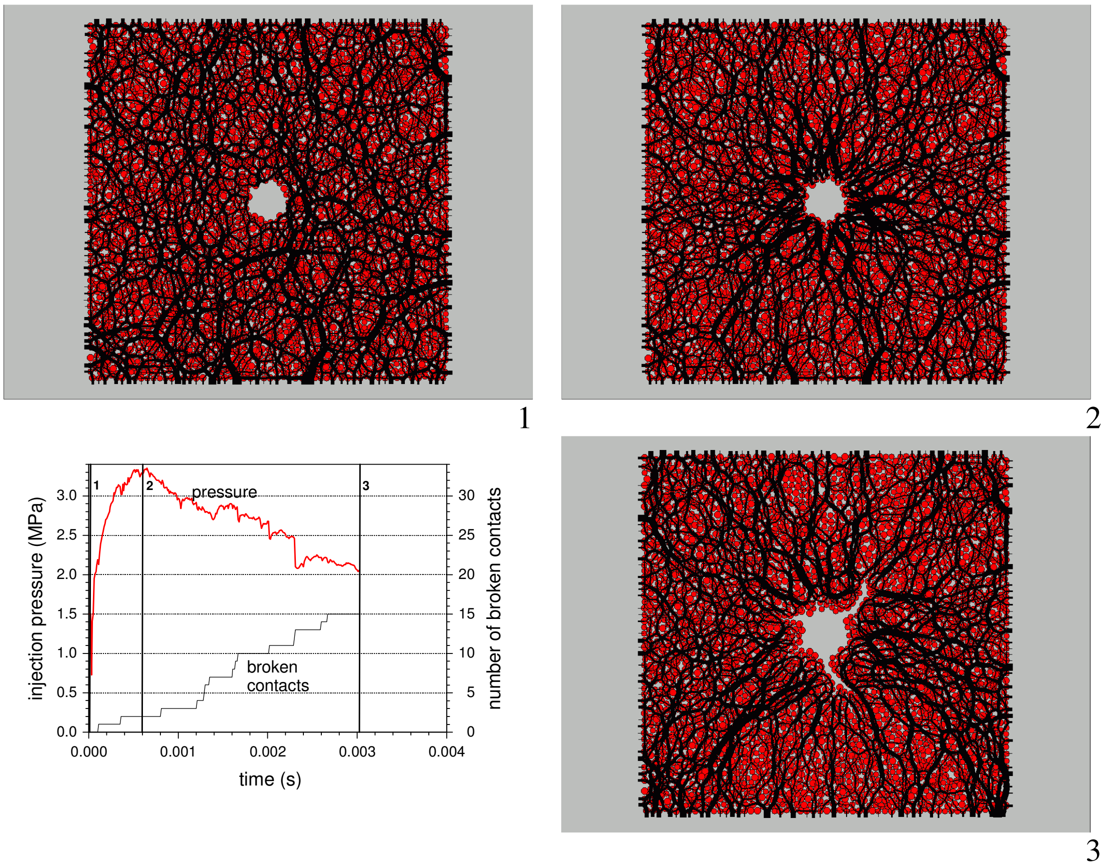

Figure 2-18: Results of DEM calculations to simulate hydraulic fractures. See also text (Pruiksma, 2002).

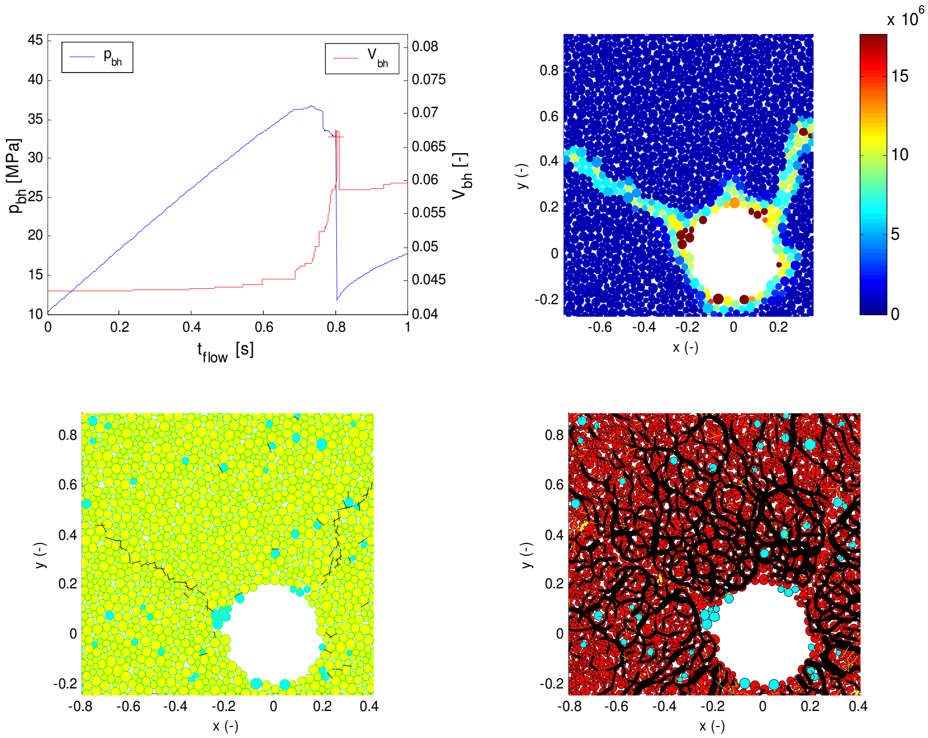

Figure 2-19. Simulation results for consolidated rock (unconfined strength of 17 MPa), with an effective confining stress of 10 MPa. The lower-left diagram shows where particles have lost contact at the end of the simulation. The diagram at the bottom right shows the forces, indicated with line thickness for the particle contacts, also at the end of the simulation. The top-left diagram shows borehole pressure and borehole volume versus time and the top-right diagram shows the pressures at the end of the simulation as colouring of the particles (Pater et al., 2003[a]).

2.4.3 Finite element calculations

The finite element calculations presented in the literature are normally not performed to investigate the micro-level, but to explore the intermediate and macro-levels (Kummerer et al., 2002, and Schweiger et al., 2004): how much grout needs to be injected to obtain a given heave? In these calculations, the impact of fracturing is modelled as a given increase in volume of some soil elements. The idea is that the various fractures that occur close to the injection pipe can be averaged to obtain a volume increase.

In some cases the ground directly around the elements is assigned different properties toinclude the hardening of the soil due to the fracturing (Schweiger et al., 2004). In the initial grouting stages, the soil properties are improved and further grouting leads to a volume increase at the injection points. Such models need to be calibrated to find the right heave at a certain grout injection. This calibration includes the influence of soil densification around the injection point due to grouting and the bleeding of the grout. The volume increase applied at the injection points will therefore always be less than the volume of grout injected. After calibrating the model, the authors claimed that there was a good match between the results of the model and the results of the measurements. A model of this kind can be used to investigate the heave that can be expected as a function of grouting, but it is not suitable as a way of investigating the mechanism that occurs during injection because the shape of the fracture and the volume loss is an input parameter in the model and not the result of the calculation.

Another approach is to concentrate all the heave in a soil layer where the TAMs are installed (Kovacevic et al., 1996). This is simulated by applying a stress in this layer acting at the grouting level at the end of a tunnel construction, with the stress being of a magnitude that is sufficient to nullify the settlement trough resulting from complete tunnel excavation. The authors argue that the method is valid for the situation simulated since they perform calculations for London clay that is over-consolidated, with a minor principal stress in the vertical direction. The fractures will therefore be horizontal. The method was used to calculate the influence of compensation grouting on the hoop lining stresses in the lining of the tunnel, which was in this case an NATM tunnel (NATM stands for New Austrian Tunnel Method, a method for tunnel excavation without the use of a TBM). Once again, the authors claimed that measurements and calculations were a good match.

The methods described above can be useful to describe the effects of compensation grouting on the surrounding area. However, the influence of the grout composition on the outcome of the compensation grouting process cannot be determined using these kinds of calculations because they do not take into account the impact of the grout composition on the results. The effect of grout composition is included only in the parameter that links the volume of the injected grout to the assumed volume increase in the soil directly around the injection point. This parameter is not necessarily the same as the efficiency of the grouting process since the constitutive models used for the soil allow for an increase or decrease of the volume of soil and it is therefore possible that final efficiency may be lower because of the densification of the soil around the area where the volume increase is fixed.

Dong and Pater (2008) present numerical calculations for describing the behaviour of a single fracture. They used FLAC to simulate the elasto-plastic behaviour of soil around a pre-defined fracture plane, varying the cohesion of the soil and the pressure infiltration properties of the injection fluid. They used a Mohr-Coulomb model in which the friction angle varies as a function of the plastic strain in an axi-symmetric grid. They found that the pressure infiltration of the injection fluid creates plastic zones around the fracture. See Figure 2-20. The injection tube is to the left of the plot. At the bottom, there is a disc-shaped fracture connected to the injection tube. The lower end of the plot is assumed to be a symmetry plane. Only half of the fracture and the soil model are modelled. The soil model in the axi-symmetric calculation is a cylinder with a hole for the injection tube. The results show that, on top of the fracture, there is a zone with high plastic stress (see the contour plot in Figure 2-19). Pressurising the injection pipe also results in plastic deformation close to the injection tube (between X=0 m and X=0.01 m) because it is assumed that, here also, the injection pressure loads the soil (the injection tube is open). The authors explain in the article that plastic deformation around the fracture is caused by the pressure infiltration from the injection liquid into the soil, leading to lower effective stresses. The fracture pressure drops from the injection tube to the tip of the fracture due to friction losses. In front of the fracture, there is an area with nearly zero vertical stress. The calculated fracture width is relatively small (100 µm or less, which is comparable to the grain dimensions). On the basis of their results, Dong and Pater concluded: “Although hydraulic fracturing in competent and tight rocks may depend only slightly on fluid properties, this assumption is invalid for fracturing sand”.

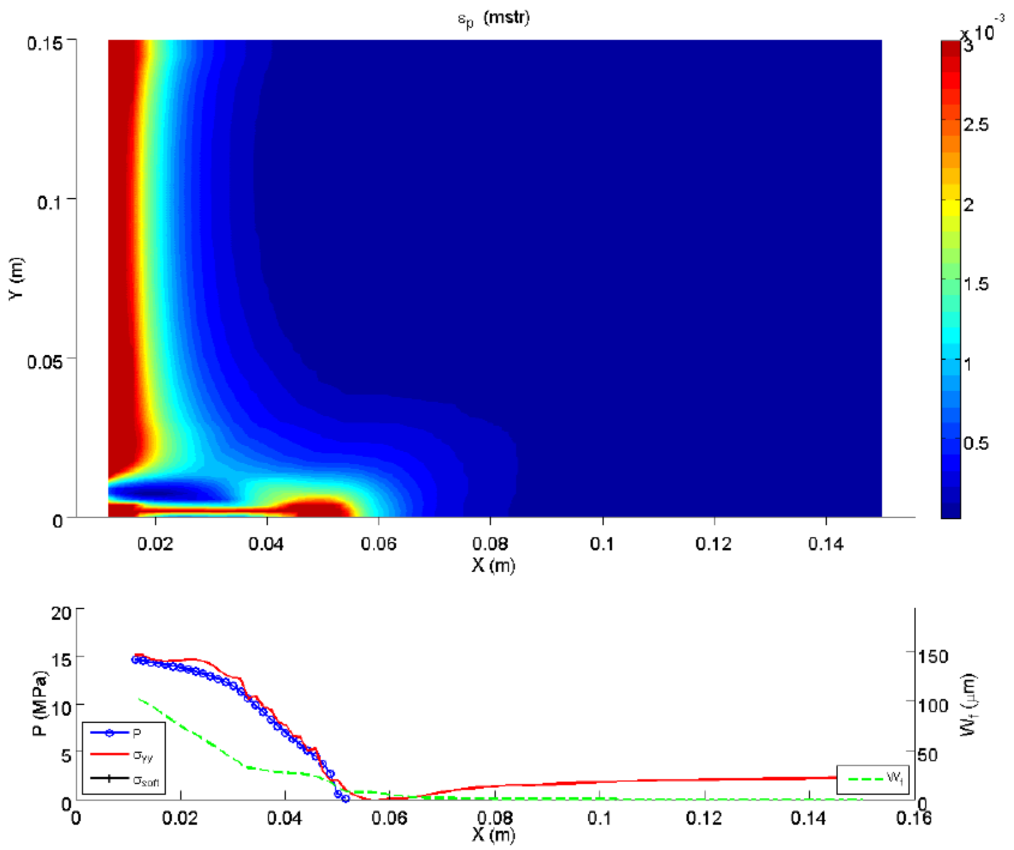

Figure 2-20: Calculation result from Dong and Pater (2008). The fracture is located between the origin. X is 0.06m and Y is 0 m. See also text.

2.5 Fracture propagation

Fracture propagation has been studied for propagation in rock (Dam, 1999) and in clay (Murdoch, 1993[b]; Chin, 1996; and Au, 2001). Fracture propagation is influenced by the yield strength of the injection liquid. Lowering the yield strength of the injection liquid results in thinner and longer fractures when injecting in clay (Harris et al., 1996). Au (2001) used the results of Murdoch (1993[b]) and Chin (1996) to explain that there will be a positive pore pressure at the propagating fracture tip when fracturing normally consolidated clay. In the case of overconsolidated clay, the pore pressure at the fracture tip will be negative because the deformation of the clay leads to dilatancy in the clay.

There is no accepted quantitative model for fracture propagation in sand in the literature. Khodaverdian and McElfresh (2000) and Zhai and Sharma (2005) present results for fracture propagation that are based on research for hydraulic fracturing for use in the oil industry. Khodaverdian and McElfresh state that: “Tip propagation in unconsolidated and poorly consolidated sand is not a 'true' fracturing process as defined by Linear Elastic Fracture Mechanics”. By contrast with fracturing in competent rocks, the fracture fluid has to invade the sand in front of the fracture for the fracture to remain open. In competent rock, the fluid front is normally behind the tip. The fractures found by these researchers in their experiments were “potentially a consequence of tip shear failure.” Using fluids with little wall-building capacity, which they call low-efficiency fluids, they found “a large number of sub-parallel fractures”. Using a high-efficiency fluid, in other words one with a high wall-building capacity, they found one, or only a few, large fractures.

Zhai and Sharma (2005) assume that plastic deformation of the sand around the injection hole leads to an increase in permeability. Since the pressure distribution around the injection hole is not symmetric, the plastic deformation means that the permeability increase will be asymmetric. This leads locally to higher permeability and a local increase in pore pressure, which finally results in a fracture. They also state:
“Classical models for linear-elastic, brittle fracture mechanics that have been traditionally applied to hard rock fracturing are not applicable for unconsolidated sands”.

Grotenhuis (2004) made the first attempt to describe fracture propagation in sand more quantitatively. Grotenhuis assumed that fracture length was determined by flow resistance in the fracture, which depends on the viscosity properties of the grout, leading to a pressure loss over the fracture in combination with pressure filtration of the grout in the fracture, reducing the thickness of the fracture in which the grout can flow. When the fracture becomes too thin, propagation will stop and another fracture will probably start. It was assumed that the minimum pressure for pressure propagation is the vertical confining stress and the maximum pressure that will initiate a fracture was estimated to be nearly twice as high. The way in which this maximum pressure was determined is not very clear.

Applying this model to determine the fracture length resulted in long and slender fractures for the grouts normally applied in compensation grouting. This result does not concur with the results obtained from the model tests described in the literature and as performed in this study. See Chapter 6. The experimental results show higher injection pressures and so the fractures are shorter and thicker.

Some additional work was therefore done in this study to improve the match between measurements and theory. See Section 6.9. However, the idea in general that pressure filtration has a major impact on the fracture results remains valid and partly explains the differences in fracturing behaviour when fracturing in sand or clay.

2.6 Fracture direction

The classical idea is that fractures propagate perpendicularly to the direction of minor principal stress, in other words vertically in normally consolidated soil and horizontally in over-consolidated soil. Many researchers have noticed this (Jaworski et al., 1981; Mori and Tamura, 1987; Panah and Yanagisawa, 1989; Mori et al., 1990; Lo and Kaniaru, 1990; Mhach, 1991; Murdoch, 1993[a,b]; Yanagisawa and Ali, 1994). The injection pressure is exerted in all directions and the direction of the minor principal stress is the first direction in which the soil stress is overcome, resulting in a fracture. The direction in which a fracture will propagate can be predicted using this idea. In normally consolidated soils, horizontal stress is less than vertical stress. This will result in vertical fractures. As a result of these vertical fractures, the horizontal stress in the soil increases and there comes a point at which horizontal stress exceeds vertical stress. From this point onwards, the predominant direction of the fractures will be horizontal. The vertical fractures are necessary to increase the horizontal stress in the soil; the horizontal fractures are the fractures that result in soil heave. In the case of concurrent compensation grouting during tunnelling, for example, it is therefore necessary to start with grouting before the tunnel reaches the grouting location. During the pre-conditioning phase, horizontal pressure is increased so that the fractures created after the pre-conditioning phase when the TBM passes are horizontal, leading directly to heave (Raabe and Esters, 1993).

This concept is not generally accepted as the sole valid concept. Massarsch (1978) and Lefebvre et al. (1991) found that vertical fractures may occur even if K_0 is greater than 1 and Jaworski et al. (1981) suggested that the fracturing direction can also follow weak zones in the soil. Fujisawa et al. (1996) deliberately created some weak zones in laboratory experiments with clay by injecting sodium silicate and found that the fractures followed these weak zones.

2.7 Installation procedure

The literature pays remarkably little attention to the installation procedure. Most researchers assume that the TAMs are, in the phrase used in FEM modelling, "wished in place". In other words, the TAM is in place but the original stress distribution remains the same as before the installation of the TAM. Wang and Dussault (1994) have shown that the installation procedure has an effect and that it is likely that the stresses around the TAM are lower than the *in situ* stresses. See Section 2.4.1.

Apart from the impact on the stress distribution the usual installation procedure also leads to the fracturing of not only the soil but also of the sleeve grout. The TAM is installed with a casing and the casing is retracted after installation while the angular space between the casing and the TAM is filled with sleeve grout. See also Section 3.3. This means that the TAM is surrounded by sleeve grout and the grout has to break through the sleeve grout before it can fracture the soil. Chambosse and Otterbein (2001) describe the influence of the sleeve grout on the injection pressure. They assume that the sleeve grout cracks during injection in conchiform (shell-shaped) clods at an aperture angle of 120^0 in both the radial and axial directions. Assuming that the crack is triggered by purely tensile forces, they found that a pressure of 40 bar is needed to crack the sleeve. This pressure is higher than the pressure they measure in a field test (18 bar). Chambosse and Otterbein do not take into account the consequences of the installation and the possible unloading on the *in situ* stresses, but they do mention the possibility of loose zones and cavities. They recommend performing pre-grouting until the injection pressures are above a certain level.

2.8 Field observations

2.8.1 Fracture shapes

The fracture shape is influenced by the grout used for the injection. As mentioned before, Harris et al. (1996) demonstrated that this was the case for injection in clay. They tested two different grouts in London clay under Waterloo Station during the Jubilee Line Extension project and found that the grout with the highest viscosity leads to thicker fractures than the grout with the lowest viscosity. In both cases, the fractures were relatively thin at 10 mm and 1–2 mm respectively. Furthermore, the difference between compaction grouting and compensation grouting also implies that the grout properties have a distinct influence on the shape of the grout body.

No field tests on compensation grouting in sand have been reported where the shape of the fractures was determined after the injection. In the compensation grouting project underneath Antwerp Central Station the grout was injected into a sandy layer of shells. There it was found that the resulting, rather long, fractures were 2–6 mm in height. The results from this field test report will be discussed in more detail in Section 3.4.

2.8.2 Projects

Where the literature reports on field observations from compensation grouting projects, the focus is mainly on the results of compensation grouting at the macro-level (as defined in Section 1.5) (Mair, 1992; Chambosse and Otterbein, 2001[a,b]; Falk, 1997; Gens et al., 2005; Haimoni and Wright, 1999). Compensation grouting is used empirically: grout is injected underneath the building where compensation is required and the heave is measured. For the purposes of this study, the reports on these results are insufficient because it is also necessary to know what fractures are made, how long they are and what levels of efficiency are achieved.

The projects in the literature are, in most cases, successful projects. As mentioned above, therefore, compensation grouting is a mature method that has developed beyond the experimental stage, even though it should be noted that successes are reported more often than failures.

Because of the rather empirical approach used in the literature to describe projects, it was decided not to discuss that literature in detail in this section. Instead, the next chapter will present some projects that closely resemble the situation in Amsterdam or projects that have been important for the development of the ideas during this study.

2.9 Summary of literature

The literature studied showed that experience with compensation grouting in sand is more limited than in clay. No calculation method is available to describe the shape and extent of the fractures in sand. Experiments both in the field and in the laboratory have shown that the grout mixture influences the extent and shape of the fractures. Fracturing sand in the laboratory with a cement-bentonite grout is not a straightforward operation. Most experiments performed to fracture sand resulted in some irregularly shaped grout bodies but not in fractures. Experiments with different injection liquids (such as the x-linked gel that is used in the oil industry) did result in fractures.

In addition to the grout mixture, the stress distribution around the injection hole and therefore the stress history also seem to have an influence. The literature pays little attention to this factor (with the exception of the theoretical work of Wang and Dusseault, 1994). Another relatively neglected area is grouting efficiency in laboratory tests. This is remarkable since this is an important issue in the field practice of displacement grouting. Most laboratory tests were performed in the context of hydraulic fracturing for the oil industry and this probably explains why efficiency received relatively little attention.

On the basis of the results of the literature study, it was decided to concentrate the experimental programme on how the properties of a cement-bentonite grout affect the shape of the fractures. Later, this research was extended to include the impact of installation and the efficiency of the fracturing process. The literature did not mention any scale effects. This made it possible to perform the experiments on a model scale. The theoretical work on fracture propagation was based on the fracture propagation model of Grotenhuis (2004). However, since this was the first attempt to describe fracture propagation quantitatively and because the predicted fractures are different from what is found in the literature, the results of the experimental programme will lead to changes to this model.

3 Field tests and observations

This chapter describes some recent projects involving compensation grouting in sand that have influenced the focus and direction of this study: the compensation grouting trial near the Sophia Rail Tunnel (near Rotterdam, Netherlands); the compensation grouting in Perth (Australia) during the construction of the New MetroRail City project; the excavation of fractures in Antwerp (Belgium) underneath the Central Station; the full-scale trial performed in Amsterdam (Netherlands) in 2007 prior to the construction of the North-South underground line; and fractures created accidentally during the construction of one of the cross-connections of the Hubertus Tunnel in The Hague (Netherlands).

3.1 Compensation grouting trial

The compensation grouting trial (CGT) was performed near the Sophia Rail Tunnel. The aim was to test whether or not compensation grouting was possible in sand below a pile foundationwith the same characteristics as in Amsterdam. The results were important to judge the applicability of compensation grouting as a mitigation measure during the construction of the North-South underground line in Amsterdam. Compensation grouting was applied during the passage of the TBM.

During the CGT, the movements of soil layers were monitored using extensometers. Ten extensometers (E01 – E09 and E016) were situated around the pile groups of a rebuilt "traditional Amsterdam foundation". See Figure 3-1.

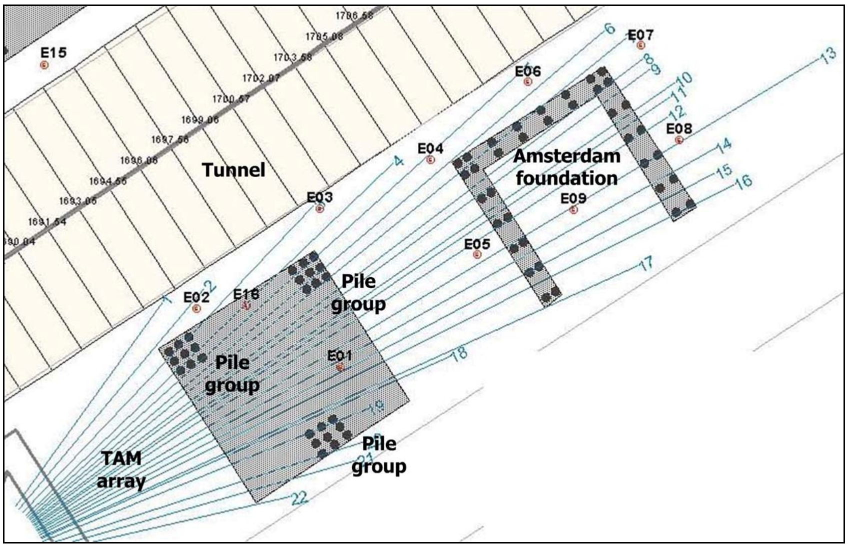

Figure 3-1: Trial site CGT (top view) (Paans, 2002)

Combining the results from the extensometers and the grout injection data allows for the investigation of the spatial relationship between an individual grout injection of about 25 litres in 3 minutes and the measured movements of the extensometers in the same time interval.

The analysis of the measurements resulted in the following observations:

- Fractures tend to develop along existing fractures.
- Fracture direction is mainly parallel to the TAMs. This and the previous observation confirm a statement found in the literature, which states that fractures tend to propagate along bedding planes (Kummerer, 2003).
- Fracture development is not radial and there is a preferred direction. The fractures were found to be very long, even extending to lengths of more than 15 metres, as response was discernable over that distance. This is illustrated in Figure 3-2 (Paans, 2002). When there was a considerable distance between the sleeve and the extensometer, this was mostly in the direction of the TAMs, indicating that fractures probably propagate in part in the direction of the TAM.

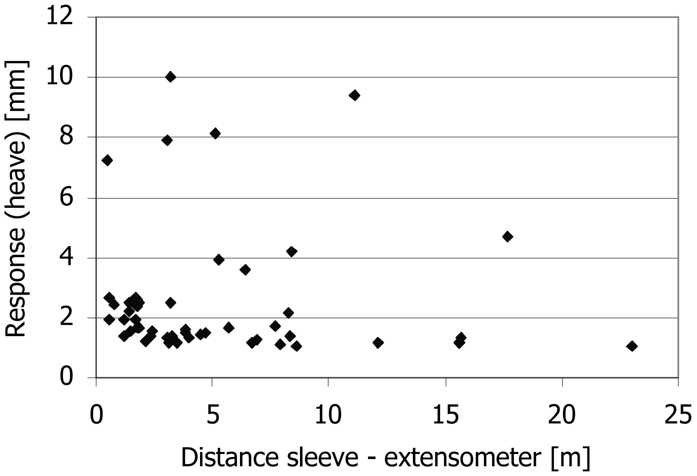

Figure 3-2: Shortest distance sleeve-extensometer and accompanying response, (Paans, 2002)

Given the results of this test, it was assumed that the fractures must have a more branch-like pattern, since the responses were found at such a large distance from the injection point (Bezuijen et al., 2008). Furthermore, it was concluded that compensation grouting underneath a pile foundation is possible but that more grout than was envisaged beforehand was necessary at some locations to achieve the necessary heave (Paans, 2002). It also emerged that it was difficult to really achieve compensation for settlement with concurrent grouting. For the geometry of the TAMs in the project, the drilling speed of the TBM (approximately 15 m/day) was such that it was not possible to compensate for all settlement during tunnelling. After the TBM had passed the foundations, it proved possible to re-level the foundations successfully.

3.2 Perth

Compensation grouting was used during the construction of the New MetroRail City project in Perth 2005-2006. The metro line was built using TBM. Just before William Street Station, the line has to pass beneath existing buildings founded on a concrete slab (Kleinlugtenbelt, 2006). The subsoil above and around the injection tubes consists of sandy material. The injection tubes were installed 5.8–8.8 m below the subsoil, close to the water table between the tunnel crown and the concrete slab of the building that forms its shallow foundation, at a distance of approximately 8 m from the tunnel crown and on average 4 m from the concrete slab. The original vertical stress at the location of the injection tubes is not known. Based on the dimensions of the building on top of it, the estimated vertical stress is between 200 and 300 kPa. Compensation grouting was applied in two phases: a pre-conditioning phase before the TBM passes and an active phase during the passage of the TBM. The pre-conditioning phase was applied to pre-stress the soil and to create a "pre-heave" of 3 mm. The pre-heave makes it possible to allow some settlement during the construction of the tunnel before the start of the active phase. Up to five injections were applied in the pre-conditioning phase to achieve the required pre-heave. Vertical displacement was measured at 33 locations.

It was found that the injection pressure was low during pre-conditioning (4 bar or less) but that it increased up to 18 bar for the last pre-conditioning injection. The efficiency of the grouting process in the pre-conditioning phase started at 0% for the first injection, due to loosening of the soil during TAM installation, and increased to 8% in the pre-conditioning phase. It emerged that the pre-conditioning phase had improved the soil conditions in such a way that, in combination with accurate TBM operations, hardly any grouting was needed in the active phase or the concurrent compensation grouting phase.

On the basis of these results, it was concluded that it was not certain that compensation grouting had really taken place. The soil improvement that was achieved could also have been the result of compaction grouting, where soil improvement is more dominant than soil heave.

3.3 Full-scale trial in Amsterdam

To test the TAM layout, a compensation grouting trial (CGT) was performed at the Rokin location in Amsterdam in 2007. TAMs were installed from an installation shaft at a depth of 15–18 m. See Figure 3-5. The subsoil consists of silty sand ("Alleröd") and standard sand.
TAMs were installed using a casing. See Figure 3-3 and Figure 3-4.

Figure 3-3: Tip and casing as used in Amsterdam

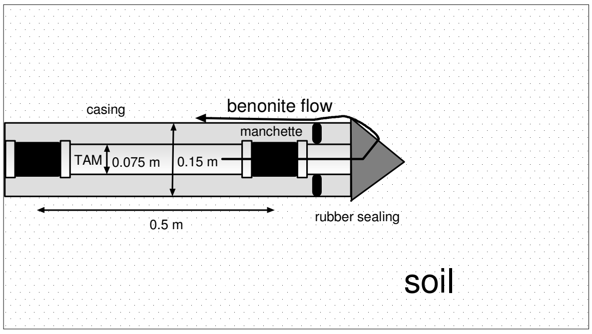

Figure 3-4: Sketch of TAM during penetrating installation (Bezuijen et al., 2008)

After installation, the installation tube was removed and only the tip and the TAM remained in the soil. The space between the installation tube and the TAM is filled with sleeve grout before removing the installation tube. Here, BlitzDämmer – a hydraulically-setting premixed dry mortar (see Heidelberg (2009) for technical specifications) with a water-solid ratio of 0.7 – was used as the sleeve grout. Two installation methods for the tubes were used. At first, the tip was flushed with bentonite supplied through the TAM and the bentonite was retrieved through an opening behind the tip before flowing back through the space between the installation tube and the TAM. The thinking is that the bentonite works as a lubricant and also erodes some of the sand to allow easy penetration of the installation tube in the sand. However, it emerged that this installation method resulted in soil settlement and settlement of the pile foundation above the TAMs of several millimetres. Consequently, the installation method was changed and only a limited amount of bentonite was applied at the tip (see Figure 3-4). This bentonite was now used only as a lubricant and no bentonite flow was allowed between the installation tube and the TAM. This installation method resulted in hardly any settlement of the foundation and it will therefore be used in the rest of the project.

Grout was injected to create a few millimetres of heave in the part of the building that is closest to the location where the tunnel will be constructed. The idea is that this allows for some settlement when the tunnel passes before more grout has to be injected and that, as in Perth, the soil is improved, reducing settlement. The results show that a very controlled heave was possible for the buildings below which the compensation grouting was performed. See Figure 3-6. However, much more grout than expected had to be injected to obtain this heave, which may indicate that the efficiency of the process below a pile foundation is less than for other foundations. Figure 3-7 shows the course of the heave during and after grouting as a function of time. The heave remains reasonably stable after the injection has stopped.

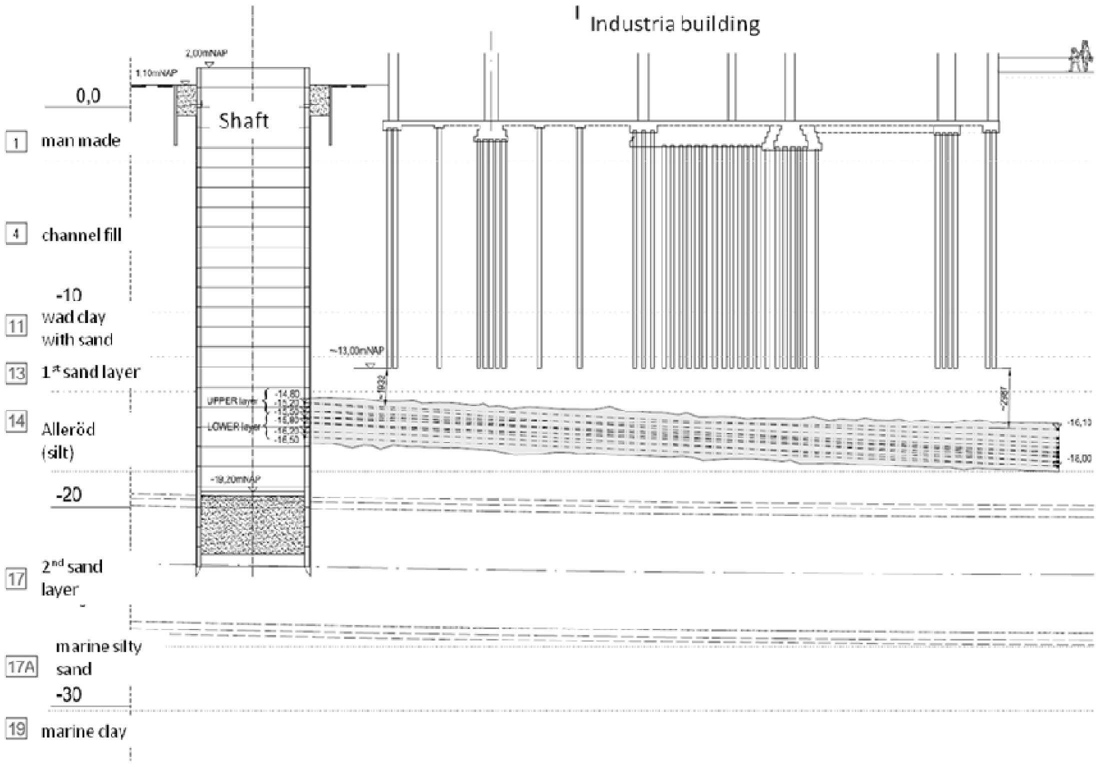

Figure 3-5: Cross-section of installation shaft, pile foundation and TAM positions in the Amsterdam subsoil below the Industria building. Only the upper TAMs were installed in the CGT.

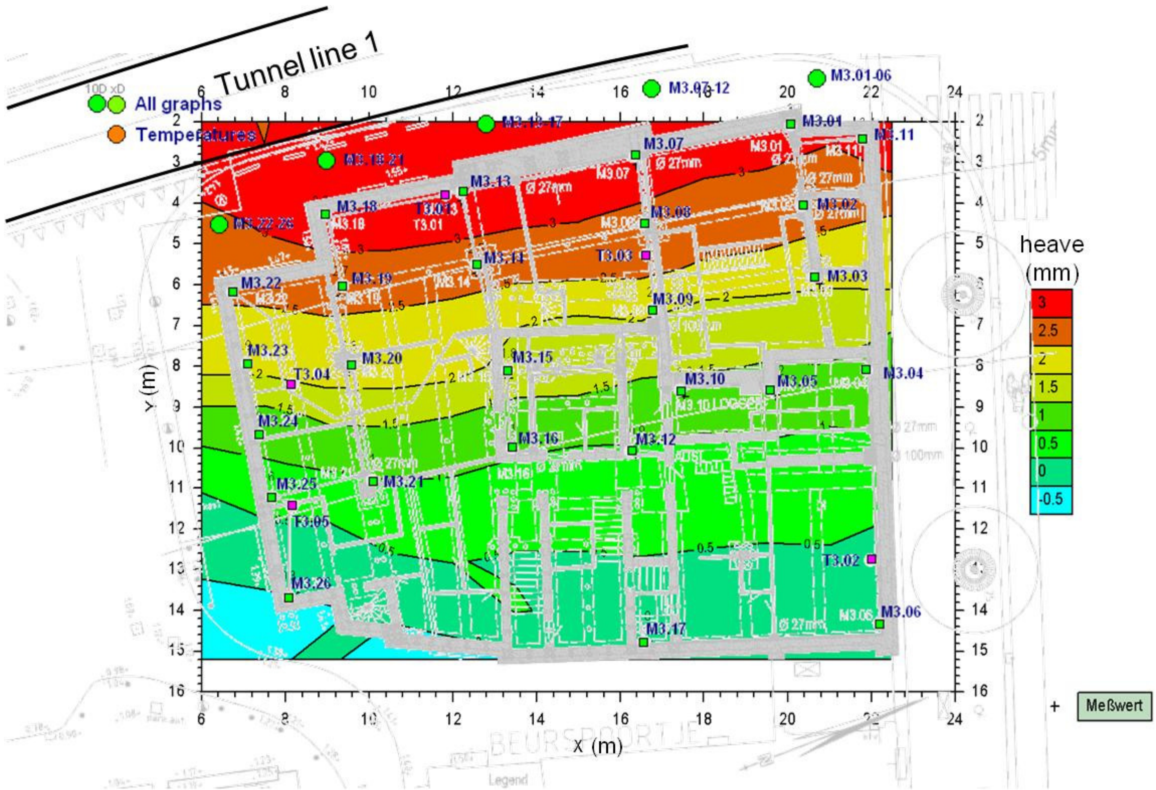

Figure 3-6: Result of CGT: Measured heave after pre-grouting. Note that the lines of equal heave are parallel to the tunnel tube. The grey lines show the walls of the Industria building. The contours show heave in mm (September 2007).

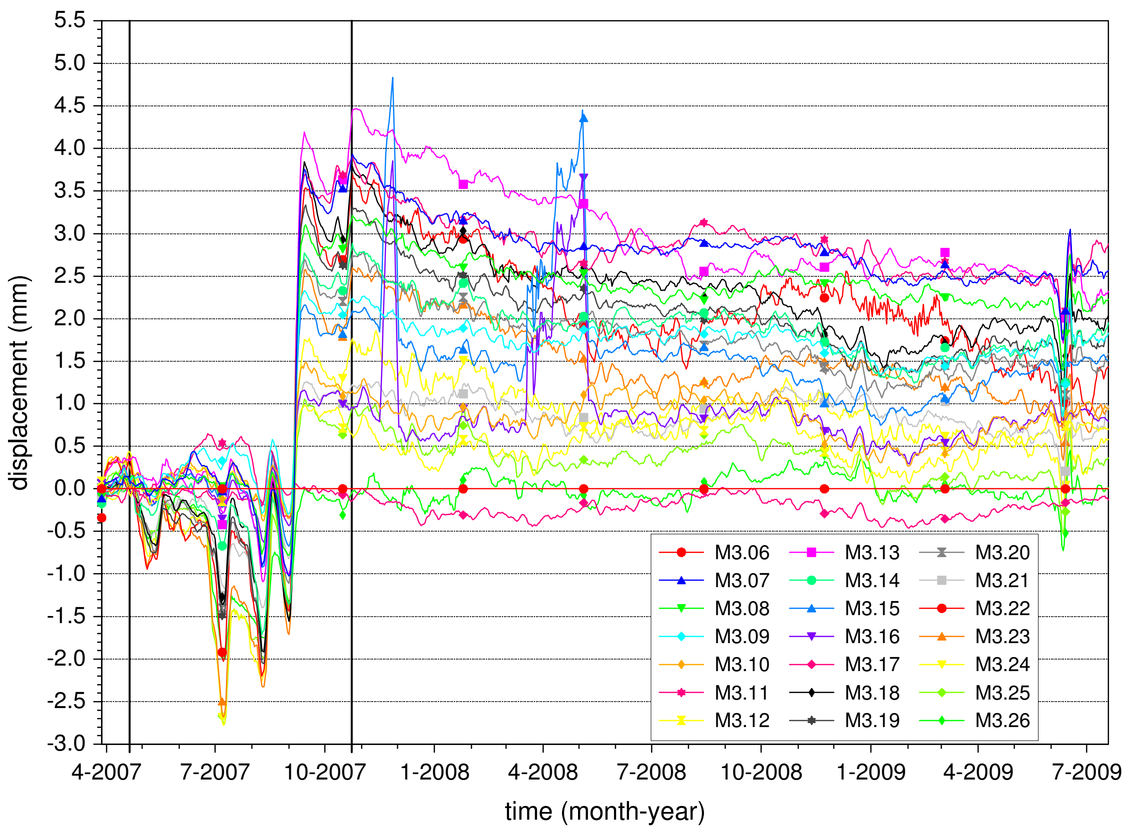

Figure 3-7: Result of CGT: Measured heave during and after pre-grouting. Numbers refer to numbers in Figure 3-6.

3.4 Antwerp Central station

The tunnel for the HSL between Amsterdam and Paris passes below Antwerp Central Station. The settlement restrictions for this historical station were rather strict and therefore compensation grouting was applied. The work was carried out from 1999 to 2001. More than 80 lances were installed for compensation grouting. The grouting was performed in "Antwerp Sand", a tertiary, slightly overconsolidated, dark grey fine sand with about 10% clay content. The sand layer is intercepted by a small shell layer and underlain by Boomse clay. An expected settlement of 20 mm was compensated for in order to obtain a maximum settlement of 4 mm. This project is of particular importance because, during the construction works, it was necessary to dig out the sand where compensation grouting had been applied. This presented a rare opportunity to see the structures created by the compensation grouting. The TAMs were used for several injections: up to 60 according to the brochure (Keller, undated reference) about this project from the contractor for this project (Keller). In some of the injections the grout was coloured and this made it possible to see what kind of fractures were made by a single grout injection. See Figure 3-8.

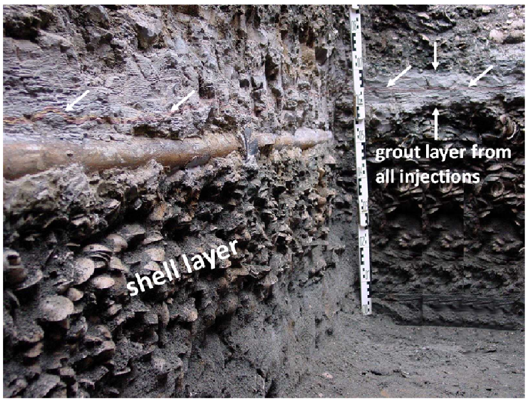

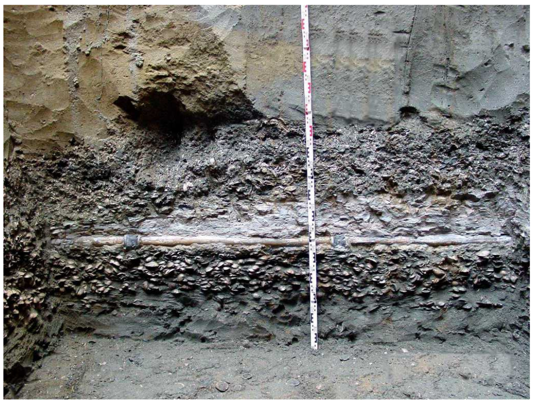

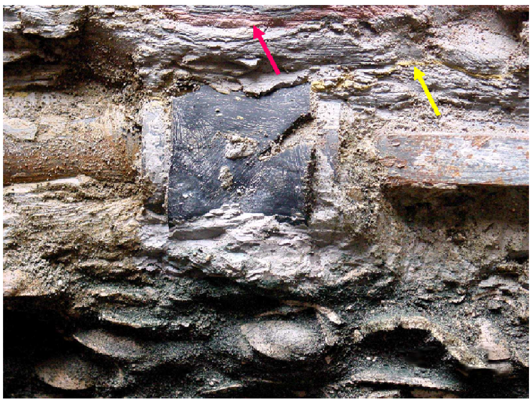

Detail of TAM in the middle of the upper right picture. The arrows point to coloured grout layers with the same colour as the arrows.

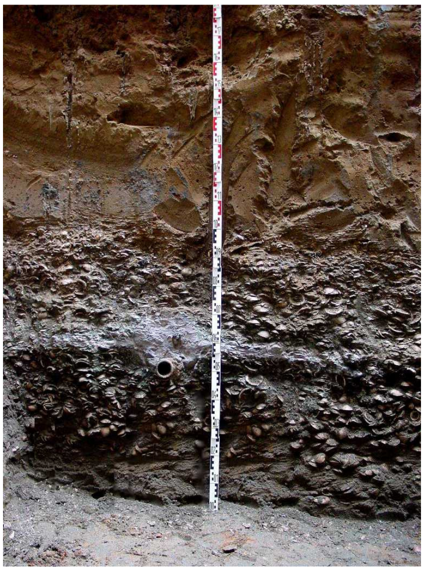

Figure 3-8: Pictures taken at Antwerp Central station. Results of compensation grouting. The red coloured grout in the upper left picture indicated with the angled arrows is the result of one single injection of 50 l grout (Watt, 2004, modified).

On the basis of the pictures taken of this site, it was concluded that compensation grouting leads to thin and long fractures. Measurements from the pictures showed that the yellow fracture in the lower left picture is about 2.5 mm wide and that the red one is 8 mm wide. The fractures shown in the pictures are not fractures through sand, but in the layer of shells and through the sleeve grout that was used for the installation of the injection tubes or through grout from previous injections. The overall picture is that relatively straight horizontal fractures are created on both sides of the injection tube. Furthermore, the injection tube proved to be located at the "bottom" of a circular body of sleeve grout and/or grout. This could have been expected since the average density of the injection tube is higher than that of the sleeve grout and therefore, as long as the sleeve grout is in a liquid phase, the tube will sink to the bottom of the hole made by the casing.

From these results Grotenhuis (2004) concluded that long thin fractures could be expected in sand. Later during the research conducted for this thesis, it was realised that the fractures were not made in the sand and that the results were probably also influenced by the sleeve grout and the layer of shells around the TAM. This result will prove to be of interest for this study, as will be discussed later.

3.5 Hubertus tunnel

No compensation grouting was performed at the Hubertus tunnel, yet the observations from the field during the construction of a cross-connection between the two tubes will be described briefly here because these observations were important for the ideas developed during this study.

The Hubertus Tunnel is a twin-track road tunnel in dune sand. The tunnels are 10 m in diameter. Five cross-connections were made between the two tunnel tubes. Soil freezing was used to make these connections. Freezing lances were positioned working from the tunnel lining into the sand. When the soil was frozen at the position of the connection, the cross-connection was dug into the frozen sand and the concrete connection structure was made. The freezing was then stopped. Figure 3-9 shows a cross-section and the frozen soil around it.

The tunnel crown is 11 m below the soil surface and the phreatic level is 5 m below the surface. The vertical pressure at the top of the tunnel is estimated to be about 140 kPa. Grout was used to install the lances for freezing. The grout used had a WCR of 1 and contained 3% bentonite. During the installation of these lances for the first cross-connection, the pressure was increased so that the grout created hydraulic fractures. These fractures became visible when the frozen soil was removed. Figure 3-10 shows an example of fractures in the sand around the tunnel and between the tail void grout and the sand.

The picture was taken with the photographer standing in the newly created opening. From left to right, we see the opening, the tunnel lining, the tail void grout, grout from a freezing lance that penetrated between the tail void grout and the sand and the frozen sand with a fracture in the upper part of the sand. There were also fractures that were only visible in the sand. Although this is difficult to determine from the available information (only one cross-section), it is likely that the fractures had the form of a plane or sheet, measuring up to several metres in length and 0.01 to 0.05 m wide. The normal pressure for injecting the grout is 3 bar. However, according to the employees on the site, the pressure could have been higher during this injection because there were doubts about the pressure gauge.

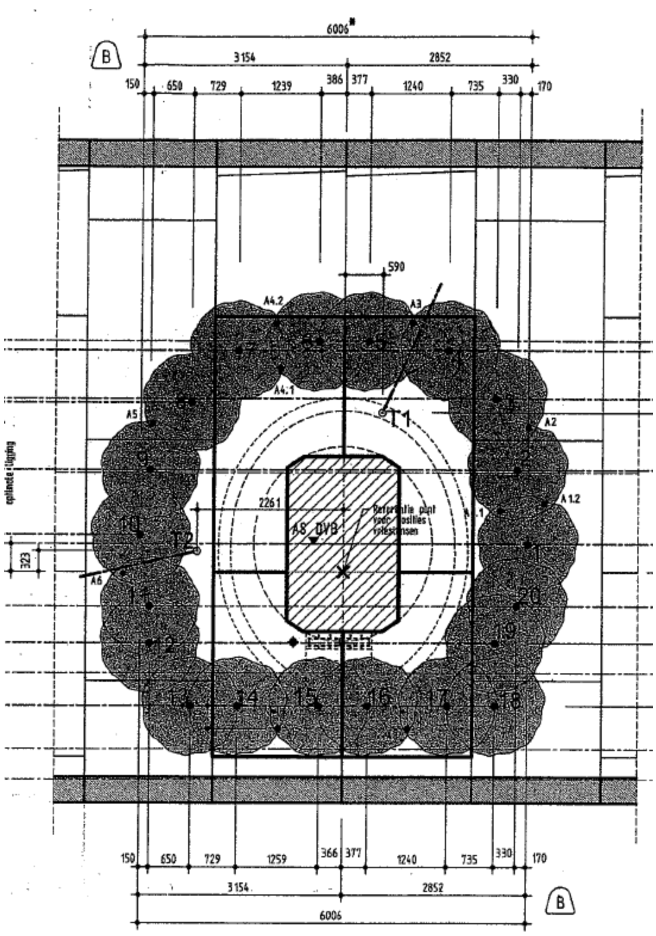

Figure 3-9: Sketch of a connection between the tubes made by freezing

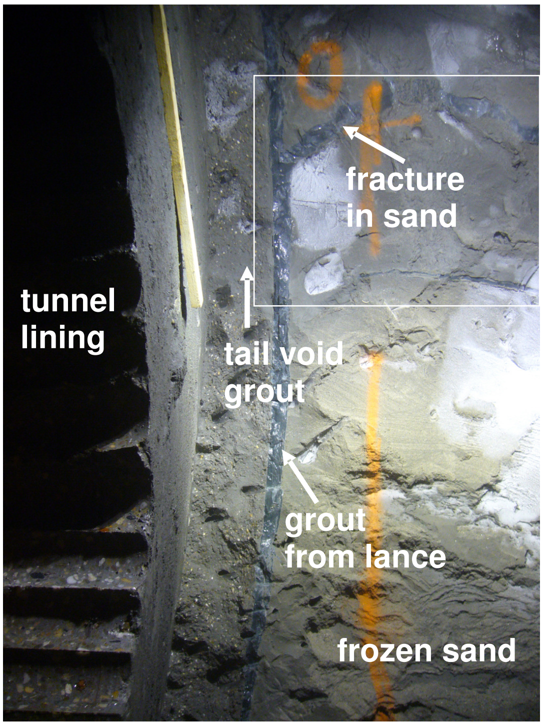

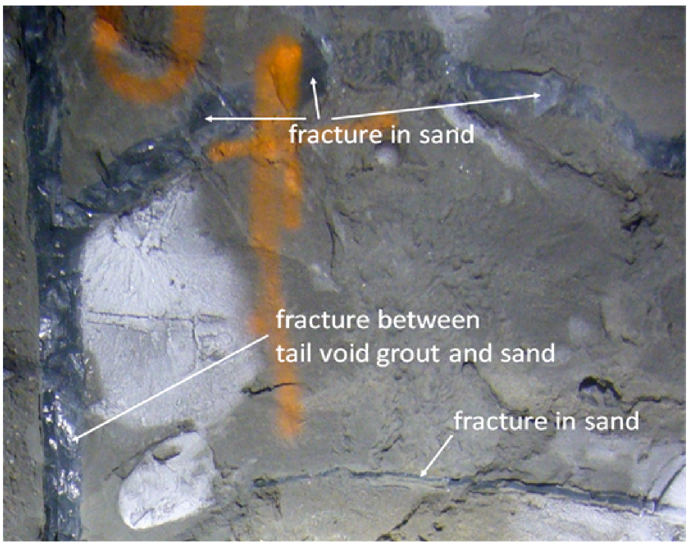

Figure 3-10: Fractures found during the construction of the first connection between the tubes of the Hubertus tunnel (left), with rectangle in detail (right)

The observations in Figure 3-10 led to two conclusions:

- Grout from the lance is injected between the tail void grout and the sand. It is likely that this is caused by a reduction in the effective stresses around the tunnel due to pressure filtration from the grout applied as tail void grout. The process is described in detail in Bezuijen and Talmon (2003).
- Fractures with a high length-to-thickness ratio (>20) can occur in sand. The fractures were predominantly horizontal. These fractures have not yet been found in laboratory experiments.

The first conclusion may seem to be of little importance for this study, but the second one may be decisive. The stresses in the sand around the injection point are important in determining whether the sand can be fractured.

Before the results of this site visit became available, it was questioned whether a fracture with a high length-to-thickness ratio could be made in sand, because all the results from laboratory tests led to low length-to-thickness ratios.

This field observation made it clear that fractures were created in sand in field conditions using grouts with a low WCR ratio (<2) and only 3% bentonite. Comparable grout mixtures did not lead to fractures in the laboratory tests and therefore it was concluded that there might be some discrepancy between the field tests and the laboratory tests.

3.6 Conclusions from the field investigations

At all the field locations, compensation grouting led to the conclusion that fractures at least several metres long had been created. These fractures were relatively thin: from 2.5 mm to 0.05 m. Fractures have a tendency to follow the direction of the injection tubes, the sleeve grout and previous fractures. The presence of a grout fracture between the tail void grout and the sand at the Hubertus Tunnel shows that there is also a preference for locations in the sand where the confining stress is lower (the observation that the confining stress is lower between the tail void and the sand was not measured; this is a result from previous research).

At the locations where efficiency was determined it was not very high: 10% or less.

The pre-conditioning in Amsterdam showed that controlled heave for a building on a piled foundation is possible using displacement grouting in the sand underneath the foundation.

The results of the field observations became available during the execution of the experimental programme (see Chapter 6), in which it was very difficult to create long thin fractures. They led to an examination of the differences between the conditions in the field campaigns and the laboratory tests. See Section 6.8.4.

4 Theoretical considerations

4.1 Introduction

The work described in this thesis emphasises the experimental side. The aim was to determine which mechanisms are important during the formation of fractures. In the case of some mechanisms, it was possible to derive theory that explains some aspects of the results. This has not yet led to a calculation model that describes all features of fracture grouting in sand. However, this chapter will end with a model that describes the relation between grout properties, soil properties and the ratio between the width and length of a fracture.

This chapter will start with a cavity expansion calculation that shows the relation between injection pressure and the increase in the diameter of an injection hole as a function of the friction angle and Young's modulus. This is followed by a more qualitative description that describes the possible start of a fracture and how this is influenced by grout properties. The movement of single grains may be important and so the following section includes a calculation of what keeps a single grain in position. Returning to a larger scale, a calculation from Verruijt (2002) is reworked to show the influence of pressure infiltration on the start of plastic deformation, followed by a calculation method to describe plastering and pressure infiltration as a function of the grout parameters. Information about plastering allows us to obtain an indication of fracture propagation and the ratio between the width and the length of a fracture. Numerical calculations show that, as a first approximation, the pressures in plane-shaped fractures can be modelled using cavity expansion theory. Combining this result with the result obtained for pressure propagation shows how the shape of the fractures is related to injection pressure.

The Discussion (Chapter 8) will compare the results of these descriptions with the results of the measurements.

4.2 Connections

The subjects mentioned above are connected and, taken together, they improve our understanding of what happens during the injection of grout in sand, as will be described below.

When soil is pressurised from an injection hole, cavity expansion results. The expansion is a function of the pressure, as will be quantified in the next section. When a fracture occurs, expansion will stop and pressure will remain constant or even fall. Without fractures, pressure increases to a certain limit pressure. Cavity expansion theory therefore produces the maximum possible pressure that can be achieved by injection. Fracturing will always result in lower injection pressures. Section 4.4 therefore looks at which mechanism can start a fracture. The ideas described were developed using the results of the DEM calculations described in Section 2.4.2. It is shown that the thickness of the filter cake present between the grout and the soil in the fracture is important. This filter cake can be formed by pressure filtration as described by McKinley and Bolton (1999) (see Section 2.2.2) but also by pressure infiltration in which water and fine particles in the grout are pressed into the soil skeleton and large particles that are also present in the grout form a filter cake. Section 4.5 describes a model for quantifying pressure infiltration.

Research by Bohloli and Pater (2006) shows that fracturing with a pure viscous liquid is difficult and that the fracturing liquid must have a "wall-building capacity". A micromechanical calculation (Section 4.6) shows that, without cake formation, the grains can easily roll and, by doing so, block a newly created fracture. An elastic cavity expansion calculation (Section 4.7) makes it clear that a pressure loading directly on the boundary between the grout and the sand, of the kind that can be achieved with a wall-building fluid, leads to plastic deformation at lower injection pressures than when there is a certain pressure gradient in the soil around the injection hole, as is the case when the injection fluid has only viscous properties without wall building.

Finite element calculations with a predefined fracture (Section 4.8) were performed to obtain an idea of the soil deformation around a fracture. The results of these calculations are used in Section 4.10 to derive an analytical formulation between injection pressure and the soil response.

The relation for pressure filtration and an assumed geometrical shape of a fracture makes it possible to estimate the thickness-to-length ratio (*d/s*) of a fracture as a function of the injection rate, injection pressure, the geometrical shape and the grout properties (Section 4.9).

Since the injection pressure is determined by the soil deformation, it is possible to relate the soil deformation to the injection pressure, once again using cavity expansion theory (Section 4.10). This model includes some simplifications, but it allows us to determine how, in the case of a sheet-shaped fracture, the injection pressure is related to the soil and grout properties. This model allows for a prediction of the injection pressure.

Table 3 presents a table with the main calculation models described in Chapter 4 and Chapter 5, and states the sections where the various models are described, the assumptions/limitations and the purpose of the model. The pressure infiltration model, the micro-mechanical model, the influence flow model and the FEM calculations have been used to increase our understanding of various processes. The other models – cavity expansion, filtration, and fracture propagation – have also been used to make a model that describes fracture propagation taking into account the combined influence of soil properties and grout properties. This model is described in Section 4.10. Figure 4-1 lists the aspects of the fracturing process dealt with in the various models, and the sections in which those models are described and investigated.

Table 3: Calculation models described in Chapter 4 and Chapter 5, assumptions and limitation and purpose of model

Model	Sections	Purpose of model (interest for this study)	Assumptions/Limitations
Cavity expansion	4.3	Relation between diameter increase and cavity pressure (result used as a base for calculations in section 4.10)	- spherical symmetry - Mohr-Coloumb failure criterion - natural strain - no dilatancy
Filtration	4.5 4.9.6 5	Establish a relation between the injection pressure, grout properties and the thickness of the filter cake as a function of time (the thickness of the filter cake determines the minimum fracture width. See 4.9, 4.10)	- also in combination with pressure infiltration - no hardening in grout during filtration - stiff filter cake - 1 D calculation
Pressure infiltration	4.5 5.9	Calculate the influence of pressure infiltration on the thickness of the filter cake (pressure infiltration can create a filter cake of coarse grains from the grout in a short time)	- in combination with filtration - Bingham liquid - 1 D calculation
Micro–mechanical	4.6	Show that some plastering is necessary to obtain stable sand grains next to the fracture (This explains why the fracturing results depend on the fluid properties)	-grains can be simulated as 2-D discs. - contact volume between grains determines force on grain. - filter cake is thinner than 0.5 grain.
Influence flow	4.7	Show that plastic deformation in the soil can be expected at lower stresses when, during injection, a filter cake creates a steep pressure gradient at the boundary between grout and soil compared to liquids that penetrate into the soil and in that way creates lower pressure gradients (plastic soil deformation is necessary, although not sufficient for fracturing)	- linear elastic soil model - Bingham liquid as grout - no fracture simulated
FEM	4.8	To find the soil deformation pattern around the fracture. (This soil deformation pattern was used to come to an analytical solution. See 4.10)	- Mohr-Coulomb model - drained and undrained - predefined fracture
Fracture propagation	4.9	Describing the shape of the fractures as a function of the injection pressure and the grout properties. (The model was used to explain measurement results and is an important basis for the model described in 4.10.)	- predefined fracture shape (plane of branch) - pressure infiltration not taken into account
Fracture and soil combined	4.10	Show how injection pressure, soil properties, grout properties and fracture shapes are related. (One of the main results of this study. Explains why injection pressures vary and shows that, for known grout properties, the injection pressures provide an indication of the shape of the fracture)	- soil reaction can be schematised as a cavity - predefined fracture shape (plane) - pressure infiltration not taken into account

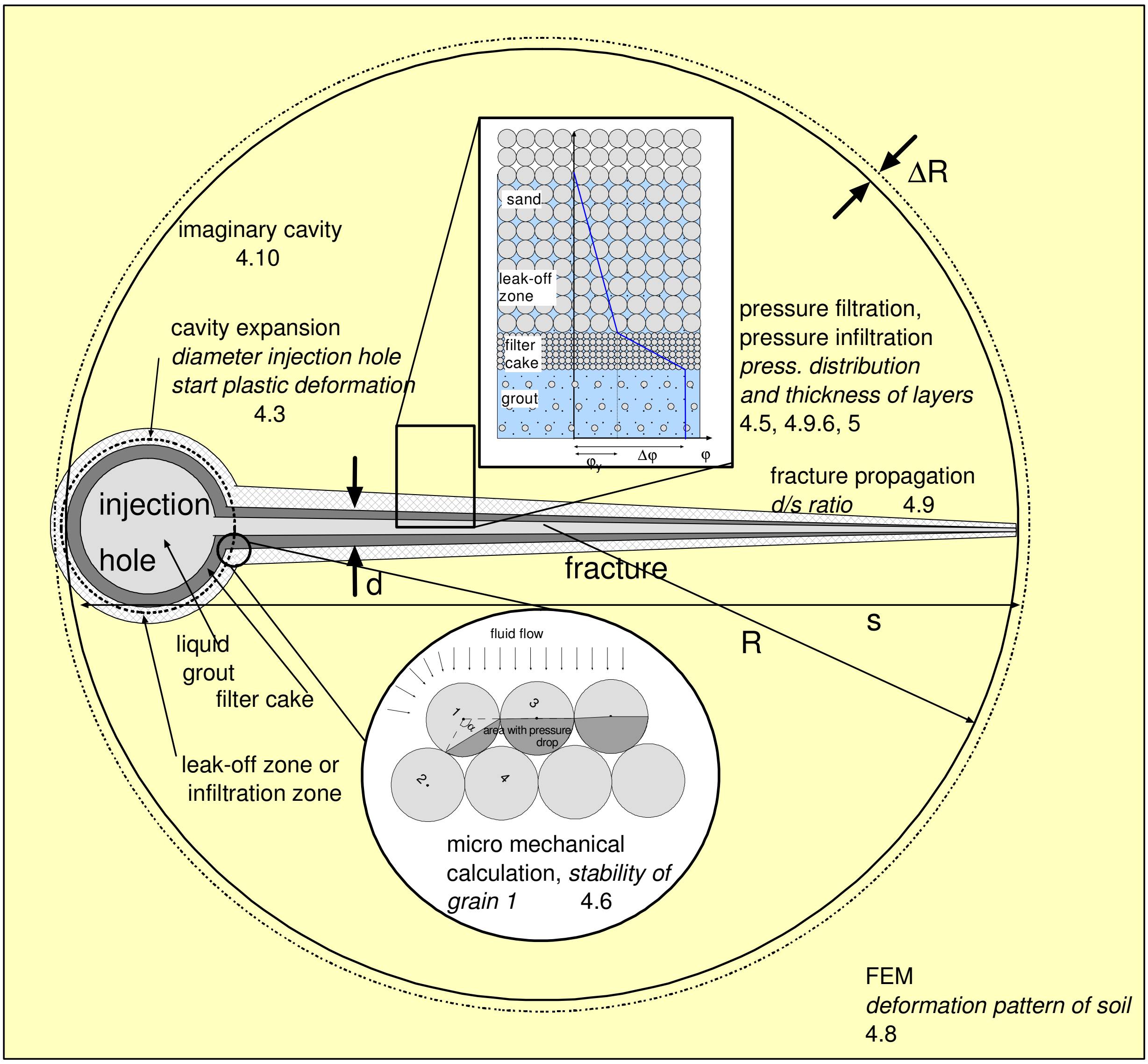

Figure 4-1: Overview of the aspects for which various calculation models were derived. The numbers refer to the sections where the models are presented. The aspects calculated are in italic. See also text.

4.3 Cavity expansion

When a cavity in the soil is pressurised, it will expand. Cavity expansion theory can be used to describe the expansion of the cavity as a function of the pressure for uniform expansion. Various authors have presented solutions for this problem, in most cases linear elastic perfectly-plastic solutions assuming the Mohr-Coulomb model failure criterion (see, for example: Vesic, 1972; Luger and Hergarden, 1988; Yu, 2000 and Salgado and Randolph, 2001). The solutions differ depending on the flow rule that is used and the way the strains are defined (small strain or natural strain). Here, we will use the solution presented by Luger and Hergarden (1988) for a plain strain situation. Their solution uses natural strain to cope with the large deformations that can be expected and assumes no dilatancy in the plastic zone, resulting in the following equations for injection pressures that lead to plastic deformations in the soil:

$$p' = (p'_f + c.\cot\phi)\left[\frac{1-(R_0/R_p)^2}{Q_1}\right]^{\left(\frac{\sin\phi}{1+\sin\phi}\right)} - c.\cot\phi \qquad (4.1)$$

with:

$$Q_1 = \frac{\sigma'_0 \sin\phi + c.\cos\phi}{G} \qquad (4.2)$$

p' the effective pressure in the bore hole,
p'_f $= \sigma'_0(1+\sin\phi)+c.\cos\phi$ the pressure where plastic deformation in the soil starts,
σ'_0 the effective stress around the hole before pressurising,
c the cohesion of the material,
R_0 the original radius of the bore hole,
R_p the radius after pressurisation,
G $=E/(2(1+\nu))$ the shear modulus,
E Young's modulus,
ν the Poisson ratio,
ϕ the friction angle.

Figure 4-2 shows the relation between the pressure increase in the cavity and the increase in diameter in the cavity according to these equations. The assumption of no dilatancy will lead to a borehole pressure that is slightly lower and a plastic zone that is slightly smaller than when taking dilatancy into account. This simplification is allowed since the model described here will be used in this study in a conceptual model to show the interaction between grout and soil. The pressure increases until the diameter is 10 times the starting diameter. The graph includes plots that show the influence of the friction angle and Young's modulus. The calculations were run for the conditions in the tests that will be described later: 100 kPa confining stress, Poisson's ratio of 0.33 and no cohesion. The maximum injection pressure varies from 1500 to 2500 kPa.

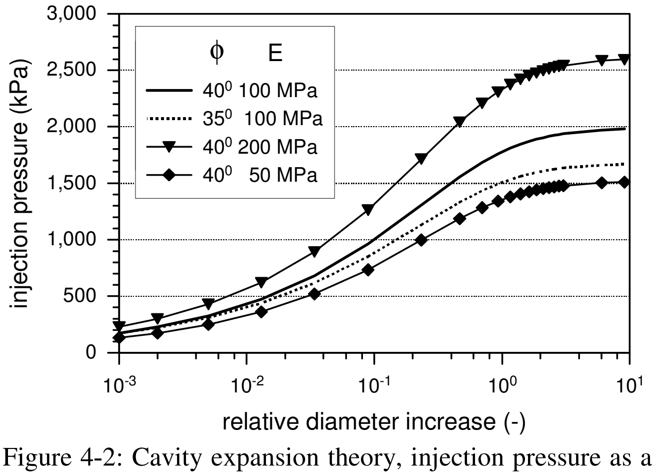

Figure 4-2: Cavity expansion theory, injection pressure as a function of the increase in diameter for friction angles (ϕ) of 35 and 40 degrees and Young's modulus (E) of the sand from 50 to 200 MPa at 100 kPa confining stress

As mentioned in Section 4.2, cavity expansion theory shows the maximum possible pressure that a cavity can resist. An asymmetric deformation of the cavity such as a hydraulic fracture is only possible when the pressure associated with this fracture is lower than the pressure necessary for cavity expansion. If it is not, cavity expansion will occur. This makes it possible to establish an idea of which process determines the width and length of the fractures during compensation grouting. A good fracture fluid will lead to fractures after only a limited amount of deformation in the soil. This means that diameter increase is only small and that only a thin fracture is possible. When the properties of the fracture fluid are less optimal for fracturing, fracturing will only occur after more soil deformation, and therefore at a point closer to the cavity expansion limit. See Section 4.9 and Section 4.10. This means that the injection pressure at which the fracture occurs will be higher and the fracture will be wider and shorter.

4.4 Qualitative description

The previous section described how injection pressure is related to diameter increase using cavity expansion theory. It also pointed out that injection pressures are lower when fracturing occurs. This section provides a qualitative elaboration of which mechanism could lead to fracturing in sand.

For fracturing in sand to occur, the contact between grains must be broken locally. Since there cannot be any tensile strength between the grains (this is different from fracturing in rock or clay), this means that the fracture pressure must overcome the effective stress and pore pressure in the direction perpendicular to the fracture. The pore pressure is exactly the same in every direction. Higher pore pressure means that all total stresses are higher. Since the effective stresses determine whether or not a fracture occurs, the analysis here concentrates on the effective stresses. It is assumed that the cavity expansion formulation is valid before the fracture starts. The pressure in the fracturing liquid will be the same as the radial stress. According to Mohr-Coulomb the relation between the radial stress and the tangential stress at failure can be written as:

$$\sigma_\theta = \frac{1-\sin\phi}{1+\sin\phi}\sigma_r \tag{4.3}$$

where σ_r is the radial stress, σ_θ the tangential stress and ϕ the friction angle of the sand. At, for example, a friction angle of 35 degrees, the tangential stress is only 0.27 times the radial stress. Classical cavity expansion theory assumes that there will be radial expansion which is uniform in all directions. However, in reality, the sand is never perfectly homogeneous. Looking at the scale of the grains at the boundary of the opening, there will be some grains that are in closer contact and some between which there is some space. See Figure 4-3.

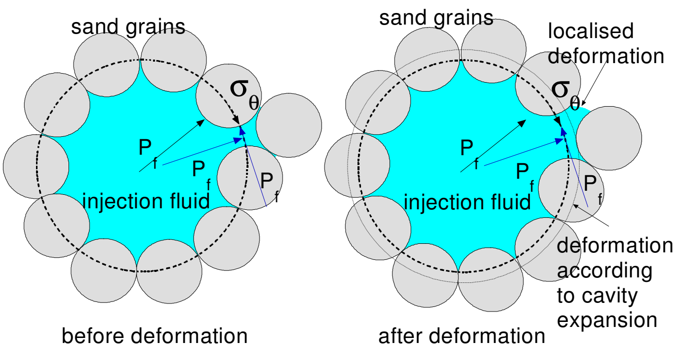

Figure 4-3: Sketch showing possible deformation modes of the injection hole. In reality there will be more grains around the injection hole. The figure illustrates the principle only.

These spaces may be such that the direction of the fluid pressure will be not only radial but also tangential. Since the fluid pressure is much higher than the initial tangential stress, this will lead to an opening of the spaces between the grains and a fracture can occur. If there is a beginning of a fracture, then the fluid pressure will penetrate further into the sand and the fracture will easily grow further. Fracture propagation will stop when the pressure in the fracture tip drops due to friction losses, pressure infiltration or an increase in the volume invaded by injection fluid. When a fracture is formed, then, the deformation will not be homogeneous over the injection hole but localised where the fracturing occurs. This was proven by the experiments described in Chapter 6. See section 6.9.5.

A consequence of this description is that the injection of grout at the beginning of a fracture more or less generates its own pressure distribution. This was also the result of the DEM calculations (Section 2.4.2) and indicates that the direction of the fractures is not necessarily determined by the K_0. The relation between horizontal and vertical stresses immediately around the injection hole changes before the initiation of a fracture.

Plastering and the formation of a filter cake in the injection hole will hamper the fracturing of the sand because possible irregularities at the boundaries of the injection hole will now be filled with plaster. See Figure 4-4. This plaster also has a certain strength and therefore prevents the fluid pressure from penetrating into the spaces between the grains.

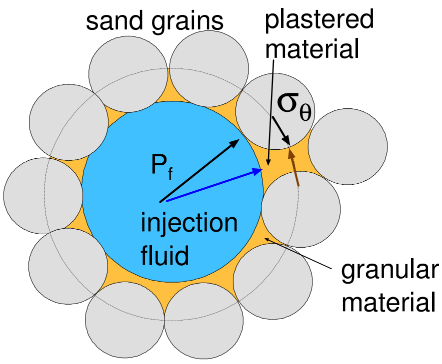

Figure 4-4: Influence of plastering

A fracture that occurs at injection pressures that are much lower than the limit pressure for cavity expansion will necessarily be only a very thin fracture, because there will be hardly any deformation of the sand at these low pressures. The thickness (*d*) of a fracture that occurs at higher pressures will be higher because, at these higher pressures, there is a larger diameter increase and when the deformation is localised at one point there is room for a fracture with a larger thickness.

As a consequence, fracturing in sand is only possible when the injection fluid satisfies certain conditions. It has been proven that Newtonian fluids (with only viscosity but no yield stress) lead to very small fractures or no fractures at all when injected into sand (Kohdaverdian and McElfresh, 2000; Bohloli and Pater, 2006). This result was also found in DEM calculations (Pruiksma, 2002): some plastering is necessary to establish a sufficient pressure gradient over the sand grains around the injection hole. However, too much plastering will fill up the irregularities around the injection hole and therefore also prevent fracturing, as will be described quantitatively in Section 4.9.

4.5 Thickness of filtrate during injection

The qualitative description presented above shows that the thickness of the plastered layer during injection is important. The thickness of this layer is determined by two processes:

- pressure infiltration;
- pressure filtration.

To describe pressure infiltration in combination with pressure filtration, the following principle was modelled. When a pressure is applied to the grout, the fine particles and the water will be pushed into the sand, causing pressure infiltration. The larger particles remain at the boundary of the sand. As a result, after some time, the finer particles and the water have to flow through the pores of the larger grout particles and the pores of the sand. There comes a point at which the pressure is not high enough to overcome the yield stress of the mixture of fine particles and water, and the flow of fine particles will stop. However, since the permeability of the fine particles for water is finite, there will be a flow of water into the sand as long as there is pressure. This will lead to an ongoing consolidation of the grout and liquid will flow continuously into the soil, but at a significant slower rate than when there is also pressure infiltration. There will be an effective stress in the sand and the coarse particles, but hardly any in the small particles since the yield strength of the slurry with the fine particles makes them interact with the coarse particles and the sand more than with each other.

This model has some limitations. It does not include any change in viscosity or yield stress parameters during the injection. However, it is known that bentonite is a thixotropic liquid and therefore these parameters will change during the injection depending on the shear stress exerted on the bentonite. Nor does the model take into account elastic deformation in the sand skeleton or the larger particles in the grout and it divides the particles in the grout rather arbitrarily into large and small particles. Furthermore, it does not take into account the difference in cake-building when the flow changes from a primarily bentonite flow to a water flow. The grain stress in the bentonite slurry between the sand grains and the larger grout grains will be small as long as the grout flow through the pores is dominated by the bentonite flow. This changes as the water flow starts to dominate. In that case the small bentonite particles will not penetrate into the coarse particles or into the sand and a cake of fine particles will form on top of the larger particles. This cake is dominated by fine particles and therefore grain stress will develop in this cake, leading to consolidation and a further reduction in permeability. Elastic deformation is not included since the calculations of McKinley and Bolton (1999) also show that, without taking elasticity into account, a close match was possible between measurements and calculations. Time-dependent effects such as the influence of thixotropy and the presence of a cake on top of the coarse particles are not included since the injection time in various experiments is relatively short (several seconds in the experiments). The presence of a bentonite cake on top of the cement particles is not included because this is a long-term process in which hardening will also start to play a role.

Formulation of the model

Let us assume that the grout is injected in a soil body with a flow resistance R_f, where R_f is the flow resistance for water with the dimension [s] and defined as:

$$R_f = \frac{\Delta\varphi}{q} \tag{4.4}$$

where:

$\Delta\varphi$: the difference in piezometric head

q : the specific discharge

The flow resistance is used to describe the water flow from an injection hole or a cylinder. Using Darcy's law it can be determined that, for example, there is a flow resistance in a spherical cavity with a radius r_0 and a piezometric head that is $\Delta\varphi$ higher than the head in the far field in a homogeneous infinite soil mass with permeability k:

$$R_f = \frac{r_0}{k} \tag{4.5}$$

During injection in the soil there will be three different flow situations in the grout:

- Grout pressure filtration starts. The larger particles will form a cake on the boundary between the sand and the grout.
- The fine particles and the water will leak into the sand.
- The water will be pressed out of the grout.

The processes are sketched in Figure 4-5. Here, the water flow resistance (R_f) is assumed to be zero, so the pressure drop is entirely over the grout cake and the grout that penetrates into the sand.

The filtration of the large particles by the sand for one-dimensional flow perpendicular to the sand surface is described by the formula of McKinley and Bolton (1999). This reads in incremental form, using porosity instead of the void ratio:

$$ds_c = \frac{k_c}{s_c}\frac{1-n_{c,i}}{n_{c,i}-n_{c,e}}(\Delta\varphi - \varphi_y)\,dt \tag{4.6}$$

where:

s_c	: the thickness of the cake with larger particles
k_c	: the permeability for the fine particle slurry through the cake
$n_{c,i}$	: the initial porosity of the larger particles in the grout
$n_{c,e}$	: the final porosity of the cake with larger particles
$\Delta\varphi$	: the difference in piezometric head over total penetration zone (see Figure 4-5)
φ_y	: the piezometric head at boundary between the grout and the soil (see Figure 4-5)
t	: time

The specific discharge of the fine particle slurry (q_s) can be written as:

$$q_s = \frac{k_c}{s_c}(\Delta\varphi - \varphi_y) \tag{4.7}$$

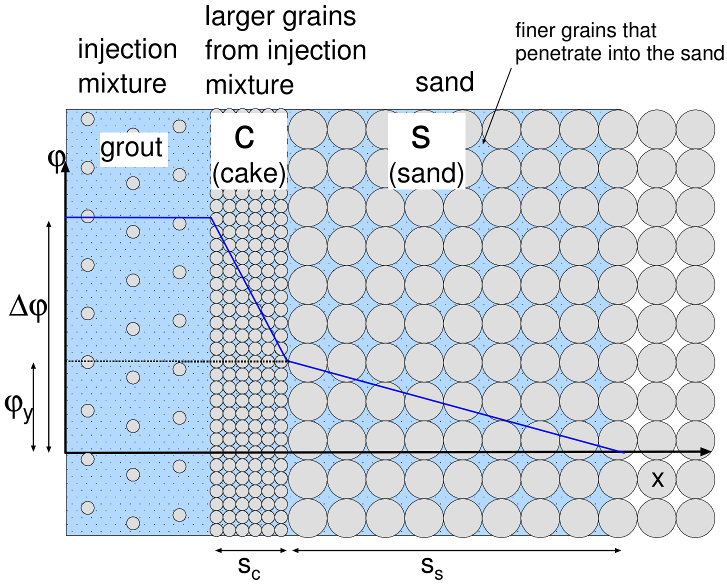

Figure 4-5: Plastering that can occur during pressure infiltration due to larger grains in the mixture that cannot penetrate into the sand and sketch of the pressure distribution over the injection liquid

The penetration of the fine particle slurry into the soil can be written as:

$$q_s = n_s \frac{ds_s}{dt} \tag{4.8}$$

where:
q_s : the specific discharge
n_s : the porosity of the sand
s_s : the thickness of the sand layer, invaded with the small-particle slurry. See Figure 4-5.

Note that, because of conservation of mass, the term q_s is the same in Equation (4.7) and Equation (4.8).

For a Bingham liquid there is an extra term in Darcy's law that now reads, for a positive gradient i in both the sand and the cake:

$$q_s = \max\left[k\left(i - \frac{1}{\rho_w g}\frac{dP_\tau}{dx}\right), 0\right] \tag{4.9}$$

where:
k : is the (Darcy) permeability of the material
P_τ : the pressure necessary to overcome the yield stress
ρ_w : the density of water
g : acceleration of gravity
x : coordinate

The influence of the last term of this formula is explained in Figure 4-6.

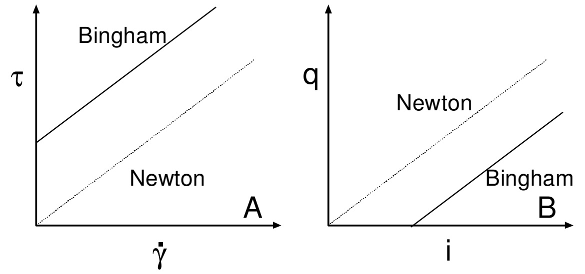

Figure 4-6: Shear stress and shear strain in both a Newtonian and Bingham liquid (A) and consequence for flow in soil (B)

The "standard" graph to explain a Bingham liquid is shown in Figure 4-6A: the shear rate remains zero until there is a shear stress, after which there is a linear relation between shear rate and shear stress. The consequence for the flow of a Bingham liquid through a granular material is shown in Figure 4-6B. A certain minimum gradient is needed to start the flow of a Bingham liquid though the soil. This minimum gradient depends on the liquid and on the soil. When this minimum gradient is not reached, there will be no flow, as indicated in Equation (4.9). For a soil material with a constant grain size distribution and a fluid with constant properties, the term in Equation (4.9) with dP_f/dx is constant and can be replaced by a parameter α.

For the fine particle material in the grout that behaves as a Bingham fluid and flows through the consolidated larger particles in the grout and the adjacent sand, the total pressure drop can be written as:

$$\Delta\varphi = \frac{s_c q}{k_c} + \frac{s_s q}{k_s} + \alpha_c s_c + \alpha_s s_s + R_f q \tag{4.10}$$

where:

α_c : parameter that describes the influence of the yield stress for the flow through the larger particles

α_s : parameter that describes the influence of the yield stress for the flow through the sand

For a given drop in the piezometric head, $\Delta\varphi$, s_c and s_b will increase and, at a given point, the terms $\alpha_c s_c + \alpha_s s_s$ match the total drop in the piezometric head and pressure infiltration will stop. Looking at Equation (4.10) in greater detail, it becomes clear that, at the very beginning of pressure infiltration, s_c and s_s will be zero and therefore that flow resistance determines the process. At the end, it is the yield stress in the grout that determines how far the grout penetrates into the sand.

A relation presented by Huisman (1998) was used to calculate the pressure drop as a function of the yield stress only. He calculates the maximum distance the grout can penetrate into the sand:

$$s = \frac{2}{3}\frac{n}{1-n}\frac{8}{78} d_{15} \frac{\Delta\varphi \rho_w g}{\tau_y} \tag{4.11}$$

where s is distance the grout can penetrate into the soil, n the porosity, d_{15} the diameter of the grains through which the grout leaks off (d_{15} means that 15% of the grains are smaller). In this relation the factor $\frac{2}{3}\frac{n}{1-n}d_{15}$ determines the average pore channel width for a soil material of given porosity and d_{15}. The factor 8/78 is a shape factor and not further defined by Huisman. The relation is comparable to the relation presented by Nash (1974), who presents the critical gradient (i_{cr}) necessary for transport:

$$i_{ir} = \frac{6}{\cos\theta}\frac{1-n}{n}\frac{\tau_y}{\rho_w g d_{15}} \tag{4.12}$$

where θ is the angle of tortuosity. Since i_{cr} is equal to $\Delta\varphi/s$ in Huisman's equation it appears that these formulae are equal for θ = 64 degrees. Nash presents a slightly lower value of 50 degrees for θ.

Using the relation from Huisman and assuming n=0.4, the coefficient α for both the sand and the filter cake can be written as:

$$\alpha = \frac{9}{4}\frac{78}{8}\frac{\tau_y}{d_{15}\rho_w g} \tag{4.13}$$

Neglecting the influence of the water flow through the grout, there is a fixed ratio between s_c and s_s:

$$s_c = \beta s_s \tag{4.14}$$

and conservation of volume determines β:

$$\beta = \frac{n_s(1-n_{c,i})}{n_{c,e}-n_{c,i}} \tag{4.15}$$

Equation (4.10) can be written as:

$$q_s = \frac{\Delta\varphi - (\alpha_c s_c + \alpha_s s_s)}{\frac{s_c}{k_c} + \frac{s_s}{k_s} + R_f} \tag{4.16}$$

Apart from the slurry flow, the difference in piezometric head will also induce a water flow: water is pressed out of grout. This process will have a completely different time scale, since the the water permeability of the grout mixture is an important factor in that process. This aspect was not therefore included in this pressure infiltration model.

To solve the equations, the procedure followed was:
The permeability of the sand and the cake for water was calculated from the particle size using the relations derived by Den Adel (1989). The maximum penetration depth in the sand and in the cake is calculated using Equation (4.11). On the basis of the given WCR value and the density of the material, the porosity of the larger particles in the mixture was calculated and, with the porosity of the sand and the cake, b is determined using Equation (4.15). Discharge into the sand q_s at t=0 was then calculated using Equation (4.10) with only the last term (s_s and s_c are 0 at t=0). For t>0 an iterative solution was used, with q_s at t>0 being determined from s_s and s_c using Equations. (4.16), (4.8) and (4.14), and then being used to determine the pressure drop over s_c

and s_s from the Newtonian part as well as the pressure drop caused by the yield stress. The sum of the different pressures has to be the total pressure drop. This is checked at every time step.

The results will be compared with the results of tests in Section 5.9.

4.6 Micro-mechanical considerations

In the section "Qualitative description" it was argued that some irregularities in the grain fabric may be important to determine whether or not a fracture occurs. This means that the movement of single grains is important. Koenders (1985) presented a description for this phenomenon using what he called "single grain" theory, in which the possibility of sliding and rotation of a single grain is analysed and compared with continuum theory. Rhee and Bezuijen (1992) used this theory to explain the stability of a sandy slope as a function of a hydraulic gradient perpendicular to the slope and showed why the relation is different for a gradient directed inwardly compared with one directed towards the outside. Here, the single grain theory is used to investigate the efficiency of a Newtonian liquid and a wall-building liquid in terms of stabilising the grains around the cavity as a fracture starts.

The situation of an injection hole with a fracture and some grains around the fracture is shown in Figure 4-7. For the sake of simplicity, a two-dimensional situation is assumed. The grout pressure will result in a force on the grain, depending on the plastering properties of the grout, and on the gradient directed inwardly. See Figure 4-8. Assuming a certain grout pressure in the grout, there will be a pressure drop (p) over the filter cake, but since this filter cake has a certain permeability there will also be a hydraulic gradient over the grain and this gradient results in a pressure drop over the grain. The force of the grout flow on the grain can be described as:

$$F_l = (p + \kappa \rho_w g i D) A \tag{4.17}$$

In this equation, D is the diameter of the grain, ρ_w the density of water, F_l the force exerted on the grain by the injection liquid, p the pressure drop over the injection liquid–grain boundary (caused by a filter cake), g the acceleration of gravity, i the hydraulic gradient in the soil just below the surface, and κ the part of the grain that is subjected to the hydraulic gradient. A is the area that is subjected to the hydraulic gradient involved.

The force exerted by the fluid as described in Equation (4.17) depends on the fluid properties but also on the position of the grain. See Figure 4-9. It is reasonable to assume that there is a pressure drop boundary over that part of the particle that is in contact with the other particles since the pressure drop in the liquid outside the grain skeleton will be negligible. The average force over a particle embedded in the grain skeleton will be determined by the average gradient. The average force on a particle lying on a flat surface will be half that force, because the pressure drop will be over only half of the grain (the darker part of grain 3 in Figure 4-9). This assumption is based on the results of experiments (Van Rhee & Bezuijen, 1992). Now it is assumed that, close to a fracture (as for grain 1 in Figure 4-9), the average pressure drop over the grain due to the flow gradient becomes lower in proportion to the part of the grain surrounded by other grains. See Figure 4-9. This means that, for grain 1, this factor is on average 0.5(1-cos(0.5α)), where α is defined in Figure 4-9 (this seems reasonable but it has not been proven experimentally). Furthermore the area over which this pressure drop acts is reduced. In the case of grain 3, the area is $\pi/4D^2$; in the case of grain 1, the area over which the pressure drop will be present will be reduced to $\pi/4[D\sin(0.5\alpha)]^2$ (see Figure 4-9) and F_l can be written as:

$$F_l = [p + 0.5.(1-\cos(0.5\alpha)).\rho_w giD].\frac{\pi}{4}[D\sin(0.5\alpha)]^2 \tag{4.18}$$

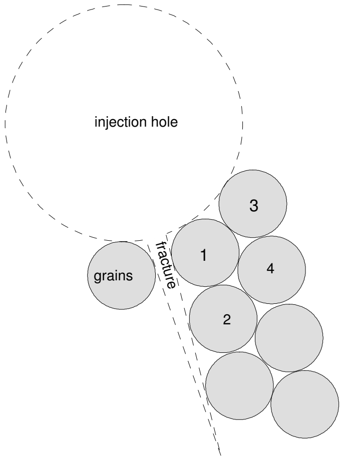

Figure 4-7: Sketch of a possible arrangement of grains around a fracture

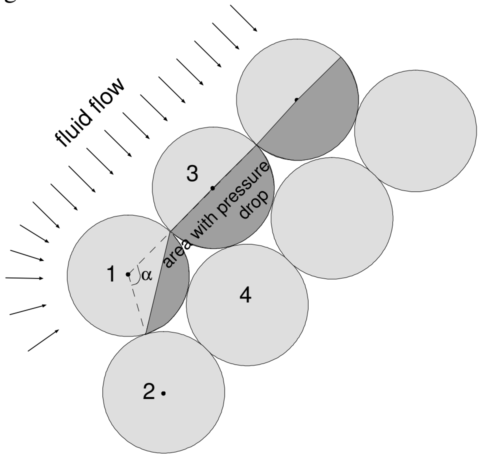

Figure 4-9: Areas where a pressure drop over the grains 1 and 2 at the boundary of a grain skeleton can be expected

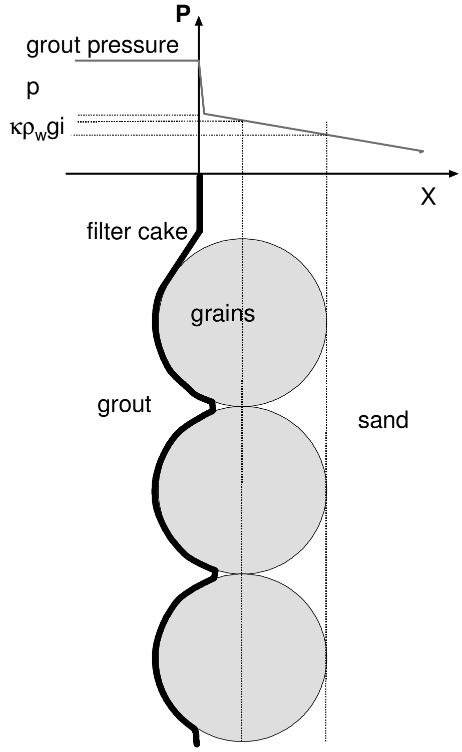

Figure 4-8: Detail showing pressure exerted by the filter cake and by the gradient

This means that, without a filter cake, the force that can be exerted by the fluid flow to stabilise a grain is much less effective where a fracture starts, as at the location of grain 1 in Figure 4-7 and Figure 4-9. Evaluation of Equation (4.18) for $\alpha=180^0$, as in the case of grain 3, leads to:

$$F_l = [p + 0.5\rho_w giD]\frac{\pi}{4}D^2 \tag{4.19}$$

at the start of a fracture with $\alpha=90^0$, as in the case of grain 1. This results in:

$$F_l = [p + 0.5(1-0.5\sqrt{2})\rho_w giD]\frac{\pi}{8}D^2 \tag{4.20}$$

When the pressure drop over a filter cake (p) is dominant, then the fluid force required to stabilise the grains at the start of a fracture is only half the value for a grain embedded between other grains. However, when the fluid flow is dominant, the force exerted by the fluid is, at grain 1, only 15% of the flow for grain 2. According to Rhee and Bezuijen's model, without plastering, a gradient directed outwardly from the cavity into the grain skeleton of around 3.5 is sufficient to stabilise a cavity in all circumstances. In the case of a fracture that starts perpendicular to such a cavity, this must be a gradient of 23.

This means that, without plastering, the grains at the starting points of fractures will be rather unstable. This can result in the filling-in of newly formed fractures with the grains at the boundary of the fracture.

The model described above shows that some cake building along the walls of the injection opening can be very efficient in terms of fixing the grains around the injection opening and therefore preventing the newly formed fractures being filled in immediately by grains from unstable boundaries. In this way, cake building along the wall increases the possibilities of fracturing because it fixes the grains around the fracture so that the fracture remains open.

4.7 Influence of flow on fracturing

4.7.1 Influence of flow on stress distribution

The possibility of fracturing sand seems to be influenced by the properties of the fluid (Bohohli and Pater, 2006). A possible reason for this is the influence of the fluid on stress distribution in the soil. For a fracture to occur, there has to be some plastic deformation of the grains to allow the grains to move apart. This section sets out the calculations that show when plastic deformation occurs as a function of the hydraulic gradient in the soil. In the case of an ideal cake-building liquid, the liquid will only exert a pressure on the boundary of the injection hole. The other extreme, an injection hole pressurised with water, will lead to an effective stress that is practically zero at the boundary of the hole and increases with the distance from the injection hole. When the injection hole is pressurised with a Bingham liquid, there will be a gradient loading on a part of the soil around the injection hole. See Figure 4-10.

The macroscopic calculation in this section calculates the effect of the way the injection hole is pressurised. Cavity expansion theory is used and a linear elastic soil is assumed. The difference with the traditional solution is that there is no force boundary condition at the boundary of the cavity, but a flow condition in a part of the soil surrounding the cavity. Since most fluids that are injected for grouting can be described as Bingham fluids, a pressure distribution that corresponds to a Bingham liquid will be chosen. The yield stress in such a liquid determines the steepness of the gradient. A high yield stress will lead to a high pressure gradient that is present only close to the injection hole. A liquid with a low yield stress will have a lower pressure gradient that is also present at larger distances from the injection hole.

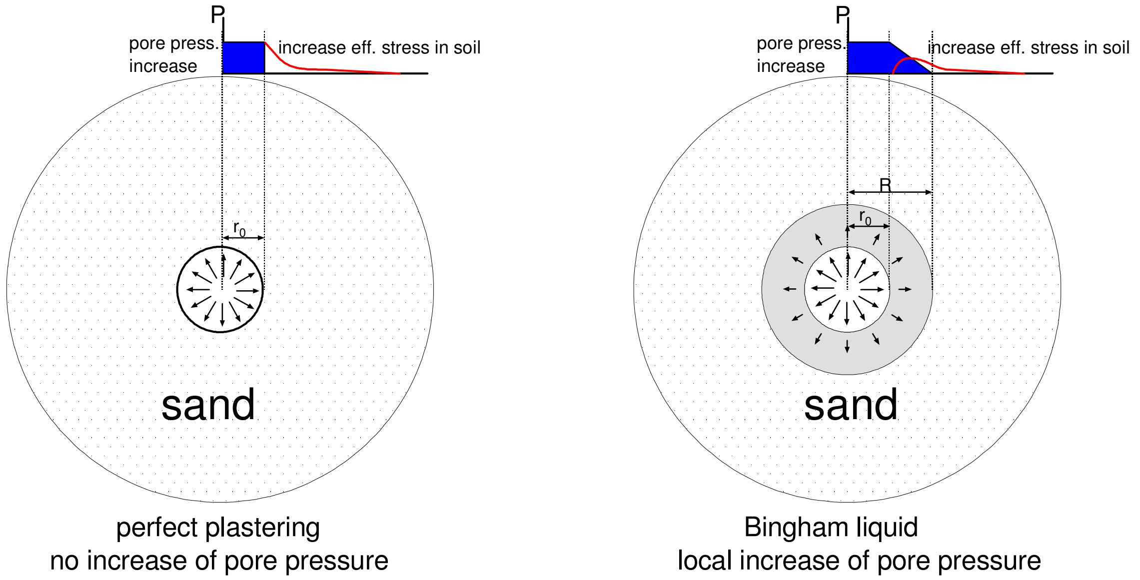

Figure 4-10: Difference in boundary conditions for an injection with a cake building fluid, assuming perfect plastering and an injection with a Bingham liquid that penetrates some distance into the sand

The aim of the calculation presented in this section is to show at what pressure in the injection hole plastic deformation in the soil starts as a function of the applied pressure gradient. Since only a linear elastic soil model is assumed, it is only possible to calculate the pressure at which the soil starts to become plastic and it is not possible to calculate the plastic deformation itself. The aim of the calculation is to calculate the minimum pressure necessary to initiate plastic deformation as a function of the boundary conditions.

The solution presented uses the basic equations derived for this situation by Verruijt (2002) (Verruijt's work has not been presented in any official publication and so the next section, “Basic equations”, presents the derivation Verruijt used to arrive at the basic equations). However, the boundary conditions used are different from the boundary conditions Verruijt used. He assumed no effective stress on the cavity and no effective stress at a distance R from the centre of the cavity. Since this is not a realistic assumption for a cavity pressurised during compensation grouting it is assumed here that the effective stress is zero at the boundary of the cavity but that, at the outer boundary of the flow at a distance R, there is still an effective stress. This will be addressed in more detail in the section on boundary conditions.

4.7.2 Basic equations

Figure 4-11 shows an element of material in a cylindrical coordinate system. If the radial coordinate is denoted by r and the angle in the x, y planes by θ, then the area of the element is: $r^2\, dr\, d\theta\, dz$.

It is assumed that the displacement field is cylindrically symmetrical, so that there are no shear stresses acting upon the element, and the tangential stress σ_{tt} is independent of the orientation of the plane. The figure shows the stresses acting on the element. The only non-trivial equation of equilibrium is now the one in radial direction:

$$\frac{\partial \sigma_{rr}}{\partial r} + \frac{\sigma_{rr} - \sigma_{tt}}{r} = 0 \qquad (4.21)$$

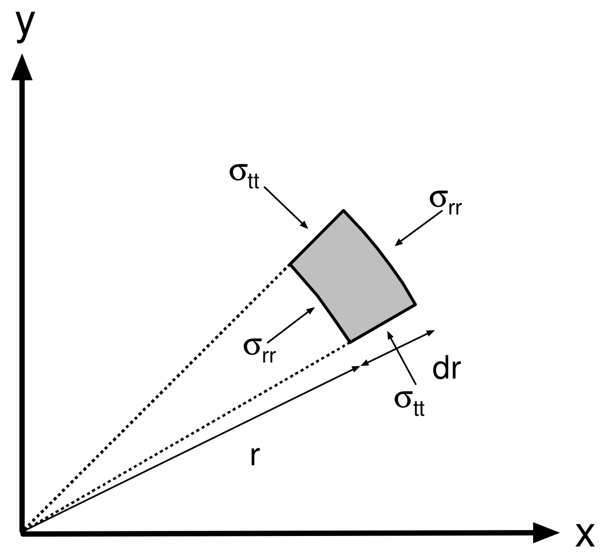

Figure 4-11: Element in circular coordinates with principal stresses for radial deformation

The total stresses σ can be separated into the effective stresses σ' and the pore pressure p:

$$\sigma_{rr} = \sigma'_{rr} + p \tag{4.22}$$

$$\sigma_{tt} = \sigma'_{tt} + p \tag{4.23}$$

Substitution of (4.22) and (4.23) into (4.21) gives:

$$\frac{\partial \sigma'_{rr}}{\partial r} + \frac{\sigma'_{rr} - \sigma'_{tt}}{r} + \frac{\partial p}{\partial r} = 0 \tag{4.24}$$

This last equation shows that, in terms of the effective stresses, the pressure gradient acts as a body force. In the elastic region, the stresses can be related to the strains by Hooke's law,

$$\sigma'_{rr} = \lambda e + 2\mu \varepsilon_{rr} \tag{4.25}$$

$$\sigma'_{tt} = \lambda e + 2\mu \varepsilon_{tt} \tag{4.26}$$

where e is the volume strain:

$$e = \varepsilon_{rr} + \varepsilon_{tt} \tag{4.27}$$

and λ and μ are the elastic coefficients (Lamé constants),

$$\lambda = \frac{\upsilon E}{(1+\upsilon)(1-2\upsilon)} \tag{4.28}$$

$$\mu = \frac{E}{2(1+\upsilon)} \tag{4.29}$$

It should be noted that both the stresses and the strains are considered to be positive for compression. The strains ε_{rr} and ε_{tt} can be related to the radial displacement u by the relations

$$\varepsilon_{rr} = -\frac{\partial u}{\partial r} \tag{4.30}$$

$$\varepsilon_{tt} = -\frac{u}{r} \tag{4.31}$$

The volume strain can be written as:

$$e = -\frac{\partial u}{\partial r} - \frac{u}{r} \tag{4.32}$$

Substitution of Equations (4.25)–(4.32) into (4.24) gives:

$$(\lambda + 2\mu)\{\frac{\partial^2 u}{\partial r^2} + \frac{1}{r}\frac{\partial u}{\partial r} - \frac{u}{r^2}\} - \frac{\partial p}{\partial r} = 0 \tag{4.33}$$

4.7.3 Boundary conditions and solution

It is assumed that the injection fluid needs a much higher pressure gradient to be transported through the sand compared to the pore water. When that is the case, the pressure gradient in the pore water can be disregarded. A significant pore pressure gradient will be present only in the part of the soil around the cavity that is invaded by the injection fluid, for example through pressure infiltration.

Furthermore, it is assumed that the injection fluid can be described as a Bingham liquid and that the yield stress is dominant in the flow. In this situation, there will be a linear pressure gradient in the part of the soil that is invaded by the injection liquid, because the pressure gradient has to overcome the yield stress.

This means that, for $r_o < r < R$, the following relation holds:

$$\frac{\partial p}{\partial r} = -G_B \tag{4.34}$$

where p is the pore pressure and G_B the pressure gradient in the Bingham liquid.

Inserting this equation into the basic Equation (4.33) gives:

$$(\lambda + 2\mu)\{\frac{\partial^2 u}{\partial r^2} + \frac{1}{r}\frac{\partial u}{\partial r} - \frac{u}{r^2}\} = -G_B \tag{4.35}$$

This can also be written as:

$$(\lambda + 2\mu)\frac{\partial u}{\partial r}\left[\frac{1}{r}\frac{\partial}{\partial r}(ur)\right] = -G_B \tag{4.36}$$

In this form the solution can be obtained by successive integration, leading to:

$$(\lambda + 2\mu)u = -\frac{1}{3}G_B r^2 + Ar + \frac{B}{r} \tag{4.37}$$

For $r>R$ the normal elastic solution is valid. In general, this reads as:

$$(\lambda + 2\mu)u = Cr + \frac{D}{r} \tag{4.38}$$

Far away from the cavity, the stresses and therefore displacements will fall to zero. In other words, $C = 0$. At $r = R$, Equation (4.37) should lead to the same displacement as Equation (4.38). At this location also, the radial stress that follows from both equations should be the same. The final boundary condition is that the effective stress should be zero at the boundary of the cavity for $r = r_o$. Together with Equations (4.37) and (4.38) these boundary conditions lead to the following set of equations:

From the boundary condition at $r = r_o$:

$$0 = (\lambda + \frac{4}{3}\mu)G_B r_o - 2(\lambda + \mu)A + 2\mu\frac{B}{r_0^2} \tag{4.39}$$

Displacement is constant at $r = R$:

$$\frac{D}{R} = -\frac{1}{3}G_B R^2 + AR + \frac{B}{R} \tag{4.40}$$

Radial stress is constant at $r = R$:

$$2\mu\frac{D}{R} = (\lambda + \frac{4}{3}\mu)G_B R - 2(\lambda + \mu)A + 2\mu\frac{B}{R^2} \tag{4.41}$$

With these equations A, B and D can be solved, leading to:

$$A = 0.5 G_B R \tag{4.42}$$

$$B = \frac{r_0^2}{2\mu}\left[(\lambda + \mu)G_B R - (\lambda + \frac{4}{3}\mu)G_B r_0\right] \tag{4.43}$$

$$B = \frac{1}{6}G_B R^2 + \frac{B}{R} \tag{4.44}$$

According to Equations (4.25) and (4.26), it is possible to write the effective stresses in the area $r_o < r < R$ as:

$$(\lambda + 2\mu)\sigma'_{rr} = (\lambda + \frac{4}{3}\mu)G_B r_o - (\lambda + \mu)A + 2\mu \frac{B}{r^2} \tag{4.45}$$

$$(\lambda + 2\mu)\sigma'_{tt} = (\lambda + \frac{2}{3}\mu)G_B r_o - (\lambda + \mu)A + 2\mu \frac{B}{r^2} \tag{4.46}$$

4.7.4 Numerical solution and consequences for fracturing

The last equations of the section above were evaluated numerically to investigate the influence of the pressure gradient in the injection fluid on stress distribution. It was assumed that sand has a confining stress of 100 kPa. The cavity is pressurised with a pressure of 1000 kPa. The sand has a Poisson ratio of 0.3. Figure 4-12 shows the ratio between shear stress and isotropic stress around the cavity as a function of the distance invaded by the injection fluid (R-r_0). The radius of the initial cavity is 0.135 m. A friction angle of 40 degrees is assumed for this graph to determine to what value of τ/P the elastic solution is valid. The resulting stresses proved to be independent of Young's modulus (although the deformations do depend on Young's modulus). This elastic calculation implies that there will be tensile stresses close to the cavity. If that is the case, the elastic model will become invalid and, in reality, there will be plastic deformation. The same is true for a stress ratio higher than 0.84, which corresponds to a friction angle of 40 degrees. However, if there is enough penetration of the injection fluid into the soil through pressure infiltration, the elastic solution is valid. This means that an injection pressure leading to plastic and elastic deformation when the injection fluid invades the soil only to a limited extent or not at all will lead to only elastic deformation when there is more penetration of the liquid in the soil. Since plastic deformation is necessary to obtain fractures, it can be concluded that fracturing will only occur at higher injection pressures when there is only a limited fluid flow into the soil, so the penetration distance into the soil is only small.

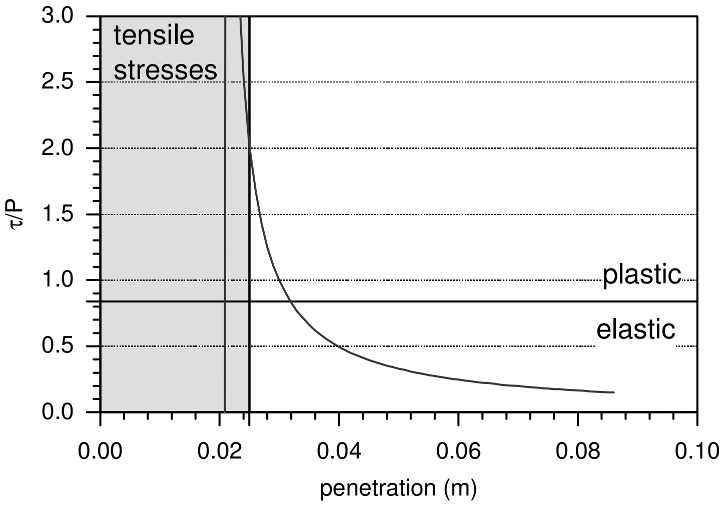

Figure 4-12: Stress ratio as a function of the pressure infiltration distance of the injection liquid into the soil

4.8 FEM simulation of a predefined fracture

The stress distribution around the beginning of a predefined fracture has been simulated numerically in two dimensions using the Finite Element Code Plaxis (Teunissen, 2006). Stress distribution was calculated using a linear elastic, perfectly plastic Mohr-Coulomb constitutive model. Two types of calculations were run, one with cohesion and no friction angle (simulating clay and undrained behaviour) and one with hardly any cohesion and a friction angle of 40^0

(simulating sand and drained behaviour). The calculations for sand are important for this study. The calculations were run for dry sand. Table 4 lists the parameters for the sand used.

Table 4. Parameters of Mohr-Coulomb model used in Plaxis simulations

Parameter	Value	Dim.
γ_{dry} (dry density)	16	kg/m^3
E_{ref} (Young's mod.)	200	MPa
ν_n (Poisson rat.)	0.2	-
ϕ (friction angle)	40	degr.
ψ (dilatancy angle)	8	degr.

The mesh was made of 1032 15-node triangular elements. See Figure 4-13 and Figure 4-14. The length and width of the full mesh were 1 m. The diameter of the tube was 27 mm and the predefined "fracture" was 14 mm long. See Figure 4-14. Calculations were run without any confining stress (only the weight of the sand above the fracture) and a vertical confining stress of 100 kPa on top of the model (as indicated by the arrows at the top of Figure 4-13). The boundary condition for the vertical walls was no horizontal movement and, for the bottom of the mesh, no vertical movement. Gravity was pointing downwards. In the calculations, the pressure in the injection hole and fracture was assumed to be the same at every location. This pressure was equal to the average isotropic soil stress at the location of the injection hole at the beginning of the calculation and increased until failure occurred.

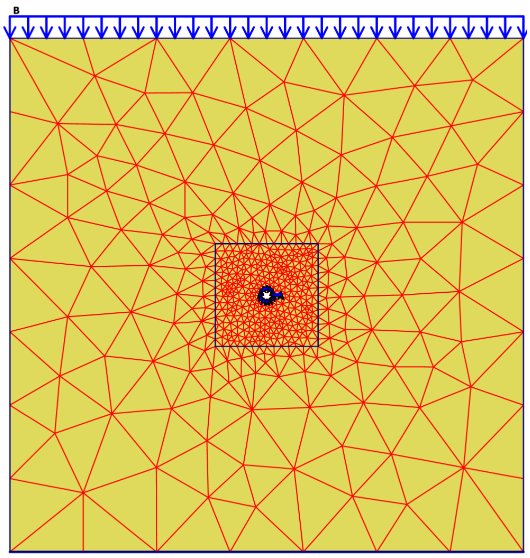

Figure 4-13: Mesh used in FEM calculations. Gravity pointing downwards

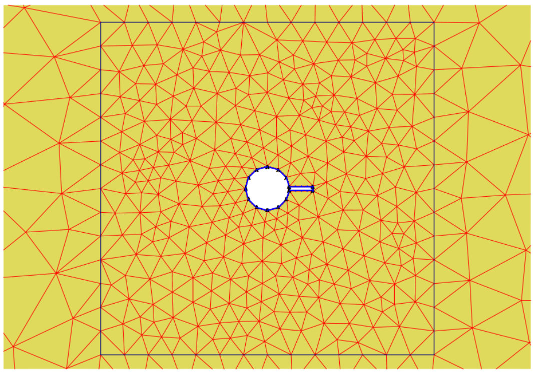

Figure 4-14: Mesh, detail with fracture

The results show the plastic points and distribution of shear strains (shear invariant) at the maximum pressure that led to a stable solution. Without any confining stress, the ultimate pressure in the fracture was 71 kPa before failure. With a confining stress of 100 kPa the ultimate pressure was 1446 kPa. The limit pressure according to the cavity expansion theory as dealt with in Section 4.3 is much higher for the situation without any confining stress (234 kPa compared to the 71 kPa found in the numerical simulation) but is very comparable for the situation with a confining stress of 100 kPa (1493 kPa, where the numerical solution gave 1446 kPa) even though the analytical calculation did not take dilatancy into account.

When there is no confining stress, the plastic points indicate that a soil wedge breaks out on top of the fracture. See Figure 4-15. This is a different failure mechanism to the failure mechanism assumed in the cavity expansion theory and so the resulting limit pressure in the numerical calculation is lower. When there is a confining stress, the plastic points are much more symmetrically distributed around the fracture. See Figure 4-17. This looks more like a symmetrical deformation and therefore the result of the numerical calculation is close to the cavity expansion solution. As was found in the simulation of Dong and Pater (2008) – see Section 2.4.3 – there is hardly any shear strain in the soil above and below the fracture itself (see Figure 4-16 and Figure 4-18). This soil is just lifted and shear strain is created at some distance from the fracture. This result will be used in Section 4.10, where the soil deformation around a fracture is schematised in accordance with the deformation that occurs during cavity expansion.

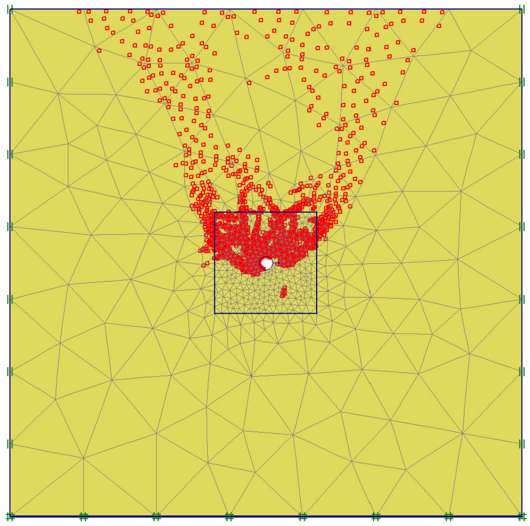

Figure 4-15: Plastic points around the fracture in the absence of confining stress and with only gravity forces (gravity pointing downwards)

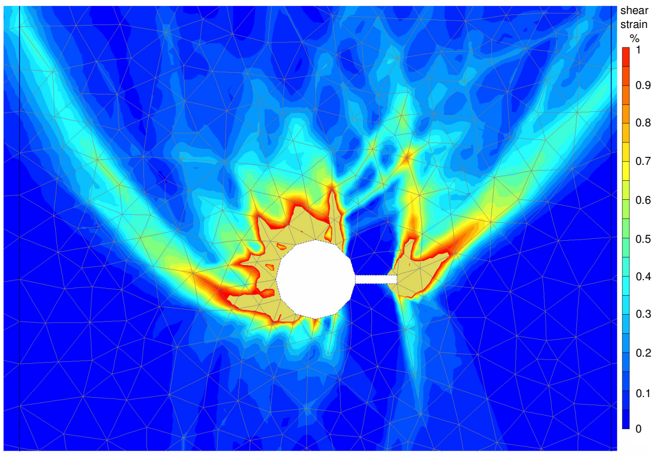

Figure 4-16: Shear strain around fracture at maximum injection pressure

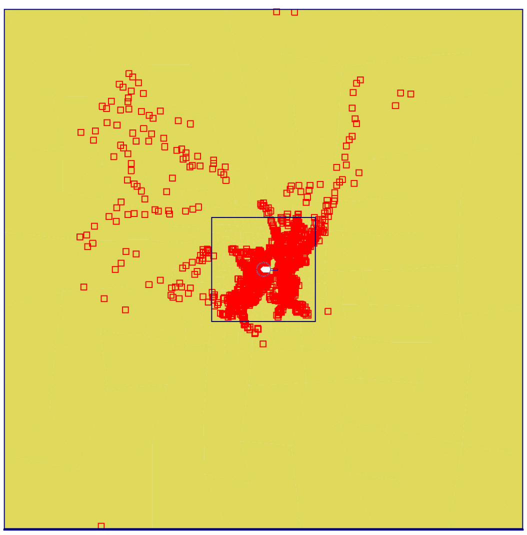

Figure 4-17: Plastic points around axis with a vertical confining stress of 100 kPa

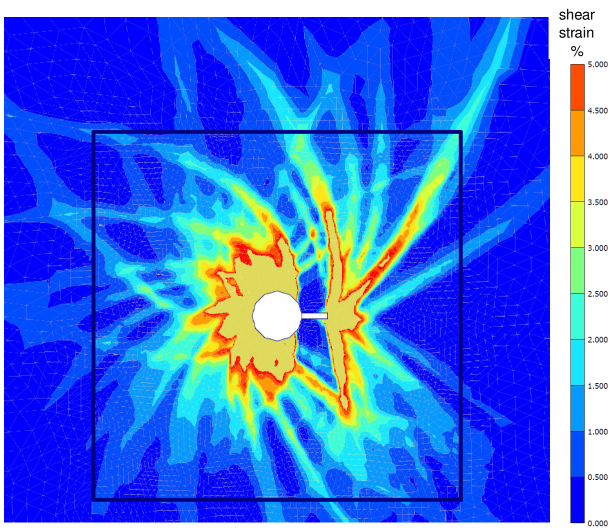

Figure 4-18: Shear strain around fracture at maximum injection pressure and a confining stress of 100 kPa

4.9 Fracture propagation

This section is a part of an article submitted to "Journal of Geotechnical and Geo-environmental engineering". The consequences of the pressure filtration of grout are investigated for some predefined shapes as a function of the filtration properties and the injection pressures.

4.9.1 Possible fracture geometries in sand

Considering possible geometrical shapes for hydraulic fractures, the following subdivision is made (Figure 4-19):
- fracture plane
- fracture path
- combination of both.

A schematic presentation of the possible fracture shapes is given in Figure 4-20. The "fracture plane" from Figure 4-19 is shown schematically in Figure 4-20a or Figure 4-20b, and a schematic "fracture path" is shown in Figure 4-20c or Figure 4-20d.

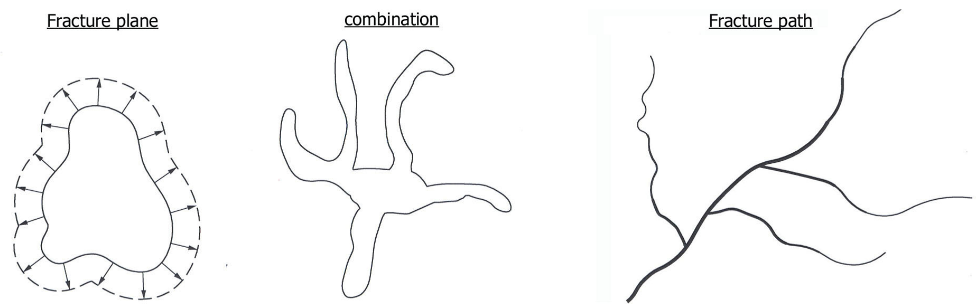

Figure 4-19: Top view of horizontal fracture plane and fracture path (Grotenhuis, 2004)

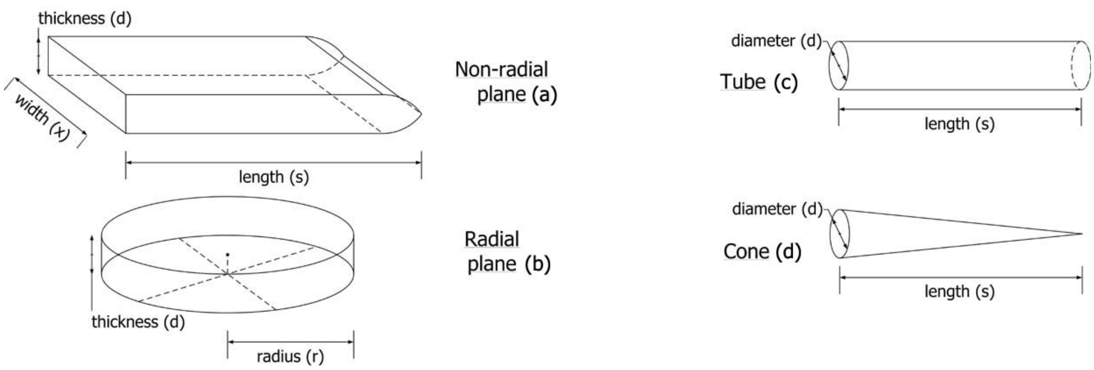

Figure 4-20: Possible fundamental fracture shapes (Grotenhuis, 2004)

From the different shapes that are seen in the field and in model tests, it seems reasonable to analyse two different geometrical shapes: a fracture plane with a certain constant fracture width, and a tube-like fracture with a constant diameter. The first shape was found to be quite general in model tests. The tube-like fracture occurs when there is a weak spot in the soil. Radial fractures (Figure 4-20b) are not considered in this model, because a radial plane fracture will barely propagate in sand due to pressure filtration of the grout. Such fractures are found in clay where no pressure filtration occurs, but not in sand (Chang, 2004).

4.9.2 Fracture propagation

The fracture process is studied using available injection pressure records and accompanying injection rates of fracture grouting works in practice. Simplified versions of the records are presented in Figure 4-21. Raabe and Esters (1993) published a plot that is shown schematically in the left-hand side of Figure 4-21 (project details are unknown). After the initial peak pressure, the pressure variations during injection are approximately 10 bar (the variation between P_f and P_{ext} in the plot. The right-hand plot is a representative record of fracture grouting at the Docklands Light Railway (DLR) extension works in London, where grouting was carried out in Terrace Gravel. This is a fluvial gravel bed, which is typically well graded, varying from silty sand to coarse gravel (Sugiyama et al., 2000). The injections were "flow-controlled" and no peak pressure is present. The injection pressure is simply a result of the "resistance to grout injection" in the soil.

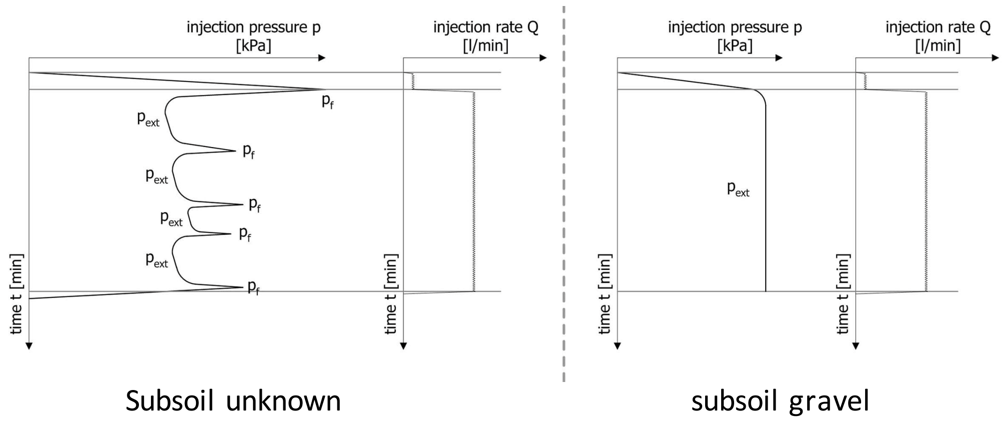

Figure 4-21: Simplified pressure records and accompanying injection rates (Raabe and Esters, 1993)

For the fracture propagation model, it is assumed that the variation in pressure as shown in the first record indicates the pressure differences between pressure at the tip and at the injection point. As a fracture starts to grow, pressure at the tip decreases. This decrease is measured at the injection point, but the pressure at the injection point starts to increase as the fracture propagates over a certain distance. This is because the grout must be transported to the tip. At a certain moment, the pressure at the injection point becomes too high and another fracture starts. This means that the minimum pressure will be slightly higher than the pressure at the tip, and that the maximum pressure can be compared with the external pressure as the fracture has reached a maximum length.

4.9.3 Fracture model and constituent processes

The fracture propagation process can be seen as a combination of three factors: (1) grout injection (2) behaviour of the injected material and (3) response of the soil. This section concentrates on the influence of the injection parameter (injection rate) and the grout properties (rheological properties and filtration properties) in the present analysis. The only influence exerted by the soil is to determine the injection pressure. This will be dealt with in Section 4.10. Furthermore it is assumed that the soil is relatively permeable compared to the grout cake (which is the case for grout injections in sand). The influence of the various parameters on the fracture shape will be described below. For the fracture shape, this is concentrated on the *d/s* ratio, the ratio between the thickness of the fracture d and its length s. For a certain volume injected, fractures with a small d/s will be long and slender and short thick fractures will have a large d/s.

4.9.4 Friction propagating grout

The injection pressure during fracture propagation, or so-called fracture extending pressure, is a function of the confining stress acting normal to the fracture and a certain driving pressure that is necessary to overcome the friction from the flowing grout along the wall of the tube plane. This is illustrated in Figure 4-22 and Equation (4.47):

$$P_{ext} = \sigma_{min} + P_d \tag{4.47}$$

where P_{ext} is the external injection pressure, σ_{min} the stress necessary to fracture the soil, and P_d is the driving force for the propagating grout. The internal pressure P decreases over the fracture length. The decrease of pressure over length is called pressure gradient dP/dl, where l is the length coordinate along the fracture.

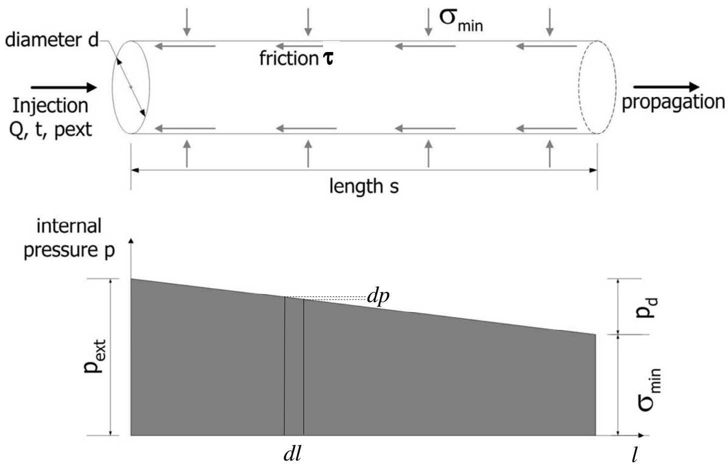

Figure 4-22: Definition of driving pressure

This pressure drop can be defined when considering the equilibrium of a small cross-section of fracture length dl; see Figure 10 and Equation (4.48). A common fracture grout can be considered as a Bingham fluid. It is assumed that the yield stress of the injected grout τ_y determines the flow and that the viscous forces can be neglected. This assumption is based on the results of rheology tests for different grout mortars (Sanders, 2007) and can be described as:

$$\frac{dP}{dl} = \frac{\alpha_1 \tau_y}{d} \tag{4.48}$$

where α_1 is a coefficient (depending on the type of fracture) and d the diameter or thickness of the fracture. The factor α_1/d is the circumference of the fracture perpendicular to the flow direction, divided by the cross-sectional area of the fracture. α equals 2 for a plane-like fracture (Figure 4-20a) and 4 for a tube-like fracture (Figure 4-20c). Integration of the pressure drop over the fracture length and using parameters and symbols from Figure 4-22 results in Equation (4.49) :

$$s = \frac{P_{ext} - \sigma_{min}}{\alpha_1 \tau_y} d \tag{4.49}$$

Equation (4.49) is a relationship between the length *s,* and the diameter or thickness *d* of a fracture. It should be noted that the influence of the soil is only included in σ_{min} in this relationship and is independent from other soil properties (for example the stiffness of the soil). For plane-like fractures, the relationship is identical to that given by Lombardi (1985). In Equation (4.49) P_{ext}-σ_{min} is generally not known. As mentioned above, the record given by Raabe and Esters (1993) is used to estimate this value. Based on the measurement presented, it is assumed that this value can be 10 bar in sand.

The length *s*, diameter *d,* and in the case of a plane-like fracture the width *w* (see Figure 4-22) determine the injected volume (*V*):

$$V = Qt = swd \tag{4.50}$$

For a tube Equation (4.50) becomes:

$$V = Q\, t = \frac{1}{4}\pi s d^2 \tag{4.51}$$

4.9.5 Pressure filtration of injected grout

Pressure filtration, also called dehydration, is the expulsion of water from the grout and leads to a decrease in porosity of the injected grout. At a lower porosity, grains in the grout come into contact with each other and dehydration stops. Consequently, the fracture needs to have a certain thickness to include both the dehydrated grout layers and the still liquid grout that causes the fracture propagation. This assumption is based on laboratory tests, to be described in Chapter 6, and special filtration tests on the grout used in the experiments. See Chapter 5. Filtration plays a particularly major role whenever the permeability of the surrounding soil is considerably larger than that of the grout filter cake that results from the filtration process. As this is the case in sand, this research takes filtration or dehydration of the grout into account. The permeability of rock and clay is generally lower than that of the filter cake, and pressure filtration will therefore not determine the shape of fractures in rock and clay.

4.9.6 One-dimensional filtration of fracture grout

Figure 4-23 illustrates the one-dimensional filtration model used. Due to the expulsion of pore water into the pores of the sand, a dehydrated layer (called the filter cake in the case of consolidated grout) originates. The thickness of this layer is x_e. This layer regulates the expulsion of water from the grout into the pores of the sand. The thickness, x_e, increases during filtration. Laboratory experiments have shown that there is a well-defined boundary between the grout that is dehydrated by filtration and the original grout. The dehydrated grout appears to be rather stiff.

According to literature (McKinley and Bolton, 1999), the following relationship holds for one-dimensional filtration with the condition that $x_e = 0$ at $t = 0$ and a constant filtration pressure:

$$x_e^2 = 2k_c \frac{\sigma}{\gamma_w} \frac{1+e_i}{e_i - e_e} t \tag{4.52}$$

where σ is the applied stress on the grout mixture, γ_w the volumetric weight of the water, e_i is the void ratio before filtration, e_e the void ratio after filtration, and k_c is the permeability of the filter cake. This model implicitly assumes that the grout does not harden during the filtration. Normally this is the case during compensation grouting since hardening takes several hours and the filtration is normally a matter of minutes. Equation (4.52) can also be written as a function of the porosity of the grout before (n_i) and after filtration (n_e) and the difference in piezometric head over the grout filter cake (Δϕ):

$$x_e = \sqrt{2k_c \frac{1 - n_i}{n_i - n_e} \Delta\varphi\, t} \tag{4.53}$$

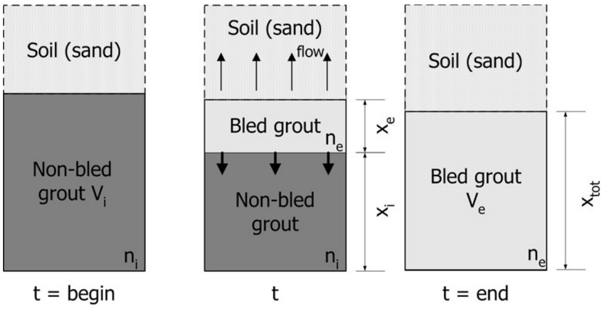

Figure 4-23: Sketch of 1-dimensional pressure filtration (Grotenhuis, 2004)

4.9.7 *Axial symmetrical filtration of fracture grout*

Filtration in the cross-section of a tube-shaped fracture must be represented as an axial symmetrical process. This was evaluated by Kleinlugtenbelt (2005), who found that the equation for the axial symmetric situation differs from the one-dimensional case. For the axial symmetric situation when the whole tube is consolidated, the equation is as follows:

$$x_e = 2\sqrt{k_c \frac{1 - n_i}{n_i - n_e} \Delta\varphi\, t} \tag{4.54}$$

For fractures in the shape of a plane or that of a tube, filtration will occur on both sides. The effective thickness of the fracture (d_{eff}) will therefore be less than the original thickness (d) with twice the value x_e (see Figure 4-24) :

$$d_{eff} = d - 2.x_e \tag{4.55}$$

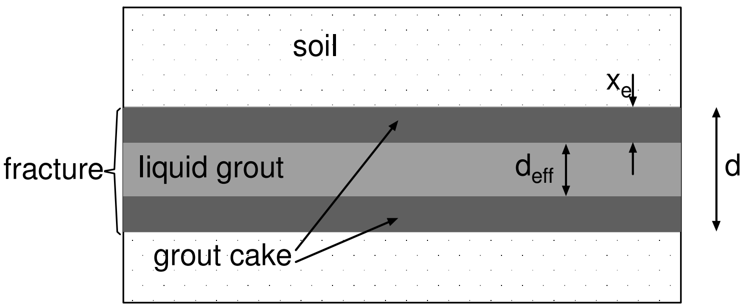

Figure 4-24: Definition sketch fracture with grout cake.

4.9.8 d/s ratio

Plane

In Equation (4.55) d_{eff} *is* the thickness of the fracture through which the grout is flowing. This thickness is described by Equation(4.49). Combining Equation (4.49), Equation (4.53) and Equation (4.55) leads to:

$$d = \frac{2\tau_y}{p_{ext} - \sigma_{min}} s + 2\sqrt{2k_c \frac{1-n_i}{n_i - n_e} \frac{P_{ext}}{\gamma_w} t} \tag{4.56}$$

Assuming that the volume loss due to pressure filtration is relatively small compared to the total volume injected, Equation (4.50) can be used to eliminate the time in Equation (4.56) as follows:

$$\frac{d}{s} = \frac{2\tau_y}{p_{ext} - \sigma_{min}} + 2\sqrt{2k_c \frac{1-n_i}{n_i - n_e} \frac{P_{ext}}{\gamma_w} \frac{wd}{Qs}} \tag{4.57}$$

with:

$$C_1 = \frac{2\tau_y}{p_{ext} - \sigma_{\min}} \tag{4.58}$$

and

$$C_2 = 2\sqrt{2k_c \frac{1-n_i}{n_i - n_e} \frac{P_{ext}}{\gamma_w} \frac{w}{Q}} \tag{4.59}$$

The solution of this equation for a *d/s* larger than the *d/s* that follows from filtration only reads:

$$\frac{d}{s} = \frac{2C_1 + C_2^2 + \sqrt{C_2^4 + 4C_1C_2^2}}{2} \tag{4.60}$$

From Equation (4.56) and Equation (4.57), it can be seen that the *d/s* ratio is determined both by the yield strength of the grout (the first term on the right-hand side of the equation) and the dehydration properties (the second term).

In cases where filtration is dominant and the influence of viscosity can be neglected it is possible to simplify Equation (4.61) to:

$$\frac{d}{s} = \frac{8wk_c}{Q} \frac{1-n_i}{n_i - n_e} \frac{P_{ext}}{\gamma_w} \tag{4.61}$$

From this formula it can be seen that high injection pressure leads to short, thick fractures (*d/s* increases as P_{ex} increases), and that a low grout permeability or a high injection rate is necessary to achieve long and slender fractures.

Tube

The situation is slightly different for a tube. Again assuming that pressure filtration is dominant, combining Equation (4.49), Equation (4.54) and Equation (4.55) leads to the relationship:

$$d = \frac{4\tau_y}{p_{ext} - \sigma_{min}} s + 4\sqrt{k_c \frac{1-n_i}{n_i - n_e} \frac{P_{ext}}{\gamma_w} t} \tag{4.62}$$

It is again assumed that the volume loss due to pressure filtration is relatively small compared to the total volume injected. Equation (4.51) and Equation (4.62) form a set of equations that can be solved numerically using an iterative procedure to determine *d/s*. In the case of a tube-like fracture, the *d/s* ratio is not constant over time but instead increases with time.

4.9.9 Numerical examples

Equation (4.60) and the set of Equations (4.51) and (4.62) have been used to calculate the *d/s* ratios for some examples. One example refers to a model set-up with relatively high injection pressures, compared to the pore pressures. See Chapter 6. Another example refers to the CGT field experiments. The main difference between these two examples is a lower injection pressure in the field, which is 2000 kPa in the model and 300 kPa in the prototype. The lower value in the prototype is presumably caused by unloading of the soil during installation of the TAMs or by inhomogeneity in the soil. In the plane strain situation, the fracture propagation can be calculated for the situation that satisfies Equation (4.60). Some examples of these calculations are shown in Table 5 for a fracture plane. For the tube-shaped fracture, it was shown that the relationship between the fracture length and fracture thickness is time dependent. The value of *d/s* was calculated for a varying injection duration for this situation, *t* in Equation (4.62). The *d/s* ratio is shown in Figure 4-25 as a function of time for both examples with a tube-shaped fracture, and for the parameters that correspond to a water-cement ratio (WCR) of 1 for a planar fracture. It is clear that the field experiment with the lower injection pressure will result in more slender fractures, and also that tube-shaped fractures will have lower values of *d/s*. The shape of the tube-shaped fractures is dominated by the shear strength of the grout when injection begins, and the difference between the injection pressure and the "fracture stress". The influence of the pressure filtration increases as the length of the fracture increases.

According to the calculation model described before, the difference between the model tests and the field experiments is due to the difference in injection pressure. The injection rate also influences the value of *d/s* when the pressure filtration term is dominant; see for example Equation (4.61), where *d/s* linearly depends on the injection pressure. Here, the tests of the 2nd series, see Chapter 6, are taken as an example, where the injection rate was the same as in the field. When a lower injection rate is used, this will lead to higher values of *d/s*. Calculations were made for different values of WCR. The WCR value itself is not a parameter in the formulas but influences both the quotient $(1-n_i)/(n_i-n_e)$ and the permeability of the grout cake (k_c). See Table 5. The values used for $(1-n_i)/(n_i-n_e)$ and the permeability of the grout cake were determined using dehydration tests for a grout mixture with 7% Colclay Bentonite and Portland cement (Kleinlugtenbelt, 2005; Bezuijen et al., 2009).

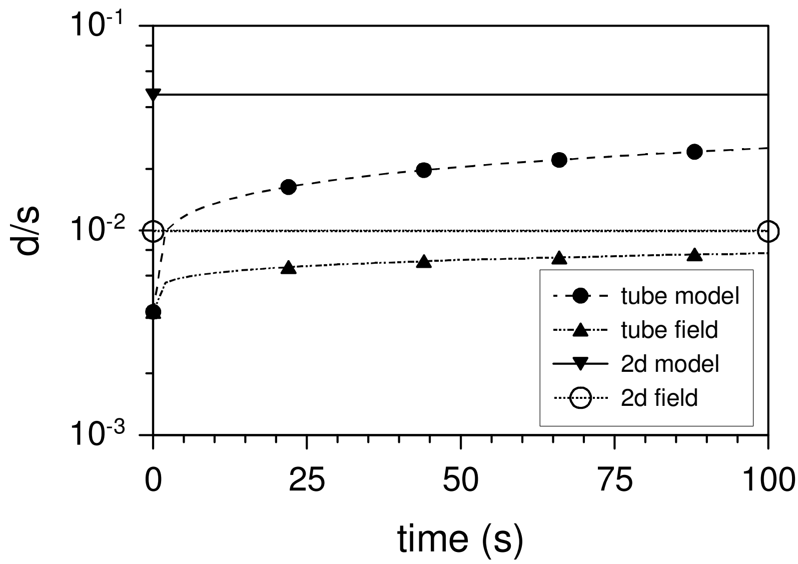

Figure 4-25: Possible d/s ratios for tube-shaped fractures (indicated as "tube" in the figure) and non-radial plane-shaped fractures (indicated as "2d" in the figure), both in the field and in a model test.

Table 5: Calculations for field situation and for a model test situation with a planar fracture with a width of 0.3 m.

WCR (-)	n_i (-)	n_e (-)	k_c (m/s)	Q (m^3/s)	*d/s* model P_{ext}=2000 kPa (-)	*d/s* prototype P_{ext}=300 kPa (-)
1	0.75	0.4	2.10^{-8}	$167*10^{-6}$	$4.6*10^{-2}$	$9.9*10^{-3}$
2	0.84	0.45	2.10^{-9}	$167*10^{-6}$	$5.7*10^{-3}$	$3.1*10^{-3}$
5	0.92	0.56	1.10^{-9}	$167*10^{-6}$	$3.8*10^{-3}$	$2.6*10^{-3}$
1[1]	0.74	0.53	1.10^{-7}	$167*10^{-6}$	P_{ext}=500 kPa $8.7*10^{-2}$	

[1] Calculation for test 1-5.

If the actual values of *d/s* are calculated using this model, it appears that in all cases the *d/s* values of the fractures are lower than the measured test results shown in Figure 4-26 where *d/s* is 0.3, even at the relatively low injection pressure of 500 kPa. The permeability of the grout cake in this test proved to be relative large because the usual step of hydrating the bentonite before mixing it with cement was omitted for this test (Kleinlugtenbelt, 2005).

The *d/s* value is therefore calculated separately and is also shown in Table 5. The value of 0.087 for *d/s* is lower than the measured value by a factor of four. This is partly caused by the assumption in the calculation model that only one fracture developed during injection. As can be seen from Figure 4-26, the grout volume injected does not only reach the fracture but also the circular shape around the axis. This means that the discharge rate of the grout that actually enters the fracture is lower. Another reason is the simplifications that were made to develop the model. For example, only the pressure filtration perpendicular to the propagation direction of the fracture is assumed. Extra filtration is possible at the tip, and this will also cause wider fractures. The CT-scan in Figure 4-26 shows clearly that the density is higher at the tip than at the start of the fracture.

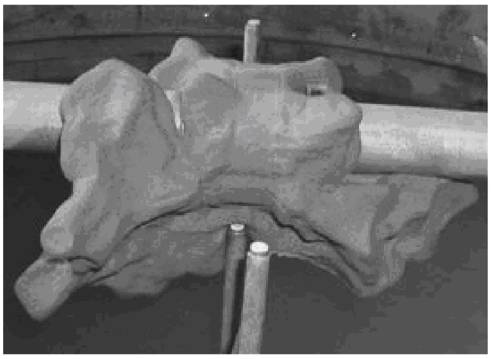

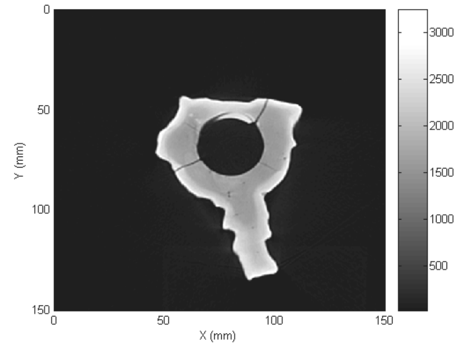

Figure 4-26: Grout sample after a test and cross-section obtained by a CT-scan through the middle of the sample, also see text (Bezuijen et al., 2006). Test information can also be found in Chapter 6 (Test 1-5). The gray scale on the left is related to the density, see section 6-10, the lighter the gray the larger the density.

As mentioned in the Introduction, the aim of this study is to develop a conceptual model. The model that has been developed explains the differences in fracture shapes found in permeable and impermeable soil, and at different injection pressures. Without pressure filtration through a permeable soil, the yield stress in the grout and the difference between the injection pressure and the actual fracturing pressure determines the fracture shape. In permeable soil and at high (>20 bar) injection pressures, the pressure filtration determines the shape.

4.9.10 Consequences for practice

A range of different fracture shapes have been found in laboratory tests (Chang, 2004; Gafar et al., 2008) and in field tests. The model described in this paper shows that these differences in shape can be explained, at least qualitatively, by taking into account the influence of pressure filtration in the grout. The mechanical properties of the soil influence the injection pressure necessary for the grout to enter the soil, but the shape of the fracture is to a large extent determined by the injection pressure (determined by the soil properties), the grout properties and the permeability of the soil. Injection of grout with a relatively permeable grout cake into a soil with sufficient permeability will lead to short thick fractures, and a high injection pressure is needed. Injections in clay or injection with grout that forms an impermeable grout cake can lead to long and thin fractures. The permeability of a cement-bentonite filter cake during injection depends on the WCR ratio (Bezuijen et al., 2009) and will be a maximum of $2*10^{-8}$ m/s using the usual bentonite preparation (24 hours of hydration in water or high shear mixing). This means that most sands and silts will be relatively permeable compared to the permeability of the grout cake. The pressure filtration will only be hampered by soil permeability in clayey soils.

For grout that is usually applied with a WCR of 1 – 2 and 3% to 7% bentonite, the model predicts that for fracture grouting in sand (where injection pressures are a few bars above the pore water pressure and injection rates are 10 l/min) it is still possible that the fractures will be long and thin and will be dominated by the yield stress of the grout. When the injection pressure becomes higher, the shape will be dominated by pressure filtration. Based on the pressure readings, this means it is possible to have some indication of the extent of the fractures made.

End of part of article submitted to "Journal of Geotechnical and Geo-environmental engineering".

4.10 From injection pressure to fracture shape

Combining the phenomena discussed in Section 4.3, Section 4.8 and Section 4.9 gives us the opportunity to acquire an insight into the fracture shape as a function of the measured injection pressures using cavity expansion theory. This section looks only at sheet-like fractures. Branch-shaped fractures are excluded because the assumptions necessary for the calculation model described in this theory are incompatible with these fractures. Furthermore, branch-shaped fractures seem to correspond to local weak spots in the soil and they were not found in homogeneous soils.

The calculations performed for this study by Teunissen – see Section 4.8 – showed that, certainly in clay but to some extent in sand also, the stress distribution around a cavity with a fracture at some distance of the fracture can be approximated to the stress distribution around a larger imaginary cavity. See Figure 4-27.

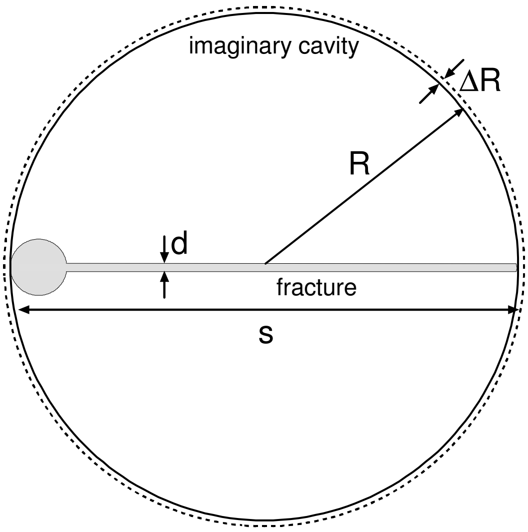

Figure 4-27: Fracture and imaginary cavity to calculate the injection pressure, see text

As a first approximation and disregarding dilatancy in the sand, the volume increase in the fracture must also lead to the same volume increase in the imaginary larger cavity. Using cavity expansion theory, it is possible to calculate the pressure needed to achieve this volume increase at the border of the imaginary cavity. Since plastic deformation close to the cavity is limited, the pressure at the border of the imaginary cavity will be comparable to the pressure in the fracture and it is therefore possible to estimate the fracture pressure.

In a two-dimensional case (with a fracture plane perpendicular to the plane shown in Figure 4-27) the fracture area is $d.s$. This fracture volume is equal to the increase in the cavity area. Assuming that the fracture is much longer than the diameter of the injection tube, the diameter of the imaginary cavity is equal to the fracture length s. On the basis of these assumptions the relative increase in area ($\Delta A/A$) can be written as:

$$\frac{A+\Delta A}{A}=\frac{\frac{\pi}{4}s^2+d.s}{\frac{\pi}{4}s^2}=1+\frac{4}{\pi}\frac{d}{s} \qquad (4.63)$$

The relative increase in the radius of the imaginary cavity is therefore:

$$\frac{R+\Delta R}{R}=\sqrt{1+\frac{4}{\pi}\frac{d}{s}} \tag{4.64}$$

This relation and the cavity expansion theory presented in Section 4.3 lead to the relation between *d/s* and the injection pressure shown in Figure 4-28.

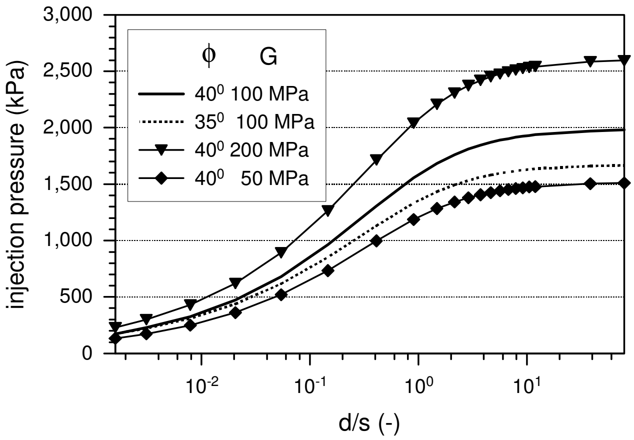

Figure 4-28: Theoretical relation between fracture shape and injection pressure using cavity expansion theory for different values of the friction angle (ϕ) and the shear modulus (G)

The relation presented in Figure 4-28 will not be valid for values of d/s larger than 1. However, the relation is also shown for large values of d/s, so that the figure reaches the limiting cavity expansion pressure. From this figure, it can be concluded that, if one knows the limiting cavity expansion pressure in the soil and the injection pressure, it is possible to estimate the width-length ratio for the fractures.

Combining this result with the relation for *d/s* found in Section 4.9 for plane-shaped fractures makes it possible to eliminate the injection pressure and to write *d/s* as a function of the soil and grout parameters only. In a zero-cohesion situation, Equation (4.1) simplifies to:

$$P'=P'_f\left[\frac{1-(R_0/R_p)^2}{Q}\right]^{\left(\frac{\sin\phi}{1+\sin\phi}\right)} \tag{4.65}$$

Since $R_p=R_0+\Delta R$, this can be written as:

$$P'=P'_f\left[\frac{1-\left(1/\sqrt{1+\frac{4}{\pi}\frac{d}{s}}\right)^2}{Q}\right]^{\left(\frac{\sin\phi}{1+\sin\phi}\right)} \tag{4.66}$$

which, for small values of *d/s*, can be simplified to:

$$P' = P'_f \left[\frac{\frac{4}{\pi}\frac{d}{s}}{Q} \right]^{\left(\frac{\sin\phi}{1+\sin\phi}\right)} \tag{4.67}$$

Without pressure infiltration, *P'* equals the injection pressure and can be entered in the equation for *d/s* for plane-shaped fractures, disregarding the influence of viscosity, as derived in Section 4.9. This leads to the following equation:

$$\frac{d}{s} = \left[\frac{8wk_c}{Q} \frac{1-n_i}{n_i - n_e} \frac{\sigma'_0}{\gamma_w} (1+\sin\phi) \right]^{1+\sin\phi} \cdot \left(\frac{4G}{\pi \sigma'_0 \sin\phi} \right)^{\sin\phi} \tag{4.68}$$

A number of assumptions and simplifications were necessary to arrive at this equation: the fracture was simplified to a cavity as shown in Figure 4-27; it was assumed that *d/s* <<1; that there is a plane-shaped fracture; that the influence of the viscosity and the yield stress on *d/s* could be disregarded; that the pressure filtration at the tip has no influence on *d/s*; that the soil in which the grout is injected is permeable compared to the grout cake; that the dilatancy in the soil during fracturing does not play an important role; and that pressure infiltration can be disregarded. All these assumptions and simplifications mean that the relation above will not be a very accurate description of *d/s*.

It emerged that, when using realistic values for the parameters, the predicted *d/s* values are much too low when compared with the results of measurements, probably because the pressure filtration at the tip has a significant influence and is not taken into account in this formula. Furthermore, some pressure infiltration can accelerate cake formation, as was explained in Section 4.5 and, at the low values of *d/s* calculated, *d* will be higher because viscosity starts to play a role and the finite dimensions of the single grain become important.

The model is of interest because it shows the influence of various parameters. Figure 4-29 shows the results of some calculations where the permeability of the grout cake is increased from the measured 2.10^{-9} m/s to 2.10^{-7} m/s. Table 6 presents the other parameters for these calculations. The result shows that *d/s* is very small for a cake permeability of 2.10^{-9} m/s but increases significantly at higher values. The reason is that higher cake permeabilities are associated with more pressure filtration, which requires a higher *d/s* (see Section 4.9). However, this is only possible when the injection pressure is increased, which results in a thicker cake and once again in higher values for *d/s*.

Table 6 Parameters used in *d/s* calculation

Parameter	Value	Dimension
injection rate	10	l/min
injection rate	166.7×10^{-6}	m^3/s
width of fracture	0.5	m
n_i	0.84	-
n_e	0.45	-
confining stress	100	kPa

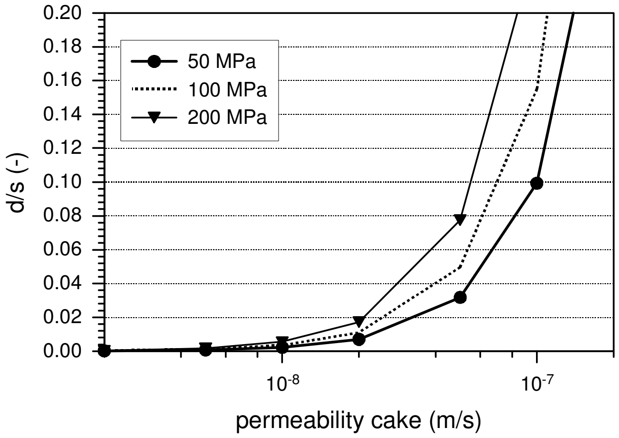

Figure 4-29: Calculated values for d/s for various cake permeabilities and shear moduli

4.11 Summary of theory

As mentioned in the introduction, it was the aim of this chapter to combine and expand existing theory to get a better idea of what determines injection pressures and fracture shapes. This information will help to interpret the measurements to be described in subsequent chapters.
The main findings are:
- A fracture in non-cohesive material occurs when a cavity is pressurised due to the difference in radial and tangential stresses in the sand that is loaded with the pore pressure that works in all directions. It is therefore possible to overcome the tangential stress with the pore pressure, and this will result in a fracture.
- Micro-mechanical (calculating the forces on a single grain) and elastic cavity expansion calculations show that, with a Newtonian liquid as an injection liquid, fracturing in sand will be difficult because the loading is applied not only at the boundary between the sand and the grout, but also slightly further into the sand. Consequently, the stability of single grains becomes less and plastic deformation will occur only at higher pressures when a Newtonian liquid is used compared to the injection of a "wall-building" fluid.
- Although some wall building is necessary to create fractures, when this wall building is obtained with a filter cake during pressure filtration, the filter cake should only have a limited thickness during the injection period. A filter cake that is too thick will hamper fracture formation because a fracture is filled with a filter cake before it is formed.
- Filter cake formation as described by, for example, McKinley and Bolton (1999) was extended to include the influence of pressure infiltration. Including pressure infiltration means, in effect, that two processes are considered. Firstly, the large particles in the injection fluid (in cement-bentonite grout, the cement particle) are filtered from the injection fluid and form a cake between the injection fluid and the sand particles. The injection fluid with the fine particle then flows into the sand. In the second phase, the yield stress of the fine particle (normally the bentonite) prevents further penetration of the fine particles into the sand and only the water is pressed out of the injection fluid. In principle, this leads to a filter cake of large and small particles on top of the filter cake with only large particles. However, since the time scale of the last filtration process is completely different from the one in the first process, this second filter cake formation was not modelled.
- The width-length ratio (*d/s*) of a fracture is, for fracturing in impermeable soils (rock and clay), determined by the yield stress of the grout and the difference between the injection pressure and the pressure at the tip. This study shows that, in the case of fracturing in a permeable soil, the filtration properties also affect the *d/s* ratio. A lot of solid particles in the injection fluid will lead

to relatively short and thick fractures. The reason is that, for the injection pressures used during the injection, the filter cake has already a significant thickness. This means that only fractures with *d/s* values that are high enough are possible. This mechanism can be shown with a one-dimensional calculation that takes into account the filter cake formation at the sides of the fracture, disregarding the effect of cake formation at the tip. Pressure filtration at the tip will be higher than at the sides of the fracture because there are more possibilities for the water to flow away. This will lead to even higher *d/s* values than mentioned in the calculations.
- A simple model was set up showing the relation between the soil parameters and the *d/s* value. It showed which soil and grout parameters determine the value of *d/s* and that higher injection pressures and higher permeabilities of the grout cake lead to higher values for *d/s*.

5 Grout properties

Sections 5.1 to 5.7 were published as a Technical Note in Géotechnique (Vol 59, Issue 8, 717-721, 2009)

5.1 Introduction

Grout pressure filtration is important in compensation grouting. Au (2001) found in compensation grouting experiments in clay that the formation of a filter cake around a cavity can inhibit fracturing of the clay. Both theoretical work (Grotenhuis 2004) and experimental work Bezuijen and Tol, 2007) indicate that filtration of the grout mixture during injection of the grout determines the occurrence and length of fractures when using the compensation grouting technique in sand.

Since grout pressure filtration is an important issue, various authors have presented the results of different types of consolidation tests on grout, for example Gustin et al. (2007), McKinley and Bolton (1999). The aim of this study was to find ways of reducing the permeability of the grout cake, as this will decrease the rate of cake building during injection. Pressure filtration is sometimes referred to as bleeding. Here the term pressure filtration is chosen because bleeding is also used for the water that comes on the surface of a grout mixture due to self weight consolidation without an external pressure applied and that is not meant here.

This paper describes the theory of pressure filtration, the set-up for the experiments and the results and ends with a discussion on the results and conclusions.

5.2 Pressure filtration of grout

A grout mixture subjected to a consolidation test will result in pressure filtration. Assume the situation sketched in Figure 5-1; the grout is partly consolidated and partly unconsolidated. The particles in the grout are assumed to be rigid. In the unconsolidated grout mixture there is no inter-grain stress and the initial porosity is n_i. After pressure filtration, the final porosity of the grout is n_e. Furthermore it is assumed that chemical reactions do not interfere significantly because of the short duration of the test and that the self weight effects are negligible.

According to McKinley and Bolton (1999), expressed here using the porosity instead of the void ratio, the thickness of the filtration layer as a function of time (t) can be written as:

$$x = \sqrt{2k_c \frac{1-n_i}{n_i - n_e} \Delta\varphi t} \tag{5.1}$$

where k_c is the permeability of the consolidated grout layer, x is the thickness of the consolidated grout layer and $\Delta\varphi$ is the difference in piezometric head between the unconsolidated grout and the drainage sand.

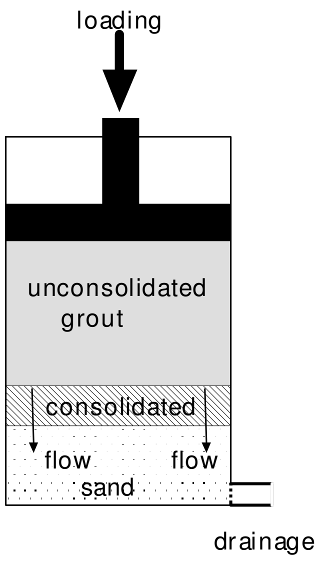

Figure 5-1: Principle of grout pressure filtration.

Since:

$$\frac{V}{A} = \frac{n_i - n_e}{1 - n_i} x \tag{5.2}$$

it follows that:

$$\frac{V}{A} = \sqrt{2k_c \frac{n_i - n_e}{1 - n_i} \Delta\varphi t} \tag{5.3}$$

In these expressions, *V* is the volume of pore water that leaves the grout mixture by pressure filtration and *A* is the area of the sample.

5.3 Properties of a grout mixture

A grout mixture used for fracture grouting consists of three main components: water, bentonite, and cement. These materials influence the properties of the fluid, but bentonite and cement also influence one another's properties (Mitchell 1976). Adding cement and thus adding calcium will lead to a higher permeability of the grout cake (Sanders 2007). The influence of calcium is shown in Figure 5-2 and Figure 5-3, which are pictures taken with an electron microscope. Figure 5-2 shows an ordinary bentonite colloid suspension with no additives. Figure 5-3 is the same type of bentonite colloid suspension mixed with calcium hydroxide. Gaps can be seen in Figure 5-3. It is assumed that this difference is also present after filtration leading to a larger permeability of the filter cake for plain grout comprising bentonite and cement.

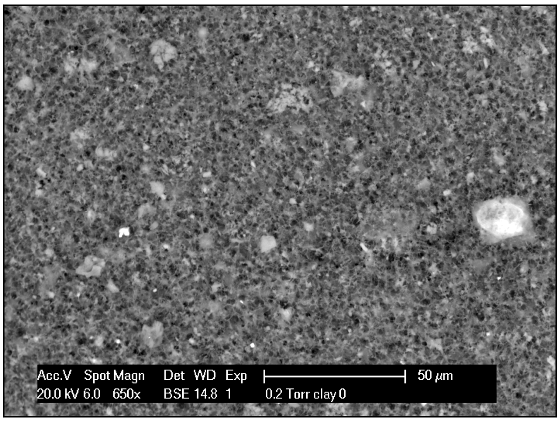

Figure 5-2: Colloid of sodium activated calcium bentonite.

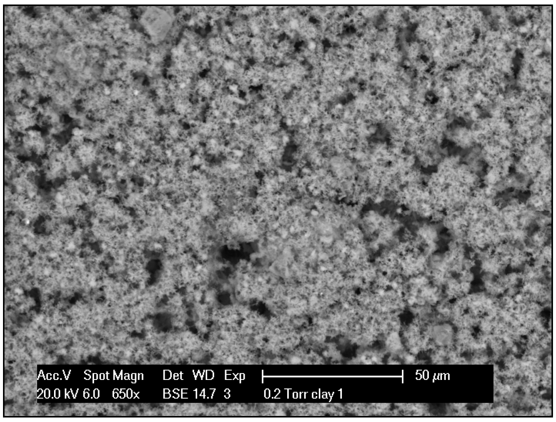

Figure 5-3: Colloid of sodium activated calcium bentonite mixed with calcium hydroxide.

5.4 Experimental method and procedure

Experimental Method

To examine the filtration properties of grout as a function of its composition, grout mixtures were tested by means of a pressure cell. The pressure cell measured 89.8 mm in height and 78.8 mm in diameter. The test set-up was modified from a standard bentonite filtration test. The grout to be tested was placed on a dense saturated sand layer in the pressure cell, pressure was then applied to the upper surface of the grout and the filtration was monitored (see Figure 5-4). Properties of the materials used are given in Table 7.

Procedure

The sand layer comprised Baskarp sand, a uniform medium fine sand with a d_{50} of 130 µm. The sand was compacted in the pressure cell by tamping the saturated sand under water on a sand-tight stainless steel wire mesh filter, forming a dense 50mm thick layer. This layer has a much larger permeability (10^{-4} m/s) than that of the grout and does not influence the filtration process.

The bentonite slurry was mixed with a high shear disperser, an Ultra Turrax device running a disintegrator at 2000 rpm in a 70 mm diameter vessel. After hydration over a 24-hour period, the bentonite slurry was mixed with the other materials (cement, fly ash and/or retarder) for 8 minutes using a rotor blade disperser running at 500 rpm in the same vessel. Immediately after mixing, the grout was poured on top of the sand layer in the pressure cell. This resulted in a grout layer measuring approximately 39 mm in thickness. The rest of the apparatus was assembled and the pressure was applied, 10 to 13 minutes after mixing additives with the bentonite slurry. The time that elapsed after mixing proved to have little influence on the results - the permeability of the grout was found to increase slightly with time after mixing.

To ensure an equal transfer of pressure over the total grout surface, a hard plastic disc was placed directly on the grout layer. An impermeable flexible plastic membrane was also placed above the hard plastic disc. This prevented air penetrating into the grout layer, which could result in the formation of preferential pathways and eventually cracks throughout the grout layer. The cap of the pressure cell was locked on top of the membrane. The chamber between the cap and the membrane was pressurised using air pressure (see Figure 5-4).

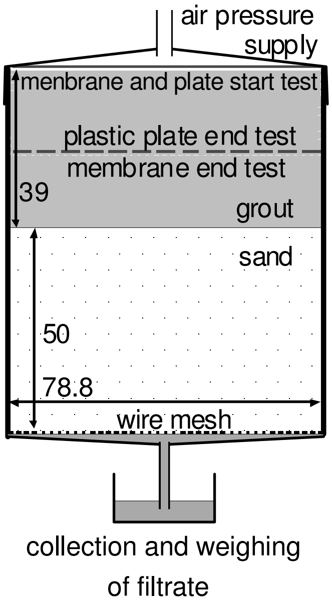

Figure 5-4: Sketch of the apparatus used for the pressure filtration tests, also see text (dimensions in mm)

The filtrate was weighed using a continuous measuring balance, which recorded the weight of the filtrate every 1.2 seconds, with a resolution of 1gram.

Table 7: Components and properties of materials used. Percentages are mass/mass (m/m). The bentonite contains for > 85% out of Montmorillonite entity.

	Benonite	Cement	Micro fine cement	Fly ash Keerkring 1	Silica flour	Sand
Name	Colclay	Portland	Dyckerhoff	Anneliese c.w.	Cebo	Baskarp
Spec. density solids (kg/m^3)	2750	2950	3100	2900	2650	2650
d_{15} (μm)	1.35	3	1.4	11	6	95
d_{50} (μm)	4.6	20	3.9	15	22	130
d_{85} (μm)	11.5	44	11.6	22	50	180
SiO_2 (%)	-	21	22.6	50	99.5	88.1
CaO (%)	-	65	66.8	5	0.03	0.55
Al_2O_3 (%)	-	4	3.9	30	0.2	5.53
Fe_2O_3 (%)	-	3	1.4	10	0.03	0.61
Others	-	7	5.3	5	0.24	5.2

5.5 Experiments undertaken

A variety of grout mixtures were tested (see Table 8). The grain size, the amount of the cement, the amount of bentonite and the applied pressure, were changed in the various tests, and fly ash was added instead of cement. Two experiments using only bentonite and silica flour were also performed, as well as one with a cross-linked gel (Borate Cross-linked Gel, a fracturing fluid used in the oil industry). In the table, we have generalised the Water-cement ratio (W/C ratio) and also use it when silica flour (SF) or fly ash (FA) is added. The amount of discharged liquid as a function of the square root of time for different tests is shown in Figure 5-5. According to Equation (5.3), there is a linear relationship between these two parameters. This relationship was apparent at the beginning of the tests. At the end of the tests, this relationship no longer applies because nearly all the grout is consolidated (e.g. the fly ash case) and water leakage from the sample ceases. However, some tests ended with membrane failure (Portland and micro cement), causing a grout fracture that leads to a sharp rise in leakage (see Figure 5-5). The permeability of the consolidated grout can be determined from the slope found in the graph showing mass of filtration versus square root of time. From Equation (5.3) it follows that:

$$k_c = 0.5\frac{\left(\frac{V/A}{\sqrt{t}}\right)^2 \frac{1-n_i}{n_i - n_e}}{\Delta\varphi} \tag{5.4}$$

The term $\left(\frac{V/A}{\sqrt{t}}\right)$ can be determined from the slope of the plots shown in Figure 5-5 that represents $\left(\frac{\rho_w V}{\sqrt{t}}\right)$, assuming that the filtrate is water. The initial porosity was calculated from the amount of material used to make the grout. The final porosity was established by taking a sample from the grout after consolidation and determining its water content and porosity.

The permeability of the filter cake determined in the various tests is shown in Table 8. The table shows that the permeability varies from $2.8*10^{-12}$ m/s to $1.2*10^{-8}$ m/s for the various bentonite slurries in different tests. This variation depends on the amount of bentonite, but, more importantly, also on the amount of cement that is added. The test with the cross-linked gel resulted in the lowest permeability: $1*10^{-12}$ m/s. In the case of the test using bentonite only (Test 5), the permeability could not be determined as the test was dominated by pressure infiltration (not only the water from the pressure filtration, but also the grout particles are pushed into the sand matrix, because only small particles compared to the pores between the sand grains are present in the grout). Substantial pressure infiltration also occurred in Test 13 with calcium chloride (see Figure 5-6).

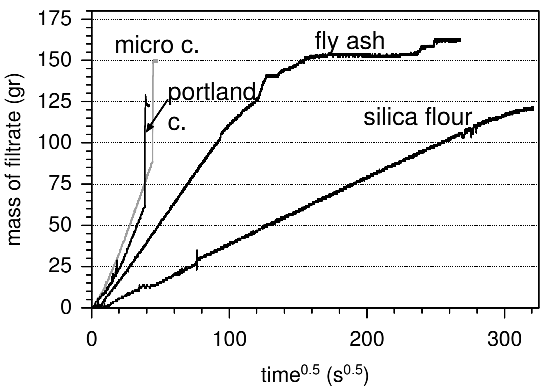

Figure 5-5: Results of experiments plotted against the square root of time.

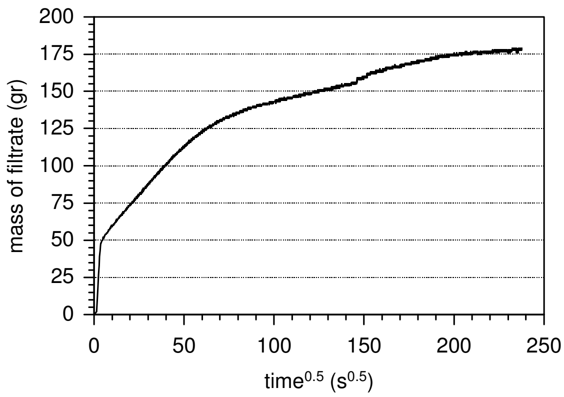

Figure 5-6: Result of experiment 13 with significant pressure infiltration at the beginning of the test.

The grain size of the cement has little influence (compare Test 6 and 7). The permeability is determined by the amount of bentonite (see Figure 5-7) and the degree of coagulation of the bentonite in the water. Permeability is lowest when only pure bentonite is used, and increases if cement or fly ash are added. See Figure 5-8. The increase in permeability when using fly ash is less than for cement, probably because fly ash contains less calcium. The addition of a retarder decreases permeability as it slows down the reaction between the calcium and the bentonite (see Figure 5-9).

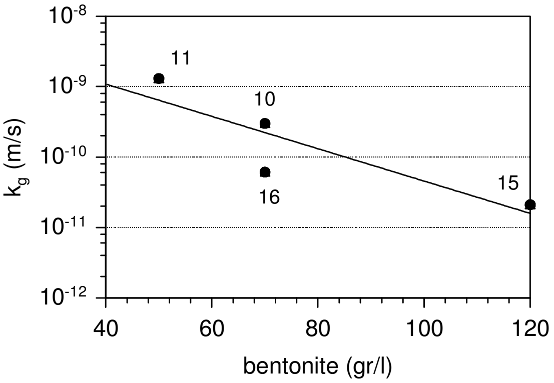

Figure 5-7: Influence of the bentonite content on the permeability of the consolidated grout. Tests performed with fly ash. Water/fly ash ratio was 3 in all tests. The numbers in the figure refer to the test numbers in Table 8.

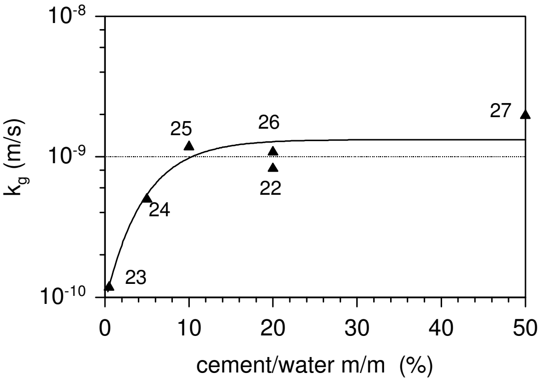

Figure 5-8: Influence of the percentage cement with respect to the water on the permeability of the consolidated grout. Tests performed with Portland cement and a bentonite slurry with 7% m/m bentonite. The numbers in the figure refer to the test numbers in Table 8.

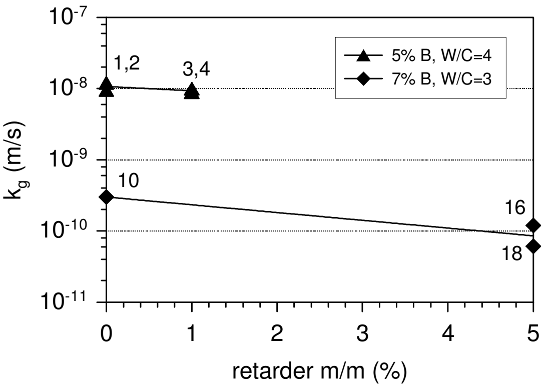

Figure 5-9: Influence of retarder on the permeability of the consolidated grout. Tests performed with different bentonite concentrations (5 and 7%) and water-cement ratios (3 and 4). The numbers in the figure refer to the test numbers in Table 8.

5.6 Discussion

There are large differences in the permeability of the grouts tested (more than three orders of magnitude), depending on the grout components. According to Mitchell (1976) the calcium content and the pH have a significant influence on the bentonite structure and therefore on its permeability. See Figure 5-2 and Figure 5-3.

If no cement is present, there is penetration of the grout mixture into the sand, known as pressure infiltration (instead of only the water from the mixture in the case of pressure filtration), at the filtration pressures used. This leads to a steeper initial section of the discharge curve (see Figure 5-6). There is no pressure infiltration when using mixtures containing cement in these tests. This is probably a result of bonding between the cement and bentonite particles. In the injection tests to be dealt with in the next chapter, there is also pressure infiltration when some cement is present in the mixture. See Section 6.7.3. Slurry with bentonite and non-reactive silica flour instead of cement also shows substantial pressure infiltration, although the silica flour had a comparable grain size distribution to cement. This means that pressure infiltration is not only blocked by the particles in the grout, but that the reaction between cement and bentonite also has an important influence on the amount of pressure infiltration.

Table 8: Performed pressure filtration experiments.

Test no	Bentonite gr/l	W/C, W/F or W/S ratio	Type of cement	Retarder[1] %	App. press. kPa	n_i -	n_e -	k_c m/s
1	50	4	PC	0	100	0.91	0.8	1.2e-8
2	50	4	MC	0	100	0.91	0.76	9.5e-9
3	50	4	MC	1	100	0.90	0.75	8.8e-9
4	50	4	PC	1	100	0.90	0.77	9.9e-9
5	70	0	-	0	100	dominated	by	p.i.
6	70	4	PC	0.2	100	0.9	0.78	4.9e-9
7	70	4	MC	0	100	0.9	0.77	6.6e-9
8	50	4	FA	0	100	0.91	0.62	2.1e-9
9	70	1.6	FA	0.95	400	0.8	0.72	9.7e-10
10	70	3	FA	0	400	0.88	0.59	3.0e-10
11	50	3	FA	0	400	0.88	0.4	1.3e-9
12	250[na]	3	FA	0	400	0.81	0.56	2.6e-10
13	50	7.4	$CaCl_2$	0	400	0.89	0.49	2.7e-10
14	70	3	SF	0	400	0.88	0.51	2.8e-12
15	120	3	FA	5	400	0.84	0.72	2.1e-11
16	70	3	FA	5	400	0.85	0.41	6.1e-11
17	70	3	SF	5	400	0.84	0.40	3.1e-11
18	70	3	FA	5	400	0.85	0.45	1.2e-10
19	70	200	SF	0	400	0.98	0.74	1.1e-11
20	70	200	PC	0	400	0.98	0.59	4.4e-11
21	0[2]	200	SF	0	400	0.99	0.47	1e-12
22	70	5	PC	0	400	0.92	0.58	8.4e-10
23	70	200	PC	0	400	0.98	0.86	1.2e-10
24	70	20	PC	0	400	0.96	0.71	5.1e-10
25	70	10	PC	0	400	0.95	0.70	1.2e-9
26	70	5	PC	0	400	0.92	0.56	1.1e-9
27	70	2	PC	0	400	0.84	0.45	2.0e-9

[1] a polysaccharide is used as retarder
[2] test with cross-linked gel
(Borate Cross-linked Gel, Schlumberger)
[na] = not activated bentonite
p.i. = pressure infiltration

PC: Portland cement
MC: micro cement
FA: fly ash
SF: silica (quartz) flour

5.7 Conclusions (filtration tests)

The experimental data presented and discussed allow the following conclusions to be drawn:
- The permeability of common grout mixtures is considerably higher (more than three orders of magnitude) than that of pure bentonite, probably due to interaction between the bentonite and the additives. The addition of relatively small amounts of cement (less than 10% of the water in the mixture. See Figure 5-8), resulted in relatively large increases in permeability of the grout.
- In the experiments, permeability was not influenced by grain sizes in the mixture but the calcium concentration seems to have a large influence.
- At the pressures applied (up to 400 kPa), the addition of cement appears to be quite effective in preventing pressure infiltration of the grout into medium fine sand (d_{50} = 130 μm). It is likely that the same mechanism responsible for higher permeability (coagulation of the bentonite), also prevents penetration of the mixture in the sand. If no cement was added, the pressure infiltration was much larger.
- The results from tests involving micro cement and Portland cement are comparable.

End of Technical note

5.8 Bentonite and ion interaction in water

The preceding sections of this chapter showed that the cement concentration affects the permeability of the bentonite mixture. A qualitative explanation of how the cement influences the permeability of the bentonite mixture is presented below. This description is based on the work of Sanders (2007).

Bentonite is a mineral which mainly consists of the clay mineral montmorillonite. Bentonite platelets have a surplus negative charge at the surface, and a surplus of positive charge at the edges. In water, this leads to the open "house of cards" structure shown in Figure 5-10. The positive edge of one platelet is attracted by the negative surface of another. In the water around the surface of the bentonite particles, there is a "double layer". This layer contains more cations than anions. Cations are attracted to the negative charge at the surface of the bentonite platelet, and are more or less fixed close to the surface of the bentonite platelets. These virtually immobile ions prevent the flow of water and therefore reduce permeability. Further coagulation is prevented because a negative potential remains at the boundary between the double layer and the water (the zeta potential). This causes the surfaces to repel each other, so that only the surface and the edge of a platelet are able to connect (see Figure 5-10).

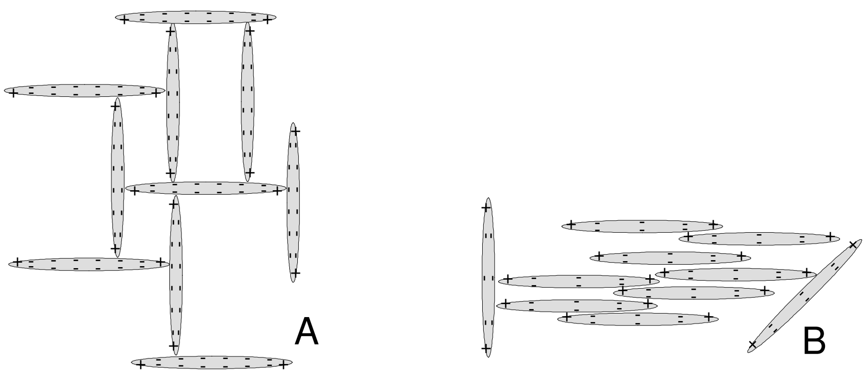

Figure 5-10: Sketch of a bentonite water solution
A. With limited cations in solution leading to a "house of cards" structure
B. Coagulated bentonite particles due to decreased zeta potential

However, adding cations (mainly sodium or calcium) to the suspension will reduce the zeta potential. As a result, the platelet surfaces no longer repel each other and coagulation occurs. This coagulation is even stronger when calcium is added, because the 2+ charged ions act as a bridge between the surfaces of two platelets (Mitchell, 1976). When this occurs, the "house of cards" will collapse, leading to larger openings in the suspension (also see Figure 5-10). This explains the difference between Figure 5-2 and Figure 5-3 in Section 5.3.

5.9 Pressure filtration and pressure infiltration

The model described in Section 5.2 describes only the influence of pressure filtration. It was not therefore possible to analyse Test 5 in Table 8 because of the significant influence of pressure infiltration in these tests. With the calculation model described in Section 4.5, it is possible to analyse these tests also.

As a first test, the model was used to simulate the one-dimensional penetration of a 5% bentonite liquid with 0.5% of quartz flour in fine sand. The model takes into account that a cake of quartz flour developed during penetration, hampering the fluid flow. The bentonite particles are so small that they will flow through the sand pores. In the model, the calculated penetration is too small when the most realistic parameters are used. However, by increasing the permeability of the sand (by reducing the viscosity of the bentonite and the grain size) a good fit appears possible. Table 9 shows the parameters used in the model. Figure 5-11 shows the results of the simulations.

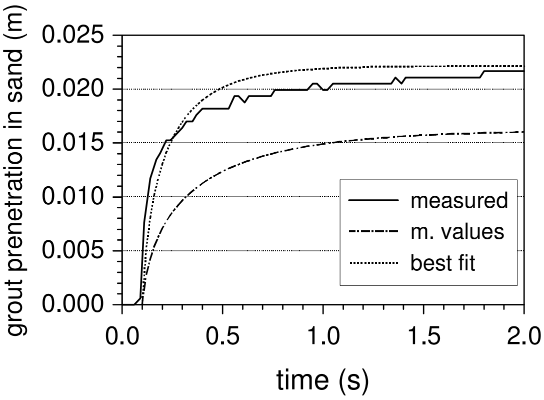

Figure 5-11: One-dimensional penetration experiments compared with calculations. The curve with "m. values" shows the result using the measured values. See Table 9.

Table 9: Parameters used in the calculation of the penetration depth.
The numbers in italics were changed to make the fit.

Parameter	M. values	Best fit	Dimension
Inj. Press	400	400	kPa
D15 sand	90	*130*	μm
Porosity sand	0.4	0.4	-
Visc. water	1e-6	1e-6	m^2/s
Visc. bentonite	1.3e-5	*6e-6*	m^2/s
Yield strength	100	*105*	Pa
Perc. quartz fl.	0.5	0.5	%
D15 quartz fl.	10	10	μm
Porosity quartz	0.5	0.5	-

This result confirms that there are two mechanisms that can create a grout cake: bleeding and the pressure infiltration of part of the grout.

A second simulation was conducted using a grout mixture with a limited amount of cement (WCR=200), as in test 2-6. It resulted in a lot of pressure infiltration. See Section 6.6. Two different measurements are available for this grout material: the pressure filtration test at 4 bar and the injection experiment, which resulted in an injection pressure of 17 bar maximum. Pressure infiltration during the injection experiment was determined from the pictures and estimated to be approximately 0.04 m. Pressure infiltration in the pressure filtration test was much lower at less than 0.01 m. When plotting the grout penetration as measured against time at the beginning of the filtration experiment – see Figure 5-12 – it is difficult to determine what is pressure infiltration and what is pressure filtration on the basis of Section 5.2. Plotting the results again as a function of the square root of time makes it possible to show the contribution made by pressure infiltration. The pressure filtration line is then a straight line. The deviation from the straight line at the beginning of the experiment shows the pressure infiltration. See Figure 5-13. The actual pressure infiltration period is only a few seconds. Before 4 s in the plot there is still some pressure build-up. From 4 to 6.5 s pressure infiltration is dominant; after 6.5 s pressure filtration dominates.

Using the measured values for viscosity and yield stress – See Table 10 – the calculated values for penetration are significantly higher than the measured ones. In the case of the filtration test, the difference between calculated and measured values is nearly a factor 4; in the injection experiment the difference is only a factor 1.45. It is clear that, if the parameter is adjusted so that the injection experiment fits, there will still be a discrepancy for the pressure filtration experiment.

The reason is that the cement-grout mixture is a shear-thinning liquid. During injection, the mixture will have to flow through the tube and the TAM and a lot of shear stress is applied to the mixture, leading to low viscosity that is comparable or even lower than the viscosity during the viscosity test. During the pressure filtration test, the grout is poured into the apparatus – see Section 5.4 – and it will take some time before the test is performed. During this time viscosity and yield stress will rise, reducing pressure infiltration.

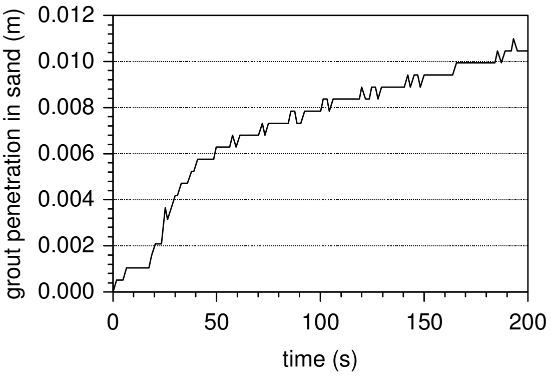

Figure 5-12: Pressure filtration experiment, grout penetration versus time, experiment S6

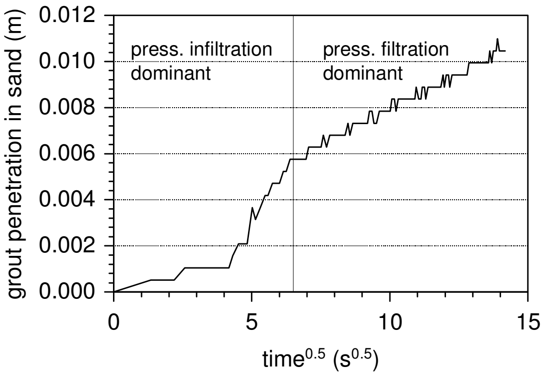

Figure 5-13: As Figure 5-12, but now plotted against the square root of time to show the parts dominated by pressure infiltration and pressure filtration

From the results presented in this section it can be concluded that pressure infiltration also depends on the non-Newtonian properties of the liquids. These depend on shear strength and they are therefore different in the filtration test than in an injection test. It is likely that pressure infiltration is more dominant in an injection test than can be expected solely on the basis of the results of a filtration test.

5.10 Summary of grout properties

The filtration tests described in Sections 5.1 to 5.7 show that the grout pressure filtration properties change considerably with the cement content: more cement leads to higher cake permeability and more solid material (cement) and higher permeability leads to a thicker filter cake. Section 5.8 explains how WCR affects the permeability of the filter cake. Since Section 4.10 showed that permeability, in theory, has a major effect on the shape of fractures, attempts were made to keep permeability in the experimental programme as low as possible, as will be discussed in the next chapter. As a result, the WCR values in the experimental programme are generally higher than would normally be seen in practice. Section 5.9 showed that pressure infiltration can also contribute to a filter cake in the fracture. In the presence of a filter cake of this kind, the *d/s* value is higher than would be the case according to the theory described in

Section 4.10. A complicating factor is that, due to non-Newtonian behaviour, there is normally more pressure infiltration in an injection experiment (or field operation) than is found in a pressure filtration test.

Table 10: Parameters used to calculate the penetration depth for cement-bentonite grout WCR = 200, 7% bentonite.

Parameter	Filtration t	Injection t	dimension
Inj. Press	400	1300	kPa
D15 sand	90	90	µm
Porosity sand	0.4	0.4	-
Visc. water	1e-6	1e-6	m^2/s
Visc. bentonite	$2.13*10^{-5}$	$2.13*10^{-5}$	m^2/s
Yield strength	50	50	Pa
Perc. cement.	0.005	0.005	%
D15 cement.	3	3	µm
Porosity cement	0.5	0.5	-
Calculated results			
Pen. depth max.	0.032	0.105	m
Pen. depth. 2.5 s	0.022		m
Pen. depth 4 s		0.058	m
Measured 2.5 and 4 s respectively	0.006	0.04	m

6 Laboratory experiments

6.1 Introduction

The literature review in Chapter 2 showed that there is no verified theoretical model to describe fracture grouting in sand. It also emerged that it is difficult to create fractures in sand using a cement-bentonite grout. Compared to the fractures created in clay, the fractures in sand were shorter and thicker, and in some cases there were no fractures at all but just a spherical grout body. The field tests described in Chapter 4 show that accurate lifting of a building is possible with the injection of grout underneath a pile foundation. The shape of the fractures seems to vary in various projects. Chapter 4 described theoretical considerations and presented some calculation models that show which phenomena can determine the width-length ratio for fractures. According to the models developed in that chapter, thin fractures and relatively low injection pressures can be expected for an impermeable filter cake of the grout. By contrast with fracturing rock, the yield stress and viscosity of the grout seems to be less important when fracturing in sand. The grout properties can be affected by the amount of cement, as shown in Chapter 5. Laboratory tests were set up to test the theoretical concepts and to generate quantitative information about injection pressures, fracture shapes and efficiency as a function of various parameters. In the laboratory experiments, the fracture grouting process was simulated at a laboratory scale.

Four test series were performed with a test set-up specially designed for this purpose. The test set-up was developed using an earlier set-up used to investigate hydraulic fracturing (Bezuijen et al., 2003). See Section 2.3.2.

The test set-ups for the first three series were identical. The third test series was performed by Khalid Eisa Gafar (Eisa, 2008). Some of the tests Eisa performed were part of the experimental programme of this research project and the results of these tests were important for the conclusions obtained from the laboratory tests. The results of these tests will be included in this thesis. Eisa (2008) also made a comparison with tests he performed at Cambridge, and performed tests using a pulsating injection strategy. This research is outside the scope of this thesis and will not be described here. Some modifications were introduced for the fourth series, as will be explained later.

The first series was performed to investigate the influence of various grout parameters (WCR and bentonite percentage) and the relative density of the sand on fracture shape and efficiency. The grout properties were varied over a wider range in the second series to investigate the effect of the grout properties on, once again, fracture shape and efficiency. The influence of the injection rate and the amount of sand above the injection tube was investigated in the third series. The results from the first three series, together with the results obtained from the literature (Eisa, 2008), showed that there was still a discrepancy between the laboratory results and the results obtained in the field described in Chapter 3. It was therefore decided to perform a fourth series in which the installation of the TAM was simulated better.

In addition to the four laboratory test series, three tests were performed in a CT scanner to study fracture growth during injection.

6.2 Aims of the test series

The aims of the test series were different for each series:

- The original aim of the first test series was to validate a numerical model for the development of fractures as developed by Grotenhuis (2004). The first tests showed that the model did not cover all the important mechanisms and that there was therefore a discrepancy between the model and the test results (Kleinlugtenbelt, 2005). The remaining tests were therefore performed to investigate the impact of various parameters on fracture shape and efficiency. It emerged that the injection pressure was much higher than anticipated. On the basis of tests with X-linked gel and bentonite slurry in sand, it was assumed that the injection pressure would be 3-5 times the vertical confining pressure (Bezuijen et al., 2003). Injection pressures were much higher for injections with cement-bentonite grout. This resulted in modifications to the injection system.
- The main objective of the second test series was to quantify the influence of the injection fluid. Ten tests were performed with different percentages of cement and bentonite in the injection fluid (the grout) (Sanders, 2007).
- After these two test series, Khalid Eisa (2008) performed another series of tests. He compared the results obtained with Baskarp sand with the ones for Cambridge sand and tested the influence of the injection rate, the influence of the amount of sand on top of the injection tube and the influence of dynamic injection on the shape of the fracture.
- The test series mentioned above generated consistent results. However, these results did not concur with field data. A site visit in Amsterdam during a compensation grouting trial – see Section 3.3 – revealed differences between the installation of TAMs in practice and installation during the tests. The literature (Wang and Dusseault 1994) indicates that this installation procedure may be important. The aim of the last test series was therefore to test the influence of the installation procedure.
- In addition to the above, a test series of three tests was performed using a CT scanner. The aim was to compare the results with the results of the test series without modelling the installation procedure and therefore to investigate the influence of the installation procedure and, in particular, the influence of the application of sleeve grout. Furthermore, the density variations measured in the grout were compared to those predicted with the theory described in Chapter 5.

6.3 Scaling

Although the literature does not discuss the scaling of model injection tests, the theory developed in Chapter 4 presents the opportunity to look at some scaling aspects. Equation (4.68) as derived in Section 4.10 can be used. This equation showed that the shape of the fracture, characterised by d/s (the ratio between thickness and length of the fracture), remains the same in the model and the prototype when the effective stress is the same (if this is not the case, pressure infiltration and pressure filtration will be different). Furthermore, grout and soil properties have to be the same, as well as the ratio w/Q, where w is the width of a planar fracture and Q the injection rate. This last requirement is difficult to achieve, because the width w is an outcome of the test and cannot be selected. Since the diameter of the tube in the model is three times smaller than in the prototype and the injection rate is similar in the model and the prototype, it is reasonable to assume that w/Q is slightly smaller in the model than in the prototype, as is the d/s ratio.

6.4 Test set-up

6.4.1 Test set-up in first three test series

A circular container with a diameter of 0.9 m was used for the tests (see Figure 6-2 and Figure 6-3). This container was filled with saturated sand up a height of 0.84 m. A PVC plate was placed on top of the sand sample. A watertight connection between the plate and the container was made using a rubber ring. This makes it possible to pressurise the sand sample using water pressure on the top plate, and therefore to simulate sand at a lower depth. The injection system in the laboratory set-up is comparable to the system developed for compensation grouting. A pipe with a rubber sleeve was used as the TAM. See Figure 6-4. The sleeve only allows outflow of the grout when grout pressure is higher than soil pressure. The injection nozzle was located 0.37 m above the bottom of the tank.
Tests were performed with Baskarp sand (d_{50} = 130 μm) with a relative density of 60% in most of the tests. Some tests in the third series were performed with "Cambridge sand" (d_{50} = 234 μm). See Section 6.4.3 for more information.

The sand was "pre-stressed" by applying a high vertical pressure before the test and relieving it to a representative in-situ value to achieve a higher K_0. This pre-stressing was only partly successful. The K_0 achieved with this procedure was around 1, as determined with the total stress transducers. See Section 6.4.1. Figure 6-1 shows, for experiment 1-2 (see Section 6.4.6 for the test numbering), the result of the total pressures measured during loading and unloading and the resulting K_0.

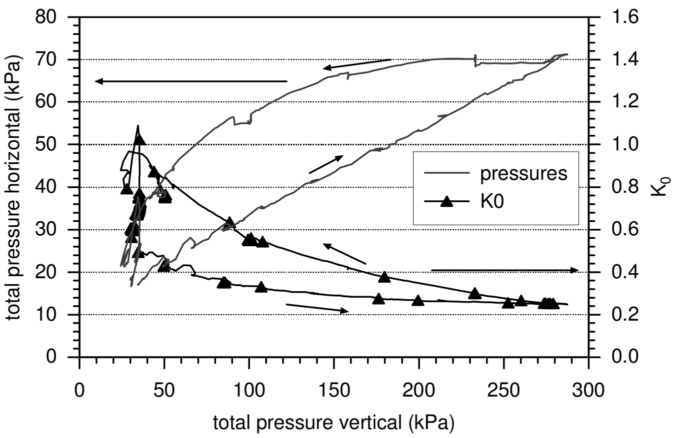

Figure 6-1: Loading and unloading of the sand sample before the test

During grout injection, K_0 at the location of the cell rises rapidly to values well above 1, and even to 4.5 in the case of dense sand. Pore pressure transducers and total stress transducers were installed at various locations in the container. See Figure 6-5. The horizontal and vertical stresses and K_0 were determined from the total stress transducers shown in Figure 6-5.

Two data acquisition systems were used to gather the data generated by the instruments: a low-frequency data acquisition system with a sample frequency of around 2 s and a high-frequency data acquisition system with a sample frequency of 0.01 s. The low-frequency data acquisition system was used to measure and store data during the whole of the test; the high-frequency system was used for measurements over a period of 40 s during the injection.

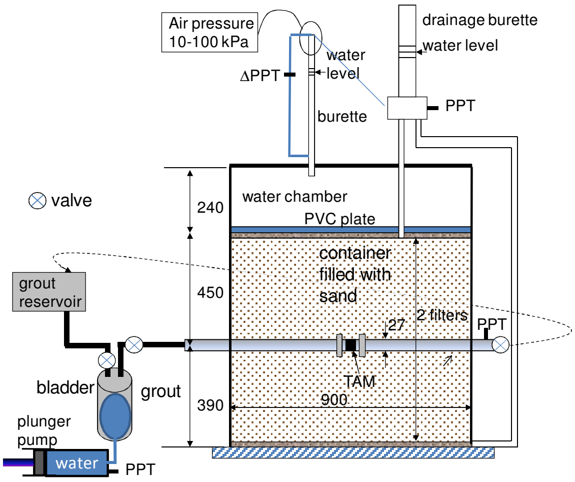

Figure 6-2: Set-up of the experiments. Note that changes in pore volume and sand volume can be measured as changes in the water levels (dimensions in mm).

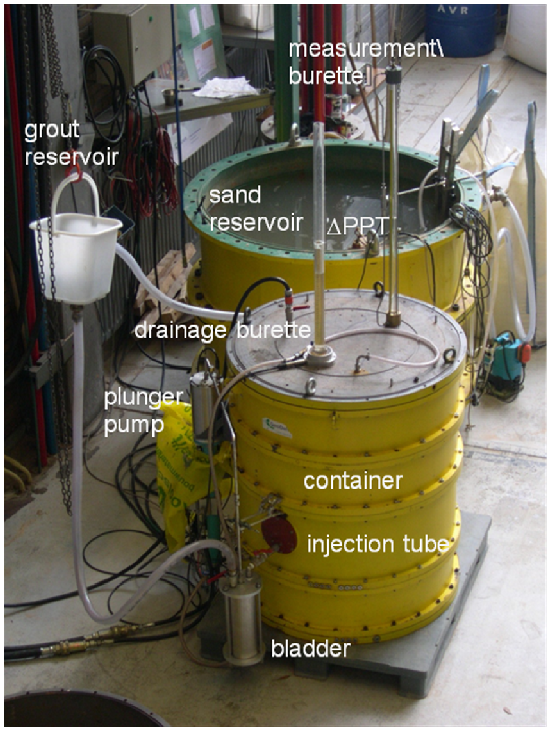

Figure 6-3: Picture of the set-up

Particular attention was paid to the measurement of the volumes. The increase in the volume of the sample due to the injection and the drainage of pore water was measured continuously during the tests. Two burettes were placed on top of the set-up to measure the volumes. In one of the burette the drainage water was collected. A pore pressure transducer measured the water pressure and therefore the water level in the burette. A second burette was connected with the water chamber at the top of the container. Here, a differential pressure transducer measured the water level in the burette.

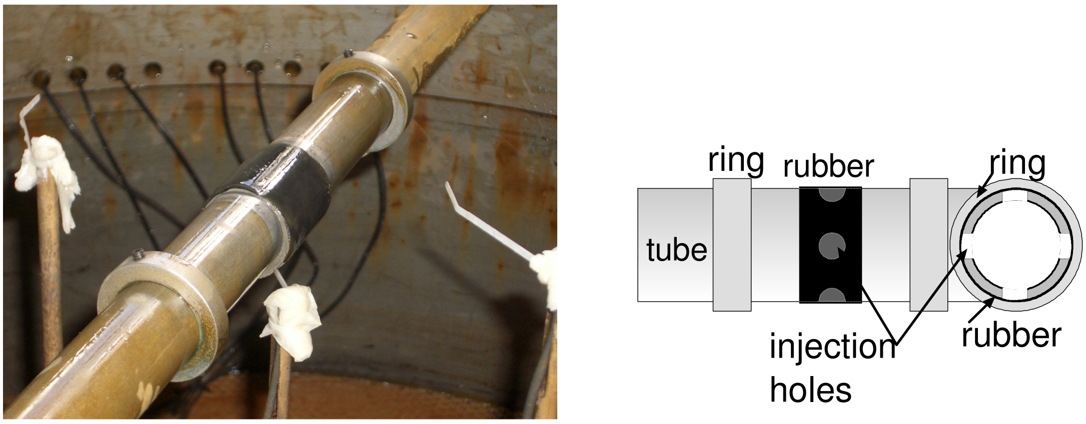

Figure 6-4: Injection system with rubber sleeve. The steel rings were placed on the tube to prevent grout flow along the tube.

Grout was injected using a plunger pump. This pump pumped water and a bladder was used to pump the grout into the system (see Figure 6-2). The bladder system was installed to prevent the granular particles in the grout from damaging the pump. The maximum injection pressure of the injection pump was 40 bar.

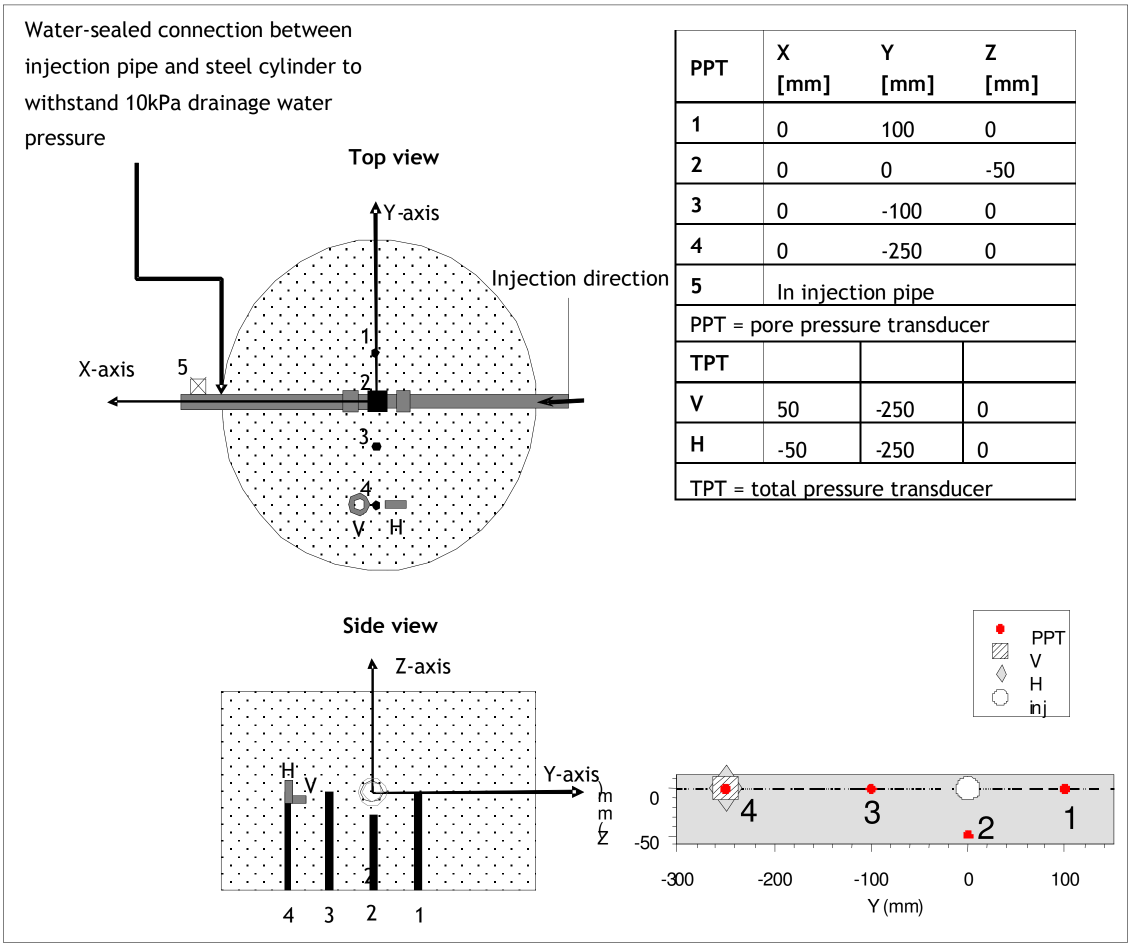

PPT	X [mm]	Y [mm]	Z [mm]
1	0	100	0
2	0	0	-50
3	0	-100	0
4	0	-250	0
5	In injection pipe		
PPT = pore pressure transducer			
TPT			
V	50	-250	0
H	-50	-250	0
TPT = total pressure transducer			

Figure 6-5. Position of the instruments with respect to the injection tube (inj). The numbered transducers are the pore pressure gauges, V measures the vertical pressure and H the horizontal pressure (modified from Kleinlugtenbelt, 2005).

The grout was allowed to harden for one day after the test before the sand was washed away and the shape of the injected grout became visible. There was no hardening of the grout in the tests without cement, or with only a small amount of cement. After the tests without or with little cement, the capillary forces in the sand were used to determine the shape of the fracture.

6.4.2 Test set-up for fourth test series

The test set-up was modified for the last test series – see Figure 6-6, Figure 6-7 and Figure 6-8 – to simulate the installation process. A second tube was constructed that fitted over the injection tube. This second tube simulates the casing that is used during the installation of the TAMs. Sleeve grout was injected between the tube that simulated the casing and the injection tube during the withdrawal of the "casing" before the injection experiment. Blitzdämmer® was used as the sleeve grout in the experiments, as in Amsterdam in the field.

Blitzdämmer® (further abbreviated to Dämmer), a product from Heidelberg Cement, is a hydraulically-setting premixed dry mortar made of natural raw materials. Its hydraulic binders are tailored to the clay component present in the inert rock flour. Combined with the high degree of fineness of the material, this produces a slurry with a flow capacity, even at relative low water contents. The product can be mixed to create a free-flowing suspension by adding water. It has comparable properties to bentonite-cement grout, but the permeability of the filter cake is considerably higher (one to two orders of magnitude). See Section 7.5.1. The relatively high permeability leads to the rapid consolidation of the material.

In these tests, the fracture started in the Dämmer and not in the sand. Furthermore, it is likely that there was unloading of the sand just around the Dämmer during the withdrawal of the second tube or casing. This unloading can be due to relatively low Dämmer pressure during the withdrawal of the casing or to pressure filtration from the Dämmer when it is still a liquid. This reduces the required injection pressure, as calculated by Wang and Dusseault (1994) on the basis of cavity expansion theory and described in Section 2.4.1.

The results from the third series, in which the changes included variations in the height of the sand in the container, indicated that the height of the sample had only a limited influence. It was therefore decided to conduct all the tests in this fourth series with a sand level of 210 mm above the injection tube instead of 450 mm. See Figure 6-6.

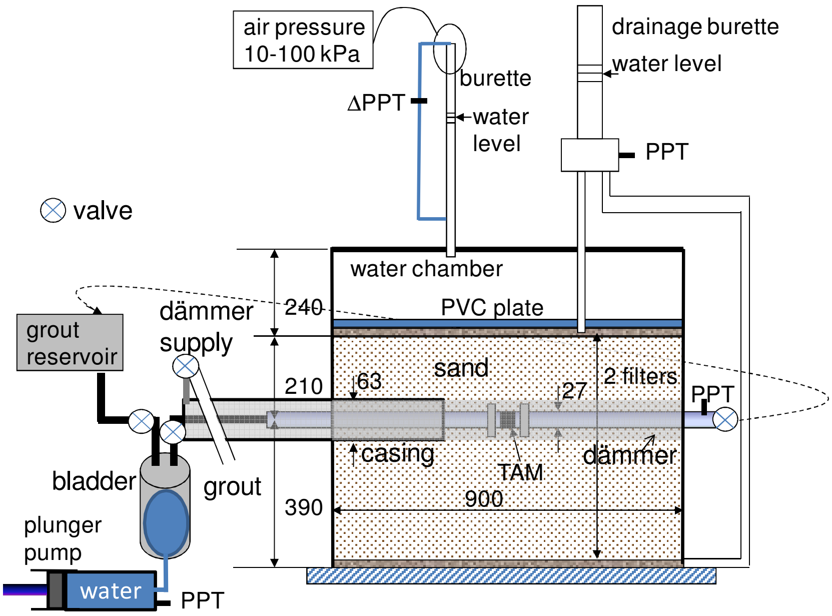

Figure 6-6: Modified set-up with Dämmer supply and casing to simulate installation (dimensions in mm)

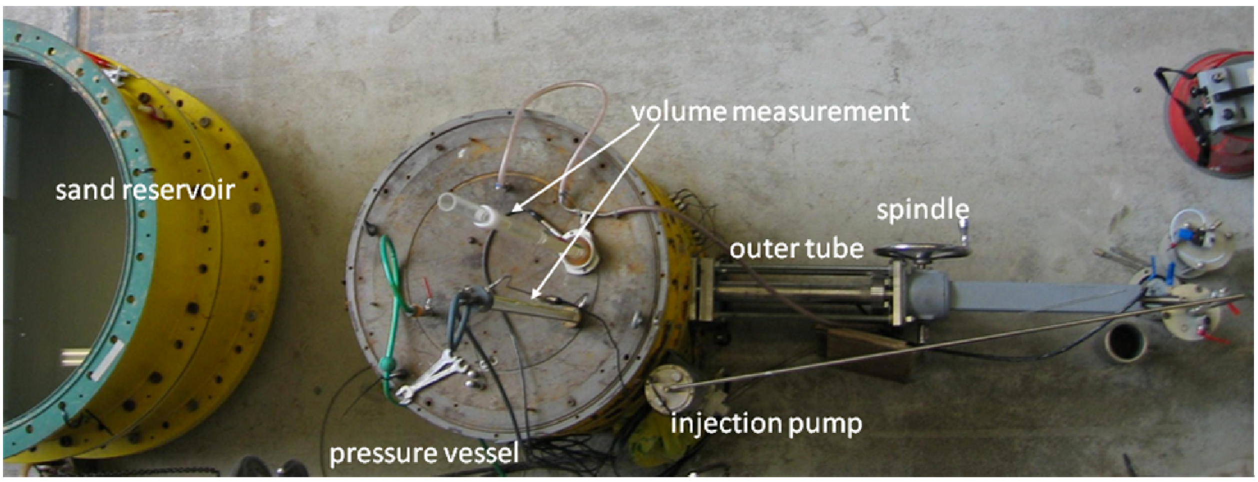

Figure 6-7: Top view of modified set-up for the fourth test series

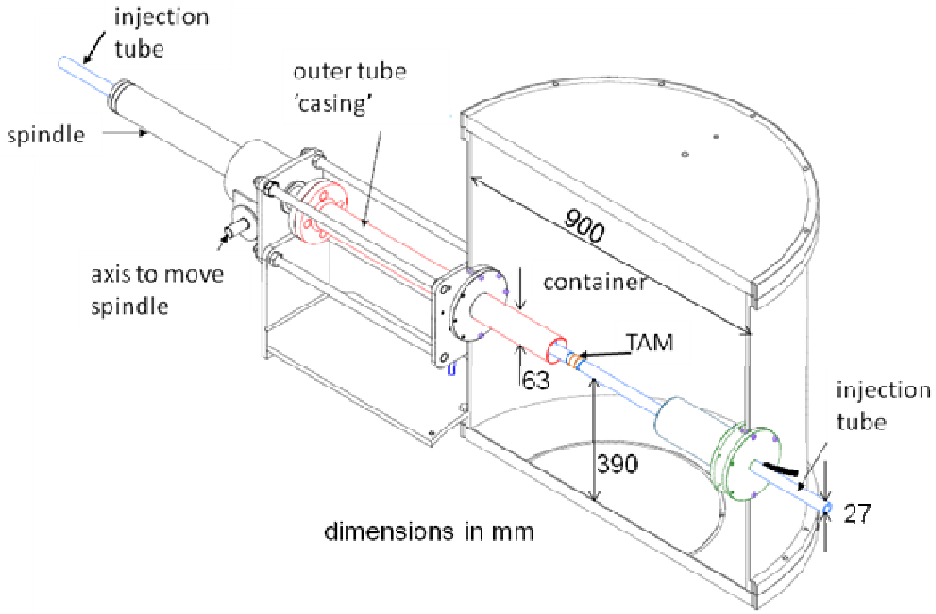

Figure 6-8 : 3-D sketch of the modified set-up

6.4.3 Sand and sand preparation

Most tests were run with Baskarp 7 sand. The d_{15} of this sand is 95 µm and the d_{50} is 130 µm. Figure 6-9 shows a particle size distribution curve for this sand.

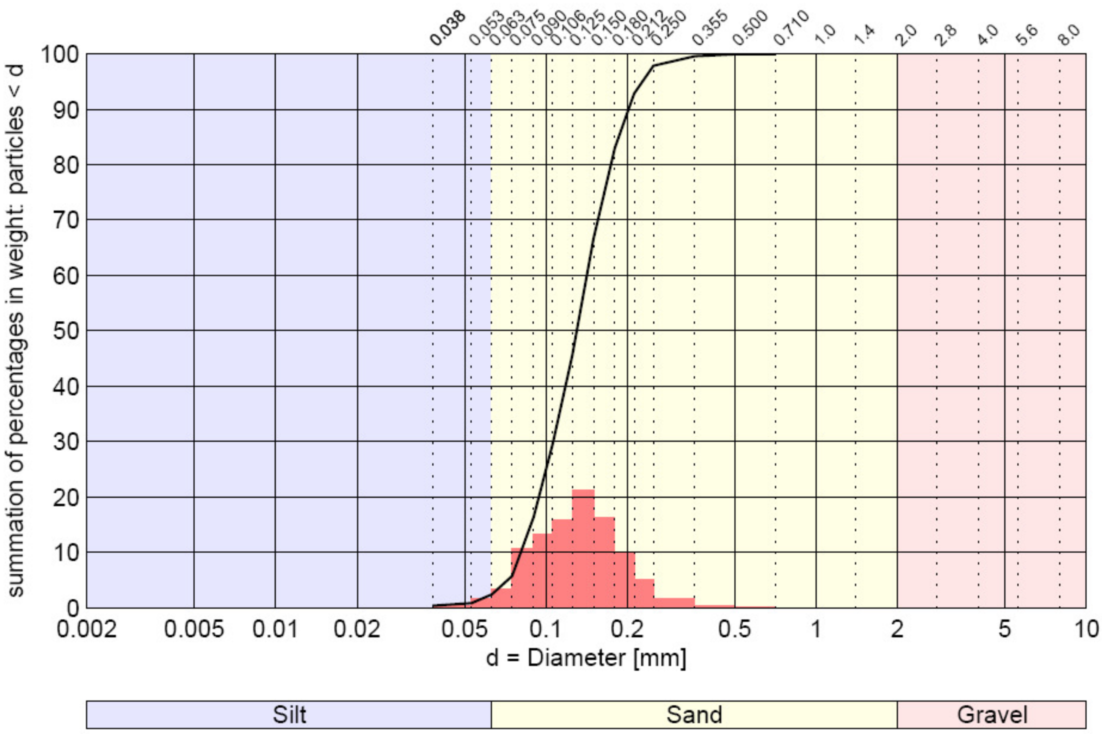

Figure 6-9: Sieve curve of the Baskarp sand used for the experiments

The friction angle and permeability were determined for different relative densities, as is shown in Figure 6-10 and Figure 6-11.

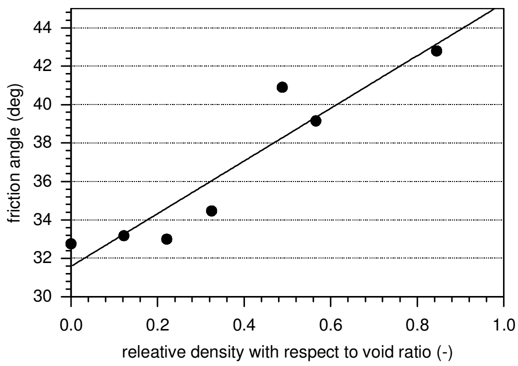

Figure 6-10: Friction angle as a function of the relative density for Baskarp sand

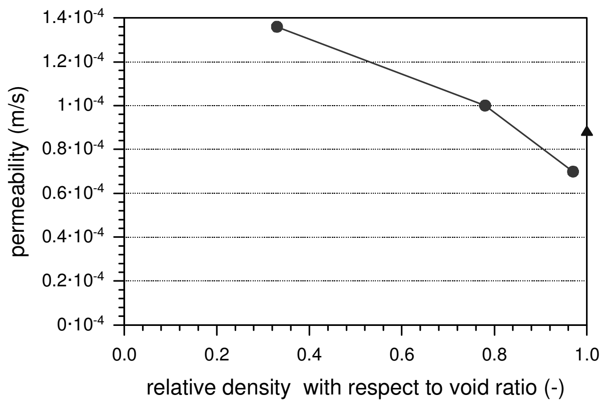

Figure 6-11: Permeability of Baskarp sand as a function of the relative density for 2 different samples (red and blue dots)

Table 11 presents other properties of the sand. A few tests in the third series were run with "Cambridge sand" (this was in fact type D Leighton Buzzard sand) with a d_{50} of 234 µm and the properties presented in Table 11 (Eisa, 2008). No major differences were found between the two types of sand. Previous tests with bentonite slurry as the fracturing liquid also proved to be fairly insensitive to the type of sand (Bezuijen, 2003) as long as the relative density was comparable. It is therefore assumed that the results of the tests are valid for medium fine sand in general.

Table 11: Properties of Baskarp and Cambridge sand (the permeability of the Cambridge sand was estimated using a correlation formula (Eisa, 2008))

Property	Baskarp	Cambridge	Dim.
d_{50}	130	234	µm
d_{15}	95	150	µm
min. porosity	34	34.0	%
max. porosity	46.9	45.1	%
friction angle			
Rd =50%	40.9		deg
R_d=80%	42.8		deg
R_d=70%		42.4	deg
R_d=93%		48.3	deg
Permeability			
R_d =50%	$1.2*10^{-4}$	$6*10^{-4}$	m/s
R_d=80%	$9.8*10^{-4}$	**n.d.**	m/s

A homogeneous soil sample is very important for the results of the tests. The tests from 2003 (Bezuijen, 2003) and the first test series demonstrated the impact of relative density on the results. The soil sample must therefore be homogeneous and reproducible. In the first test series, a dry pluviation method was used. This method had been tested before (Poel van der and Schenkeveld, 1998). The homogeneity of the soil samples also emerged from CT scans made of soil samples using a comparable technique. See Section 6.10.

In most tests, a "wet pluviation method" was used (Rietdijk et al., 2010). This is a further development of the dry pluviation method. The advantage of the wet pluviation method is that there is no need to dry the sand between the tests. The method results in a loose sand model due to the raining of sand under water. This sand sample is compacted by dropping the model container on the floor from approximately 1 cm height. Hitting the floor results in liquefaction of the sand, after which it settles in a higher density. Sanders (2007) has described the details of this method. The sample was dropped between 15 to 20 times before a relative density of around 60% was reached.

Above the pipe there will hardly be any difference in density. This was also clear from the CT scans. Below the pipe, there can be some disturbance. However, in previous experiments with a cylinder with a diameter of 122 mm in a 0.6 m diameter container filled with sand, it was concluded that, with the preparation method described above, the 122 mm cylinder had no significant influence on the density of the sand (Schenkeveld, 1996). Porosity underneath the cylinder proved to be around 2 per cent lower – and so density was higher – than next to the cylinder. Given these results, it is to be expected that this disturbance in only limited (up to 10 per cent in relative density). The resulting densities were measured in three tests (Test 2-8, 2-9 and 2-10) using a ring with a known volume at various locations in the container. The results are plotted in Figure 6-12. Tests 8 and 9 showed a slight increase in relative density with depth. At the injection point (0.39 m above the bottom of the container) the relative density was 62%, which is equal to the average value in the Table of tests in Appendix 1. The relative density in Test 10 varied more. The relative density at the injection point is approximately 60%, which is slightly higher than the average value of 58%.

The fourth series, with the casing around the TAM, showed that the homogeneity of the sand sample with respect to the porosity can be influenced by the way the densification is performed. Dropping the container and pallet (see Figure 6-3) from a low height (0.01 m) flat onto the floor resulted in a more homogeneous sample than when the container was dropped over a larger distance (0.02 m) over which it was difficult to keep the container and pallet horizontal.

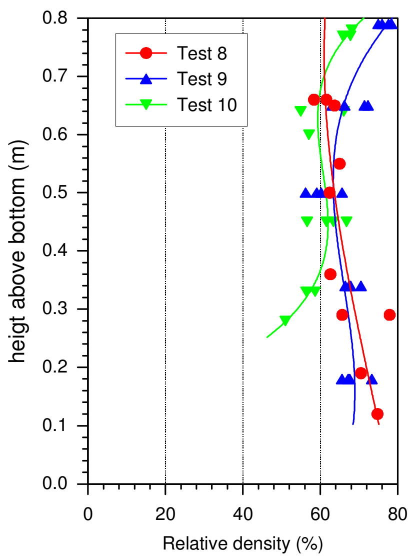

Figure 6-12: Relative density as a function of height measured in various tests

It emerged that the relative density found in the three tests is quite similar and that it is also reasonably uniform over the height. The injection tube was located at 0.36 m from the bottom. This means that it is in the area where the densities are comparable in the three tests. Only in Test 10 was the relative density rather low at the lower end of the soil sample. No reason was found for this relatively low density.

The method used requires the weighing of the container with water, and with water and sand. Sanders (2007) made an error analysis and found that errors of 3% in relative density due to measurement errors are possible. However, in Test 2-5 there was a systematic weighing error due to a problem with the weighing equipment. It emerged that the number of times the container is dropped on the floor is an accurate measure for the density for a given type of sand. This number was therefore monitored and the equipment was checked when deviations occurred.

The preparation method was different from the one used at Cambridge University (Eisa, 2008). In Cambridge, dry sand raining is used. It is known from the literature (Garnier, 2002) that dry sand raining also leads to homogeneous sand samples. The advantage of dry sand raining is that very dense samples can also be obtained with a relative density of up to 100%. With wet sand raining and densification by dropping, the maximum relative density that can be achieved is about 70% for the Baskarp sand used in the tests. Wet sand raining was chosen because, in tests with saturated sand, the dry sand raining method is quite labour-intensive since the sand has to be saturated before the test and dried afterwards. Neither saturation nor drying is necessary with wet sand raining and the quality (homogeneity, reproducibility) of the samples is similar.

6.4.4 Test procedure

The test procedure was the same for all test series except the last one, which included some extra steps to simulate the installation procedure.

The grout mortar was prepared after preparation of the soil sample. Bentonite slurry was prepared by mixing the required amount of bentonite with water and ripening for at least 12 hours. Twenty minutes before the injection, the cement was added to the bentonite slurry and the injection system was filled with the mortar. Sanders (2007) found that the time between the adding of the cement and the test has an effect on the filtration properties of the grout and so a fixed time was chosen. The grout mortar is circulated in the injection system (still without injection) to de-air the injection system. Injection then took place with a predefined volume and injection rate. Shortly after injection, the rheology of the grout and permeability of the grout cake (the last one in a pressure filtration test, as was seen in Chapter 5) were measured. The injected grout was left to harden for at least 24 hours. The sand was then removed and the grout body was investigated. The sand was removed by rinsing the sample with water. With careful rinsing, all the sand could be removed, apart from the sand that stuck together due to the pressure infiltration of grout into the sand. Increasing the water velocity during rinsing removed all the sand, leaving behind the grout body. Rinsing at a higher velocity was only possible when the grout contained enough cement, more than 20% (WCR values of less than 5). With less cement, the grout body was not strong enough and collapsed when the sand was removed.

The fourth test series included some additional steps in the procedure. First, the sand sample was prepared as in the earlier tests. Blitzdämmer (further abbreviated to Dämmer) was used as the sleeve grout and injected into the space between the "casing" and the injection tube. After the injection of the Dämmer, pressure on the Dämmer was kept constant. As this pressure was applied, the casing was removed and the Dämmer was allowed to harden for 3 to 24 hours, depending on the test. In the meantime, the bentonite slurry was prepared as described above and injection took place.

6.4.5 Tests performed

All the tests performed in the series 1, 2, 3 and 4 are summarised in Appendix A.

Theoretical considerations – see Chapter 4 and the literature survey in Chapter 2 – and the results from the first test series had shown that fracturing could only be expected when grouts with a high WCR (more than 2) were used. Most attention therefore focused on these grouts. According to the literature based on different injection materials (Bezuijen et al. 2003), the injection pressure has to be equal to the pore pressure and approximately 3-5 times the vertical effective stress. Since the planned vertical effective stress applied was 100 kPa and the pore pressure just a few kPa in all tests, an injection pressure of a few kPa above 500 kPa should be sufficient. However, this proved not to be the case and the confining stress had to be lowered in the first test series to make an injection. In the second test series the maximum allowable pressure of the pump was increased up to 4,000 kPa so that higher pressures could be applied. Injection pressures of up to 2,900 kPa were found.

In one test (Test 2-3), two injections were performed in one soil sample from the same injection point, the second one day after the first. All other tests involved just one injection.

A bentonite-water-cement mixture was used in most of the tests. One test (Test 2-4) was performed with cross-linked gel, an injection liquid that is used in the oil industry to create hydraulic fractures. Some tests were performed with fly ash instead of cement. The idea was that, with fly ash, there is less calcium in the grout and therefore the grout is less permeable. For the same reason, retarder was used in a number of tests. Silica flour was used in some tests to minimise pressure infiltration.

6.4.6 Test numbering

All the tests were performed as part of a Masters or a doctorate project. These tests are therefore also described in the Masters reports of Kleinlugtenbelt (2005) (first series) and Sanders (2007) (second series) and the doctorate report of Eisa (2008) (third series). Only the fourth and final series has not yet been published in a final Masters or doctorate report. An interim report by Au and Massini (2008) was drafted on this series after the tests.

To compare the tests, all the tests were assigned a series number and a test number in the order set out in the previous paragraph. This means that Test 2-7 is Test 7 in Sanders' Masters report (2007).

6.5 Introduction to test results

The various test series can be seen as attempts to create long and thin fractures as described in the literature, as in Antwerp, for example – see Section 3.4 – and of the kind found more or less by accident at the Hubertus Tunnel. See Section 3.5.

The first series did not result in long and thin fractures. It created no fractures at all, or relatively short and thick fractures. The composition of the grout injected had a clear effect on the shape of the fractures, as will be described later. Quite a number of tests resulted more in compaction grouting than in fracture grouting.

The first tests in the second series also created no real fractures and so doubts arose about the test set-up. A test was therefore performed with X-linked gel, a liquid that is used in the oil industry for fracturing and that worked well in hydraulic fracturing tests performed at Delft University for the Delfrac project (Bolholi and Pater, 2006.). The test with X-linked gel also created fractures in the set-up for this study – see Figure 6-29 – and it was therefore concluded that the problem was not related to the set-up. The remaining tests in the second test series showed that fracturing with a cement-bentonite slurry was possible, but only with high WCR values. Reducing the WCR value from 20 to 2 showed that pressure infiltration decreases and fractures become shorter and thicker. At a WCR of 2 the grout body had an irregular shape that is expected more as the result of compaction grouting than of fracture grouting.

In the third test series, the results were compared with results obtained in Cambridge and another type of sand was tested. It was concluded that the results obtained in the test set-up for this study were rather similar to the results obtained in Cambridge.

The fourth test series was performed because it was realised that the effective stress around the TAM in the field can be lower than the in situ stress. This could be caused by the installation of the TAMs and the consolidation of the grout around the TAMs. The last test series simulated the installation of the TAMs using a casing and the injection of Blitzdämmer. In this series, lower soil stresses around the cavity were found and so the fractures were thinner.

During the course of the research, it became clear that it is not certain that long and thin fractures are a feature of all field applications. For example, the description by Kleinlugtenbelt of a compensation grouting project in Perth (Kleinlugtenbelt, 2006) also suggests that the resulting injection process has more in common with compaction grouting than with fracture grouting. It also became clear that the grout shapes found in this research are comparable with the results of other laboratories. See Section 2.3.

Since the aim of this research is to acquire a more fundamental understanding of the grouting process, the results will not be presented and evaluated with only the practical application of compensation grouting in mind (the efficiency of the grouting process, for example). The results will also be evaluated independently and comparisons will be made with the results of other laboratory tests looking at compensation grouting.

6.6 First test series

6.6.1 General

A clear result from the first test series (Kleinlugtenbelt, 2005) was that the theory as developed by Grotenhuis (2004) was not correct in quantitative terms. This theory predicted long and thin fractures. However, these were not found in the tests. A typical result for this series is shown in Figure 6-13 and Figure 6-14. The figures show the result of a test that can hardly be described as a fracture (Figure 6-13) and the test with the most "fracture"-like behaviour in this first test series (Figure 6-14). In the first test, it looked as though the fractures tended to develop, but that this process was stopped before the fracture got any longer. Later in this research, it emerged that, by contrast with what is usual in practice, the bentonite had not been allowed to "ripen" in the water for 24 hours. Since the ripening was only performed for Test 1-9 and Test 1-10, the permeability of most of the grout cakes was relatively high.

The first four tests in this series can be seen as start-up tests for getting the equipment ready. In the remaining tests, the relative density of the sand, the percentage of bentonite and the injection rate were varied to investigate how these changes affect the shape of the fracture.

Figure 6-13: Grout body, Test 1-5

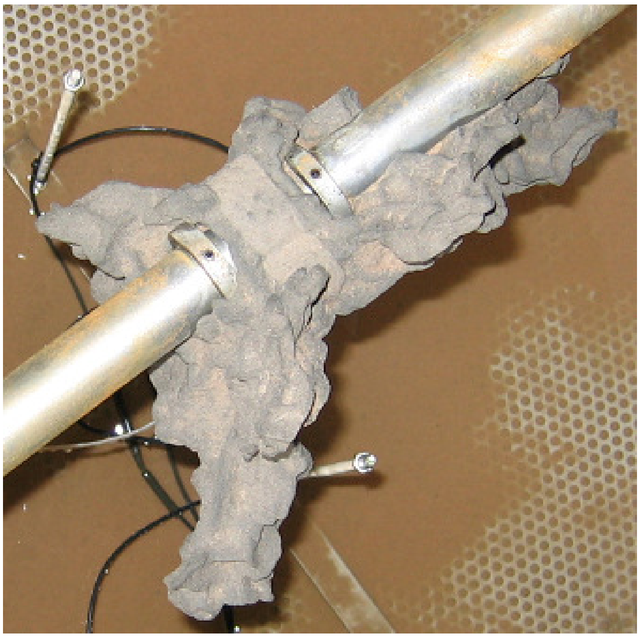

Figure 6-14: Grout body, Test 1-8

6.6.2 Typical measurement results

Figure 6-15 and Figure 6-16 show typical measurements during a test. The increase in the vertical total stress is mainly caused by the increase in the pore pressure in the sand. The lower plots in Figure 6-15 and Figure 6-16 show the measured volumes. It emerged that, in Test 1-10, most of the injected grout volume was traced back to the volume of drainage water and that it did not therefore contribute to the volume increase in the sand body. With 670 cc of grout injected, less than 100 cc contributed to a volume increase, and so efficiency was low. Efficiency was better in Test 1-7 (Figure 6-15). Efficiency falls as injection stops because of the filtration of the injected grout volume and the ongoing densification of the sand, as can be seen from the drainage of the sand.

6.6.3 Injection pressures

The test results also showed that injection pressures were much higher than predicted. On the basis of results from tests with bentonite and cross-linked gel (Bezuijen et al., 2003), an injection pressure of 3–5 times the confining stress was expected. However, the actual values were between 7.2 for the loose sand (relative density 40%) and as high as 62.8 for the dense sand (relative density 75%). See Figure 6-17. At the beginning of the tests, the high injection pressures required could not be obtained with the injection system. So Tests 1-1 to 1-6 (incl.) and Test 1-9 were performed with a vertical total confining stress that was approximately 25 kPa (Test 1-1 to Test 1-5 and 1-9) or 50 kPa (Test 1-6). Since the tests were performed at different confining pressures, the injection pressures are stated not only as absolute values but as ratios to the vertical confining stress in Figure 6-17. Tests 1-1 and 1-2 failed: Test 1-1 because there was no grout injection and Test 1-2 because the measurement of the injection pressure failed (Kleinlugtenbelt 2005), so there is no plot for pressure registration. In Test 1-4, the injection was limited by the pump capacity and so the pressure remained high. The results presented as a pressure ratio between the injection pressure and the total confining stress show clearly that the dense sand results in the highest pressure ratios and the loose sand results in the lowest pressure ratios. All the other tests had comparable pressure ratios. In the figure, the pressure rises at different times in the various experiments. This is because the time is the time after starting the high-frequency data acquisition system and is not related to the start of the plunger movement.

When the injection stops, the pressure in the injection system falls rapidly. Most of the excess pressure is gone within 5 to 6 seconds. This means that the driving force for the pressure filtration also falls rapidly and pressure filtration is confined to a relatively thin layer. This can be seen in Figure 6-18 (Kleinlugtenbelt, 2005) and it also emerged from the CT scan that was taken of the grout sample from Test 1-5. See Figure 6-72.

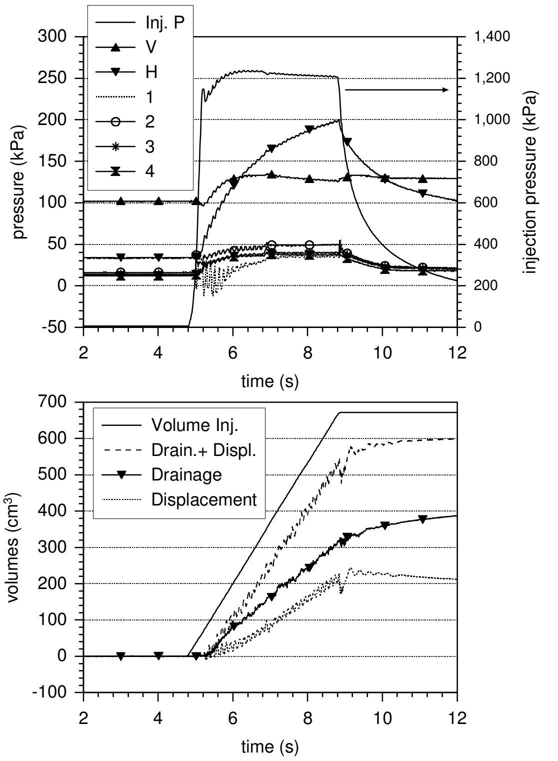

Medium dense sand (R_d = 60%), Test 1-7

Figure 6-15: Example of measured pressures and volume changes during a test. V is the vertical pressure, H the horizontal pressure and 1, 3 and 4 are pore pressure gauges. Volume Inj. is the injected volume, drainage what comes out of the drain, and displacement gives the volume change measured by the displacement of the top plate.

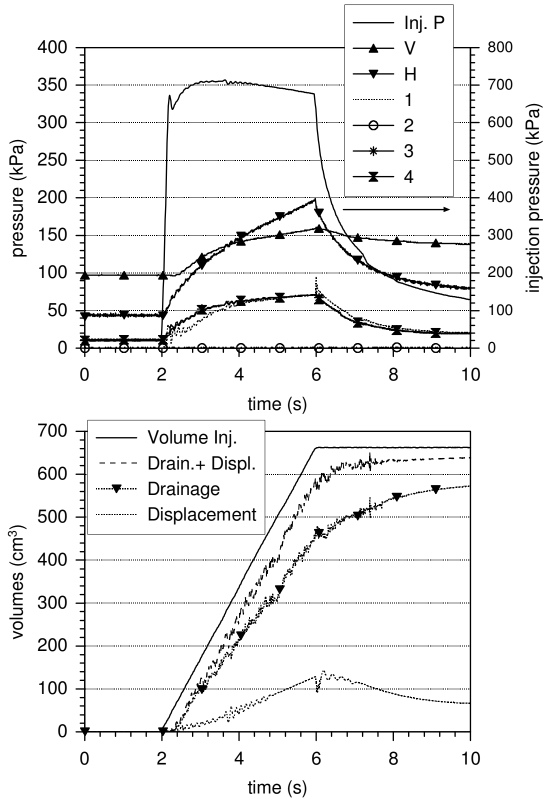

Loose sand (R_d = 40%), Test 1-10

Figure 6-16. Result of test presented as in Figure 6-15, but now for loose sand

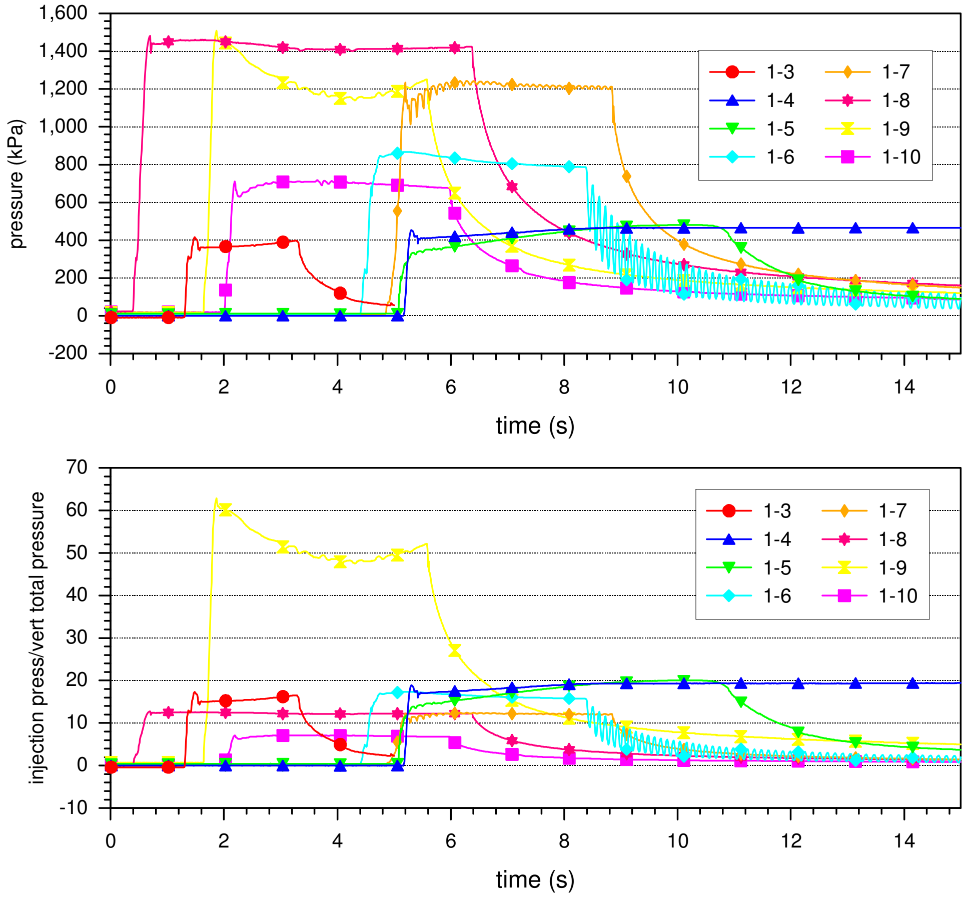

Figure 6-17: First test series. Injection pressures and relative pressures relative to the vertical total stress

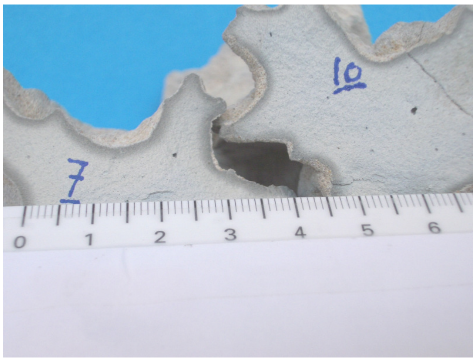

Figure 6-18: Test 1-7 and 1-10: broken grout bodies.
The colour differences indicate density differences due to pressure filtration.

6.6.4 Pore pressures and effective stresses

In most cases the pore pressure gauges showed limited variations during injection. The usual range was about 20 to 50 kPa, as shown in Figure 6-15 and Figure 6-16. The density of the sand affected pore pressures. See Figure 6-19. This figure shows the pore pressures measured in the last three tests of the first series, in which the densities of the sand model were different. In Test 1-8, in which the density was moderate (Rd=60%), the pore pressure for PPT 1 fell at the beginning of the test, probably due to dilatancy. Later during the test, the pore pressures rose at all locations due to water being expelled from the grout by the injection pressure on the grout. In Test 1-9, which was performed in dense sand (Rd=75%), dilatancy was dominant during most of the injection period. Test 1-10 in loose sand (Rd=40%) shows hardly any dilatancy. In this test,

there was certainly densification of the sand also, leading to a higher pore pressure during injection than in Test 1-8.
All pressure changes were relatively limited compared to the injection pressure, which was several hundreds of kPa in all cases. Figure 6-20 shows the influence of pore pressure on vertical effective stress. During injection, the pore pressure may affect the injection pressure by changing the effective stress. An increase in pore pressure will lead to a decrease in effective stress. The results in Figure 6-20 show that the pore pressures do have some influence on the vertical effective stress, albeit a limited one. The horizontal total stress increases much more than the vertical effective stress during injection and reaches higher values than the vertical stress. In relative terms, therefore, the horizontal stress will be influenced even less by the pore pressure generated during the injection process. It was therefore concluded that the pore pressures have only a limited effect on the fracturing process.

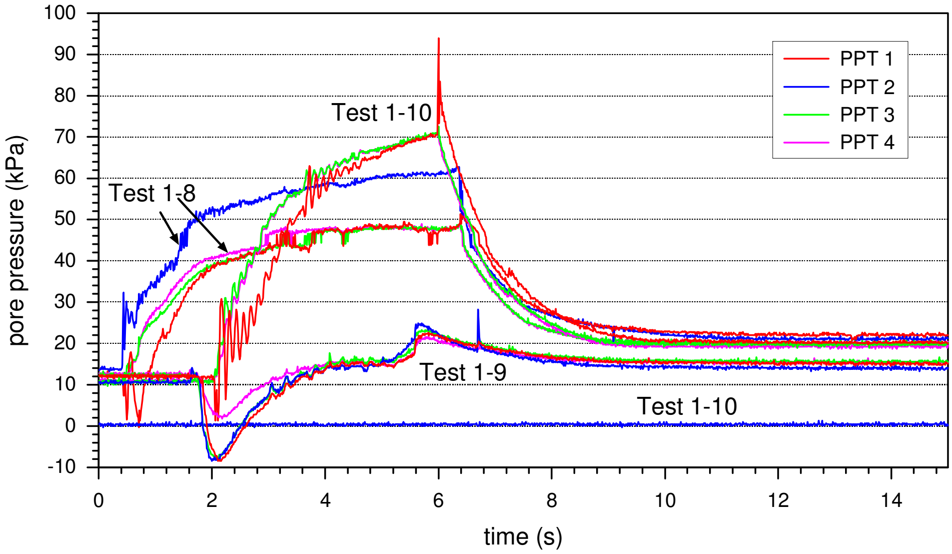

Figure 6-19: Pore pressures measured in the last three tests of the first series. (Test 1-8: Rd=60%, Test 1-9: Rd=75%, Test 1-10 Rd=40%). PPT 2 failed in Test 1-10.

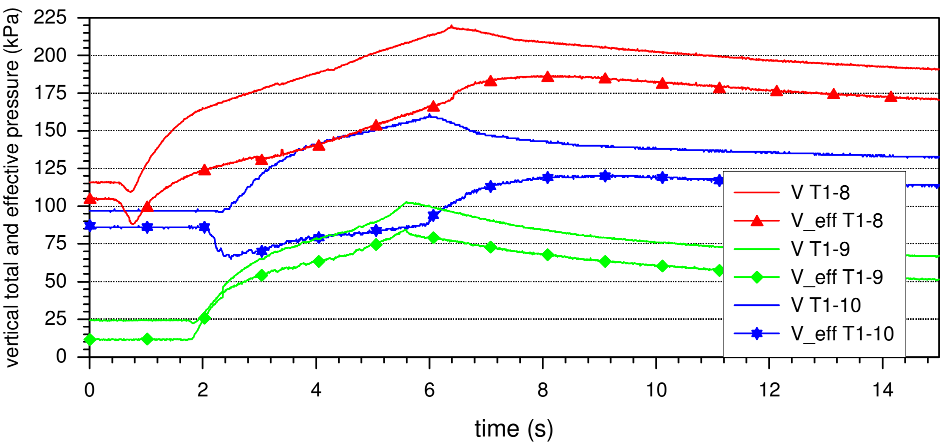

Figure 6-20: Vertical stress (V) and vertical effective stress (V_eff) measured in the last three tests of the first series

The pore pressure at the end of each experiment was slightly higher than the pore pressure at the beginning of the experiment. This does not mean that there was still some excess pore pressure that has to drain away. This phenomenon is caused by the set-up of the experiment. The drainage water was collected in a burette that was connected to the drain, causing an increase in the water pressure in the sample. The higher the water in the burette, the higher the pore water pressure, and so the increase in pore water pressure was lowest in the test with dense sand, where there was hardly any compaction and therefore hardly any drainage.

6.6.5 Shape of fractures

In Test 1-1 no grout was injected at all because the maximum possible injection pressure that could be delivered by the pump was too low. Tests 1-2 to 1-5 resulted in very rounded forms in which fractures hardly even began. Cake permeability was relatively high ($1–2.10^{-7}$ m/s). In the light of the theoretical results described in Section 4.10, it is understandable that, given this cake permeability, fractures could not be expected. In tests 1-6 to 1-9, cake permeability dropped from 5.10^{-8} to $1.4*10^{-8}$ m/s. Here, the shapes of the grout bodies look like short, thick fractures. In all tests, the grout body is longer in the direction of the tube and shorter perpendicular to the tube. The differences between the various tests were only small.

A remarkable result of the tests from the first series is that the rubber ring was visible in the grout body in most of the tests. See Figure 6-13 and Figure 6-14. In these tests, the ring itself was still at its original location around the tube, but it looks as if it was present around the grout. The most likely explanation is that the imprint of the ring in the grout is a "negative" from the shape of the sand. Before the grouting, the sand was present around the rubber ring. The injection pushed the sand away from the ring, but since there are only parts that are deformed and most of the sand retained its original shape (with the rubber "imprint"), the original form remained intact and is found later as a "negative" in the grout. Figure 6-21 proves that deformation was limited. It shows the result of a CT scan which will be discussed in greater detail in Section 6.10.4. The grey area in the middle is the injection tube and there are two identical circles in the corners of the grout body. These circles show that the sand did not deform at these locations. The circular shape it acquired from the injection tube was simply displaced without any deformation and it is only between the circles that there was deformation. This deformation must also have been gradual because the imprint of the rubber ring is also visible in the deformed area. See Figure 6-22. It was only at the lower end, where a fracture began, that the imprint could no longer be found. See Figure 6-13.

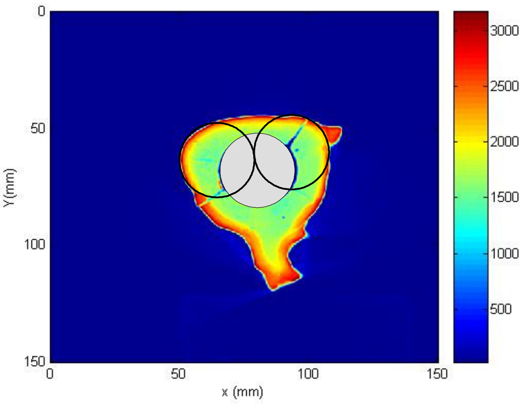

Figure 6-21: Result of CT scan with circles to show areas without deformation

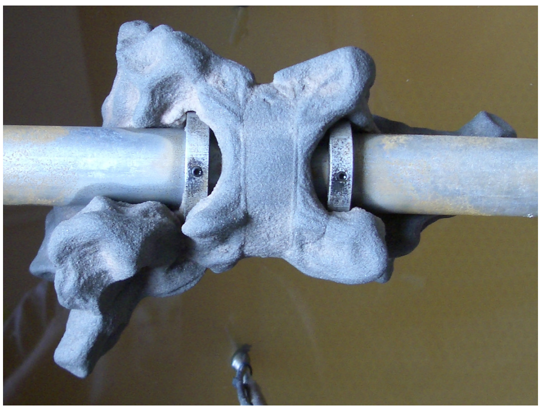

Figure 6-22: Top view of Test 5

6.6.6 Ratio between vertical and horizontal stress, K_0

The stress distribution in the sand sample will change during the test. The horizontal and vertical pressures were measured at one location only, and the results from that measurement cannot be more than an indication of what happened to the stresses in the soil sample. However, it is useful to compare the results from different tests. Figure 6-23 shows the result for K_0 determined with the total pressure transducers and PPT 4. The results show that, as could be expected, K_0 was highest in the test with dense sand (Test 1-9). In this test, the starting value for K_0 is already well above 1. In all tests, a value of above 1 was reached. The usual assumption is that a K_0 below 1 gives vertical fractures and a K_0 above 1 gives horizontal fractures. That would mean that Test 1-9 should result in only horizontal fractures. This proved not to be the case, as can be seen in Figure 6-24 and Figure 6-25, which show the excavated grout sample from Test 1-9 (Kleinlugtenbelt, 2005). The fracture is oriented horizontally, but it certainly has some vertical branches also.

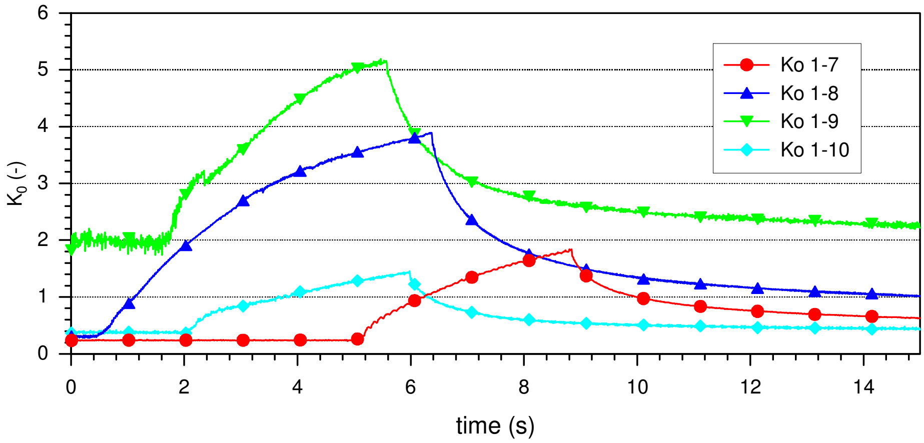

Figure 6-23: K_0 as measured in various tests in the first series

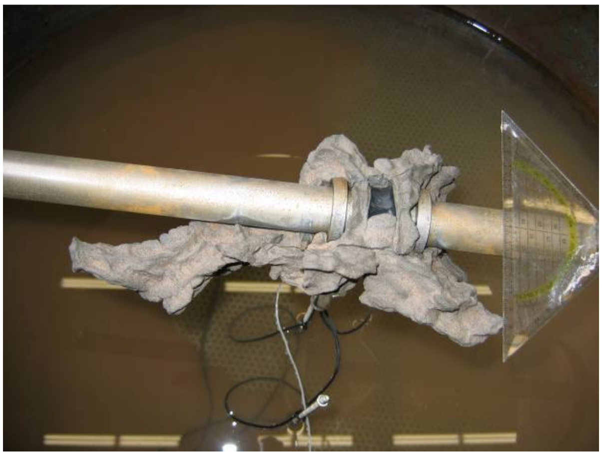

Figure 6-24: Horizontally and vertically oriented fracture of Test 9 (angled view)

Figure 6-25: Excavated grout fracture in Test 9 (top view)

6.6.7 *The influence of the relative density of the sand*

Most of the tests in all the series were performed in sand with a relative density of 60–70%. In the tests, most attention was focused on the impact of the grout properties on the results. In the first test series, the density of the sand was also varied. Tests were conducted with relative densities of 40, 60 and 75%. It emerged that relative density has a major impact on injection pressure. It has already been seen here that injection pressure increases with relative density. This relationship is plotted in Figure 6-26. Furthermore, the efficiency of the grouting process increases with increasing relative density. See Figure 6-27.

The relative injection pressure increases because the denser sand will have a higher friction angle and also behave in a more dilative way during injection. All the tests showed, at least in part, cavity expansion behaviour. According to cavity expansion theory (Vesic, 1972) both dilatancy and the friction angle lead to an increase of the injection pressure. Using the equations derived by Vesic, it emerged that the increase in dilatancy was a particularly important factor in higher injection pressures.

Efficiency increases when injecting in sand with a higher relative density because, in loose sand, the injection will also cause compaction of the sand. In dense sand, compaction will be much lower.

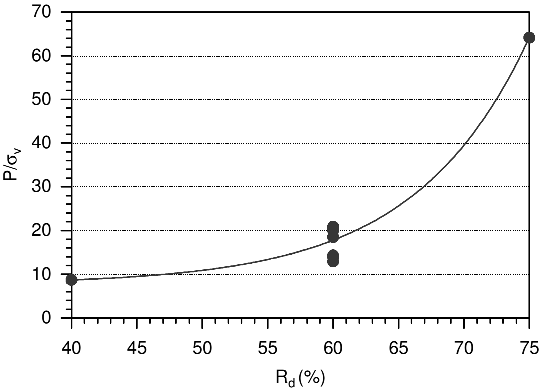

Figure 6-26: Ratio of injection pressure/vertical confinement pressure as a function of relative density

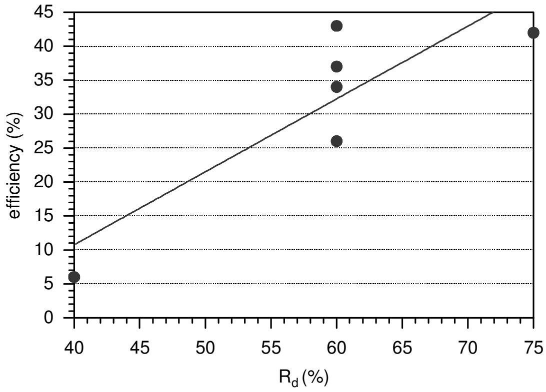

Figure 6-27: Efficiency as a function of relative density

6.7 Second Series

6.7.1 General

Since the first test series did not find much of a difference in the shape of the "fractures" created, it was decided to conduct a more systematic investigation in the second series of the influence of the grout properties on the fractures. Most tests in this series were performed with a comparable relative density of the sand sample: values varied between 58 and 69% (the exception was Test 2-1, in which the relative density was 76%). Two tests were performed with fly ash instead of cement, because the permeability of a bentonite/fly-ash cake is lower than that of a cement-bentonite cake. The percentage of bentonite with respect to the water varied from 6.2 to 12%. However, more importantly, the water-cement ratio varied from 2 to 200. The WCR was varied over such a wide range because small-scale tests (Sanders, 2007) and pressure filtration tests (see Chapter 5) had shown that the cement affects the bentonite. The permeability of the grout cake becomes higher with more cement, as was described in Section 4.9 and 4.10. This affects the shape of the fractures.

Apart from the variation in bentonite and cement, the influence of a second injection in the same soil sample was investigated and a test was performed with X-linked gel, a fracturing fluid from oil industry.

The wider variation in the input parameters was also reflected in the results. This test series did not have a "typical" result. Results differed significantly according to the different injection liquids.

6.7.2 Injection pressures

Figure 6-28 shows the injection pressures measured during the second series. All tests were performed with a vertical confining stress of 100 kPa. This means that the ratio between the injection pressure and the confining pressure is 1% of the measured injection pressure in kPa. In Figure 6-28 it can be seen that this ratio varies from 7 to 29. Clearly, the test with the X-linked gel resulted in the lowest injection pressures. This test resulted in thin fractures only. The higher the injection pressure, the thicker the fractures were, as can be seen in Figure 6-29. This concurs with the theory developed in Section 4.10. There is one exception: the peak pressure in Test 2-9 is higher than in Test 2-10, probably due to slightly higher compaction of the sand in Test 2-9. Furthermore, the influence of the grout on permeability is not very high at higher cement contents (i.e. lower WCRs). See Section 5.5.

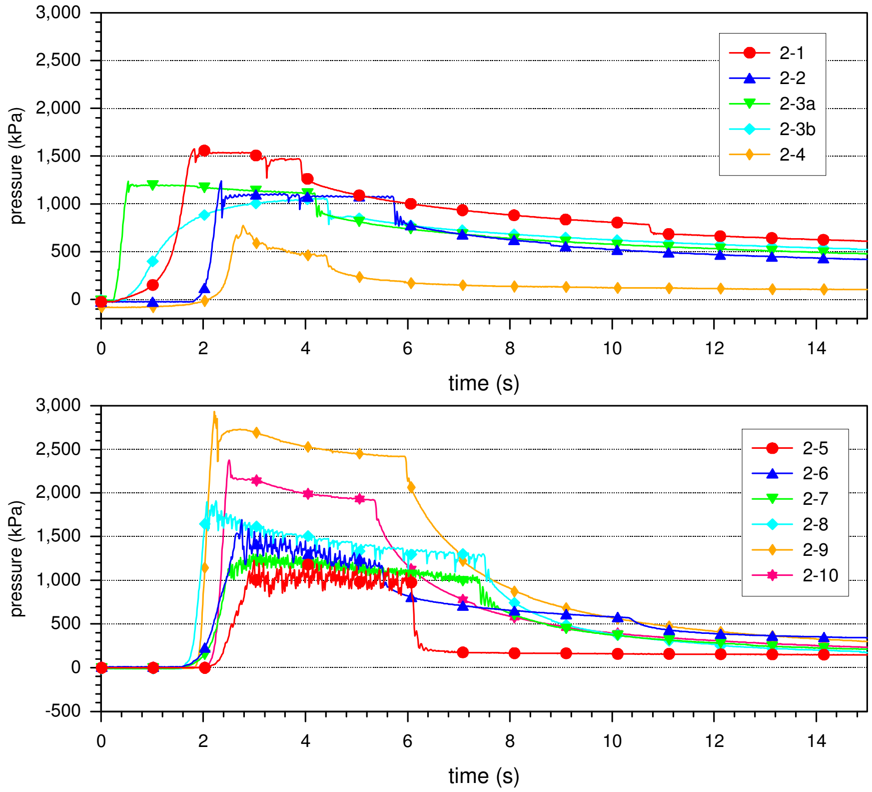

Figure 6-28: Injection pressures in the second test series

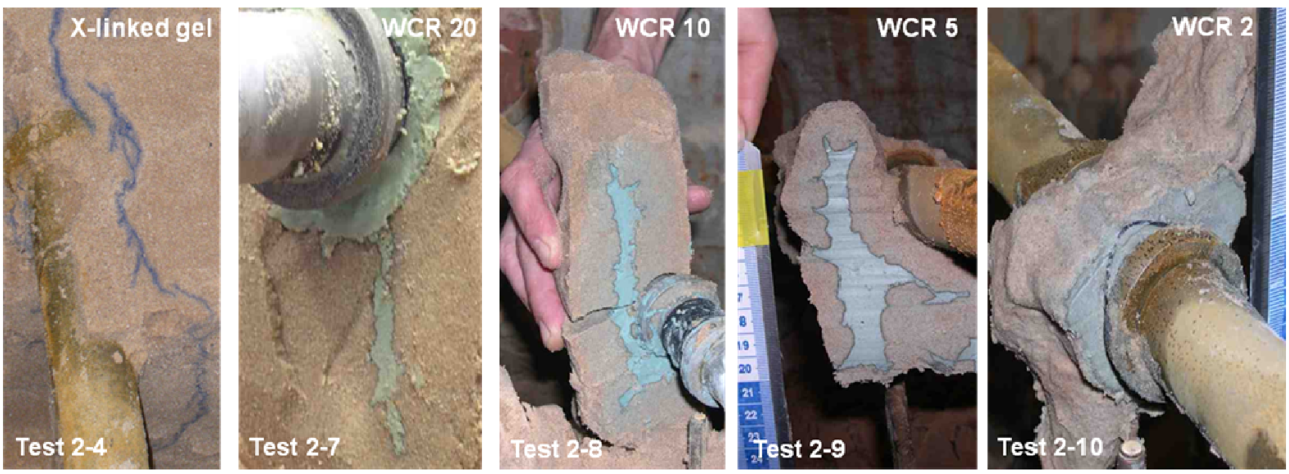

Figure 6-29: Shape of fractures as cement content increases

A remarkable result relating to the injection pressures are the fluctuations seen in Tests 2-5, 2-6, 2-7 and 2-8. These were the tests with considerable pressure infiltration. It is therefore assumed that these fluctuations are caused by the pressure infiltration. The creation of new fractures created new areas where pressure infiltration could occur. This led to a decrease in pressure until most of the pressure infiltration stopped. Pressure then increased until another new fracture occurred or an existing fracture grew further.

6.7.3 Shape of factures

As mentioned in the previous section, the shape of the fractures is determined by the cement content in the grout and related to the injection pressure. In this test series, it was remarkable that a number of tests were characterised by considerable pressure infiltration, as can also be seen in Figure 6-29. The sand around the grout mixture was more or less fixed to the grout mixture by pressure infiltration. Even in Test 2-10, with a WCR of 2, there was some pressure infiltration. Pressure infiltration reduces the efficiency of the injection.

In the picture of Test 2-9 in Figure 6-29, it can be seen that the boundaries of the grout body are darker than the rest of the grout. This is probably caused by pressure infiltration. Figure 6-30 and Figure 6-31 are microscopic pictures of the boundary between the sand and the grout for Tests 2-9 and 2-10 respectively. The picture of Test 2-10 shows that the grout contains some larger, dark particles. Pressure infiltration pushed the grout into the sand. This cannot be seen from the colour of the sand but it results in the sand sticking to the grout. The larger particles cannot penetrate into the sand and remain at the boundary. The sand grains in both pictures are from Baskarp sand, which means that the average diameter will be 130 μm. This gives an idea of the dimensions.

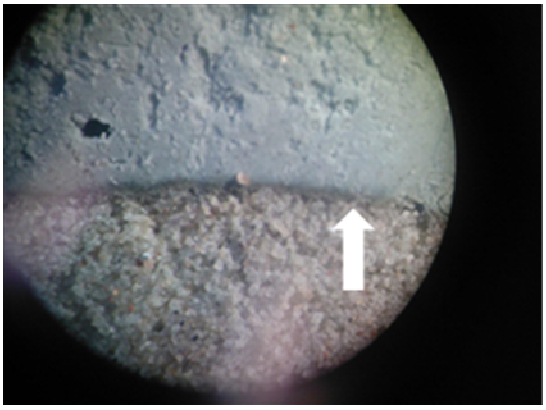

Figure 6-30: Test 2-9, boundary between sand and grout

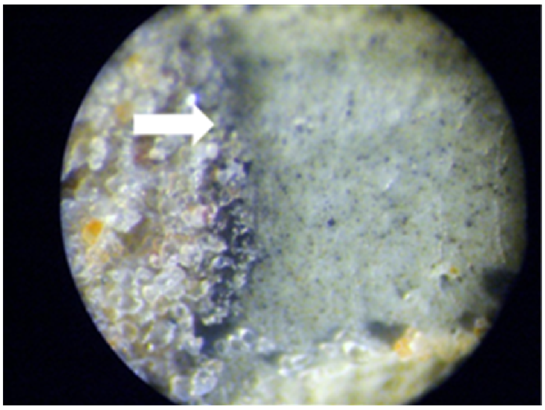

Figure 6-31: Test 2-10, boundary between sand and grout

It emerged from the tests that the pressure infiltration in an injection experiment can be quite different from what is found in a pressure filtration test (Section 5). There will be more pressure infiltration during an injection. This is caused by the higher pressures that occur during injection and possibly also by shear thinning of the grout during injection (Section 5.9) and/or by the soil deformations that occur during an injection experiment. Dilatancy of the sand around a fracture may cause larger pore sizes and therefore more pressure infiltration.

This test series showed that, with a cement-bentonite grout, it can be difficult to find an optimal mixture for fracturing projects in sands with the d_{50} used in these tests. A lot of cement in the mixture will lead to short fractures or no fractures at all and a high injection pressure. A limited amount of cement leads to a lot of pressure infiltration. This will be addressed in more detail in the next section.

The grout bodies created in tests where the WCR was 10 or more proved to be rather weak. In practice there is no need for the grout body to be much stiffer and stronger than the surrounding sand since there is no extra loading on the grout body. However, the grout bodies with a high WCR are probably not very stable and this may result in further volume reduction due to consolidation, or in ongoing chemical reactions which may also lead to a volume reduction. This issue was not investigated further.

Sanders (2007) investigated the permeability of the grout and the amount of pressure infiltration in the tests as a function of the dry mass in the grout. A modified version of the graph presented by Sanders can be found in Figure 6-32. Plotting the same results as a function of the WCR on a logarithmic scale (excluding the X-linked gel) results in more or less straight lines for the tests with cement – see Figure 6-33 – and this indicates an increase in pressure infiltration and lower permeability as WCR increases. It is of interest to note that the points with the fly ash (where the WCR is the water/fly-ash ratio) result in pressure infiltration that is in line with the pressure infiltration that would be expected if the same amount of cement were added, but with a much lower permeability. This result concurs with the theory developed in Section 5.8 and Section 5.9. Section 5.8 showed that it is likely that calcium in the cement raises permeability. And Section 5.9 showed that pressure infiltration is determined by the solid particles in the cement. Since the particle content in the grout with the fly ash and the cement are more or less the same, pressure infiltration will be comparable but fly ash contains much less calcium per unit weight and so the impact on permeability is less.

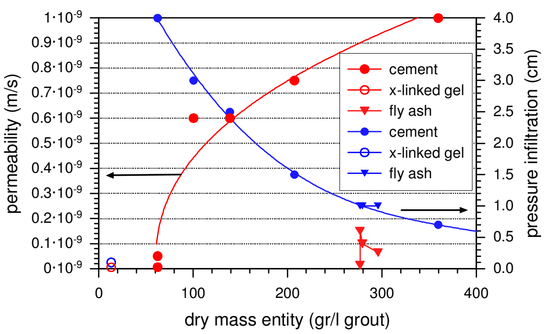

Figure 6-32: Permeability (red lines and markers) and pressure infiltration (blue lines and markers) measured in the second test series as a function of the dry mass in the grout

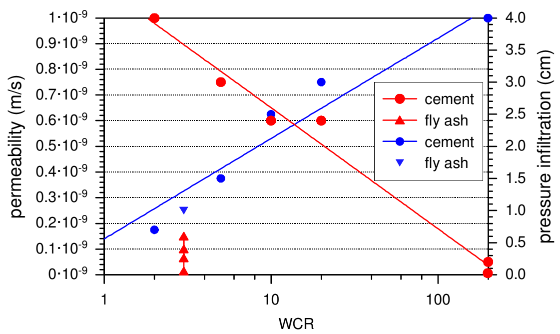

Figure 6-33: As Figure 6-32, but now as a function of the WCR

The cake permeability of the grout with fly ash is lower than in most grouts with cement. Better fracturing behaviour was therefore expected. However, this result was not found in the tests. In fact, the results are slightly inconclusive. The injection pressure was relatively low (compared with the tests with cement) – see Figure 6-28 – certainly when the high relative density (76%) of the sand sample in Test 2-1 is taken into account, but the shape of the grout body is rather rounded and does not look fracture-like. Looking more in detail at sections throughout the grout body to prevent pressure infiltration from influencing the picture, there seems to be more fracture-like behaviour. See Figure 6-34 and Figure 6-35.

A possible explanation for why the test did not result in the long thin fractures that were expected could be the grain size of the fly ash. The cement contains finer particles. See Table 12.

These fine particles will influence the permeability of the cake in the pressure infiltration phase. See Section 5.9. According to the model described there, the filter cake due to pressure infiltration is nearly 3 times thicker after 4 seconds of grout injection in the case of grout with fly ash compared to grout with cement. This would mean that finer graded fly ash could have resulted in longer and thinner fractures because the finer particles hamper the pressure infiltration of the bentonite.

Table 12: Grain size distribution in cement and fly ash

	Cement (μm)	Fly ash (μm)
d_{15}	3	11
d_{50}	22	15
d_{85}	55	53

Figure 6-34: Test 2-1, grout body

Figure 6-35: Test 2.1, fracture details in grout body, (colours changed)

6.7.4 Efficiency

The efficiency of compensation grouting according to the experiments in the first and second series performed using cement-bentonite grout was evaluated by Sanders (2007) and is shown in Figure 6-36. Efficiency is defined as the heave volume created at the end of the fast registration divided by the volume of grout injected.

In these tests, optimal efficiency is reached at a WCR of 5. Higher WCR values result in an efficiency reduction due to pressure infiltration. At lower WCR values, efficiency is reduced due to volume loss by pressure filtration through the relative permeable cake. The plot showed that there is some variation in the results at low WCR. Whether this would actually be the optimal WCR in a practical application depends on the stability of the grout at these high WCR values and the confining stress around the injection tube during the injection. See also Section 6.9.

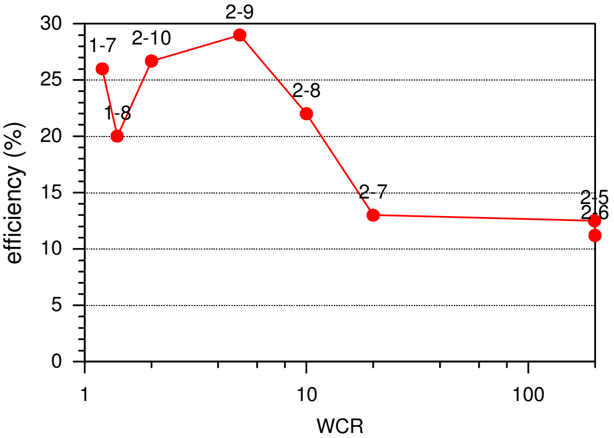

Figure 6-36: Last tests in first and second series: efficiency as a function of WCR

Efficiency was calculated both by Kleinlugtenbelt (2005) and Sanders (2007) roughly 40 seconds after the beginning of the test. This was the last record with the high-frequency data acquisition system in operation during the actual injection. This was not the point where equilibrium was reached, as can be seen from Figure 6-37, where efficiency was calculated in the last three tests of the second series over a longer time using the low-frequency data acquisition system. Efficiency falls for several hours. The real efficiency, obtained after a compensation grouting campaign, will be lower than the values shown in the figures and stated in the Table in Appendix A.

The reason the values in the tables were retained rather than the values some hours after injection is that, in some experiments, there was slight leakage between the container rings and the top plate. This would also lead to a decrease in efficiency. In a short-term measurement, this decrease can be neglected, as will be shown when looking at the fourth test series. In long-term measurements, it has a major effect on the calculated efficiency, leading in some cases to negative efficiencies. So the short-term efficiencies were adopted, even though long-term values will be 5 to 10% lower, as can be seen in Figure 6-37. However, this figure also shows that, although the WCR varied from 10 to 2 in the tests plotted, the difference in efficiency found shortly after the grout injection is comparable to the difference after a few thousand seconds.

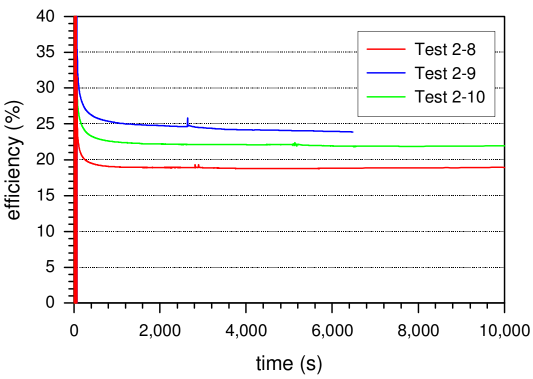

Figure 6-37: Development of efficiency after injection

6.7.5 *Two injections*

In compensation grouting, the usual procedure is to perform several (up to 70) injections through the same TAM openings. Repeat injections of this kind are difficult to reproduce in laboratory-scale experiments since the amount of soil around an injection opening is relatively small and the influence of the fixed boundary conditions in the model increases. So only one test was performed with more than one injection in the same soil sample: Test 2-3. This test comprised two injections, the second three days after the first injection. Two different injection fluids were used. For the first injection mixture, water was used with 120 gr bentonite per litre of water, fly ash with a water to fly-ash ratio of 3, 5% retarder and 0.5% silica flour. In the second injection, the mixture from Test 2-1 was used. This is a comparable mixture, but it contained 70 gr bentonite/l water instead of 120 gr/l. The second mixture had a different colour from the first mixture so that it was possible to identify which grout body was made by each injection. The results are shown in Figure 6-38 and Figure 6-39. It emerged that the second injection fractured through the first one, but that the fracture stopped when the sand was reached. This probably explains the slow rise in the injection pressure during the second injection. See the line for Test 2-3b in Figure 6-28. The injection pressure was relatively low when the grout was fracturing the material from the first injection, but pressure infiltration starts when the injection grout reaches the sand, stopping the fracture and inducing a more cavity-expansion-like pattern that requires higher pressures.

Figure 6-38: Test 2-3, grout body after 2 injections marked 1 and 2

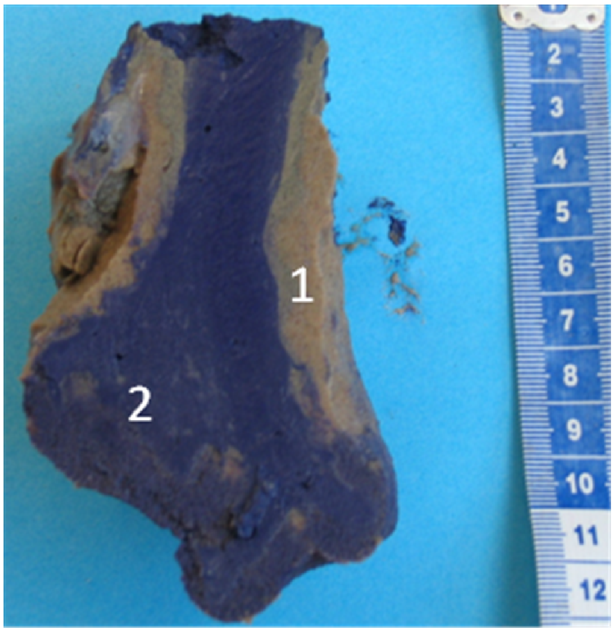

Figure 6-39: Test 2-3, a slice through the grout body. The two injections are marked 1 and 2.

The efficiency of the first injection was lower than the second (15.8 and 20% respectively), probably because there was some densification of the sand in the first injection. The horizontal and vertical stresses in the sand at the location of the total pressure transducers were slightly higher before the start of the second injection but the peak horizontal and vertical pressures were lower for the second injection.

The results of this two-injection experiment showed that, even when a fracture has started, as was the case when the grout of the first injection was fractured during the second injection, propagation may stop when the fracture reaches sand and pressure infiltration and/or pressure filtration start to play a role.

6.8 Third series

6.8.1 General

Research similar to that described in this thesis took place in Cambridge (Eisa, 2008). The third series of tests in Delft were performed by a Ph.D. student from Cambridge in order to link the results from Cambridge to the Delft results. Eight tests took place. The experiments investigated the repeatability of the results obtained by Sanders (2007) described in Section 6.7, as well as the effect of the injection rate, WCR and grout materials on soil-grout interaction. The "dynamic injection" method, in which the injection rate varied during the injection, was also tried. Furthermore, the height of the sand sample above the injection tube was varied.

The height of the sand sample was varied after it was found that there was a remarkable difference between the vertical pressure patterns from the experiments in Cambridge and Delft. The measured vertical pressure during injection decreased in Cambridge, but increased in Delft. This will be addressed in greater detail in Section 6.8.3.

6.8.2 Injection pressures

The injection pressures measured in the third series are plotted in Figure 6-40. Again, the confining stress was 100 kPa in all tests. Two tests were run with a lower injection rate of 2 l/min (instead of 10 l/min in the other tests). These two tests with a lower injection rate were still in the injection phase after 15 s. Since no pressure fluctuations occurred after 15 s it was decided to retain the X-axis, as in the other test series, to make good comparison possible.

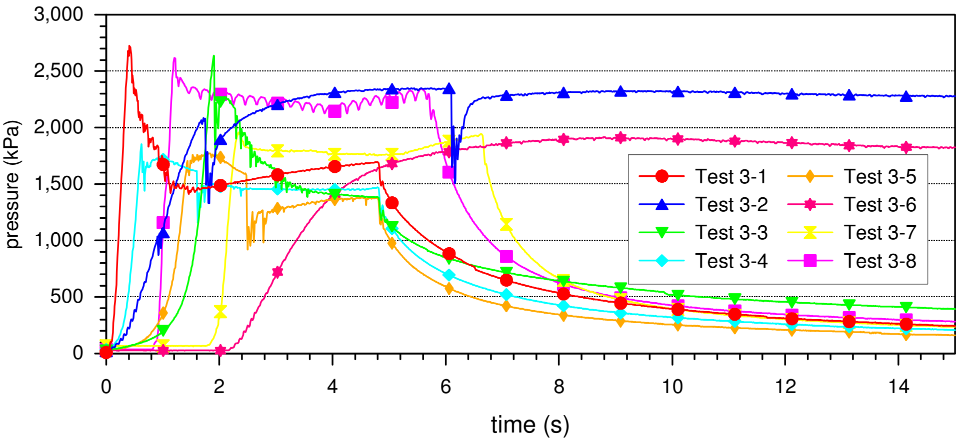

Figure 6-40: Injection pressures measured during third test series

Although different injection rates, different sands and different grout mixtures were applied, the injection pressures did not vary greatly. In Test 3-1, there was probably a lack of homogeneity in the soil sample caused by the soil preparation. This resulted in just one big fracture. See Figure 6-41. There was probably an "easy" path for the grout to follow, resulting in the pressure drop. Test 3-2 was a test with a low injection rate of 2 l/min. It is likely that the dips in the pressure are caused by fractures during the experiment. New fractures lead to new pressure infiltration. At an injection rate of 10 l/min the injection rate was sufficient to keep the pressure more or less constant for this grout composition, but there is a fall in pressure at this lower injection rate. Test 3-8 is performed with a cyclic injection rate of 10 l/min with a 5 Hz cycle with an amplitude of 5.66 l/min. The variation in the injection rate seems to have only a limited influence on the injection pressure.

Figure 6-41: Result of Test 3-1: one big fracture starting from the injection point on the right-hand side of the picture

Comparing the injection pressures of this test series with the results of the second series, the differences in the injection pressure are less marked in the third series. In the second series, the grout properties were varied over a wide range; here, the sand and the injection rate were varied. From the results it can be concluded that the grout properties have more impact on the injection pressures than the parameters varied in the third series.

6.8.3 Vertical pressure during injection

Comparing the results of the tests performed in Cambridge with the results obtained in Delft, there was one remarkable difference. Total vertical pressure rose during the tests in Delft, but fell during the tests in Cambridge. A test result from Cambridge is shown in Figure 6-42; Figure 6-43 shows a result from the first test series. This figure presents pressure as a function of the injected volume rather than as a function of time, as elsewhere in this thesis. This is because that was how the Cambridge results were presented. Since the pressure decrease after injection can also be important and because this is not clear in a plot against the injected volume, most plots are given as a function of time.

For the purposes of comparison, Tests 1-7 and 1-9 were chosen because the grout mixtures of these tests are comparable with the grout mixture used in Cambridge and dense sand was used in Test 1-9, as in Cambridge. It is clear that the vertical pressure decreased in Cambridge and increased in Delft, with the exception of the effective vertical stress in Test 1-7, which remained more or less constant. The confining stress in Test 1-9 was very limited and so a significant increase in pressure was measured for Test 1-9. The position of the stress transducer was 230 mm from the wall in Cambridge, where the diameter of the container was 850 mm, and 200 mm from the wall in Delft, where the diameter of the container was 900 mm. So the positions are quite comparable.

Theoretically, a fall in pressure as seen in Cambridge can be described as follows. The vertical force on top of the sand sample remains constant during a test. This is determined by the air pressure that is applied. The injection with grout results in a local increase in the stress around the injection point. Since the total force on the sand remains the same, a local increase in stress is only possible if there is also a local decrease at some distance from the injection point. A decrease in vertical stress of this kind has been found in previous tests (Bezuijen, 2003).

Eisa (2008) suggests, as a possible explanation for this discrepancy, that the confining pressure is applied with a stiff plate. However, this is unlikely because the Cambridge tests found that the injection caused heave of the sand in the centre of the container. With a stiff plate, most of the force would be through the centre and, once again, the vertical stresses closer to the wall must decrease. Furthermore, the PVC plate used is not very stiff compared to the sand.

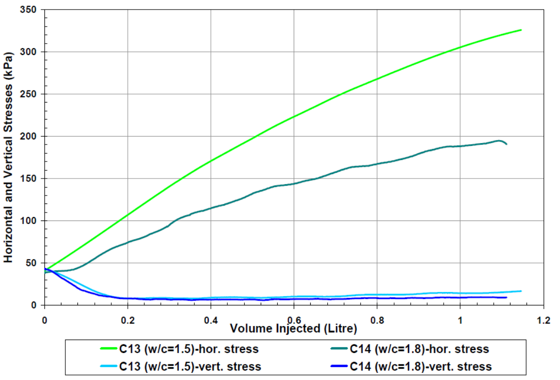

Figure 6-42: Measured horizontal and vertical total stress in Cambridge tests (Eisa, 2008)

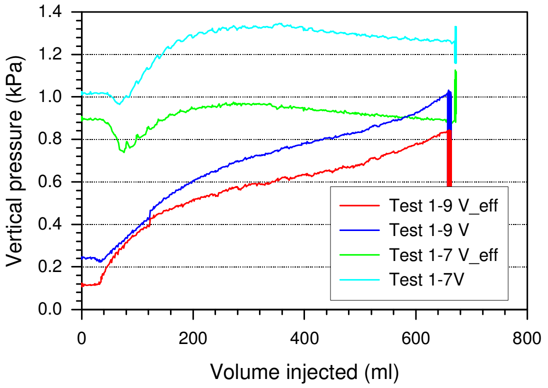

Figure 6-43: Measured vertical pressures in first series

A significant difference between the Cambridge and Delft tests was the height of the sample. In Cambridge there was only 180 mm of sand above the injection point; in Delft there was 450 mm in the first two test series. A possible explanation could be the friction of the sand against the walls. Since horizontal stress increases significantly during a test it is likely that the friction with the walls increases during a test. To test this hypothesis, it was decided to reduce the amount of sand above the injection tube by 240 mm (the height of the rings used to build the sand container), so that only 210 mm of sand remained above the injection point. Eisa evaluated the results (2008). See Figure 6-44. The vertical stress for Test 3-3 in this figure is much too low and must be wrong. The values presented in the figure are also in the original data file. It is probable that the instrument failed. Eisa found no clear impact of sample height in the tests performed in Delft. All the tests showed some increase in vertical pressure during injection. Tests 3-4 and 3-5 first show a pressure decrease. The most likely explanation is that the increase in vertical stress is caused by friction with the walls, so that the difference between the Cambridge and Delft tests is the friction coefficient between the walls and the sand.

In the Delft set-up, it seems as if the sand above the injection hole is like an inverted arch with its lowest point in the middle above the injection hole, blocking vertical movement of the sand. See Figure 6-45. This figure compares the measured effective horizontal and vertical stresses for Test 2-9 and Test 3-4. These tests had grout bodies with comparable shapes after the test and the only difference is the difference in sand sample height. The height of the sand sample in Test 2-9 was 0.84 m; in Test 3-4 this was 0.6 m. The input pressure in Test 2-9 was 1100 kPa than in Test 3-4 (2900 and 1800 kPa respectively) and vertical stress was also higher. See Figure 6-45. Nevertheless, horizontal effective stress was higher in Test 3-4. The sand "wedged" itself against the walls and the higher horizontal stress is necessary to mobilise enough friction from the walls to compensate for the upward vertical force exerted by the injection pressure.

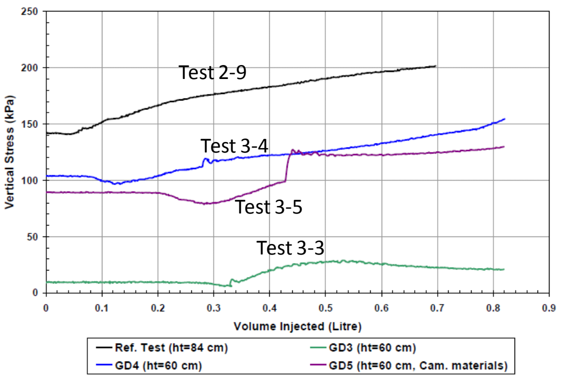

Figure 6-44: Vertical pressure as a function of the injected grout volume for various tests (Eisa, 2008)

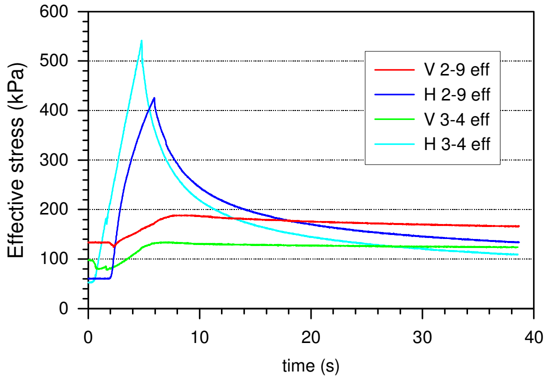

Figure 6-45: Comparison of effective stresses measured in Test 2-9 and Test 3-4. See also text.

6.8.4 Efficiency

The efficiency of the grouting process was also measured in this test series. Figure 6-46 plots the results together with the results of the second series, which were presented above. Efficiency in the third series is slightly higher than in the second series. This is not a genuine difference; it is related to the slightly different calculation methods used by Kleinlugtenbelt (2005) and Sanders (2007) on the one hand and Eisa (2008) on the other. The main difference is that Kleinlugtenbelt and Sanders used the displacement of the plunger to calculate the injected volume, while Eisa's starting point was the moment when the pressure started to build up in the plunger pump. He assumes that the plunger movement that is not associated with an increase in pressure at the plunger pump does not really pump grout into the system. This initial absence of pressure may be linked to air in the system, or some play in the various connections, although no connections were found that could have caused the problem. Another difference is that Kleinlugtenbelt and Sanders calculate the efficiency approximately 40 seconds after the end of the injection and Eisa calculated it immediately after the injection. Taken together, such differences in assumptions can become significant. Sanders reported an efficiency of 29% for Test 2-9. Using Eisa's method, efficiency would be 37%. Since the relative efficiencies are important and to maintain the link with the publications of Kleinlugtenbelt, Sanders and Eisa, it was decided to adopt the efficiencies as reported by these authors.

The second series resulted in optimal efficiency at a WCR of 5. Adding the results of the third series resulted in a more confusing picture. There proved to be no significant difference in the efficiency of the grouting process when WCR = 1 and WCR = 5. At lower injection rates, efficiency was even lower when WCR was 5 because, at lower injection rates, there is more time for water loss due to pressure filtration from the grout, resulting in a lower efficiency (see also Eisa, 2008).

6.8.5 Repeatability of tests

Different test series have been performed by different researchers and although all the researchers followed the same procedures, there are always differences. This is even the case when there is just one researcher, but differences increase as more people become involved. Furthermore, as stated in the chapter on theory, a fundamental aspect of the fracture grouting process is that it starts with some irregularity in the grains around the tube. The repeatability of the tests therefore becomes important. Can there be large variations in, for example, injection pressure because of small variations in the test set-up? Since the first test series and the first half of the second generated results that were different from the results expected, repeatability was not tested.

The third test series afforded some opportunities for checking repeatability. Test 3-1 was intended to be a copy of Test 2-9, and Tests 3-3 and 3-4 were also more or less replications. The only difference was that the height of the sand above the injection was less in Test 3-4: only 210 rather than 450 mm (see the previous section). The injection pressures for these tests are compared in Figure 6-47 and the efficiencies measured are compared in Figure 6-48.
The results show that the maximum injection pressures for three of the tests (2-9, 3-1 and 3-3) are quite comparable. Test 3-4 has a lower peak value in the injection pressure; the "plateau" during the injection (from 2 to 5 seconds) is more or less the same as in Tests 3-1 and 3-3. There is a striking delay in Test 3-3 before the pressures actually increase. The reason for this delay is not known. Tests 2-9 and 3-1 have exactly the same rise curve for the pressures to approximately the same maximum. The injection pressure in Test 3-1 then falls by 1000 kPa, while the pressure for Test 2-9 remains more or less constant. This difference is likely caused by a different fracture pattern. As described in 6.8.2, Test 3-1 resulted in one large fracture – see Figure 6-50 – probably due to some inhomogeneity in the soil. In the case of this large fracture, propagation pressure was lower than with the fracture in Test 2-9. Comparing the measured injection pressures (Figure 6-47) for these tests with the resulting grout bodies (Figure 6-49, Figure 6-50, Figure 6-51 and Figure 6-52), it emerges that there is a larger fall in pressure after the initial peak in the tests with larger fractures in one direction (Test 3-1 and Test 3-3) than in the other tests (Test 2-9 and Test 3-4).

The pressure decay after injection is the same for all tests and is hardly affected by the shape of the fractures.

Figure 6-48 shows that efficiency in all four tests is comparable.

In conclusion, the tests show some variations in the injection pressure even in duplex tests, as could be expected on the basis of the mechanisms described. Different fracture patterns lead to different peak pressures or propagation pressures, although the difference in the peak in two of the four tests compared is only limited. The pressure decay after injection and the efficiency is not influenced as much by the fracture pattern and is therefore quite comparable in all four tests.

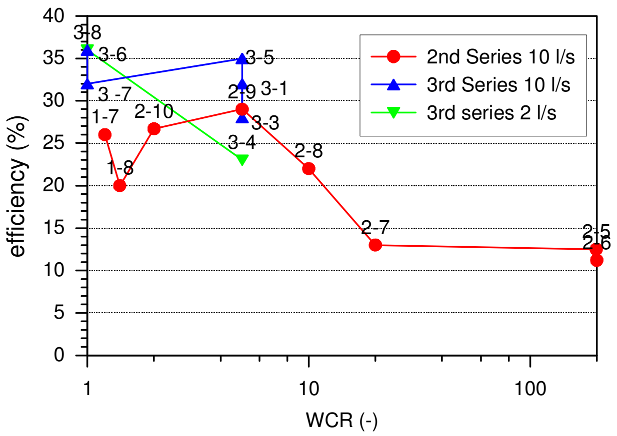

Figure 6-46: Efficiency of compensating grouting in second and third test series

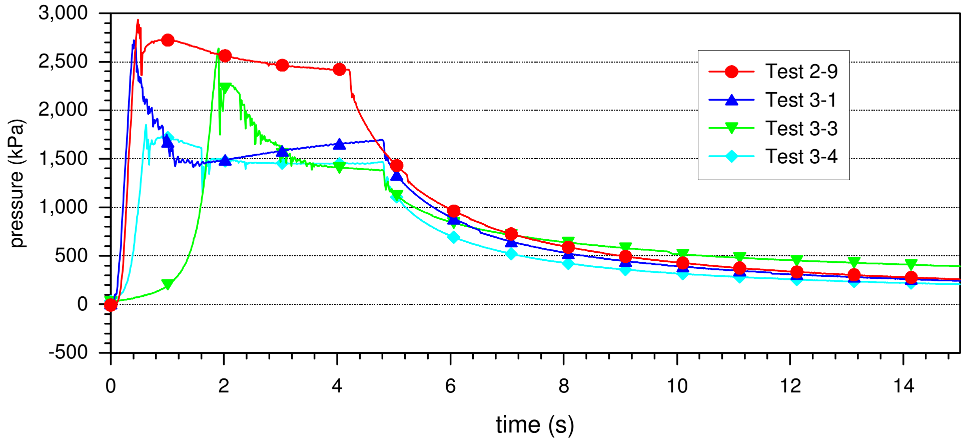

Figure 6-47: Injection pressures of comparable tests from Series 2 and 3 compared

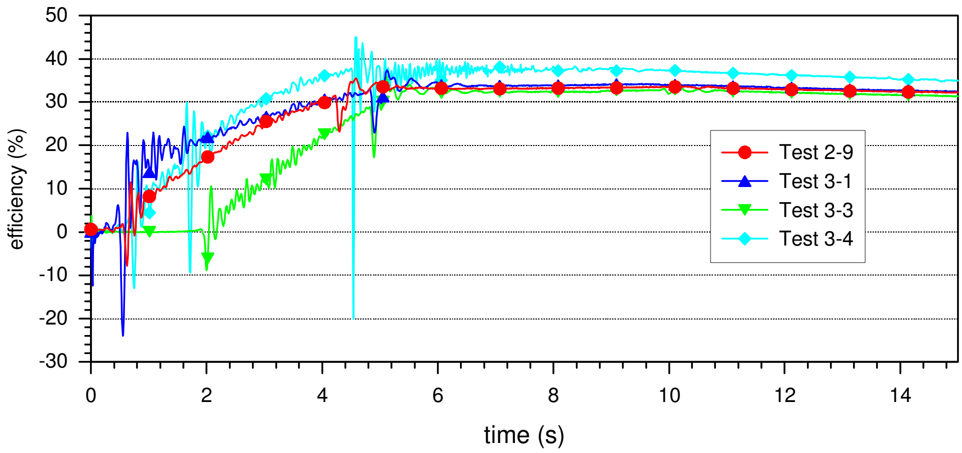

Figure 6-48: Measured efficiency of comparable tests from Series 2 and 3 compared

Figure 6-49: Grout body, Test 2-9

Figure 6-50: Grout body, Test 3-1

Figure 6-51: Grout body, Test 3-3

Figure 6-52: Grout body, Test 3-4

6.9 Fourth series

6.9.1 General

Comparing the results of the first three test series with the results of field measurements suggests a discrepancy. Field observations showed fractures in conditions where no fractures were found in the model tests. On the basis of the theory of Wang and Dusseault (1994) – see Section 2.4.1 – it is assumed that unloading of the soil around the fracture could explain this discrepancy. In a field situation, the installation of the TAM in the casing and the withdrawal of the casing afterwards may lead to local unloading around the TAM. The consolidation of the Dämmer around the TAM may lead to further unloading close to the TAM. This unloading due to the consolidation of grout has been measured in TBM tunnelling (Bezuijen et al., 2004) and described in a calculation model (Bezuijen and Talmon, 2003) and the same process can be expected around a TAM.

For the reasons mentioned above, it was decided to perform a fourth series of experiments taking the installation procedure into account. The set-up is described in Section 6.4.2.

6.9.2 Test procedure for the fourth test series

After preparation, a sand sample was pressurised to 100 kPa using air pressure and a watertight plate that was placed on top of the sand sample. The Dämmer was then injected into the casing and the casing was removed by using the spindle. See Figure 6-6 and Figure 6-8. Three hours after the retraction of the casing, the grout was injected through the TAM. In two tests (4-2 and 4-3), the time interval was 24 hours. After the injection, the Dämmer and the grout were allowed to harden for 24 hours before the sand was removed and the result of the injection studied. The tests performed are shown in Table 13. In different tests, the amount of cement in the grout – the Water-Cement Ratio (WCR) – was varied, as were the pressure on the Dämmer during the retraction of the casing (p_d) and the time the Dämmer was allowed to harden before the experiment was performed (t_d). In the field, there is no constant pressure on the Dämmer during the retraction of the casing. The casing in the field consists of tubes with a length of 2 m. When the casing is removed in the field, there is some pressure on the Dämmer but there is no pressure when a tube is disconnected. In the laboratory experiments, the pressure on the Dämmer was kept constant during the retraction of the casing. The Dämmer between the casing and the injection tube was by a tube (not the injection tube) connected to a bladder filled with Dämmer outside the container. This bladder was mounted in a pressure chamber with a constant air pressure. After a time t_d the pressure was removed from the bladder and the Dämmer was more or less at atmospheric pressure.

Table 13. Tests performed, fourth series

Test	WCR (-)	t_d (h)	p_d (kPa)
4-1	5.0	3	85
4-2	5.0	24	85
4-3	5.0	24	85
4-4	5.0	3	85
4-5	1.8	3	20
4-6	1.8	3	110

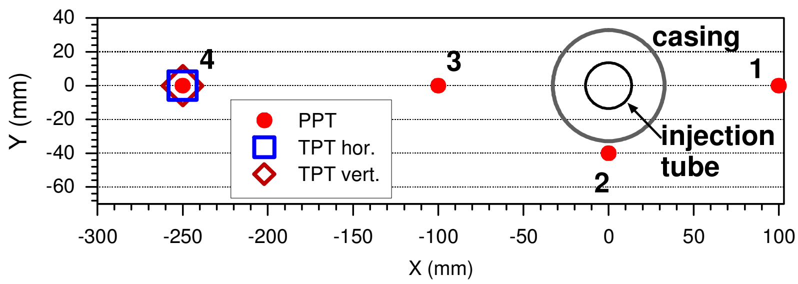

Figure 6-53: Instrumentation. The radius of the container is 450 mm. The injection tube is located in the middle of the container (x=0 mm).

The grout injection was volume controlled. 680 cc of grout was injected in each experiment at an injection rate of 10 l/min.

6.9.3 Parameters measured

During and after the introduction of the Dämmer, the pressure in the Dämmer was measured. The injection pressure and injection volume were measured during grout injection. The burettes (see Figure 6-6) were equipped with pore pressure gauges to obtain continuous measurements of drainage and heave, as in the original set-up. In a plane perpendicular to the injection tube at the position of the TAM, four pore pressure gauges (PPT) were installed in the sand and two total pressure gauges were installed to measure the horizontal and vertical pressures. See Figure 6-53. More details about the instrumentation are given in Au and Masini (2008).

6.9.4 Results of measurements with casing

Figure 6-54 provides an example of the measured pressures and the water volumes in the burettes for Test 4-4 before injection and during the retraction of the casing. A pressure of 60 kPa was exerted on the Dämmer for approximately 30 minutes (1800 seconds). During that time, the amount of water in the drainage burette increased due to pressure filtration from the Dämmer. When the pressure was removed from the Dämmer, filtration stopped and the amount of drainage water actually decreased, probably due to the hardening of the Dämmer, which draws water from the vicinity. During the whole of this process the volume of the water in the burette (volume of burette water in Figure 6-54), which indicated the volumetric change above the sand due to heave at the top, remained more or less constant. The horizontal and vertical total pressures at some distance from the tube also remained constant. At the end of the measurement period shown in the graph the amount of drainage water in the drainage burette fell sharply. This was simply to prevent overflowing of the burette during the injection experiment.

Figure 6-55 shows some of the measured parameters during a "typical" test. The injection pressure in Figure 6-55 increases sharply, followed by a decrease at the very beginning, presumably when the Dämmer around the TAM is broken. Then there is a further increase in pressure until the injection stops, when the injection pressure falls. There are only minor variations in pore pressures and vertical pressure during injection but horizontal pressure increases significantly. The average vertical pressure, as in all tests described in this chapter, is applied as a boundary condition by exerting a pressure on the plate on the sand, and therefore the variation of the vertical pressure was only limited.

There was a reasonable match between injected volume and the total drained volume (Figure 6-55). The total volume measured from the drain and the volume change due to heave was slightly smaller than the total injected volume. This may be caused by some air that is entrapped during the set-up of the experiment and escapes during the injection, or by the fact that the finite stiffness of the container allows for some volume deformation during injection. It emerged that efficiency increased during injection before decreasing afterwards, probably due to consolidation of the grout and the Dämmer. The "final" efficiency of this test was less than 10% and therefore relatively low.

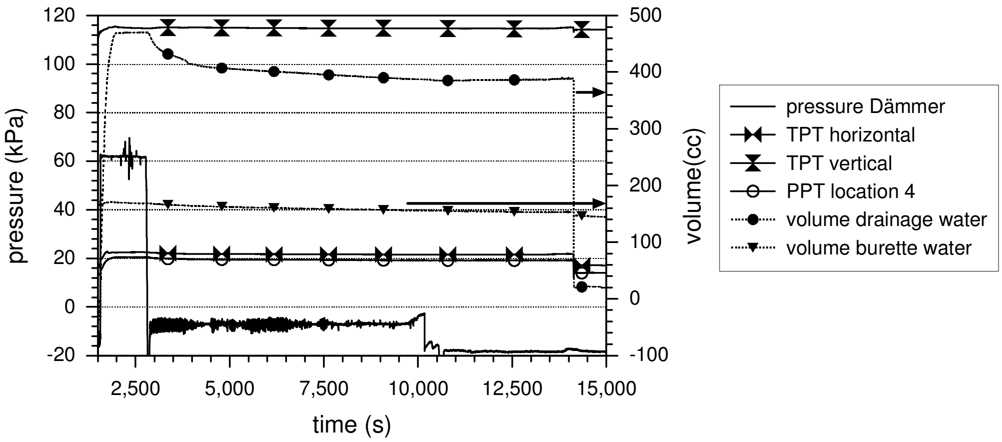

Figure 6-54. Test 4-4, pressures and drainage during retraction of the casing and waiting afterwards. The casing was retracted at approximately 2000 s.

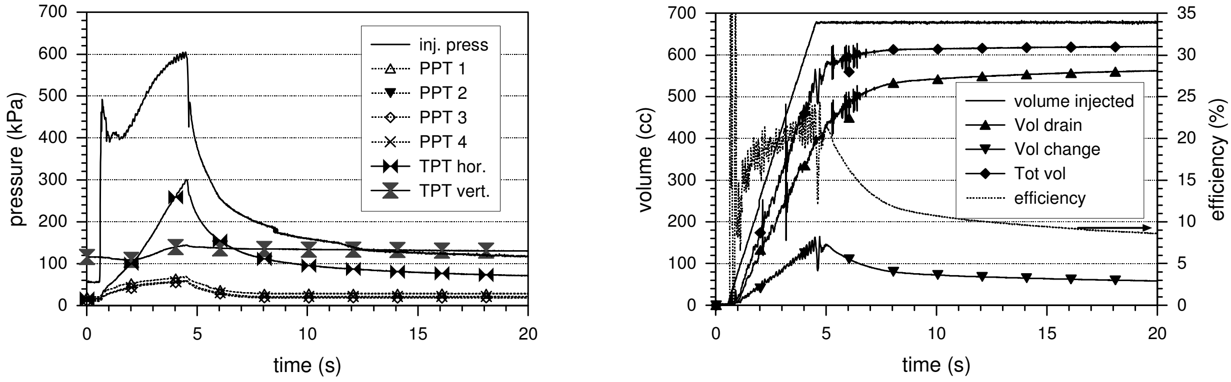

Figure 6-55. Test 4-4, pressures during injection (left) and volumes (right). The volume change (volume change in the right-hand plot) is caused by the heave that is created.

Injection pressures

All injection pressures measured in the fourth series are shown in Figure 6-56. The pressure peaks to break the Dämmer in Test 4-2 and Test 4-3, where the Dämmer was allowed to harden for 24 hours, dominate the graphs. The pressures up to 700 kPa have therefore been set out in a second plot in Figure 6-57. Comparing the results with the results from the second and third series (see Figure 6-28 and Figure 6-40), it is clear that, with the exception of the pressures to break the Dämmer, the injection pressures are significantly lower. The grout mixtures used in Tests 4-1 to 4-4 are comparable with the grout mixtures used in Test 2-9, with a peak injection pressure of 2900 kPa. The combination of Tests 4-5 and 4-6 is comparable to Test 2-10, with a peak injection pressure of 1550 kPa. In the fourth test series, after breaking the Dämmer, there is no injection pressure higher than 600 kPa. The difference in injection pressure between the two different grouts is only limited.

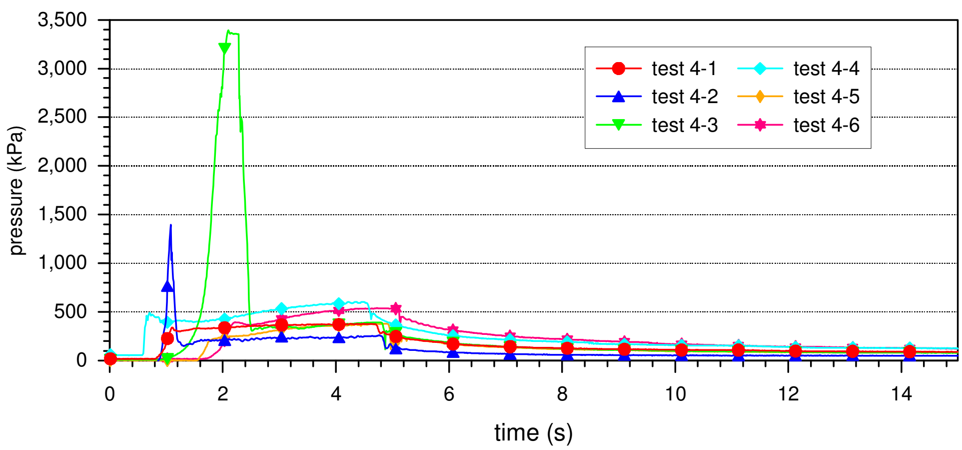

Figure 6-56: Injection pressures measured during fourth test series

6.9.5 Dämmer consolidation time and pore pressures

Tests 4-3 and 4-4 are comparable tests. The only difference is that the Dämmer was allowed to harden for 24 hours in Test 4-3 and for only 3 hours in Test 4-4. In Test 4-3, the Dämmer made a stiff cake around the injection tube and therefore a very high injection pressure was needed to break the Dämmer. The difference in behaviour also emerges from the pore pressures that were measured in both tests. See Figure 6-58. In Test 4-3 there was a large peak in the injection pressure which is only partly shown in the figure. At the end of the pressure peak (compare Figure 6-58 with Figure 6-56) the pore pressure in the container increased abruptly. The result of one PPT only is shown but the trend for the others is comparable. In Test 4-4, pore pressure started to increase as soon as injection started and there was a steady increase during injection. After the sudden increase in the pressure, the trend for the pore pressure in Test 4-3 was comparable to Test 4-4.

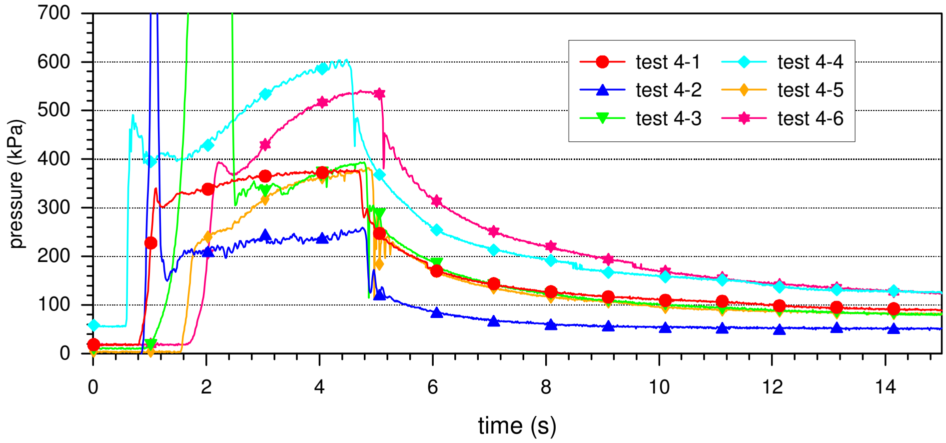

Figure 6-57: Detail of the injection pressures measured during fourth test series

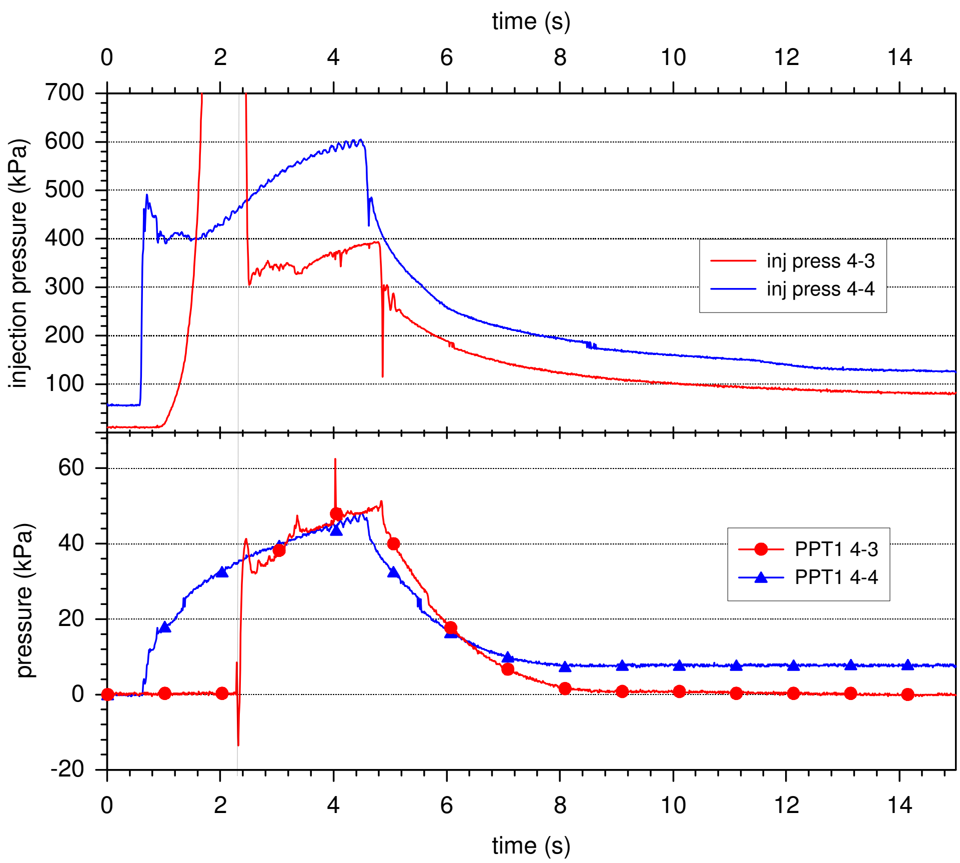

Figure 6-58: Measured injection pressures compared with pore pressures at PPT 1. See Table 13, Test 4-3 and 4-4.

6.9.6 Efficiency

Figure 6-59 shows efficiency as measured in the fourth series. Compared to the other series, maximum efficiency is significantly lower, but the fall in the measured efficiency during the first 30 seconds after the test is more significant than in the earlier tests. Consequently, the realised efficiency after 30 seconds is rather low. Even in Test 4-4, where maximum efficiency was reached, it was still less than 10%. Efficiency was lowest in Test 4-2, but it emerged that, during this test, there was a leak between the plate on top of the sand sample and the container. This means that water can flow to the sand sample when pressurising the plate. This leak is in fact very small. Correcting the efficiency data for this leakage shows a difference in efficiency of less than 0.2% for Test 4-2. This effect can be neglected. However, it remains possible that leakage is higher during injection when the plate on top of the sand will move due to the heave created.

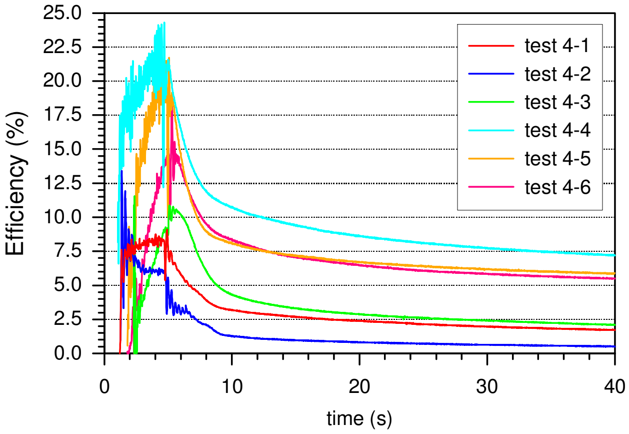

Figure 6-59: Efficiencies measured in the fourth test series

6.9.7 Discussion of the results of tests with casing

The pressures measured for the set-up described above were compared with the results of earlier tests in which the sand was installed directly around the TAM. See Table 14 and Figure 6-60. The injection pressure was significantly lower in the set-up for the fourth series. The sample height and WCR were the same in the tests shown in Figure 6-60. Test 3-3 and Test 3-4 were performed under the same conditions and show the possible variation due to different fracture patterns in two tests with the same conditions. Test 4-4 shows the effect of differences in the installation procedure. The lower injection pressures found in Test 4-4 were found in all the tests of the fourth series. See Table 14, Figure 6-56 and Figure 6-57. There are only pressure peaks when the sleeve grout has to be broken. Furthermore, it was found that the shape of the fractures was different. As expected on the basis of the considerations stated in Section 6.9.1, the fractures are thinner in the present set-up compared with earlier tests. See Figure 6-62. The lower injection pressures for the tests with sleeve grout led to less pressure filtration and less pressure infiltration (grout mixture being pushed into the sand). The lower pressure infiltration level results in a thinner sand layer around the grout after the injected grout is rinsed after the test. It can therefore be concluded that the installation procedure is important for both the injection pressures and the shape of the fractures during fracture grouting with a cement-bentonite-based grout. The installation procedure with a casing leads to a lower stress level in the sand just around the sleeve grout, resulting in fracturing at lower injection pressures.

A remarkable result is that the efficiency of compensation grouting is higher in the earlier tests (29%) compared with the fourth test series (around 20% at maximum). It is generally accepted that fracture grouting at lower injection pressures is more efficient than compaction grouting at higher injection pressures. A possible reason for the results found is that, in earlier tests (such as Test 9 from 2006), the injected grout formed a relatively compact body. See Figure 6-62 (upper left picture). This was not the case in the present tests. Some fractures were formed, but the grout also created a "film" around the sleeve grout. See Figure 6-61. The volume loss in the grout as a result of pressure filtration in a film of this kind will be significant because there is a relatively large area in which filtration is possible. The film is created because of the volume loss in the sleeve grout, resulting in a low stress state of the sand around the sleeve grout. A comparable situation was found near the Hubertus Tunnel in the Netherlands (see Figure 3-10 in Section 3.5). The reason in that location was consolidation of the tail-void grout (Bezuijen and Talmon, 2003). In addition, there is also the possibility of some further water loss from the sleeve grout when this is pressurised by the grout and has not hardened completely within the three hours allowed for hardening in some of the tests. The setting times for the Blitzdämmer used as the sleeve grout are, according to the manufacturer, 210 and 315 minutes. This means that setting will not yet have started within 3 hours and therefore that the Blitzdämmer is still a liquid and will lose water when pressurised.

Table 14: Influence of installation. Pressures and stresses without simulation of the installation (second series, 2006, and third series, 2007) and with the installation procedure (fourth series, 2008).

Test nr.	WCR (-)	Max. injection pressure (kPa)	$\sigma'_{v;initial}$ (kPa)	$\sigma'_{h;initial}$ (kPa)	Max. σ'_v (kPa)	Max σ'_h (kPa)	Sample h. (m)
2-9	5	2900	133	61	188	426	0.84
2-10	2	2350	133	45	216	550	0.84
3-3	5	2638	n.m[1]	62	n.m	185	0.6
3-4	5	1852	97	53	143	541	0.6
4-1	5	370	102	17	102 ($\sigma'_{v;final = 85}$)	95	0.6
4-2	5	1390	100	6	101	22	0.6
4-3	5	3400	105	19	105	107	0.6
4-4	1.8	605	103	4	115	242	0.6
4-5	1.8	370	78	6	87	80	0.6
4-6	1.8	550	103	13	115	197	0.6

[1] n.m means not measured. The reading for the vertical stress transducer was not correct in that test.

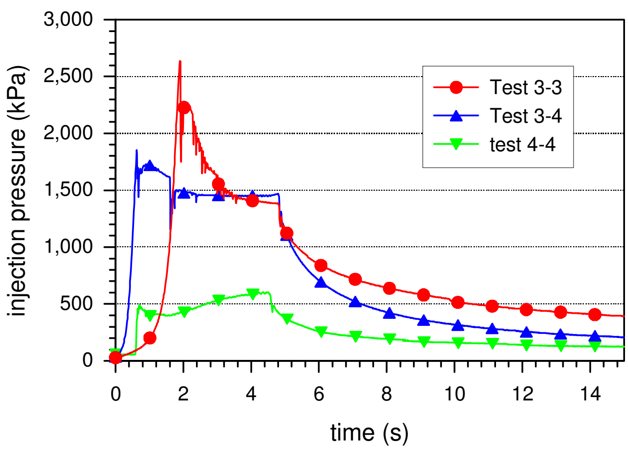

Figure 6-60. Test 4, comparison of injection pressure with results of an earlier test

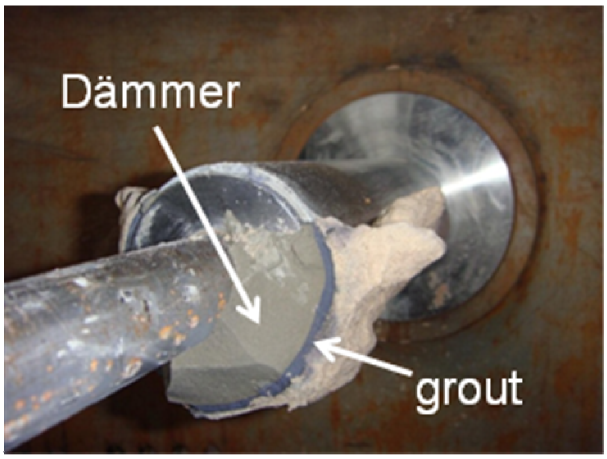

Figure 6-61. Test 4: Sleeve grout (Dämmer) surrounded with a thin layer of grout from the injection

6.9.8 Conclusions about the effect of installation

The installation procedure is important when modelling the fracture grouting process in a physical model test. Without the right installation procedure the predicted injection pressures measured in a test will be higher than in the field and the shape of the fractures will be different. The water loss due to pressure filtration leads to a low stress situation around the Dämmer. In our set-up, it resulted in a large contact area between the injected grout and the sand, leading to the de-watering of the injected grout due to pressure filtration. Efficiency is therefore low.

The experiments present an explanation for the result of the field test near the Sophia Tunnel (Section 3.1), where it was found that, in some cases, heave occurred at a considerable distance from the injection point but in the direction of the TAM.

The results concur with those of Wang and Dussault (1994) based on the cavity expansion theory.

Figure 6-62: Fracture shapes from an earlier test (pictures left, TAM directly in sand, Test 9 2006) compared with the results of Test 4, 2008 (pictures right)

6.9.9 Implications for practice

The results of the fourth series have implications for the practice of compensation grouting. They confirm that injection pressure affects the shape of fractures. Increasing the confining stress will lead to less slender fractures when the other conditions are the same. When the confining pressure and friction angle of the sand are known, it is possible to estimate the shape of the fracture in accordance with the theory developed in Section 4.10.

These tests showed that relatively low efficiency was achieved when the grout after injection remains between the sand and the Dämmer and/or created thin fractures (the tests did not make it possible to determine whether the grout flow around the Dämmer causes the low efficiency or the thin fractures). Both the grout flow around the Dämmer and the thin fractures lead to a relatively large contact area between the grout and the sand which, depending on the permeability of the filter cake, may lead to a significant volume loss due to pressure filtration. Since, at a water-cement ratio of 2, 66% of the injection grout by weight is still water and more than 80% by volume, pressure filtration may have a significant impact on efficiency. Section 8.3.2 will discuss this point in more detail.

6.10 Fracturing tests with CT scan

6.10.1 Motivation and description of test set-up

Two fracturing tests were performed with a CT scan during the injection process. The equipment developed at Delft University of Technology for the Delfrac Consortium was used for the tests. The CT scanner used was also from the Delft University of Technology. This test set-up makes it possible to see how a fracture develops during injection. It also shows the distribution of the density in the sand and in the grout. Since a different set-up was needed, the tests also show the influence of the set-up on the results. Tests could only be performed as an additional part of an ongoing research programme on hydraulic fracturing and so only three tests were performed.

These tests took place in a different and smaller set-up. An aluminium container was used to allow the passage of X-rays through the container. See Figure 6-63. The container was 217 mm long, with a diameter of 152 mm.

In these tests the injection tube is positioned vertically. There is a rubber sleeve around the soil sample and oil is pressed between the sleeve and the aluminium container. The axial stress is applied by the end plates. This set-up makes it possible to control the horizontal and vertical stresses, as in a triaxial set-up. In principle, it is also possible to keep the stresses constant during an injection by controlling the amount of oil and the end plates. In practice it emerged that the control loops installed were too slow for the injection rates chosen and so the stresses increased during injection.

These tests were conducted with relatively slow injection rates of 0.5 and 1 cm^3/s. The slow injection rates were necessary because the capacity of the injection pump was limited. As mentioned above, the set-up was designed for higher pressures that occur during hydraulic fracturing as applied in the oil industry and the slow injection rate was sufficient for that research. The design for high pressures also made it necessary to use a higher confining stress than in the other test series. A radial stress of 10 MPa was applied and the axial stress was 15 MPa.

By contrast with the large set-up described above, the injection opening was made by removing a tube. See Figure 6-63. This injection opening contained some notches so that a preferential fracture path was created before the injection started. Figure 6-64 shows a cross-section of the sample taken by the CT scan with the openings created by the notches.

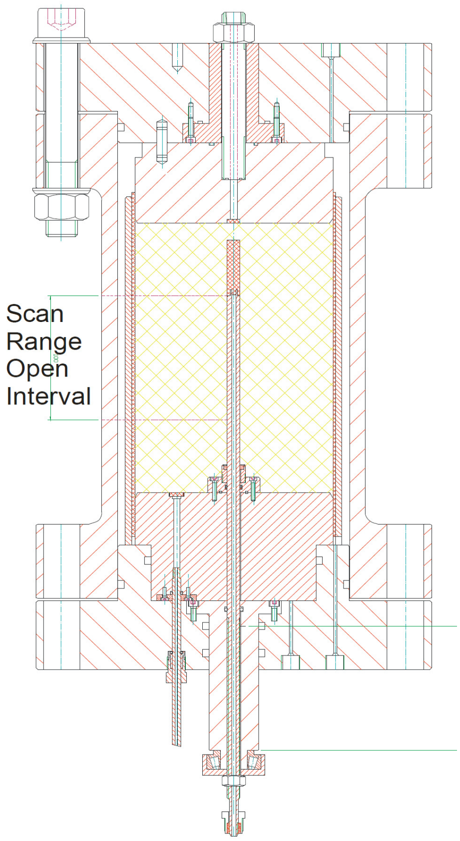

Figure 6-63: Sketch of set-up for the tests with CT scan (Dong and Pater, 2008)

Figure 6-65 shows the principle for the CT measurement. The container (referred to in the figure as the "vessel") moved horizontally through the scanner, a SIEMENS_S5VA47A of the type used in hospitals. It produces scans with a resolution of 0.3*0.3*1 mm.

6.10.2 Tests performed

Three tests were performed. The first test, Test CT 27, was run using a bentonite/silica flour/water mixture with 100 grams of bentonite (Colclay D90) per litre of water and 333 grams of silica flour per kg water. The second and third tests (CT 41 and CT 42 respectively) were both conducted with a grout mixture of 7% bentonite and Portland cement with a WCR ratio of 5.

The first test was performed because the mixture used in the first test had been tested before in the large set-up described in Section 6.7 and, by then unexpectedly, did not produce fractures. The test was performed to see whether or not this result was also found using a different set-up.

The second and third tests were performed using the grout mixture from Test 2-9, the grout mixture that performed best in the second series. The aim here was to observe actual fracture growth during injection. The second test was not successful because the opening collapsed before the injection of the grout. Injection was still possible but only at very high pressures. The third test was performed with an open injection hole and showed the development of a fracture. Table 15 shows some basic information about the tests performed. Tests 2 and 3 were conducted with Baskarp sand. The first test was conducted with Sibelco 39 Sand, which is slightly finer

(d_{50}=90 μm instead of 130 μm for Baskarp), but has the same friction angle at 50% relative density.

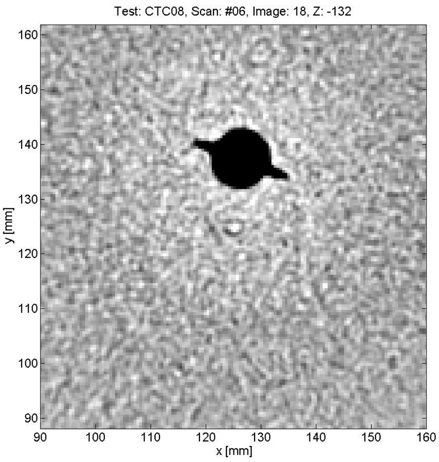

Figure 6-64: CT-scan picture of sample with pre-defined notches

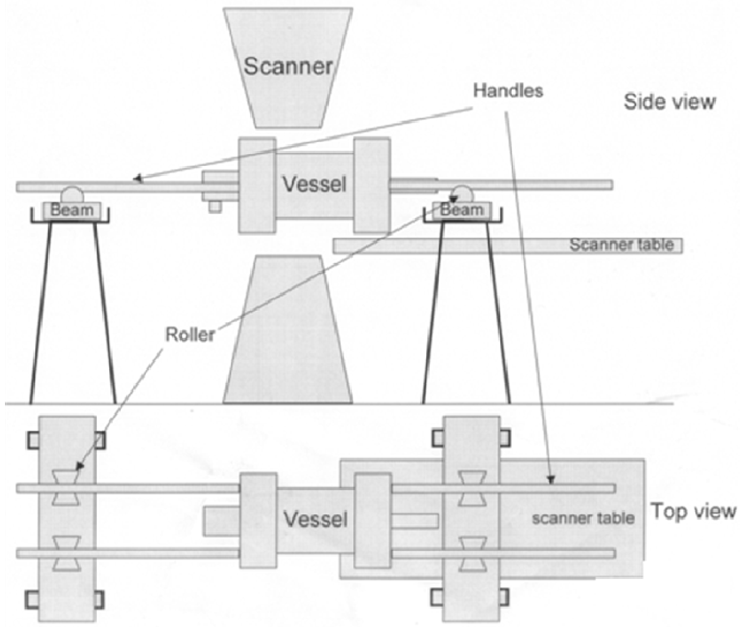

Figure 6-65: Set-up for CT scan tests

Table 15: Information about the fracturing tests in the CT scanner

Test	Flow rate (cc/s)	Peak pressure (bar)	R_d (%)	Fractures
CT 27	0.5	122	68%	No
CT 41	0.92	1013	53%	Yes
CT 42	1.2 – 1.45	92	57%	Yes

6.10.3 Results of tests

Test CT27

Like the large set-up, Test CT 27 did not produce any fractures. The hole around the injection opening was larger because of the high pressures. This process is comparable to cavity expansion. The water-bentonite-silica flour mixture that was used as the injection fluid was mostly concentrated around the injection tube after the test. Some pressure infiltration occurred.

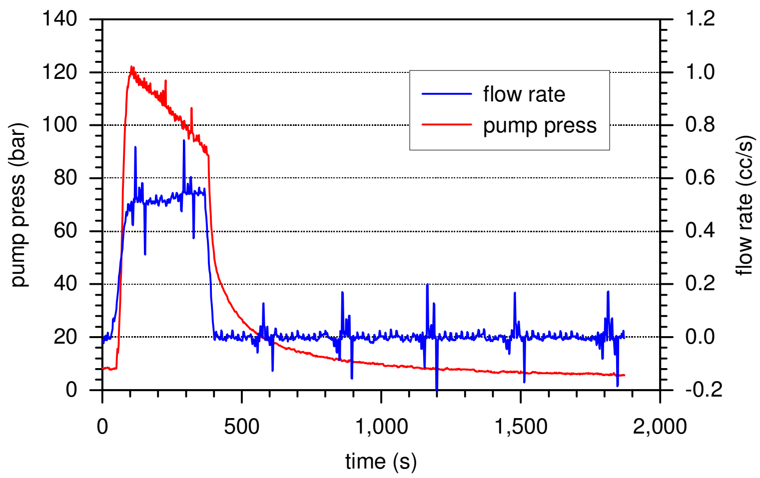

Figure 6-66: Test CT27, injection pressure and flow rate

Injection pressure falls from the beginning to the end of the injection. The decrease is linearly related to the volume of liquid injected. See Figure 6-66. This drop in pressure is not expected for pure cavity expansion because, in cavity expansion, a pressure increase to a limit value is expected. It is likely that there was some fracturing, although this is not evident from Figure 6-67.

The CT scan – see Figure 6-67 – shows some variation in density through the sample in a small area around the injection tube before, and in a slightly larger area after, the injection. In this figure, the amount of X-ray attenuation is presented in "image values". More attenuation leads to higher image values. A change of 100 in the image value corresponds roughly to a variation of 70 kg/m^3. However, different materials also have different values. The middle of the bottom plot shows, in a cross-section, the shape of the injected bentonite mixture. The injected bentonite mixture has a low image value because the density is also low. The density of sand directly around the injected liquid is higher after the injection than before, partly due to densification and partly due to the invasion of the injected material into the pores, replacing the water. Further away from the injected liquid, there are some lines indicating lower densities. These are probably shear bands caused by the plastic deformation of the sand during the injection.

In this test, the fractures did not follow the path of the notches.

Test CT 41

Test CT 41 was more or less a failure. The pressure on the injection liquid, a water-bentonite-cement mixture, was too low during the withdrawal of the tube that creates the opening. As a result, the opening collapsed before the injection could start. A very high pressure peak of more than 1000 bar was necessary to re-open this collapsed opening. Since the equipment was designed for a high-pressure environment, it was possible to reach this pressure. After this pressure peak, there was a rapid decrease to a level comparable to the other tests. See Figure 6-68

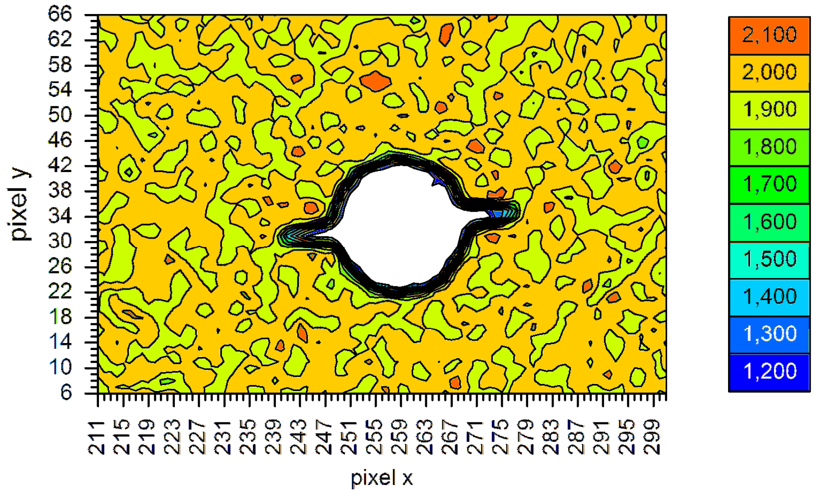

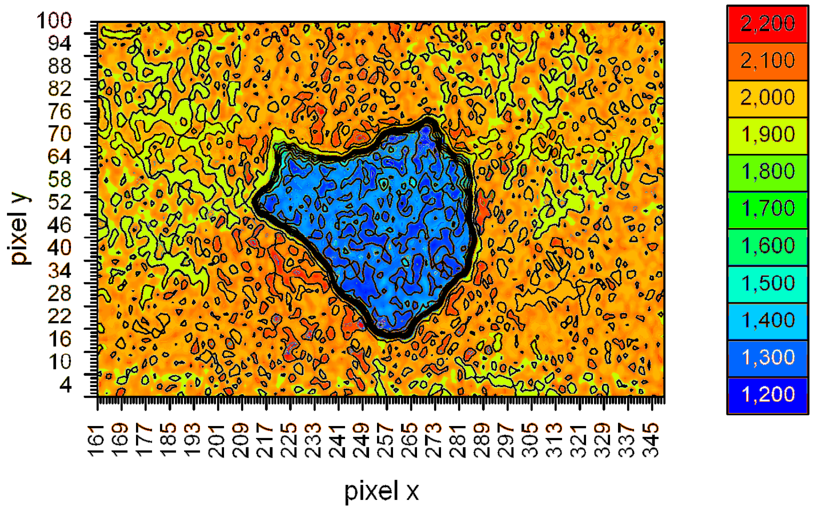

Figure 6-67: Density variations in the sand before the injection (top) and in the injection liquid (the blue section) and sand after the injection (bottom). Density variations in the sand after injection are possibly due to shear bands. See text (note different length scale in the two plots).

.

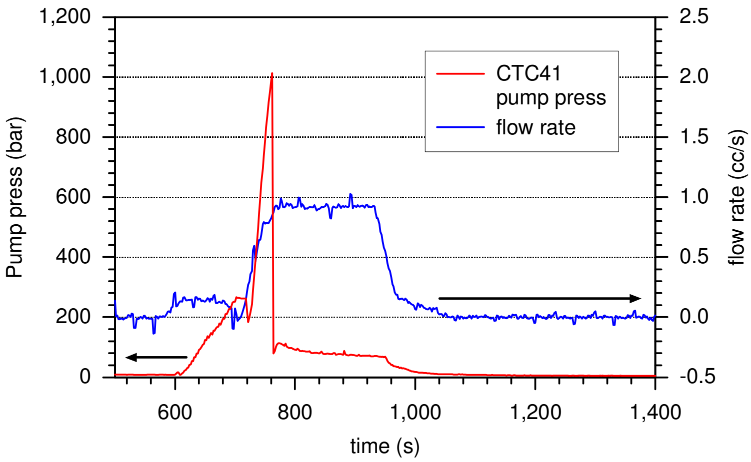

Figure 6-68: Test CT41, injection pressure and flow rate

The high pressure peak resulted in considerable pressure infiltration. See Figure 6-69. The pressure infiltration is shown in the picture by the cylindrical shape. After the grout body was rinsed with water, some sand was still attached. This indicates that bentonite particles were pressed into the sand. In the contour plot, the pressure infiltration is not so clear, since the density of the bentonite slurry pressed into the sand is only slightly higher than the density of water. The shape of the injected grout (the blue area in Figure 6-69) is more suggestive of fracturing behaviour than the shape in Figure 6-67. The density of the grout is higher close to the sand (the green, yellow and reddish areas). This is probably caused by pressure filtration from the grout during the high pressure. No shear bands were found.

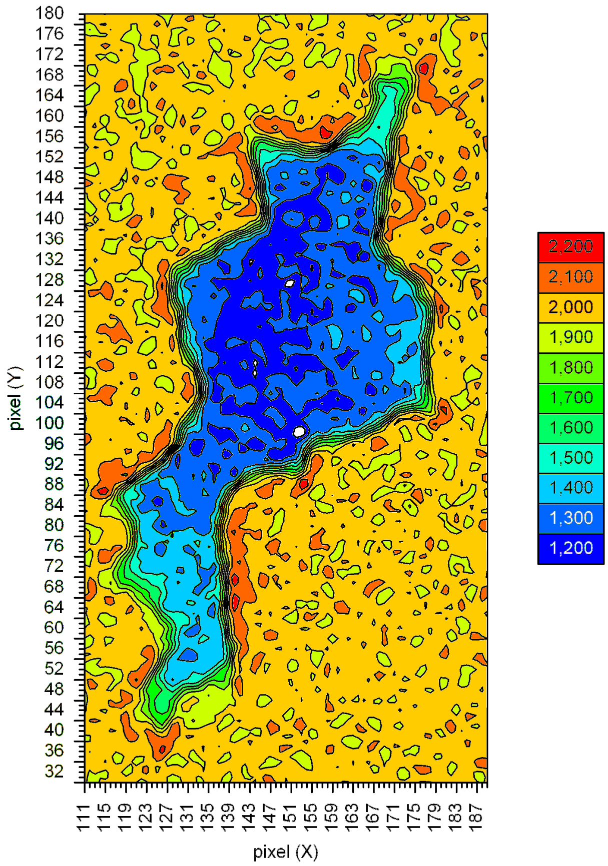

Figure 6-69: Test CT 41, Picture and density variations in the injected liquid and in the surrounding sand in a cross-section

Test CT42

Test CT42 was conducted with the same grout properties as Test CT41. However, in this test, grout pressure during the opening of the injection hole was higher to prevent the collapse of this hole. This resulted in a much lower maximum injection pressure in this test compared to CT41. See Figure 6-66. In this figure, injection pressure increases with the increasing volume of the grout injected. This is likely caused by the increase in radial stress during injection into this sample. At the higher flow rate in this experiment compared to CT27, it was not possible to keep radial pressure constant. The fracture initiation slits made in the sand led to a flat fracture. See Figure 6-71.

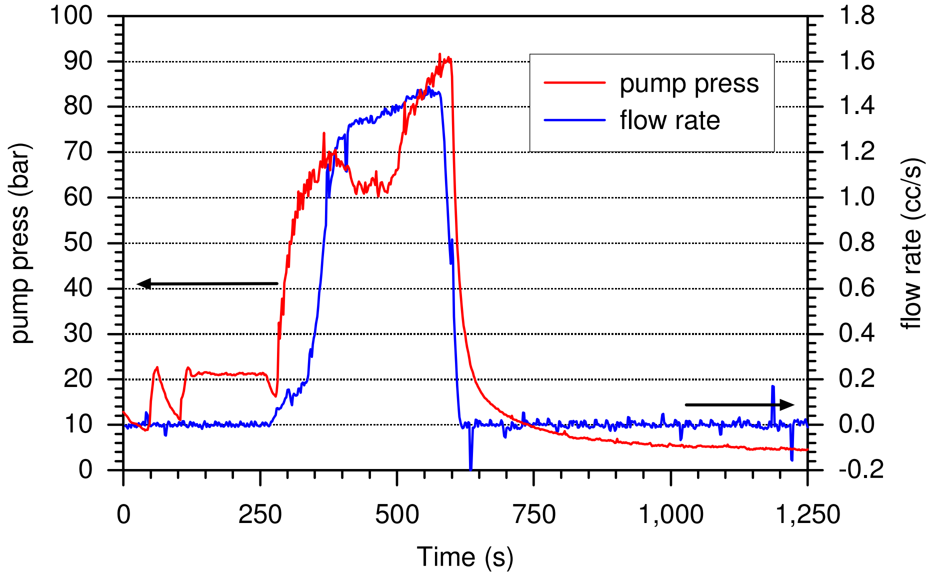

Figure 6-70: Test CT42, injection pressure and flow rate

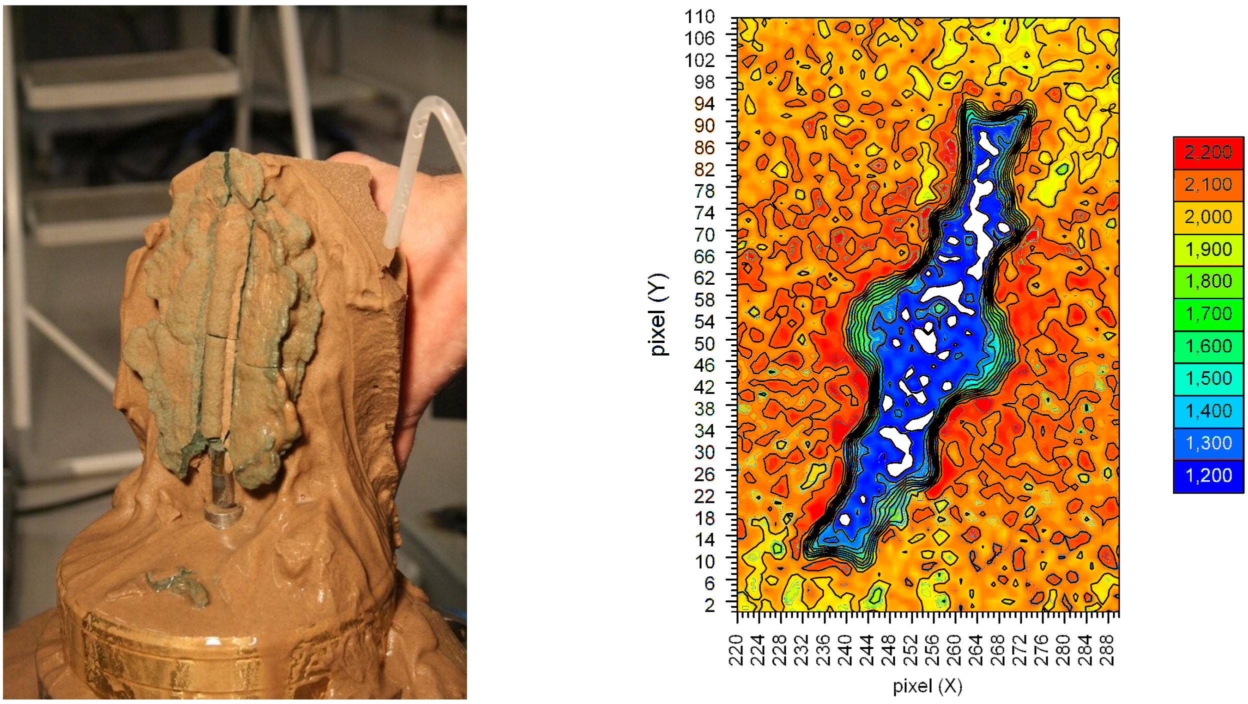

Figure 6-71: Test CT 42, Picture and density variations in the injected liquid and in the surrounding sand in a cross-section. The white areas are areas with densities lower than values corresponding to an image value of 1200. In order to keep the pictures comparable, the colour palette was not changed.

In Test CT 41, the density of the injected grout as measured with the CT scan was more or less constant through the sample. See Figure 6-71. Pressure filtration was less influential than in Test CT41, probably due to the lower injection pressures compared to CT41. The density in the sand is higher than in Test CT41. However, there are some areas at the tips with slightly lower density (the yellow areas). This may be the result of shear failure and dilatancy in the sand.

6.10.4 Additional CT scans

In addition to the three tests described above, the density was determined of a grout sample obtained in the first test series (Test 1-5). The grout sample was removed from the injection tube (see Figure 6-13) after the test and only the grout body formed during the test was placed in the CT scanner. Figure 6-72 shows the result for one cross-section of this CT scan.

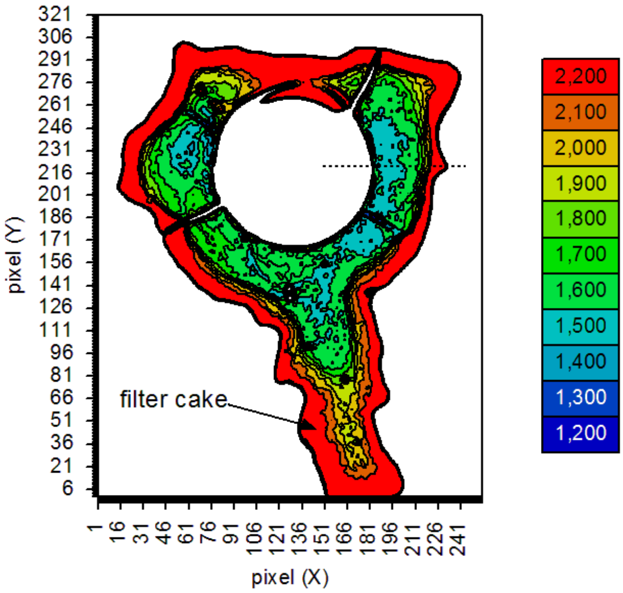

Figure 6-72: CT scan showing a cross-section of a grout sample obtained from Test 5 of the first test series

A comparison of this result with the results of the other scans showed that the density of the grout is much higher. This was to be expected because the grout used for this test had a lower water-cement ratio. Figure 6-72 also shows that there is more variation in density. The density increases moving away from the centre, where the pipe was located, to the outside, where the grout was in contact with the sand. This increase in density is partly caused by beam hardening – see the next section – but mostly by pressure filtration from the grout. The high permeability of the grout with the WCR of 1 leads to significant pressure filtration during injection before the grout is hardened. The grouts used in tests CT41 and CT42 had a lower cement concentration and therefore lower density. In addition, and again due to the lower cement concentration, the permeability of the filter cake that will form due to the pressure filtration was lower. As a result, the image values are lower and also more constant through the grout body.

6.11 Beam hardening

As mentioned in the section above, the result shown in Figure 6-72 was affected by beam hardening. Beam hardening always occurs when making a CT scan. The X-ray light used has different wave lengths. The X-rays with the longest wave length will attenuate more than the X-rays with shorter wave lengths. Further into the sample the X-rays with the shorter wave lengths are the only ones left. However, at the boundaries, the X-rays with longer wave lengths are also present. The results of CT scans therefore always have higher image factors at the boundaries of a sample.

It is possible to correct for this “beam hardening effect” (Bezuijen et al., 2006). However, this correction cannot be very accurate since the effect also depends on the material through which the X-rays are sent and the density of that material. A correction was made using data obtained from an aluminium cylinder. The result is shown in Figure 6-73. The effect of the correction is shown at the bottom of the plot. It is clear that this effect is only present over a range of approximately 3 mm (from 12 to 15 mm).

The beam hardening effect is not present in the figures from Test CT 41 and CT 42. In these tests, the grout was evaluated in the sample and the beam hardening effect is present in the aluminium tube around the sample but no longer in the sample.

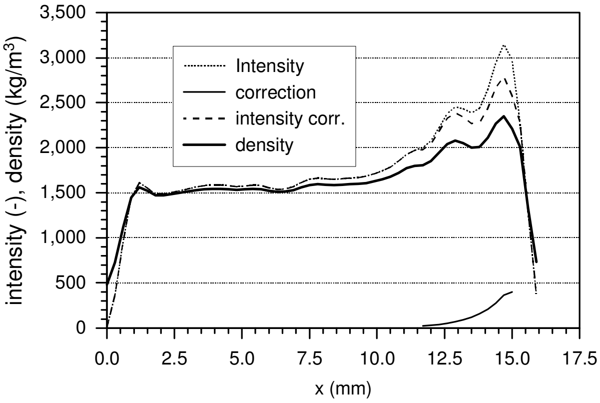

Figure 6-73: Intensity measured with a CT scan. Correction for beam hardening effect and calculated value of the density of the grout along the dotted line shown in Figure 6-72. The correction in intensity can be seen at the bottom of the graph.

6.12 Conclusions from experiments

The tests were designed to acquire a better understanding of the mechanisms that determine fracture shape and efficiency. The first three series showed that the grout parameters are dominant in determining fracture shape. For the sand and confining pressure chosen, it proved not to be possible to define an ideal grout type (a type that would lead to fractures and result in a grouting process with a high efficiency). A high WCR results in a lot of pressure infiltration and therefore in low efficiency. During the tests of the second series, it emerged that the increase in pressure infiltration is more or less linearly related to the logarithmic value of the WCR. Grout with a low WCR will have limited pressure infiltration but results in grout bodies that can hardly be called fractures, being more like irregular spheres. It emerged that efficiency was relatively independent of the shape of the fracture.

The reproducibility of the tests proved to be good when it comes to maximum injection pressures. The shape of the grout body can vary in different tests with identical sand, grout properties and injection rates. This shape may depend to a large extent on local weak spots.

Although, in some tests, especially those of the first test series, the results are more reminiscent of compaction grouting than fracture grouting, the results show that there was no homogeneous cavity expansion during the injection, but that only some of the sand deformed, with other parts being only translated without deformation. This result shows that, in tests without clear fracturing also, there is localised deformation. The reason why these tests did not lead to a clear fracture is not that there is no localised deformation but that conditions such as the grout properties were not favourable for fracturing.

The fourth series showed that it is likely that the confining stress around a TAM is less than thestress caused by the weight of the soil above. TAMs are installed using a casing and sleeve grout. This results in the unloading of the sand directly around the TAM. The lower stresses in the soil just around the sleeve grout led to thinner fractures but also to grout flow between the sleeve grout and the soil. This grout flow was present along the entire injection tube and it may give the grout the opportunity to spread quite a distance in the direction of the TAM tube.

During injection, K_0 increased considerably during the tests. At the end of injection, K_0 was always greater than one and values up to 5 for K_0 were found in the first test series (in a test with a relative density of sand of 75%). According to theory (Raabe and Esters, 1993) this would mean that, at the end of injection, the fractures are predominantly horizontal. The results show fractures in all directions and no dominance of horizontal fractures could be found.

The tests with CT scans showed that, in tests where grout was used with a WCR value of one, density increases at the boundaries of a grout sample. With a WCR of 5, grout density is more homogeneous, indicating that the filter cake is much thinner.

7 Vijzelgracht field measurements

7.1 Introduction

In June 2008, there was a leak in a diaphragm wall built for the Vijzelgracht station of the Amsterdam North-South underground line. A sand-water mixture passed through the wall, resulting in significant settlement (up to 0.15 m) of a block of four adjacent buildings (Korff et al., 2009). Not only had the piled foundations under two of these buildings settled because of the sand that was lost, bearing capacity was also significantly reduced, as emerged from the results of cone penetration tests (CPT) performed before and after the incident. The incident probably resulted in a reduction in the density of the remaining soil around the pile tips and there was also a reduction of soil stresses. The brickwork walls of the buildings were braced with timber beams immediately after the incident in order to prevent the progressive collapse of the buildings. After this bracing was put into place, it was decided to use corrective grouting to restore the bearing capacity of the sand and therefore to raise the buildings by an agreed maximum of 10 mm. If this proved possible, the thinking was that it would constitute implicit proof that end bearing capacity had been restored, guaranteeing that the stability of the buildings had been restored. Moreover, a successful operation would prove that it was possible to compensate for possible future settlement resulting from the ongoing construction of the station.

This chapter presents a brief description of how leaks affect soil properties, followed by the measurement results and an analysis of the compensation grouting project at this location.

7.2 Sand-water leakage

The mechanisms that occur during a leak in a diaphragm wall 12 metres below the groundwater table, and the resulting outflow of a sand-water mixture, have not been studied systematically. What is known is that the cone resistance of the sand behind the diaphragm wall is greatly reduced directly behind the wall and that, some 10 metres from the hole in the wall, the soil layers seem undisturbed. There has been, however, some systematic research into this phenomenon in the oil industry. Sometimes, during the extraction of oil from sand, the well produces oil and sand. This is done to raise the porosity of the sand around the well and therefore the permeability of the sand and, in turn, oil production. During the leak in Amsterdam, there was a comparable situation, with a water flow resulting in instability and the erosion of the sand. This section looks at the results of small-scale experiments that show which mechanisms can occur during the erosion of sand.

Tremblay and Oldakowski (2003) describe small-scale experiments to investigate the behaviour of a sand body from which sand and water are removed. They also present a numerical model. However, here, the qualitative description of the process is important to understand the mechanism involved. Their experiments led to a "wormhole": an area comprising very loose sand, some "tensile failure" bands and the original sand core. See Figure 7-1. The stiffness of the original sand is more than 30 times higher in their experiments than in the centre of the wormhole and the wormhole acts as a high permeability channel. The sand directly around the wormhole is in a very loose state.

On the basis of the experiments described above and experiments investigating the stability of the front face of a tunnel in sand (Leca and Dormieux, 1990) which found a high-porosity zone in front of an instable tunnel face, it is assumed that the leak in the diaphragm wall leads to a high permeability channel with, around that channel, an area of high porosity. The stresses in this high-porosity area are just enough to support the arch that separates the high-porosity sand from the original sand.

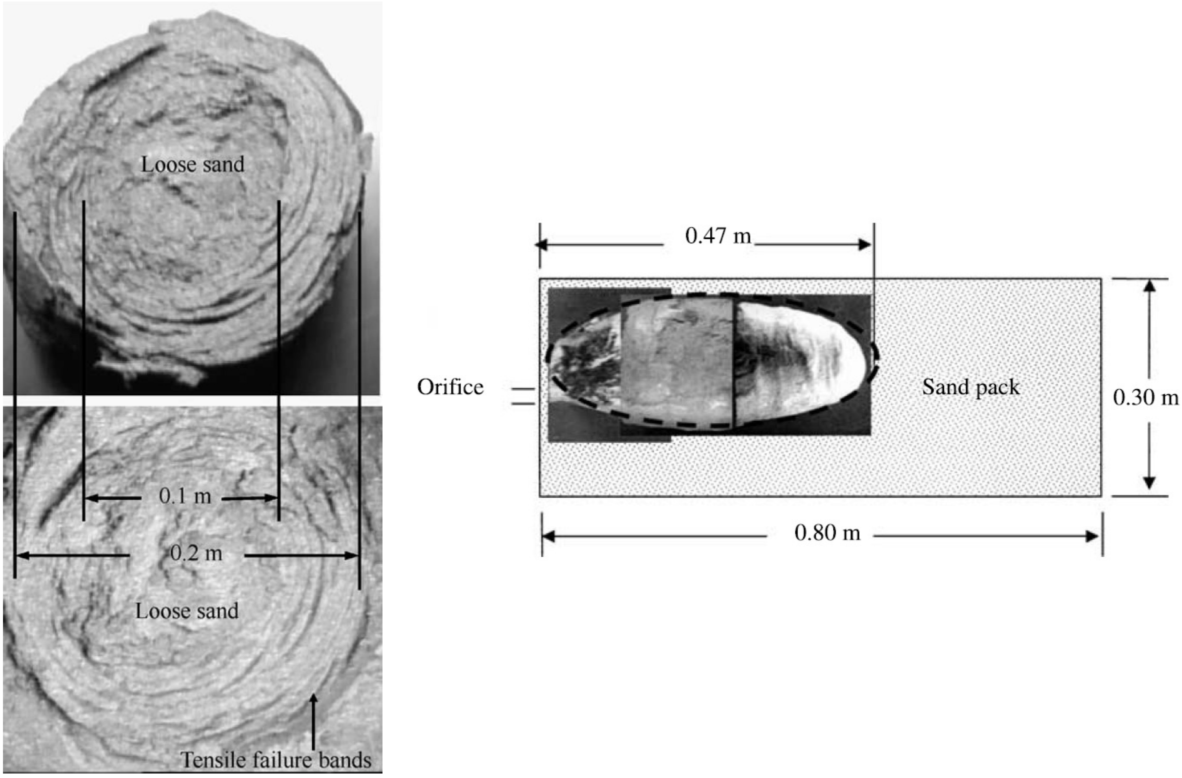

Figure 7-1: Longitudinal view and cross-section of "wormhole" created by extracting oil and sand from oil-saturated sand

In this situation, even a limited amount of sand leakage can affect quite a large volume of sand. Assuming an initial porosity of 38% and a maximum porosity of 48%, 1 m^3 of sand flowing through the diaphragm wall will affect the porosity of about 5 m^3 of sand.

7.3 Compensation grouting, installation

The partly excavated station between the diaphragm walls allowed for the installation of the lances with the TAMs through the diaphragm wall. The layout is shown in Figure 7-2. The TAMs were installed at an angle of 16 degrees from the horizontal. At the diaphragm wall, the installation depth was 12 m –NAP. Underneath the foundations close to the liquid levelling instruments LL12, LL13 and LL14, the depth was 17.66 m –NAP. This means that the TAMs were only around 1.5 m below the pile row closest to the diaphragm wall, around 3.1 m below the middle pile row and around 4.7 m below the pile row furthest away from the diaphragm wall. See also Figure 7-3.

Grout injection was performed using Blitzdämmer, a hydraulically-setting premixed dry mortar (Heidelberg, 2009), as the injection grout. Three types of water-Dämmer ratios were used: 1.4, 1.6 and 2.0, designated as M6, M8 and MF respectively. The different mixtures were used for all pumps and sleeves, and at the beginning and the end of the grouting operations. However, MF was used more in the beginning, M8 in the middle and M6 was used most at the end. It is not known why these different grout mixtures were used. The thinking was probably to create fractures with the MF with the lowest viscosity and then to use materials with larger solid contents to increase efficiency. Table 16 lists the number of litres injected, the number of injections and the average injection dates, showing which mixture was used during the various injection phases.

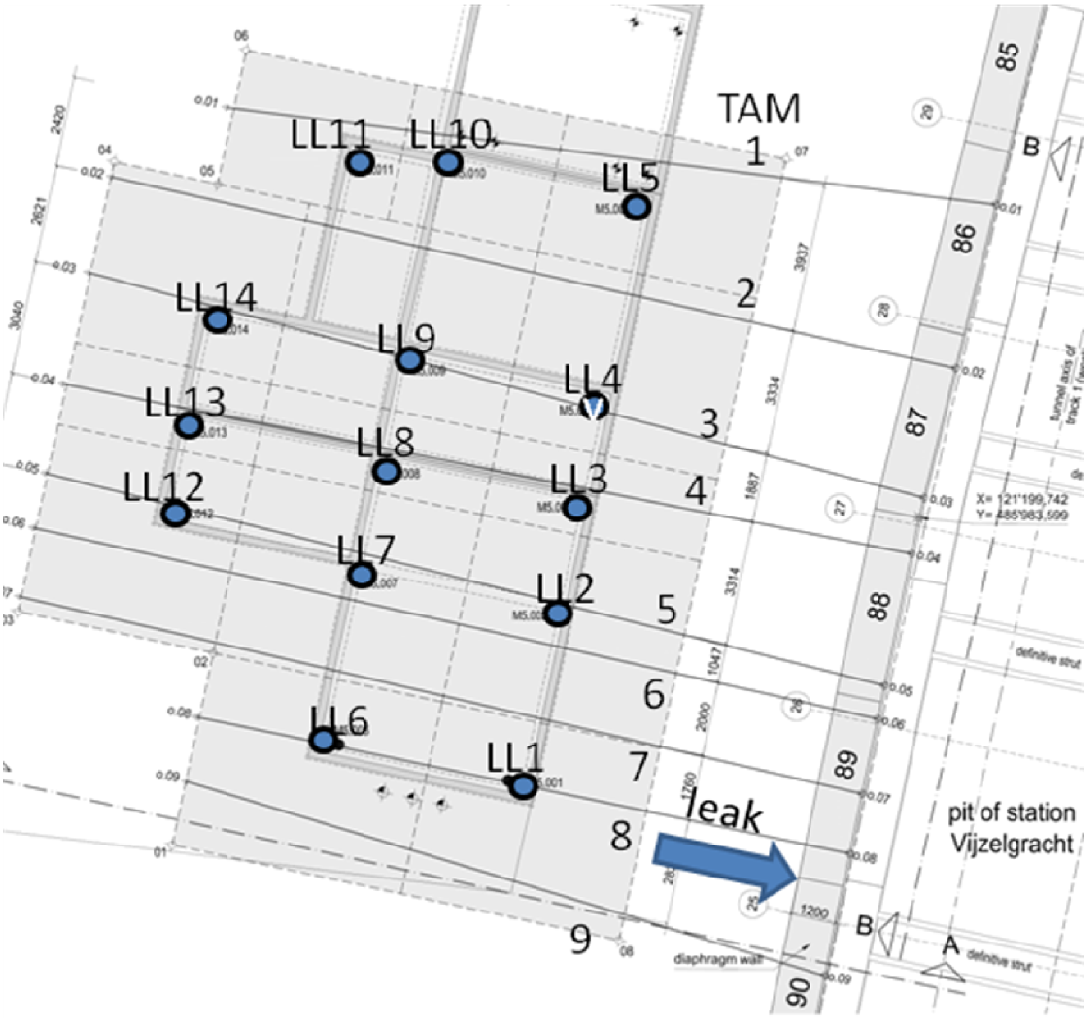

Figure 7-2: Overview of Vijzelgracht compensation grouting area. Lines 1 to 9 show the TAMs. Positions LL11 to LL14 (the blue dots) indicate the positions of the liquid levelling system. The leak was between panels 89 and 90.

Table 16: Data for injection grout mixtures used. See also text.

Mixture	kg Dämmer/ litre water	Density kg/m^3	Number of injections	Total litres	Average Date
M6	0.714	1360	1636	41735	24-09
M8	0.625	1323	1298	29315	09-09
MF	0.5	1269	601	12500	23-08
Total			3535	83550	

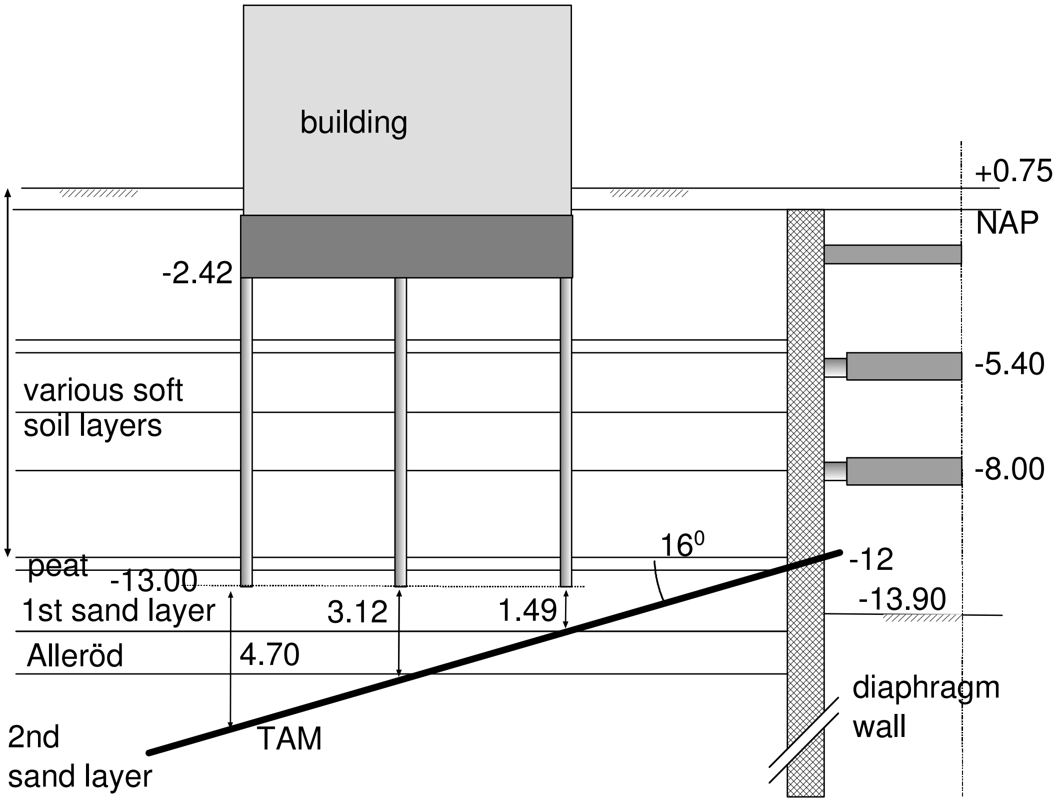

Figure 7-3: Cross-section of location. Dimensions in m. The angled line represents the TAMs.

The leak in the diaphragm wall occurred between panels 89 and 90. So it was here that the loosest sand conditions could be expected.

The results of the measurements were analysed for this study to investigate the extent of the area affected by compensation grouting. It was also possible to study some long-term effects.

7.4 Limitations of field measurements

A relatively common problem when using field measurements is that the data are collected for quality control and not really for study. There can therefore be some inconsistencies or errors in data collection or data processing. Our data also suffer from this problem. The injection reports were not complete; the injection report for 10-8-2008 was copied over the reports for 12-08-2008 and 14-08-2008 in the spreadsheet used for the reports. Only three lines were left from the report for 14-08-2008 and so this report was disregarded. More than half of the report for 12-08-2008 was still available and so this report was used. Consequently, the results for 10-08-2008 were included twice in the overall report (more or less to compensate for the missing values) and the results for 14-08-2008 and some of the results for 12-08-2008 are missing. Altogether, 100 injections are missing or have been replaced by the 10-08-2008 injections. This leads to some inaccuracy, but this is limited since more than 3500 grout injections were performed.

Another inaccuracy in the data is that the time records for the grout injections and the measured heave seem to be out of phase in the first part of the injection process. This can be seen in Figure 7-4.

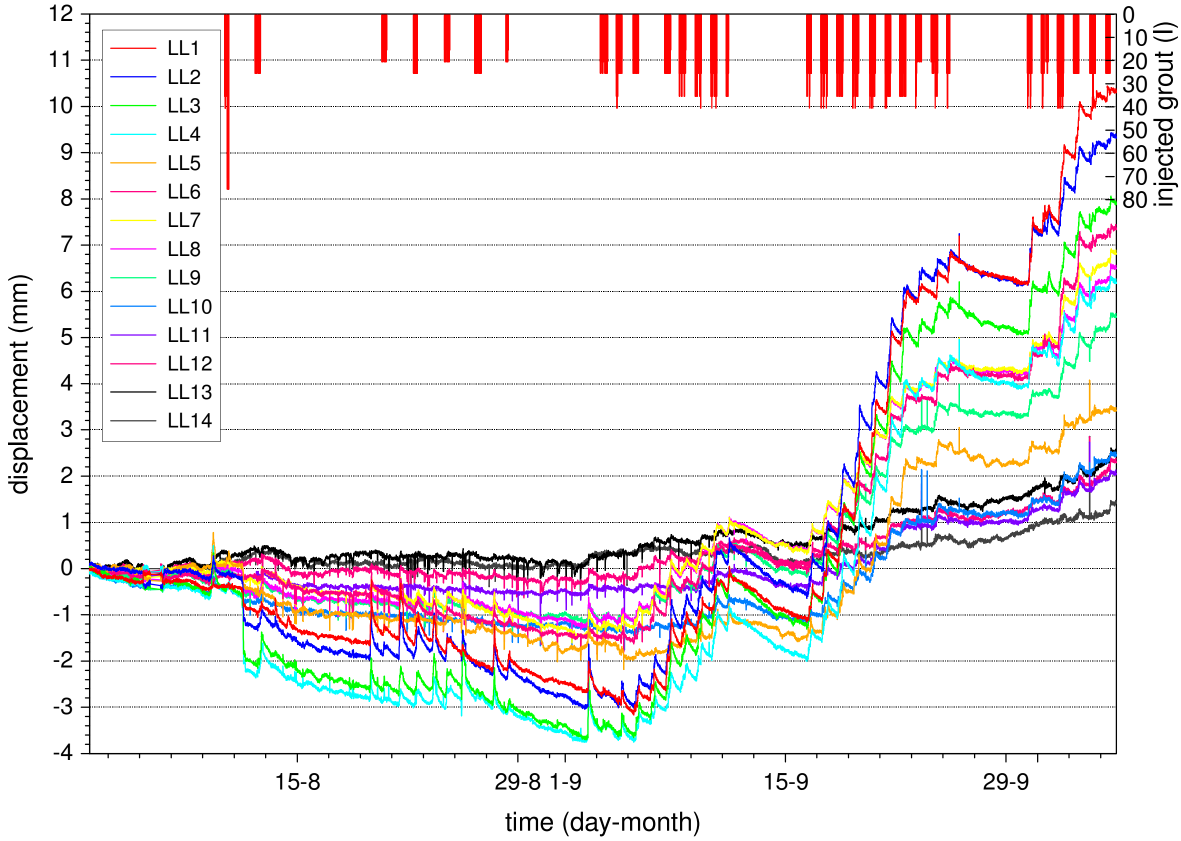

Figure 7-4: Vijzelgracht, measured displacement as a function of time and the periods of grout injection. The periods of grout injection are shown in the red lines at the top of the graph. The length of the line represents the amount of grout injected during one injection. The red lines overlap and are therefore not an indication of the total amount of grout injected (top).

Figure 7-4 shows the measured displacements and when grout was injected. The periods of grout injection coincide with periods of heave in the measurements for September, but not in the measurements for August. Because of this discrepancy, it was decided to focus on the results obtained in September.

7.5 Measurement results

7.5.1 Properties of the injection fluid

The filtration properties of the injection fluid were tested using the consolidation cell as described in Chapter 5. Blitzdämmer M6, M8 and MF were prepared and tested using a confining stress of 500 kPa. The permeability of the Blitzdämmer cake proved to be much higher than that of a normal cement-bentonite grout. This meant it was difficult to determine permeability for the various mixtures. The high permeability explains why a significant part of filtration occurred during the adjustment of the pressure for the filtration test. Consequently, the values found from the filtration test will not be very accurate. The values were determined using the approach described in Chapter 5 and stated in Table 17. Since, during the first part of the test, the pressures applied were too low, it is likely that actual permeability is even higher. No pressure infiltration was found; there was a clear boundary between the Blitzdämmer and the sand and no Blitzdämmer penetrated into the sand.

The results found were more than two orders of magnitude higher than the permeability of a cement-bentonite grout. See Section 5.5. This means that fracture propagation will be limited. The fractures will be localised around the injection point. See Section 4.9 and 4.10.

Filtration also leads to a significant volume loss. The percentage of the remaining volume compared to the original volume is also presented in Table 17 for a constant pressure of 500 kPa in the pressure filtration test. It emerged that, after filtration, the remaining volume of the cake (V_c) is only about 30% of the original volume of the slurry (V_s). At higher pressures this volume will be even lower. Volume loss will be largest for MF and smallest for M6 grout, but the differences are relatively small.

Table 17: Permeability of Blitzdämmer and theoretical efficiency from filtration tests

Mixture	permeability (m/s)	V_c/V_s (-)
MF	4.10^{-7}	0.27
M8	6.10^{-7}	0.31
M6	1.10^{-6}	0.34

7.5.2 Pressure losses in the injection system

The pressure losses in the injection system were determined so that the injection pressures for the TAMs could be evaluated. Using the M8 mixture, with a Marsh funnel time of 36 seconds, an injection with a discharge of 10 l/min was performed in the open air and in a TAM that was in the open air. The last test was performed to measure the additional resistance of the rubber sleeve of the TAM. It was found that, at 10 l/min, the resistance of the injection system in open air was 5.5 bar. The resistance of the injection system with the TAM attached increased to 7.5 bar. This means that the flow resistance in the TAM added another 2 bar to the pressure drop. In the tests, the outflow point was at approximately the same height as the pump, so no correction for hydrostatic pressures was needed. The flow through the injection system will be laminar; this means that the pressure drop will depend on the type of grout, its viscosity and yield stress. The flow through the TAM will be turbulent and therefore the pressure drop through the TAM will depend hardly at all on the viscosity, and almost exclusively on the density. Adopting these assumptions, it is possible to correct for the pressure drop that can be expected in the injection system and the TAM for the MF and M6 Blitzdämmer mixtures based on the experimental results for the M8 mixture and the measured Marsh funnel times for the MF, M8 and M6 mixtures. The following parameters were used in the calculations:
- length of injection string 90 m
- the discharge is 10 l/min, corresponding to $1.6667*10^{-4}$ m^3/s.
- diameter 0.010 m
- viscosity based on the Marsh funnel values obtained, using the standard formula:
$\mu = \rho(t_{marsh} - 25)$ with t_{marsh} being the Marsh funnel time in seconds
- the shear strength is 2000μ when using [pa.s] for μ and [pa] for the shear strength. This is a rather rough estimate based on Sanders' (2007) measurements for cement-bentonite grout.
- the total pressure drop in the string (ΔP_{tot}) is determined by adding the pressure drop according to the Hagen-Poiseuille relation (ΔP_{visc}) to the pressure drop due to the yield stress (ΔP_{yield}). Strictly speaking, these two pressure drops cannot be added because the yield stress changes the flow pattern in the injection system. However, this was done here as an approximation. Littlejohn (1982) suggests the same procedure.
- The pressure drop in the TAM (ΔP_{dyn}) depends on the density only and is the measured 200 kPa for the M8 material. For the M6, the calculated pressure drop in the TAM is increased in

proportion to the density increase and, in the same way, the calculated pressure drop in the TAM is reduced for the MF material.

Using these parameters, the results summarised in Table 18 were found.

Table 18: Calculated pressure drops for various Dämmer mixtures, measured values for the Marsh times. Directly measured values in italics.

					Pressure drop injection string (tube)				Pressure drop TAM
Type	Marsh Time [s]	Density [kg/m^3]	Viscosity [Pa.s]	Yield stress [Pa]	ΔP_{visc} [kPa]	ΔP_{yield} [kPa]	ΔP_{tot} [kPa]	Rey -	ΔP_{dyn} [kPa]
MF	*38.15*	*1270*	0.0167	33.4	1021	383	1403	1614	194
M8	*40.41*	*1310*	0.0202	40.4	1234	463	1696	1377	*200*
M6	*42.78*	*1360*	0.0242	48.4	1478	554	2032	1194	208

The results show that the calculated pressure drop is much higher than measured. The measured total pressure drop ($\Delta P_{tot}=\Delta P_{visc}+\Delta P_{yield}$) for M8 in the injection string was 550 kPa; the calculated value is 1696 kPa.

It is likely that there is some shear thinning in the injection line. This means that the shear forces lead to an effective lower viscosity and yield stress in the injection string. The calculations were therefore repeated, but now with a Marsh time that is adapted so that the total pressure drop over the injection string ($\Delta P_{tot}=\Delta P_{visc}+\Delta P_{yield}$) for M8 due to viscosity and yield stress is only 550 kPa. The other viscosities and yield stresses are scaled down by the same percentage. Table 19 shows the results. The calculation for the pressure drop in the TAM (ΔP_{dyn}) was not changed.

Table 19: Calculated pressure drops for various Dämmer mixtures, fitted values (directly measured values in italics)

					Pressure drop injection string (tube)				Pressure drop TAM
Type	Time fitted [s]	Density [kg/m^3]	Viscosity [Pa.s]	Yield stress [Pa]	ΔP_{visc} [kPa]	ΔP_{yield} [kPa]	ΔP_{tot} [kPa]	Rey -	ΔP_{dyn} [kPa]
MF	29.3	1270	0.0054	10.8	331	124	455	4974	194
M8	30.0	1310	0.0066	13.1	400	150	*550*	4244	*200*
M6	30.8	1360	0.0078	15.7	480	180	659	3678	208

The resulting pressure drop using these fitted values is, for M6, approximately 100 kPa higher than for M8 and the pressure drop for MF is again approximately 100 kPa lower. The pressure drop in the TAM hardly depends at all on the type of mixture. The pressure losses proved to be significant when compared to the injection pressures measured. For these fitted values the Reynolds numbers (Rey) are larger than 2000, the boundary for laminar flow in pipes. However, since the yield stress dampens turbulence, it is assumed that this laminar flow is still a reasonable assumption.

Figure 7-5 shows the measured injection pressures with and without correction. The figure shows clearly with the different colours the dates when the different mixtures were injected. With some exceptions, the first grouting was MF only, followed by M8 and finished with M6. The figure also shows some regression lines for the different grouts. It is clear that the pressures measured when MF was injected were lower on average than for the other two mixtures, whether or not the data were corrected for the pressure losses in the injection system. The average injection pressures using the M8 or M6 grout are more or less the same without any correction. Using the correction described above, the average injection pressures for the injections with M6 and M8 move even closer to each other. Neither the filtration tests nor the analysis of the field measurements produced results that justified a preference for one of the grout mixtures used.

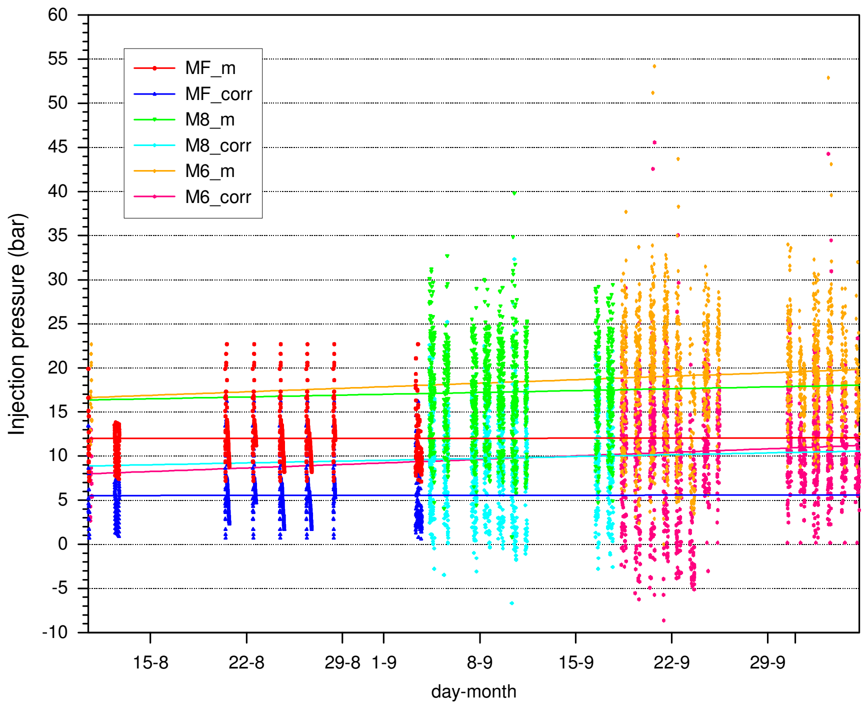

Figure 7-5: Injection pressures as measured (m) and after correction (corr)

7.5.3 Pressure required to crack the sleeve grout

Chambosse and Otterbein (2001) present a calculation method to calculate the injection pressure needed to crack the sleeve grout. They assume that the crack is triggered by pure tensile forces and that the aperture angle of the clods is 120^0 in both the axial and radial directions. Adopting this calculation method and after entering in the diameter of the casing (0.15 m), the TAM (0.075 m) and a Blitzdämmer compressive strength of 8 MPa – this strength is reached within 3 days (Heidelberg, 2009)) – the pressure required to crack the sleeve is 30 bar.

Looking at the injection pressures measured – see Figure 7-5 – it is clear that the injection pressure is less in most cases, certainly at the beginning of the injections. The calculation method of Chambosse and Otterbein (2001[b]) probably over-predicts the necessary pressure, but it is also likely that there were already some cracks in the sleeve grout after installation. Since the records analysed with pressure over time that will be discussed in the next section did not indicate a distinct pressure peak, the most likely option seems to be that there are already cracks after installation.

7.5.4 Injection pressures

Course of injection pressure

The project organisation provided some examples of the pressure records made during injection. Figure 7-6 and Figure 7-7 present two examples of a pressure record of this kind, with the injection rate. In principle the injection rate is controlled at 10 l/min. However, pressure variations have an influence on the rate. At pressures above 45 bar, injection can stop completely (see Figure 7-7, right-hand plot), because the maximum pressure that can be exerted by the pump system is reached.

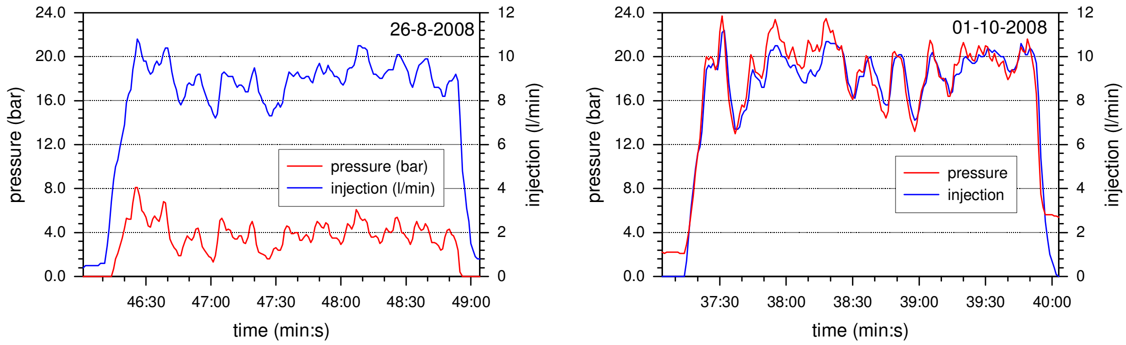

Figure 7-6: Vijzelgracht, injection pressures at the beginning and at the end of the compensation grouting project

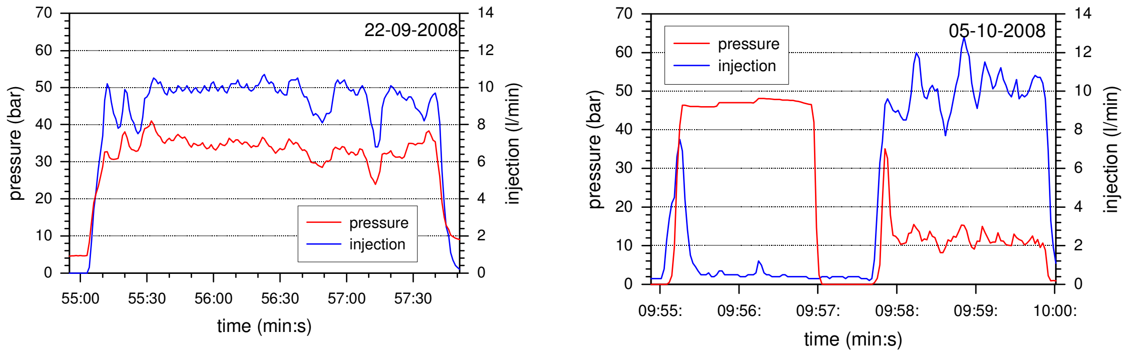

Figure 7-7: Vijzelgracht, remarkable injection pressures during the compensation grouting project (note that the scale is different from the scale used in Figure 7-6)

The left-hand plot in Figure 7-6 shows the pressures in the first part of the compensation grouting project; the plot on the right was measured at the end of the project. The left-hand plot shows, apart from the fluctuations, that there is also an overall decrease in pressure as a function of time. This may be caused by a fracture. The right-hand plot shows fluctuations but no overall decrease in pressure during the course of the injection, probably because there is no fracture.

Figure 7-6 makes it clear that, in most cases, the pressure fluctuations measured correspond to fluctuations in the injection rate. This indicates that the fluctuations in the injection pressures were not determined by the fracturing process, because the pressures necessary for fracturing are more or less independent of the injection rate. It is likely that the dominating mechanism determining the fractures is a flow restriction in the injection lines, the packer and/or in or around the TAM.

The pressure and injection records in Figure 7-7 include some "unusual" values. The left-hand plot shows a rather high injection pressure of 30 to 40 bar, yet the fluctuations in the injection pressure follow the fluctuations in the injection speed. This means that, for these high injection pressures also, flow resistance is dominant. The right-hand plot shows a record in which the necessary injection pressure exceeded the capacity of the pump. As a result, injection stops even though the pressure remains high. In a second attempt, there was again a pressure peak (at about 9:58 in the right-hand plot), but then the flow starts and the pressure drops to normal values (around 10 bar). This plot is from the last day of the compensation grouting campaign, so it is likely that the TAM was constricted, for example by hardened grout, and that this constriction was removed only in the second attempt, after which the grout started to flow.

Injection pressures for repeated injections

It is generally accepted that injection pressures increase during a compensation grouting campaign (Chambosse and Otterbein, 2001[b]). The idea is that, during the initial injections, horizontal pressure is still relatively low; the grout fractures may extend in a vertical direction. However, after a number of injections, horizontal pressure rises and the principal direction of the fractures will be horizontal. The higher horizontal pressures and the hardened grout around the injection sleeves lead to higher injection pressures.

This theory was tested using the injection data. A few sleeves were selected in which quite a number (50–70) of injections were performed. The injection pressure measured at the end of the injection was plotted for each of these injections. The results are shown in Figure 7-8.

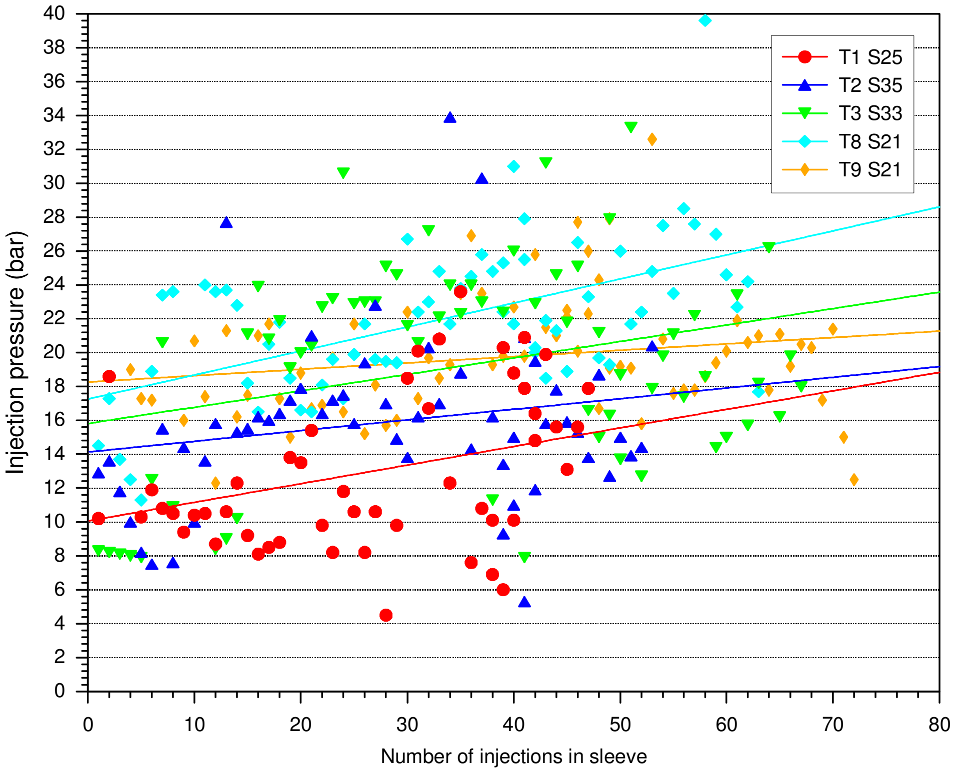

Figure 7-8: Pressure measured at the end of the injection for subsequent injections in one sleeve. The legend presents the tube number (T) and the sleeve number (S) for which the pressures are given.

The figure shows that the injection pressure may indeed tend to increase when the number of injections through the same sleeve increases, but the tendency is rather weak. The scatter for the subsequent injections is much larger. It is possible that an injection pressure of more than 34 bar is followed by much lower injection pressures slightly higher than 5 bar.

This result means that the relation between the number of the injections in the sleeve and the injection pressure, and therefore the relationship between the amount of grout injected and the injection pressure (because 25 litres were injected in all the injections shown), is not as straightforward as is sometimes assumed. A possible cause is that the injections in various sleeves of one TAM interact with each other. The injection at one point probably sometimes creates a low stress situation around another injection point, resulting in lower injection pressures when that other injection point is used.

The hardening of the grout itself seems to have only a limited effect on the injection pressures. If hardening played a role, the injection pressures would be higher in the morning when all the grout has hardened. Plotting all the injection pressures according to the time of the day when the injection started does not confirm a trend of this kind. See Figure 7-9.

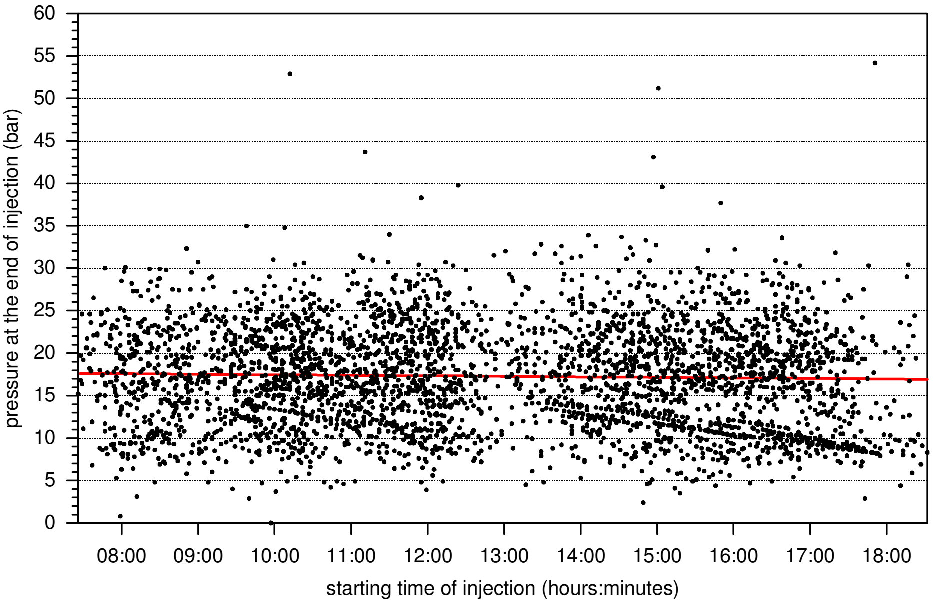

Figure 7-9: Injection pressure as a function of the time of the day. The red line is a linear regression line.

Position of high and low injection pressures

In addition, the locations of the injections with the lowest grouting pressures were investigated. The 100 lowest and 100 highest pressures found (of the total of 3,535 injections) were selected and their locations are plotted in Figure 7-10 (some injections with low or high pressures were at the same location and so there are not 100 markers for each selection). The resulting plot shows that a lot of injections with low injection pressures were performed from TAM 1 (the highest black line in the plot) and hardly any with high pressures. TAMs 7, 8 and 9 have a lot of injections with the highest pressures.

It was expected that the injection pressures would be lowest at the locations close to the location of the leak – TAMs 7, 8 and 9 – and higher at larger distances from the leakage point. However, the measurements show the opposite. The lowest grout injection pressures were found furthest away from the leak (for example at TAM 1). A possible explanation could be that the injections at injection pipes 7, 8 and 9 lifted the building slightly and that, due to that the tip forces on the piles and the soil, stress around the piles close to TAM 1 and 2 fell, leading to lower injection pressures

7.5.5 Injections and foundation movements as a function of time

Figure 7-4 shows that, in the early stages of compensation grouting, the process results only in more settlement, especially for instruments LL3 and LL4. This is a remarkable result since LL1 and LL2 are the instruments closest to the opening in the diaphragm wall and it seems reasonable to assume that sand density will be lowest around LL1 and LL2 (see also Section 7.6) due to sand and water leaking through the wall. The reason for the settlement is most likely the loose sand conditions due to the leak. In such a situation, every disturbance leads to densification of the loose sand and therefore to settlement. This result shows that, in such a loose sand situation, compensation grouting involves some risks. The first injection led to a significant settlement of 2 mm. The following injections did not create heave and stopped settlement only temporarily. It emerged that, after 26 August, without compensation grouting, the settlement rate only increased compared to the initial situation: by up to more than 0.2 mm/day for several instruments between 30 August and 2 September.

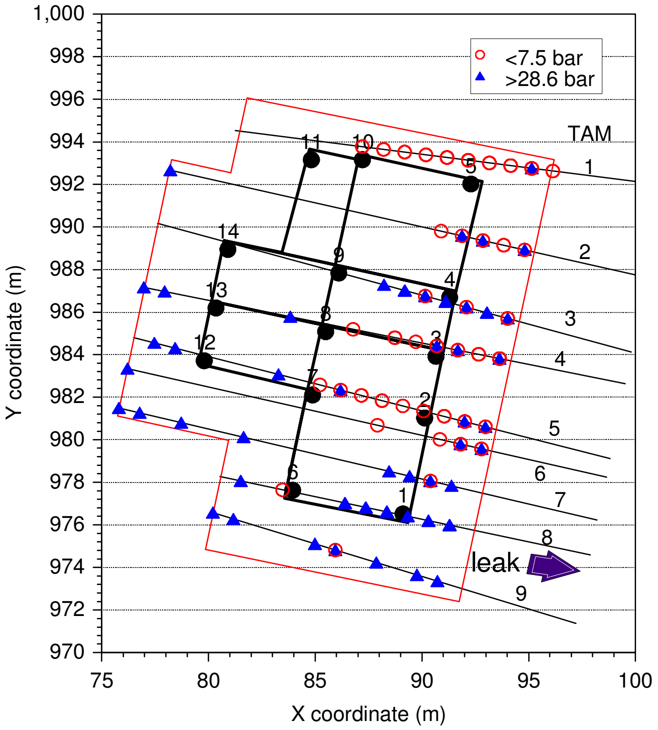

Figure 7-10: Locations where low and high injection pressures were found

After 6 September and the injection of approximately 21,000 litres of grout, the foundation started to rise. It is striking that, in the periods without grouting, settlement continued for most of the instruments. Instruments LL1 to LL12 settled more in the periods without grouting than before grouting (the far left of the plot). At the end of September (around the 29th), instruments LL13 and LL14 continued to rise even if no grout was injected. The grouting at other locations probably led to unloading of this section of the buildings. The other instruments still indicate some ongoing settlement, but less than in the August period.

After the injection period, the settlement of the foundation was as in Figure 7-11. It emerges that most of the liquid levelling instruments indicate ongoing settlement for more than 5 months. Instruments LL4 and LL5 seem to settle even at the end of the measurements shown in Figure 7-11, nearly 8 months after the termination of compensation grouting. This settlement means that most of the heave created was lost and that, for five instruments (LL4, LL5, LL12, LL13 and LL14), the total heave was negative. Eight months after the corrective grouting campaign, then, there was more settlement than before the start of the campaign. This result is quite different from the result shown in Figure 3-7 for the Amsterdam full-scale trial. In the Amsterdam full-scale trial, where there was much less disturbance of the soil before the grouting started, heave appeared much more stable.

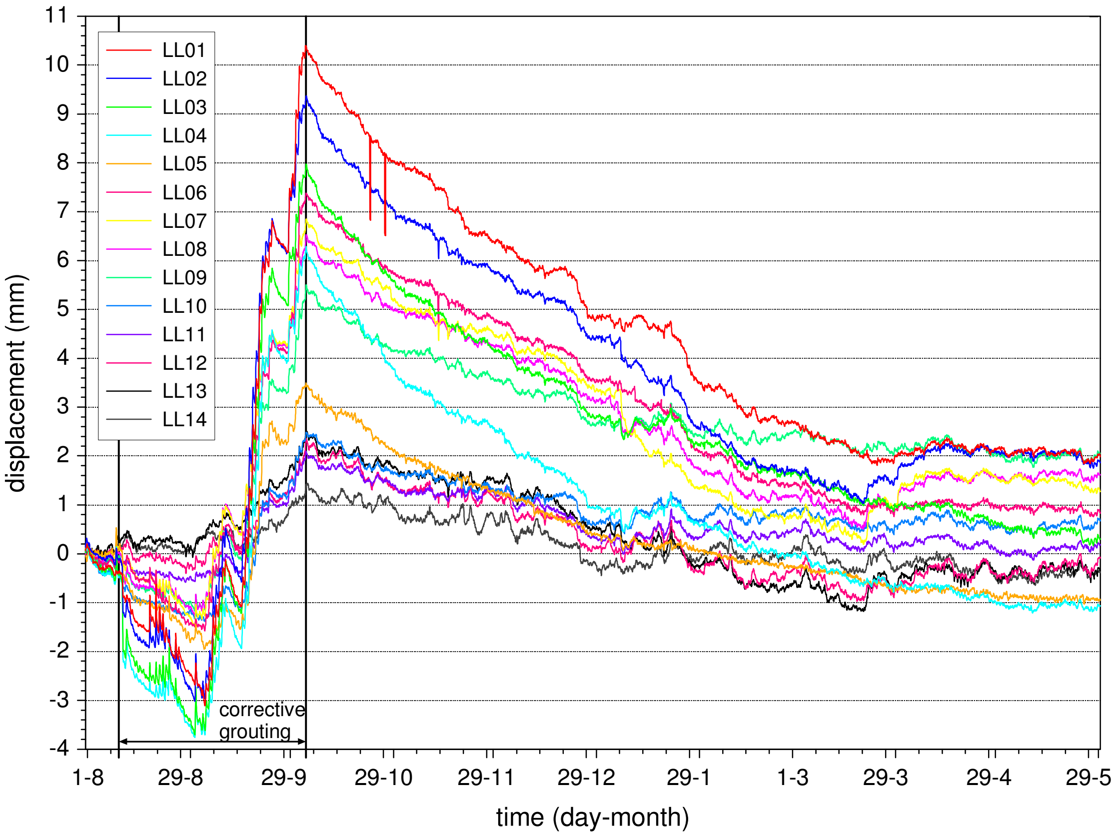

Figure 7-11: Vijzelgracht, ongoing settlement of the foundations after compensation grouting, measurements until 30 December 2008 (data smoothed by using a moving average over 5 measurement points)

The ongoing settlement raises the question: was there already comparable settlement before the compensation grouting as a result of the leak or is the settlement induced by the compensation grouting? The liquid levelling system was installed only days before the start of the compensation grouting work, so the data from before the compensation grouting are limited. Figure 7-12 shows the results for the first measurement days. To smooth the picture, a moving average over 17 measurement points was applied; the markers in the figure are drawn for every 500 data points. Since the markers present the positions of single data points and the line is the moving average, the markers are normally not on the corresponding line. Figure 7-12 shows the short period before corrective grouting. In this figure, broadly speaking, there are two periods: from day 1 to day 4 when average settlement is 0.10 mm/day, and from day 4 to day 7 when there is much less settlement. The average settlement for LL1 from day 1 to day 7 was 0.049 mm/day (in this analysis, day 0 was skipped because there are probably some installation effects also, as can be concluded from the data from LL5). After corrective grouting, the settlement measured with LL1 was, according to Figure 7-11, an average of 0.048 mm/day from 10 November to 30 December 2008. This value is in line with the average value measured before compensation grouting, so it is possible that the settlement after the compensation grouting operation was also a feature before this operation started but after the leak occurred in the diaphragm wall. It is therefore probable that the leak caused the soil disturbance that started the settlement and that this settlement continued after the compensation grouting campaign.

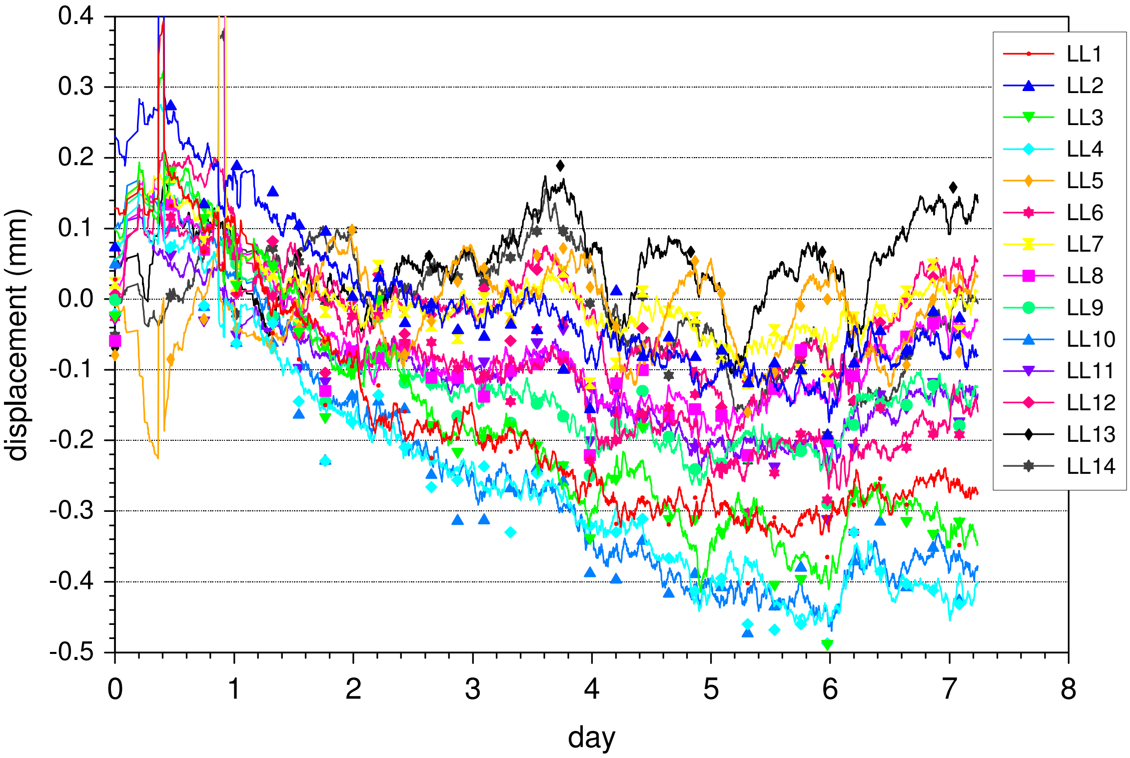

Figure 7-12: Results of settlement records just after the installation of the liquid levelling system (31-07-2009) (data smoothed by using a moving average of 17 points)

7.5.6 Spatial information relating to the total volume injected and the resulting deformation

Figure 7-13 shows the total amounts of injected grout and the resulting deformation based on the data available. The heave at the end of the injection period is interpolated between the measurement points. No extrapolation outside the measurement area was applied, since this could lead to inaccuracies. The circles at the injection points show the amount of grout injected. Not all the numbers can be read, but the diameters of the circles are proportional to the amount of grout injected. The lines on which the circles are drawn indicate the positions of the TAMs. Figure 7-13 shows that most of the heave is generated in \the bottom right of the graph, where a lot of grout was also injected. Although a lot of grout was also injected through the TAM at the top of the graph (TAM 1, see Figure 7-2) this leads only to very limited heave.

7.5.7 Horizontal distance between injections and deformations

The amount of grout injected during each injection was the usual amount for compensation grouting. Nearly all the injections involved 40 litres or less (Figure 7-4, upper part). Larger volumes were used in the trial at the Rokin location (see Section 3.3) where 250 or even 500 litres were injected during one injection at the start of the test. One reason was that, during the Rokin trial, the installation of the TAMs created some settlement and this had to be compensated as quickly as possible. Another reason for the smaller injection volumes compared to the Rokin trial can probably be seen on the left of the plot (upper part). There, 70 litres were injected, resulting in the settlement of 2 mm shown for instruments LL3 and LL4 in Figure 7-4. So large injection volumes probably led to instability in the loose sand underneath the foundation, and therefore to this settlement. However, this remains guesswork: it cannot be proven that the settlement was caused by the 70 l grout injection because, as mentioned before, for this part of the injection operation, there are discrepancies between the time records for the injection system and the deformation system. The small injection volumes for each injection mean that it is not straightforward to determine the deformation result for a single injection. An analysis of this kind is also difficult for another reason: the layout of the injection tubes through the diaphragm wall from the partly excavated station – see Figure 7-2 – made it possible to inject from different locations at the same time and this was done regularly.

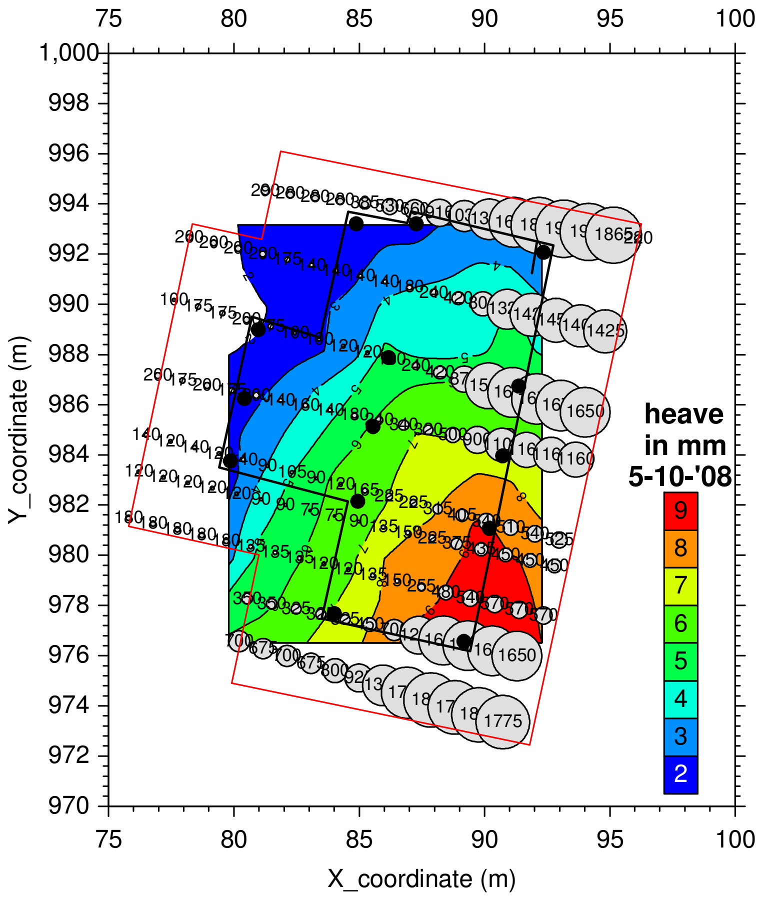

Figure 7-13: Vijzelgracht, injected grout (total amount in litres at each location) and heave realised at the end of the compensation grouting campaign 5-10-2008. See also text.

To establish a picture of the extent of the amount and location of the heave caused by a single injection, two strategies were applied:

1. The amount of grout injected was plotted for a limited period, together with the heave caused by that amount. When grout is applied locally, it is possible to investigate whether a local injection results in local heave.
2. The measured heave was averaged using a moving average for 5 measurement points (as in the plots for Figure 7-4 and Figure 7-11) to reduce the noise in the measurements. From these data, the moments that resulted in a movement of more than 0.05 mm between 2 measurement points in time, which means within 2 minutes, were selected for the measurement positions LL1, LL2 and LL3. It was then determined for these moments whether or not there was an injection within 10 minutes before the measurement of the heave and whether or not the heave measured at that position was the maximum heave measured for all the liquid level points. When these conditions were fulfilled, the distance from the measurement position to the injection point was determined.

Figure 7-15 and Figure 7-16 show some results for the first method. These figures analyse the data from 19 September 2008.

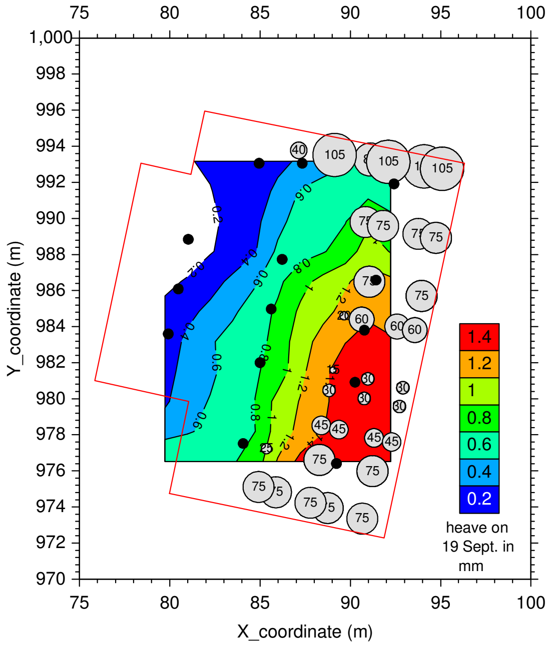

Figure 7-14: Vijzelgracht, overview of injected volumes and heave created on 19 September 2008

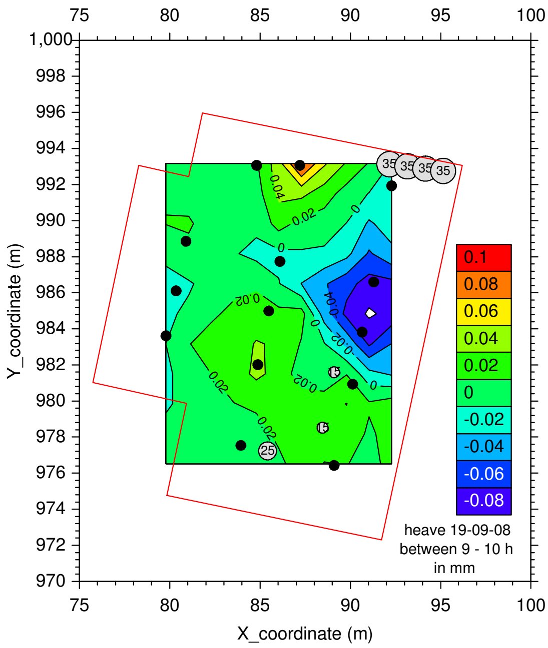

Figure 7-15: Vijzelgracht, injected volumes and heave on 19-09-2008 between 9:00 and 10:00

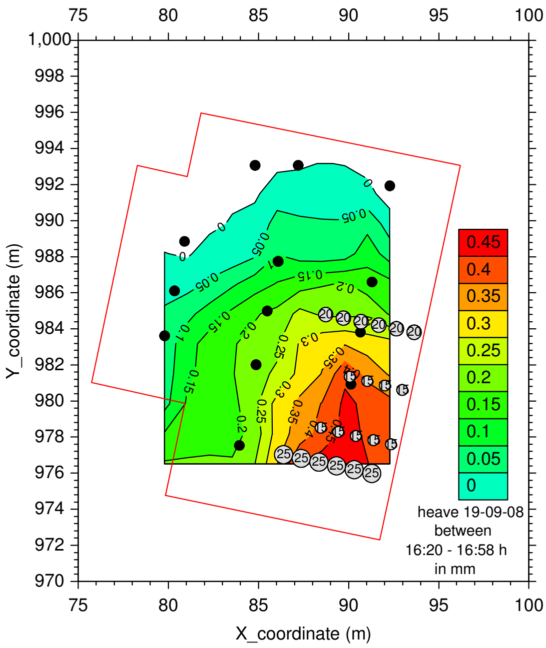

Figure 7-16: Vijzelgracht, injected volumes and heave on 19-09-2008 between 16:20 and 16:58

These figures show that the result for the whole day in Figure 7-14 is generally comparable with the overall result (Figure 7-13), except that there is less heave. Here also, considerable heave was achieved in the lower right-hand corner of the area and a lot of grout was injected in the upper part of the area (without any significant heave). Between 9 and 10 a.m., only a limited number of injections were performed. More heave might have been expected from these injections in the upper right of the measurement area, the location of most of the injections in that period.

Towards the top, in the middle of the measurement area, there is some heave. The injections with a limited volume at the other locations do not seem to have any impact on the heave.

Between 16:20 and 16:58, there were a considerable number of injections towards the lower part of the area and this is where most heave was found.

The second method described above did not establish any relation between heave and distance. It looks as though there can be a given heave at all distances from the injection points. See Figure 7-17. It should be realised that the foundation and the building were rather stiff because the building had been strengthened with stiff timber beams – see Figure 7-18 – to prevent further damage after the incident. Heave was measured at the building. Heave can be localised and caused by one injection beneath the measurement point, but it may also be a result of the rotation of the entire foundation. Therefore no correlation was found between the position of the injection point and the location where heave was measured.

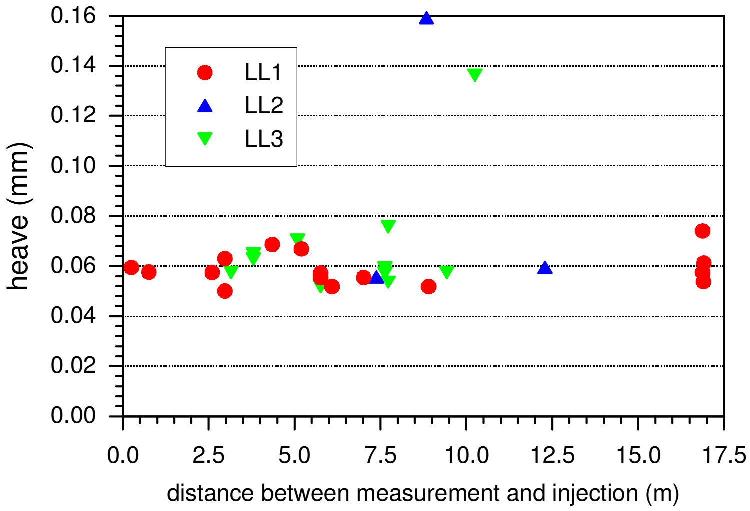

Figure 7-17: Heave as a function of distance from the injection

Figure 7-18: Example of braced houses at the Vijzelgracht location. Timber beams are also present inside the buildings, as can be seen through the windows.

7.6 Cone penetration tests

Cone penetration tests (CPTs) were performed before and after the compensation grouting. One CPT was performed close to the buildings affected by the diaphragm wall leak; the others were performed inside the buildings after the leak but before and after the grouting. Figure 7-19 shows the positions used for this work. The black lines in the figure are the outline of the buildings. The CPTs numbered 1, 2, 3 and 4 were performed before the compensation grouting; numbers 112, 102, 103 and 104 took place after the compensation grouting campaign. The CPTs performed before and after compensation grouting were not taken at exactly the same location but very close to each other at intervals of only 0.5 to 1.0 m. Figure 7-20 lists the results of the CPTs. In these results, soil layering also proved to provide an indication of which layers are affected by the compensation grouting.
Comparing the results of the CPTs after the leak through the diaphragm wall with the CPTs performed before the leak, it is clear that the resistance of the first sand layer was severely affected by the leak. Cone resistance was significantly reduced up to CPT3, with hardly any effect for CPT4.

Compensation grouting leads to an increase in cone resistance. Comparing the results in Figure 7-19 with the results in Figure 7-20, it emerges that, by contrast with the heave, the increase in cone resistance found with the CPTs before and after the compensation grouting roughly corresponds to the amount of grout injected at that location. For example, at location 2, only a limited amount of grout was injected and so the increase in resistance as shown in CPT 102 is also only limited. At locations 1, 2 and 3, resistance increased more, and more grout was injected at these locations. Cone resistance increased in the first sand layer as well as in the Alleröd, although the cone resistance in the Alleröd was less affected by the leak through the diaphragm wall.

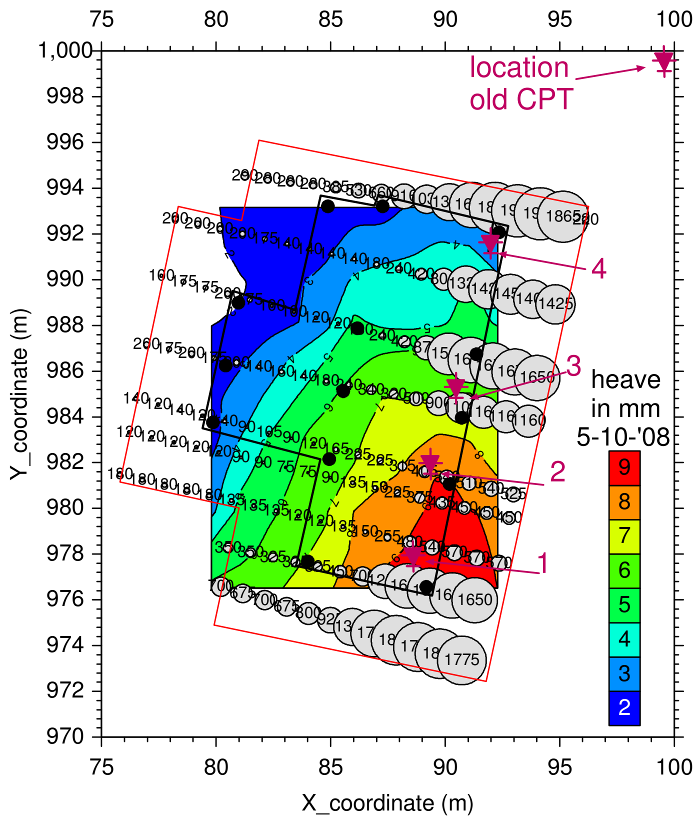

Figure 7-19: Vijzelgracht, locations of CPTs

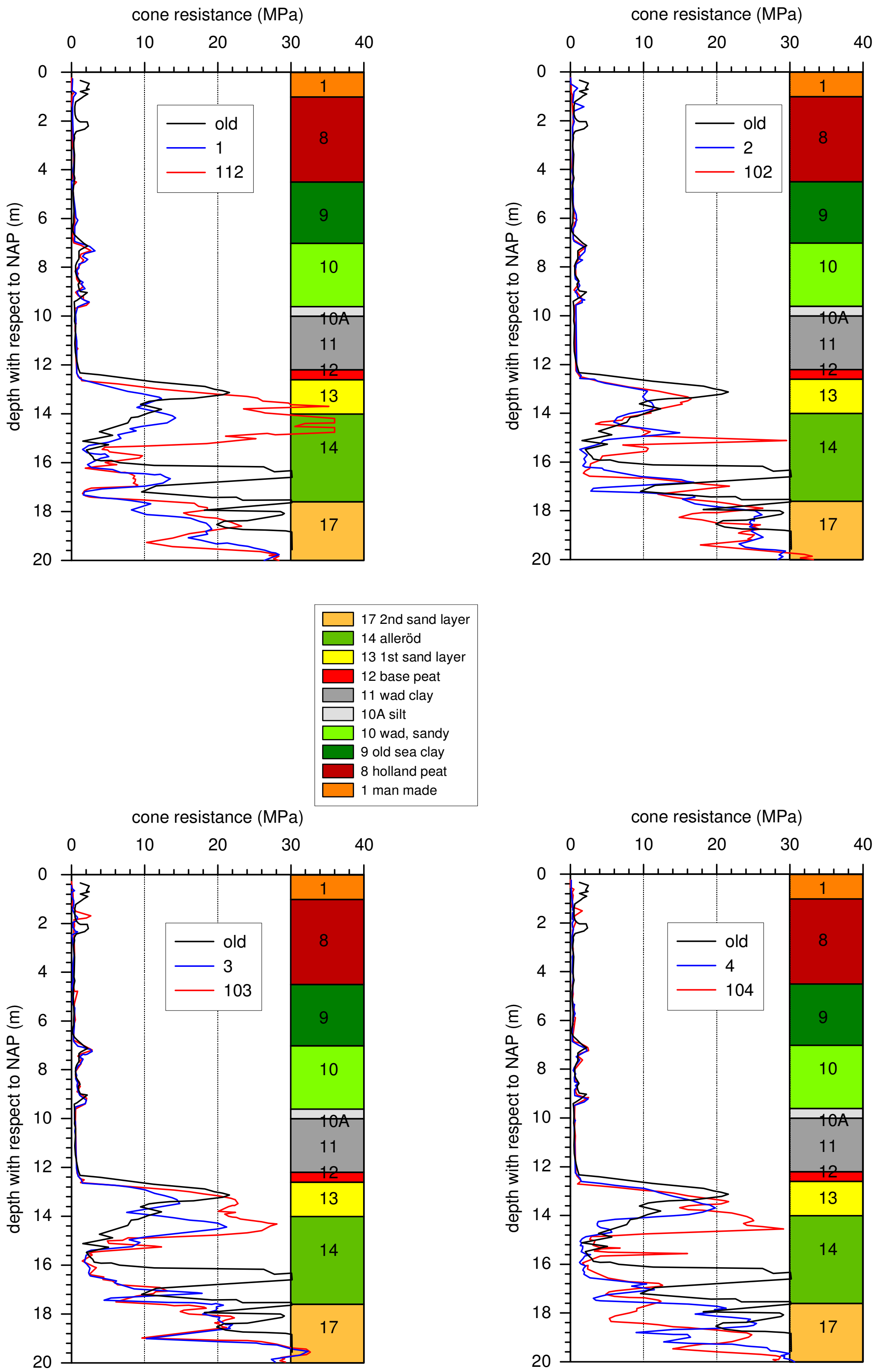

Figure 7-20: Vijzelgracht, results of CPTs and soil layering. For the locations, see Figure 7-19.

It was mentioned above that the heave acting on the foundations as measured with the liquid levelling system was only limited, and so the efficiency of the compensation grouting was low. A possible explanation may be that the tip resistance of the pile was affected by sand erosion and that the piles do not follow the heave of the sand. In the CPTs, the transition from the Old Dutch peat (12 in Figure 7-20) to the first sand layer (13 in Figure 7-20) is very clear in the CPTs. This transition is slightly more evident in the "old" CPT at some distance from the buildings. In the CPTs conducted before and after the compensation grouting, the increase in resistance caused by the first sand layer starts at almost exactly the same depth. This means that, within the accuracy margin for height measurement in a CPT (less than the accuracy in liquid levelling, but in Figure 7-20 a difference of 0.1 m would have been discernable), the soil layers remain more or less in the same positions. If then, due to the compensation grouting, there has been some raising of the sand layers with respect to the foundation of the building, this effect cannot exceed 0.1 m.

7.7 Analysis of the results

7.7.1 Volumes injected

As was already mentioned in the report from Witteveen and Bos (2008), the volumes injected do not correspond to the heave measured. In the southern section of the buildings, close to the hole in the diaphragm wall, there was extensive grout injection, and this generated some heave. In the northern section, there was also quite extensive grout injection, but this did not generate any significant heave (see Figure 7-13). Furthermore, no grout, or only very limited amounts, was injected into the central part of the settled area, but significant heave was measured here. The report states that the stiffness of the foundations may play a role. The injected grout led to a strengthening of the soil, as emerged from the cone penetration tests, but no heave.

The volumes injected are quite considerable: more than 600 l/m^2 in the lower right corner (Witteveen en Bos, 2008). This amount corresponds to an average grout height of 0.6 m. Since the maximum heave created was only 10 mm, the question arises of where all the grout has gone that was injected. This question will be addressed in the next section.

7.7.2 Efficiency of compensating grouting in these conditions

The efficiency of the compensation grouting at Vijzelgracht is remarkably low: 10 mm heave was achieved after the injection of 600 l/m^2 grout. This means that efficiency is only 1.7%, where efficiency of 10-20% is normal for compensation grouting. The grout itself loses quite a lot of volume when injected in sand. For the Blitzdämmer mixtures used here, efficiency was 30% or less in the small-scale consolidation experiments (see Section 7.5.1). Furthermore, a loose sand package reduces efficiency. This study did not address the influence of the relative density of the sand. Figure 7-21 presents the clearest illustration of the influence of relative density in the results from the first series of model tests. The plot shows a lot of scatter and it is questionable whether or not it is permissible to draw the line through the measurements that is plotted in the graph, but it is clear that, in a model test also, low relative density leads to only low efficiency. In the first test series, the "theoretical efficiency" of the grout itself was calculated using the small-scale pressure filtration tests described in Chapter 5. The theoretical efficiency is the volume of the cake after the test compared to the volume of the slurry. It was found that, for the grouts used in the first test series, which resulted in Figure 7-21, theoretical efficiency is 70 to 80% (Kleinlugtenbelt, 2005). For the Blitzdämmer, theoretical efficiency is about 30% only (see Table 17), and this will lead to lower overall efficiency.

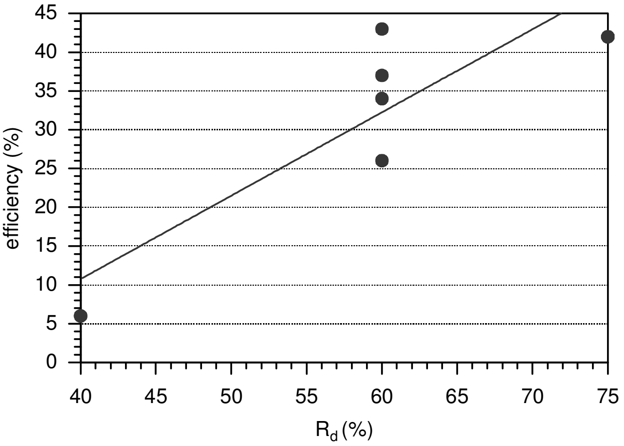

Figure 7-21: Model tests, efficiency as a function of relative density

Figure 7-20 shows a reduction in cone penetration resistance underneath the buildings in the first sand layer and some parts of the Alleröd after the incident. Numerical simulations (Bosch and Broere, 2009) of the incident also led to the conclusion that the second sand layer had been affected. This means that relative density was lower over a height of several metres (for our purposes here, roughly 2 m on average). Assuming that the grout itself has a "theoretical efficiency" of 30% and that porosity increases by an average of 10% (from 38% to 48%, for example), this means that approximately 0.64 m^3 grout/m^2 would be necessary to restore the original relative density and also that the most affected parts, where the sand layer is disturbed over a height of up to 5 m, need a much larger grout volume than has now been injected to restore the original relative density.

At the northern end of the building (north is at the top in the figures with top views), the bracing of the walls of buildings with timber beams may also have a negative impact on efficiency. Corrective grouting was performed under only one of the buildings. However, this building was firmly connected to the adjacent building by the timber beams. Heave is only possible if the adjacent building is also lifted.

7.8 Pile tip resistance versus cone tip resistance

Looking at the measurement results, there seems to be a discrepancy between the behaviour of the piles and the results of cone penetration tests. After the compensation grouting operation, cone resistance was comparable with the cone resistance measured before the leak in the diaphragm wall. However, the foundation settled for more than 5 months after the compensation grouting operation. This settlement could be caused by the consolidation of the top layers. The following sequence of events is possible:

1. The leak leads to a reduction of the pile tip resistance. The pile and the building on top of it start to settle.
2. The negative skin friction present along the piles is reversed, becoming a positive skin friction. This happens when there is only limited movement of the piles (a few centimetres) with respect to the soil layers (Bezuijen and Schrier van der, 1994). However, the piles still settle because the skin friction and the reduced pile tip resistance is insufficient to withstand the loading. Settlement stops when the building is partly supported by the soft soil layers just underneath it, which then act like a kind of raft foundation.

3. The installation of the TAMs, and possibly the first grout injections in the corrective grouting operation, led to a further reduction of tip resistance and consequently to some more settlement. See Figure 7-4. The ongoing grout injections led to heave in the entire soft soil package and the densification of the sand layers, although it is unlikely that this operation also enhanced the density of the sand just around the pile tip, since the pile tip is located in the upper part of the first sand layer and, if grout with a relative high pressure is present close to the pile tip, it will "break through" to the soft layers. Another consequence is that the grout operation leads to some excess pore pressure in the soft soil layers above the sand layer. Such excess pore pressures during compensation grouting were calculated by Au et al. (2003), although they grouted in a homogeneous clay layer.
4. The excess pore pressures decrease in time, leading to a decline in positive skin friction and possibly even leading to the restoration of negative skin friction around the piles and therefore to further settlement.
5. This settlement stopped when the excess pore pressures had been dissipated. This took more than five months, but this is a reasonable assumption since there are 12 m of soft layers on top of the sand layer.

7.9 Discussion of measurements

This corrective grouting project took place in rather disturbed soil conditions. The ground loss through the diaphragm wall will result in localised areas in the first sand layer (the layer that supports the piles) with lower densities than other areas. It is clear from the CPTs in Figure 7-20 that cone resistance was significantly reduced close to the location of the leak (CPT 1 and to a lesser extent CPT 2). In addition, CPT 3 shows a reduction of cone resistance in the first sand layer. This was not the case for CPT 4 only.

The achieved heave pattern (see Figure 7-13) corresponds almost exactly to the target values. However, the correlation with injected volumes is not immediately apparent. A lot of grout was injected using TAMs 8 and 9 (see Figure 7-2 and Figure 7-13) before some heave was created in this area. The soil had to be strengthened in areas of former ground loss before heave could be achieved. The achieved heave decreases gradually in the direction of TAM 1. One might expect a fall in injected volumes from TAM 9 in the direction of TAM 1 as well. This is not the case, as can be seen in Figure 7-13. Above TAMs 5, 6 & 7, relatively low grout volumes were used. The reason is the presence of the timber stability beams used to brace the buildings. The process operators also observed heave above TAMs 5, 6 & 7 when injections were performed in the TAMs 8 & 9. The stabilising timber cross beams had stiffened the buildings so much that the buildings acted like girders themselves, spanning the support area above TAMs 8 & 9 and 1 to 4. When this phenomenon was observed, the bolts connecting the temporary timber cross beams were loosened and the building settled 1-2 mm in the area above TAMs 5-7. During the remainder of the grouting operation it proved unnecessary to make disproportional increases in the injected volumes in TAMs 5-7 in order to maintain a smooth heave pattern. The explanation for the injection of relatively large grout volumes through TAMs 1-4, and the relatively small levels of the anticipated (and achieved) heave, is related to the fact that this area is connected to an adjacent building in the block, the load of which also has to be partly lifted. Shortly before the target values were reached, the stabilising timber cross beams were “locked” again. However, it was decided not to remove them but to finish the corrective grouting process to meet the target values, as had been agreed beforehand with the city authorities.

The ongoing settlement of the buildings after the termination of the grouting process exceeded the expected values, but settlement seemed to stop after 5.5 months (see Figure 7-11). A possible explanation was given above: during the incident, the weight of the building is partly supported by the friction between the piles and the soft soil layers above the first sand layer. When the grouting stops, the soft soil layers will consolidate (these layers were disturbed by the leak and the grouting) and a negative skin friction will develop on the piles. The pile foundation is still loaded onto the ultimate bearing capacity and so the development of negative friction will lead to extra settlement. This settlement continued until the consolidation of the soft layers stopped and the friction piles became end bearing piles again.

The construction with the stiff timber beams explains why there is hardly any correlation between the location where the grout is injected and the location where the heave is measured. Apart from the loose sand and the ongoing settlement, there is an additional reason for the low efficiency and that is the use of the Blitzdämmer as the injection material. The permeability of Blitzdämmer cake is 100 times higher than the permeability of a bentonite-cement cake. Research by Bezuijen and Van Tol (2008) and Sanders (2007) has shown that this will prevent the formation of fractures and lead to compaction grouting with a lower efficiency. Furthermore, all the liquid will be pressed out of the Blitzdämmer into the permeable soil before the hardening starts. This consolidation of the Blitzdämmer alone reduces the maximum possible efficiency to about 30%, depending on the type of mixture used.

The low injection pressures found around TAM 1 continue to be puzzling. Compaction grouting should result in higher injection pressures. It is possible that inhomogeneous soil conditions create easy pathways for the injection fluid or, as mentioned above, there may have been some stress relief in this area when the building was lifted by compensation grouting at the other end.

7.10 Conclusions from Vijzelgracht field measurements

The field measurements led to the following conclusions:

- A first and obvious conclusion to be drawn from this measurement campaign is that the reality is more complex than the experimental model. Factors such as localised differences in sand properties due to sand leakage, pile foundations and soft soil layers were not included in the model tests. However, the model tests were useful for understanding some aspects of these field measurements.
- The corrective grouting led to a significant increase in the CPT values for the layers injected. Although the buildings were successfully lifted and stabilised, it was found that the efficiency of the corrective grouting (on the basis of measurements of the upward movement of the foundation) was very low at 1.7%, and that it decreased due to settlement that persisted for more than five months.
- The pressure losses in the injection system were tested separately and proved to be significant compared to the overall injection pressures. They must therefore be taken into account when injection pressures from various sites are compared.
- The buildings are relatively stiff due to temporary stabilising timber beams and cross-beams, and so it was not possible to determine the impact of single injections on deformation.
- In these sandy soil conditions, it is probably better to use a grout that produces a grout cake with a lower permeability. On the basis of the available data, it was not possible to select a preferred grout mixture from the three mixtures used.
- From the field tests evaluated, it emerged that the installation of the TAMs causes (in the Amsterdam situation) settlement of 2–2.5 mm. After the compensation grouting campaign, there will be some long-term settlement. In the Industria and Peek &

Cloppenburg locations, this was 2 mm or less. In a disturbed soil situation, as was the case for the Vijzelgracht site, settlement after grouting of up to 8 mm was found. Since, in all cases, the measurement system for heave and settlement was installed only weeks before the start of the grouting campaign, it is not possible to state whether this settlement was natural settlement at that location. At another location in Amsterdam, Bridge 404, long-term measurements (over a period of 10 months) were made of the settlement of the bridge without intervention. At the bridge, 2 mm of heave and 2 mm of settlement were sometimes measured during the 10 months, but there was no significant downward settlement.

The overall conclusion must be that the application of compensation or corrective grouting below a piled foundation can lead to additional settlement during and after the compensation grouting operation. Au et al. (2003) found the same result for compensation grouting in soft clay. Compensation grouting will lead to more predictable results when applied in stiff sand and hard clay layers. When applied beneath a pile foundation, tip loading has to be significantly smaller than tip resistance to prevent additional pile settlement.

8 Discussion

8.1 Introduction

On the basis of the literature (Chapter 2) and the findings from field tests (Chapter 3), calculation models were developed to describe the shape of a fracture made by fracture grouting in sand. The important grout properties were tested (Chapter 5) and experiments (Chapter 6) were performed to test calculation models and to acquire additional insight into the mechanisms that are important for the fracture shape and the efficiency of the fracture process. The results were checked against the results of a field project in which more information than usual was available about grout pressures and deformations. This field project (Vijzelgracht) was an example of corrective grouting: a leak in a diaphragm wall had resulted in major deformations in the soil, more than could be expected in a compensation or corrective grouting project, and the results were affected accordingly.

In this discussion the results from the literature study, the field tests and the results of the experiments will be compared with results from literature and results from theory. This will lead to a different concept for describing what happens in the soil and the kind of fractures that can be expected during compensation or corrective grouting in the subsoil. Arguments for this different model will be presented.

8.2 Comparison of tests with literature

8.2.1 *Fracture shape*

The results of the first three test series show that, as in the literature (Chang, 2004; Eisa, 2008; Cho, 2009), grout injection in sand will not always lead to fractures. A good comparison between the results described in the literature and the results obtained in this study is not possible because of the wide range of test conditions and injected materials in various publications.

Comparable elements did concur. The fracture obtained with the x-linked gel (Test 2-4) is comparable with the results from Dong and Pater (2008) and the shape of the grout bodies obtained in this study is comparable to results obtained by Eisa in Cambridge (2008) and by Younes (2008). Relatively high injection pressures (the total of the pore pressure plus more than 10 times the vertical effective stress) were found in both the literature and in this study in experiments where the fractures had a higher *d/s* ratio. Compare, for example, the experiments of Younes (2008) with a P_f/σ_v ratio of 10 to 16 with the experiments in the third series, where this ratio varied between 15 and 27. There may be differences in this ratio due to differences in the density of the soil sample.

According to Haasnoot et al. (2002), fractures often propagate in the direction of the TAMs. The results of the fourth test series have shown why: pressure filtration from the sleeve grout around the TAM during installation and the resulting stress relief allow the grout to penetrate between the soil and the sleeve grout. The same phenomenon was observed at the Hubertus Tunnel. See Section 3.5. This stress relief due to pressure filtration from the grout is the same mechanism as the one found in field measurements of the pressure in the tail void grout around the lining of a TBM (Bezuijen and Talmon, 2003). Wang and Dusseault (1994) showed that soil stresses can fall rather rapidly after the reduction of the volume of a cavity in the soil that is first created by expansion. For this project, this means that, although a high injection pressure on the grout is needed to inject the grout into the soil by creating a fracture or by expanding the injection hole, some volume reduction of the grout due to pressure filtration will lead to a reduction in the stresses around the fracture or bore hole. A consequence will be that a new injection will start at the boundary between the soil and the bore hole.

8.2.2 Permeability variations in the soil

In sand, fractures cannot occur due to tensile failure of the sand, as in rock and clay, because tensile stresses cannot develop in the sand. The fracture description developed for fractures in rock and clay based on tensile failure cannot therefore be used to describe the fracture behaviour of sand. A range of possibilities have been presented for fractures in cohesionless soil. Zhai and Sharma (2005) suggest a local increase in permeability in the soil due to plastic deformation of the soil. In their view, this local permeability increase leads to local increases in pore pressures that may initiate a fracture. They believe that pressure variations and plastic deformation may cause this increase in permeability. However, apart from the local permeability increase caused by the fracture, the experiments found no indications that there was a significant increase in permeability in the soil next to the fracture. Permeability was not measured, but a consequence of the theory of Zhai and Sharma should be that, in the tests where pressure infiltration is present, there will be areas where the sand layer influenced by pressure infiltration is significantly thicker (where permeability is high) than in other areas (the areas of lower permeability) and no difference of this kind was found. See Figure 6-29. The only indication of a difference in permeability is the CT scan shown in Figure 6-69. This CT scan shows that the density of the sand in front of the tips of the fracture is lower than at the sides of the fracture. Using the normal correlation formula to relate the density of the sand to permeability showed that permeability at the tip can be nearly twice as high as at the sides of the fractures. Although this is a significant difference, it is still much less than predicted by Zhai and Sharma, who calculated a factor of 10 difference between the highest and lowest permeability. In this study, the relative density of the sand was, in most tests, between 60 and 65%. When relative density is higher, there will be more dilatancy during plastic deformation and it is likely that, in sand of this kind, the permeability increase due to plastic deformation will be higher and become significant. This means that it is unlikely that a local increase in permeability is the cause of the fractures in the tests described in this thesis. The mechanism may have an effect in very dense sand.

Recent research looking at polymer injection in sandy soil (Pater, 2009) has shown, however, that this discussion is still open. Experiments have shown that the permeability of sand loaded to the yield stress and close to fracturing, or in which there are already some small fractures, can be higher by one order of magnitude than the normal permeability applicable to "matrix flow" without such loading. A permeability difference of this kind is not caused by porosity difference but probably by some permeable shear bands or small fractures, although the exact mechanism is not yet known. These recent results may bring into question the assertions in the previous paragraph about porosity differences and their effect on permeability. What remains is that the tests with pressure infiltration show no significant anisotropy.

8.2.3 Fracture direction

The theory that fractures propagate in the direction of the main principal stress, as described by Raabe and Esters (1993), was not proven by the results of these tests. However, it should be noted that the principal stress changes significantly during a test. The principal stresses were not measured during the tests, but the horizontal and vertical stresses were measured. Figure 8-1

shows how the measured K_0 changed during some tests in the first test series. This means that fractures were possible in all directions. Field tests will not have the horizontal restrictions of the model tests presented in this study, but the same change in K_0 will occur during injection, or even before the injection during the installation of the TAM.
The DEM calculations (Pruiksma, 2002) showed that pressurising the bore hole around the injection tube leads directly to a change in stress distribution around the bore hole. It is therefore questionable to what extent the original stress distribution still has an influence during fracture initiation directly around the bore hole. During the retraction of the casing, the sleeve grout will still be a liquid and that means that the radial stress in the sand close to the sleeve grout will be more or less constant during and after extraction (there will be a small hydrostatically-induced stress variation due to the weight of the grout). This means that, in the field where a casing is used, the original stress distribution is already disturbed before the injection of grout starts.

The only test in the four series that included two injections (Test 2-3) did not produce conclusive results. During the first injection, K_0 increased. See Figure 8-1. However, before the second injection (3 days later), K_0 had returned to its original value. In the second injection, K_0 rose much faster, but this did not lead to a different fracture pattern. As mentioned in Section 6.7.5, the fracture created in the second injection followed the existing fracture. From that test, it can be concluded that it is more likely that a fracture will follow an existing fracture than that the fracture direction will be influenced by a different stress pattern.

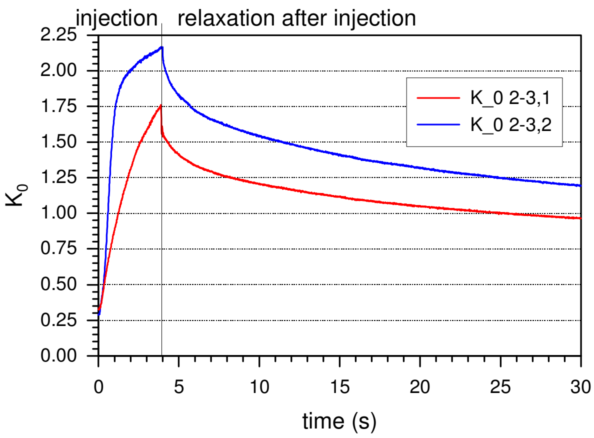

Figure 8-1: K_0 for the first and second injection in Test 2-3

8.3 Comparison of tests with theory

8.3.1 Injection pressures

The first test series showed that the injection pressures in the experiment were higher than anticipated. This made it necessary to raise the maximum possible injection pressure in the set-up. Furthermore it emerged that it was difficult to obtain fractures. As explained in Chapter 4, these two results are related: because only short and thick fractures were created, the injection pressures were close to those predicted by cavity expansion theory. Injection liquids that allow long and thin fractures will result in lower injection pressures. For sheet-like fractures, Equation (4.68) was derived in Section 4.10, linking the *d/s* value of the fracture with the grout and soil properties:

$$\frac{d}{s}=\left[\frac{8wk_c}{Q}\frac{1-n_i}{n_i-n_e}\frac{\sigma'_0}{\gamma_w}(1+\sin\phi)\right]^{1+\sin\phi}\cdot\left(\frac{4G}{\pi\sigma'_0\sin\phi}\right)^{\sin\phi} \tag{8.1}$$

In this formula:

d : the thickness of a fracture
s : the length of a fracture
w : the width of a fracture
k_c : the permeability of the grout cake
Q : the injection rate
n_i : the initial porosity of the grout
n_e : the porosity of the grout cake after pressure filtration
σ'_0 : the effective stress
γ_w : the volumetric weight of the water
ϕ : the friction angle
G : the shear modulus of the soil

The maximum injection pressures measured in the first series were analysed using this formula. The shear modulus of the sand (*G*) is an uncertain parameter in this formula. This value was fitted using the results of Test 1-8. The fitted value of 125 MPa is in reasonable agreement with the E_{50} (Young's modulus at 50% of the shear strength) measured in triaxial tests. Triaxial tests with Baskarp sand, as used in the tests, were performed at a slightly higher consolidation stress of 160 kPa with a relative density of 35 and 80% and these resulted in values for E_{50} of 160 and 180 Mpa respectively. In this first series, only Tests 1-5, 1-6, 1-7 could be used to compare the results of the calculations with the measurements. The earlier tests involved some uncertainty or were limited by the capacity of the pump system. Test 9 and Test 10 had a different soil density. The parameters from Table 7-1 in Kleinlugtenbelt (2005) and the fixed parameters from Table 20 were used to obtain the results in Table 21.

Table 20: Parameters with constant values in the calculations

Parameter	Value	Dimension
shear modulus	125	MPa
injection speed	10	l/min
width of fracture	0.5	m

Table 21: Parameters used to calculate injection pressures

Test	n_e (-)	n_i (-)	Permeability grout cake (m/s)	Confining stress (kPa)	Pressure calculated (kPa)	Pressure measured (kPa)
5	0.53	0.74	9.6*10-8	24	500	845
6	0.55	0.77	4.7*10-8	50	1000	1000
7	0.55	0.77	4.7*10-8	100	1400	2002
8	0.59	0.8	2.7*10-8	116	1500	1500 (fit)

These results were compared with the measured values – see Figure 8-2 – and although quite varied confining stresses were applied and the permeability of the grout cake also varied quite significantly, there was reasonable agreement.

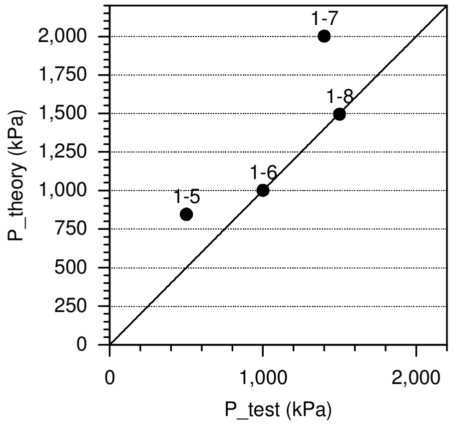

Figure 8-2: Calculated maximum pressures compared with measurements

Equation (8.1) was also applied to the tests in the second and third series. It emerged that, for these test series, the calculation method results in excessive injection pressures. The rather low permeability of the grouts used in test series 2 and 3 results in low calculated injection pressures. The measured injection pressures are much higher. This is likely caused by the filter cake formed by the pressure infiltration that occurred in these tests and is not taken into account in the model described with Equation (8.1). The pressure infiltration creates a filter cake of large particles that is much thicker than the filter cake predicted by pressure filtration only. See Section 5.9. A formula like (8.1) that does not take pressure infiltration into account will therefore underestimate both the thickness of the filter cake and the injection pressure.

The calculation method will therefore only produce reasonable results when the influence of pressure infiltration can be neglected. Most grouts used in compensation grouting projects until now have had a WCR that is low enough to prevent grout pressure infiltration and the model can be used for these grouts. Where pressure infiltration can be neglected and the parameters necessary for the model are available, the model can be used as an indicative method to investigate the kind of fractures and the injection pressures that can be expected for an injection directly in sand.

For an injection of grout through sleeve grout, as tested in the fourth series, and with retraction of the casing (this is, as mentioned above, the usual procedure in the field), the situation is more complicated. Pressure filtration from the sleeve grout means that the effective stress in the sand around the sleeve grout is lower than in experiments where the grout is injected directly into the sand. This leads to fractures at lower injection pressures and also causes grout flow between the sleeve grout and the sand. It is not possible to calculate the injection pressure and the shape of the fractures with the calculation model: the sleeve grout around the TAM has to be broken first and the stress distribution in the soil is difficult to predict because it depends on the amount of pressure filtration in the sleeve grout. In all probability, the relatively permeable Blitzdämmer used as the sleeve grout in the fourth test series will lose volume due to pressure filtration until the driving force for the pressure filtration, the soil pressure on the Dämmer, is gone and the radial pressure in the sand close to the Dämmer just exceeds the pore pressure in the water. Low pressures of this kind due to pressure filtration in tail void grout have been measured (Bezuijen et al., 2004). The measured pressures in the Blitzdämmer after the retraction of the casing in Test 4-4 are also low, and even negative in some cases (see Figure 6-54). The negative pressure must be a measurement error, but the actual pressure was low and it is therefore likely that fracturing is relatively easy. The model predicts very thin fractures and these were also found. However, a quantitative comparison was not made since the pressure distribution is different from that assumed for the derivation of Equation (8.1).

Equation (8.1) also explains why, until now, the literature has distinguished only between fracture grouting and compaction grouting. Figure 4-27 shows that *d/s* rapidly increases with cake permeability and, furthermore, that a lower WCR results in a higher value for $(n_i-n_e)/(1-n_i)$. It is clear from this formula that, when k_c and $(n_i-n_e)/(1-n_i)$ both increase, *d/s* also increases rapidly. When the filter cake reaches a certain thickness, then, the injection pressure starts to increase, and this leads to more pressure filtration and therefore to an even thicker filter cake, and so on. This process explains why most fracture results from the field comply with one of the extremes: fracture grouting with limited pressure filtration and relative low injection pressures, and fractures or compaction grouting with relative high injection pressures and no fractures. The relative high effective stress in Series 1, 2 and 3 (because there was no stress relief due to pressure filtration), combined with the relatively high WCR in most of the tests from those series, meant that it was only the results from these series that were sometimes in the "intermediate" area, producing only some small fractures, but high injection pressures.

The results of this study indicate that the difference between fracture grouting and compaction grouting is, for injection in sand, not caused by the difference in viscosity, as has sometimes been claimed (ASCE, 1980), but by the difference in pressure filtration properties. At the relatively high *d/s* values found in most of the tests, the pressure fall in the fracture is only limited. In all the tests from the first three series (with the exception of Test 2-4 with the cross-linked gel) the *d/s* value is higher than 1/100. It follows from Equation (4-49) that the relation between the pressure drop (ΔP) in the fracture and the *d/s* can be written as:

$$\Delta P = 2.\frac{s}{d}\tau \tag{8.2}$$

where τ is the yield stress in the grout. The yield stress was measured in the test series, but the measurements proved not to be very accurate. In the second test series, the values found for the yield stresses varied between 50.6 and 97.7 Pa for cement-bentonite grouts with a WCR varying between 200 and 2. Comparable values were found in the first test series. Assuming the maximum value found of nearly 100 Pa and a *d/s* (note that the equation here uses *s/d*) value of 1/100, the pressure drop in the fracture is 20 kPa. Since the injection pressures exceeded 1000 kPa for these grouts, the pressure drop of 20 kPa over the fractures can be neglected.

This complies with the result of Test 2-4 with x-linked gel. Although this gel had the highest yield strength of all the injection fluids used in the second test series, it produces the fractures with the lowest *d/s* values because the very low permeability of the gel and the limited amount of solids produced only a very thin filter cake.

The description of the shape of a fracture with the *d/s* ratio appears to be useful, as is shown above. However, it should be realised that this is a simplification. A real fracture can be so complicated that it is not possible to describe it as a *d/s* ratio only. See, for example, Figure 8-3. For a fracture with this shape, it is difficult to determine a reasonable *d/s* value. And even more so because the fracture is not in a radial direction from the injection tube: it forms almost a semi-circle around the tube and the injection point itself is still in the sand. In this thesis, therefore, the *d/s* value is used as an indication of what can be expected in terms of injection pressure. No attempt was made to determine *d/s* values for all experiments, because the results would be highly subjective.

Figure 8-3: Fracture found after Test 2-7

8.3.2 Pressure filtration

The influence of grout pressure filtration during and after injection on the result of the compensation grouting process is an important outcome of this study. On the basis of the work of Bezuijen and Talmon (2003) for tail void grouts, this effect was first suggested by Grotenhuis (2004) and it has been proven experimentally by the work of Eisa (2008) and the work described in this thesis. The influence of pressure filtration on injection pressure was already covered in the previous section. Pressure filtration also affects the efficiency of the compensation grouting process.

Although, in this study, some WCR values in the experiments were very high, the WCR values of grouts used for fracture grouting in practice vary between 1 and 2. In a normal grout, the weight of the bentonite is 3 to 5% of the water. Using the densities presented in Table 5 (Chapter 5), this means that a grout with a WCR of 1.5 and 5% bentonite is 80% water by volume. The amount of pressure filtration is therefore important for the efficiency of the grouting process. The porosity of a filter cake is approximately 50% (see Table 6 in Section 5.5). The volume of the filter cake as a percentage of the slurry volume is calculated in Table 22 for different WCR values, assuming 5% bentonite by weight and, as stated, filter cake porosity of 50%.

Table 22: Volume cake/volume slurry for different WCR values

WCR	volume cake/ volume slurry
1	0.53
1.5	0.39
2	0.31

The results show that, for a WCR of 2, the volume of the filter cake is only 31% of the original volume. Consequently, complete filtration of the grout leads to an efficiency with the grout only that cannot exceed 31%. Complete filtration of this kind is unlikely for low *d/s* ratios and relatively limited injection pressures. For example, the results of the first test series (Section 6.5.3) and the CT scan (Section 6.9.3 and 6.9.4) showed density variation in the grout, indicating only partial dehydration. Kleinlugtenbelt (2005) reported a few mm of grout with a higher density due to pressure filtration. He determined this on the basis of colour variations in the first test series (see Figure 6-18). In his case, this reduced the maximum possible efficiency from 80 to 63%. If the value for *d/s* is low, the average thickness of the grout layer will be greatly reduced and so maximum efficiency will be lower because there can be more pressure filtration. In the fourth test series, most of the sleeve grout was covered with grout from the injection through the TAM during the compensation grouting operation (see also Figure 6-61). This means that, even if there are no fractures, the average thickness of this grout layer around the sleeve grout is only 8.3 mm, as calculated on the basis of the injected volume and the surface of the sleeve grout. Since there were fractures, the average thickness of the grout layer is even lower. With a cake permeability of 2.10^{-9} m/s, it can be calculated (using Equation 5.1) that during the four-second injection with an injection pressure of 600 kpa in the fourth test series there is already a filter cake of 1 mm. After injection, the pressure on the grout decreases but, given an average value of 200 kPa, it will take 400 seconds before 6 mm is consolidated. In this case, that is effectively all the injected slurry.

The conclusion is that the grout in a thin fracture will be dehydrated due to pressure filtration before the fracture grout has time to harden. This result means that, in the case of thin fractures with a relatively large area in contact with the sand, the efficiency of the grouting process falls due to pressure filtration.

8.4 Consequences for fracture model

To explain what happens in the soil during compensation grouting, pictures like the one in Figure 8-4 are often used (Kummerer, 2003, Raabe and Esters, 1993, Keller, no date). In this picture, compensation grouting results in a number of rather thin fractures. The picture is two-dimensional and it is therefore uncertain what the fracture will look like perpendicular to the plane in the drawing. However, since the fractures as drawn are not in the direction of the tube, it seems reasonable to postulate that this picture assumes a branch-like fracture. If that is the case, Figure 8-5 shows what this fracture would look like in three dimensions. In some cases (Kummerer, 2003), it has been stated that in normal consolidated soils where K_0 is less than 1, the first fractures are in a vertical direction. Due to these vertical fractures K_0 will increase and, when it is higher than 1, more horizontal fractures will occur.

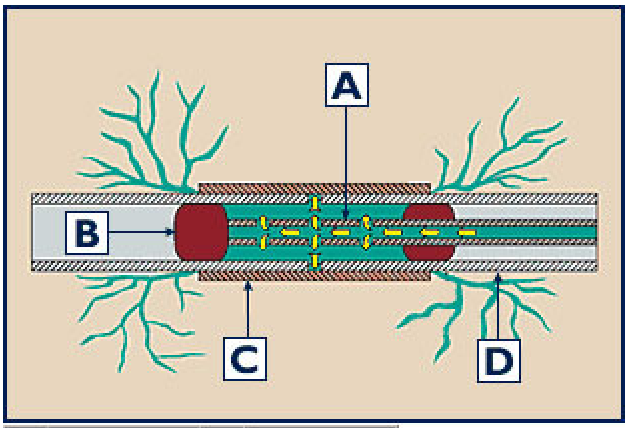

A =	Inner Pipe	C =	Rubber Sleeve
B =	Inflatable Seal	D =	Main Pipe

Figure 8-4: Usual picture to illustrate compensation grouting

On the basis of the results of both the experimental research in the laboratory and the field tests, this model would seem to be incorrect for compensation grouting or corrective grouting in sand. Given the results of the research described in this thesis, a different picture is more plausible. See Figure 8-6.

The following arguments support these changes:
- branch-like fractures were seldom found in tests or in the field.
Only Test 3-1 resulted in a clear branch-like fracture, but this was caused by a non-homogeneous soil sample and there was only one branch and not a lot of branches as shown in Figure 8-5. The results of the field observations (Antwerp Central Station and Hubertus tunnel) seem to be closer to sheet-like fractures of the kind found in most of the experiments. From a theoretical point of view, a branch-like fracture in homogeneous soil is only possible when there is a kind of cavity expansion in the soil. Fractures are normally created with lower pressures than the pressures predicted by cavity expansion theory (see Section 4.2).
- The sleeve grout is normally thicker than shown in Figure 8-5. This may seem a triviality but this implies that there can be more consolidation of the sleeve grout, resulting in lower effective stresses in the soil directly surrounding the sleeve grout.
- The field observation in Antwerp and one experiment (Test 2-3) showed that fractures follow existing fractures. The number of fractures will therefore be limited.
- The field observations at the Hubertus Tunnel showed that grout has a tendency to follow the boundary between the tail void grout of the tunnel and the sand. This is a location where, due to pressure filtration from the tail void grout, the effective stress is low. In the light of the experiments of the fourth test series, it is assumed that the grout will also follow the boundary between the sleeve grout and the sand. This also explains why, at the Sophia Tunnel, the effects of compensation grouting are also found in the directions of the TAMs.
-The injection pressure that is applied and the unloading due to pressure filtration that occurs after each injection have a significant impact on stress distribution in the sand around the fracture. These mechanisms, which determine stress distribution around the sample, probably have a greater effect than the original K_0 and so the grout will follow existing paths.

Although, as mentioned above, there are quite a number of arguments in favour of assuming that the grout in this soil creates a fracture of a kind that is different from the fracture shown in Figure 8-5, it should be pointed out that Figure 8-6 is not completely "evidence-based". The number of field tests where it is actually possible to see fractures is very limited. Only one of the experiments included a second injection through the first injection. This is also a rather limited basis for drawing conclusions about injection campaigns where up to 70 injections are sometimes made through the same injection opening. So Figure 8-6 must be seen as a best guess with the knowledge available but not as the definitive description of fracture grouting. Nevertheless, this picture has been included here because it is very likely that it is an improvement on Figure 8-4 and Figure 8-5.

Figure 8-5: Artist's impression of fracture grout after injection according to literature (2-D picture from literature reworked to 3-D drawing)

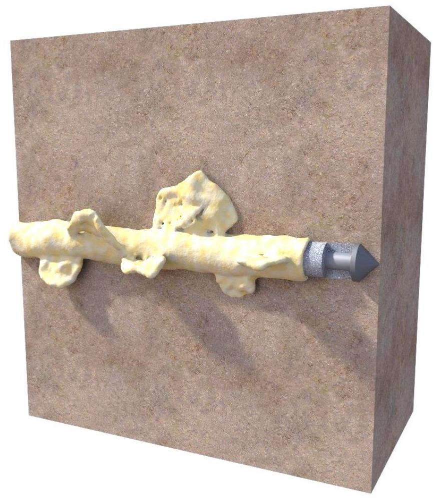

Figure 8-6. Artist's impression of grout body after injection according to the results of this study

8.5 Consequences for practice

Although the primary aim of this study was to improve our understanding of the mechanism involved, the results also have consequences for the practice of compensation grouting.

The results show that, given normal confining stresses in compensation grouting (100 kPa or more) and using a cement-bentonite grout, long thin fractures in sand are only possible when there has been unloading of the soil, for example by pressure filtration of the sleeve grout around the injection tubes.

The unloading of the soil around the sleeve grout allows the grout to flow around the sleeve grout after injection, as emerged from the results of the fourth test series. This can occur over quite a distance. So heave can occur at some distance from the injection point.

It is possible to prevent the flow of grout across large distances by increasing its permeability. This was done in the case of, for example, the Vijzelgracht grouting. The consequence is that there is a lot of pressure filtration before settling and hardening starts and so the theoretical maximum efficiency (the efficiency assuming that the volume deformation in the sand is zero) of the grouting process will be limited. Furthermore, the result will be compaction grouting, not fracture grouting.

The results of the tests show that the pressure filtration properties have a major impact on injection pressures and fracture shape, and the theory developed showed which mechanisms play a role and influence the shape of the fracture. It was found that there is an optimal WCR for the efficiency of the grouting process. At high WCRs, efficiency is relatively low due to significant pressure infiltration. At very low WCR values, efficiency decreases again due to pressure filtration and a more compaction-grouting-like pattern.

In the tests performed for this study where the effect of installation was not taken into account, the optimal WCR based on the second test series was around 5 (Sanders, 2007). However, it should be noted that nothing is known in practice about the stability of grout mixtures over time with this limited amount of cement.

The third test series found hardly any difference in efficiency between grouts with a WCR of 5 and 1. The experiments in the fourth series that took the effects of installation into account showed a higher volume loss after the injection, probably due to the combination of the unloading of the sand before the injection and the fact that pressure filtration can occur over a larger area.

Although a final conclusion about efficiency is therefore impossible, the effect of the fracture shape on efficiency seems to be relatively limited. When the sand has a relative density of 60% or more, the densification of the soil during grouting will be limited, even during cavity expansion. Grout pressure filtration seems to be the dominant factor affecting efficiency. Following this line, it is not necessary to "design" the grout in a way that the injection will lead to a fracture. The grout can be "designed" so that the grout will consolidate within a reasonable distance to prevent heave in areas far away from the injection point.

The time scale for pressure filtration in the experiments was around one hour. If settlement occurs over a much longer time scale, as was found at the Vijzelgracht location where the time scale was five months, this must be a different mechanism and cannot be caused by grout pressure filtration.

9 Conclusions and further research

9.1 Conclusions

In this study, four series of laboratory test series were performed looking at compensation grouting. The first three series had comparable set-ups; the last one took place with a changed set-up to take the influence of installation into account. In addition, three tests were performed in a set-up that made it possible to observe fracture growth using a CT scan, and the field data for the corrective grouting at the Vijzelgracht location were analysed. The results of the tests show the impact of the grout properties, the confining stress, the injection rate, the density of the sand and the installation procedure on the results. Various factors could be explained quantitatively or qualitatively with analytical models developed during this study. Analysing the data from the Vijzelgracht location (see Chapter 7) made it possible to explain why efficiency is unexpectedly low and why there is ongoing settlement after grouting.

This thesis has focused on the mechanisms that determine fracture initiation and propagation, and also appraised the efficiency of the fracturing process. It did not examine the distribution of the resulting soil movements around the injected grout.

The results of this study show that pressure filtration and pressure infiltration (as defined in Chapter 5) are important mechanisms when it comes to understanding fracture initiation and fracture propagation. Fracture initiation pressure is not only determined by the confining stress and the sand properties; it also depends very much on the grout properties. Pressure filtration and bleeding both lead to higher injection pressures. This study shows that there is a relation between fracture shape and injection pressures.

Fractures start at the location of inhomogeneities in the soil in the immediate vicinity of TAMs. A macro-mechanical constitutive model describing sand as, for example, an elasto-plastic material will not lead to fractures. Pressurising a cavity (as described in cavity expansion theory) causes yield, but not fractures. Describing the sand as randomly placed grains makes it possible to explain that the fluid pressure in the fracturing liquid can separate grains because the fluid pressure is much higher than the tangential stress (see also Section 4.4). Some plastering is necessary for this mechanism to occur because the water pressure has to be transferred to a pressure on the sand grains. When the filter cake becomes too thick, the pore pressure cannot surmount the tangential stress in the grains, there will be no fracturing and the increasing radial pressure on the grains will lead to cavity expansion.

A conceptual calculation model was developed to describe the shape of the fracture. This model defined the shape of fractures as d/s, where d is the thickness of the fracture and s the length. It emerged that d/s and the injection pressure depend on the permeability of the grout cake, the amount of solid material in the grout, the injection rate, the friction angle and the shear modulus of the soil. According to the model developed there is no real boundary between fracturing and non-fracturing behaviour. More solid material in the grout, higher confining stresses or a higher permeability of the cake will lead to higher d/s values. So there is a more or less gradual transition between fracturing and non-fracturing. The distinction between fracture grouting and compaction grouting results from the relatively rapid increase in the injection pressure needed when the fractures have some width, as shown in the calculation model using the cavity expansion model. This is why the shift between fracturing and compaction seems rather abrupt, although the transition is a gradual one and a gradual transition would be found in experiments with different grout properties if the confining pressure were to be adapted to keep the injection pressure more or less constant.

The dependencies mentioned above make the description of fracturing in sand more complicated than the description of fracturing in clay. However, there is an advantage in that it is possible to control the width and length of the fractures. Within the limits of this study, it was not possible to develop a "recipe" that results in the ideal grout for a given situation, but it was possible to identify the important parameters and indicate how changes to the parameters affect the results.

For an injection directly into sand (without taking into account the sleeve grout that is normally present around the TAM), and looking at short-term efficiency, the optimal WCR for the set-up used in the laboratory tests is 1 to 5. Efficiency of more than 30% was attainable. Higher WCR values reduce efficiency due to pressure infiltration and lower values lead to a fall in efficiency due to pressure filtration. For long-term efficiency in sand, it may be worthwhile to look at efficiency as the volume of heave created divided by the volume of solids injected, since the volume of water will be always partly drained when executing compensation grouting in sand.

With respect to physical modelling in general, the results of the study show the importance of modelling the relevant features of a process. Modelling always means simplification and a good physical model simplifies reality but still retains the relevant features. It emerged in this study that the installation process is important.

Installing TAMs using a casing and sleeve grout to fill in the gap between the casing and the injection tube causes pressure filtration, which in turn causes a reduction in the volume of the sleeve grout and pressure release in the soil around the TAM. This pressure release reduces injection pressures significantly (compared to the injections directly into sand without sleeve grout) and consequently to more fracture-like behaviour (lower values for *d/s*).

It can therefore be concluded that, although the physical model used in the first three test series was sufficient to investigate the influence of confining stress and grout parameters on the type and shape of the fractures, it was too simple to investigate the shape that can be expected when grout is injected in a field situation. This means that, with each physical model, it is of the utmost importance to bear in mind what should be tested and what mechanisms can be expected, and therefore where simplifications are possible and where they are not.

Comparing the injection pressures found in model tests with the injection pressures measured in the field, it should be realised that the injection pressure in the field is normally measured at the grout pump and that there can be several bars of pressure difference between the pressure at the grout pump and the pressure at the injection point. For the equipment and grout used at the Amsterdam Vijzelgracht location, a pressure drop of 7.5 bar was found. This pressure drop is comparable to the lowest injection pressures found at the Vijzelgracht and slightly less than half of the average injection pressure – see Figure 7-8 and Figure 7-9 – and it cannot therefore be neglected.

Installing TAMs beneath buildings causes some settlement of these buildings. In the Amsterdam situation, this proved to be 2 to 2.5 mm. Au et al. (2003) have shown that compensation grouting in clay causes long-term settlement. The evaluation of the field data in Amsterdam showed that compensation or corrective grouting underneath piled foundations in sand and silt (the Alleröd) also leads to the long-term settlement of the buildings on top of the piles. If the soil is disturbed only by the installation of the TAMs, this long-term settlement is limited to a few millimetres, as measured in the Industria location. In disturbed soil conditions (as was the case at the Vijzelgracht location), this can be much more. Settlement of up to 8 mm was measured there.

In disturbed soil conditions, as in Amsterdam at the Vijzelgracht location after the leak through the diaphragm wall, the efficiency of the grouting process is very low (less than 2%). This is probably caused by the decrease in tip resistance when the soil was loosened. The heave caused by corrective grouting can push up the sand around the tips of the pile without creating enough tip resistance to move the piles with the sand. Furthermore, it was shown that grout used with a permeable grout cake also leads to a low efficiency. The grout used was not the usual cement-bentonite grout. The benefit of the grout used at this location may be that the injected grout was localised around the injection points to a certain extent.

The conceptual model developed to describe the shape of the fractures tends to underpredict the *d/s* value for a fracture. This is because it does not take into account the effect of pressure infiltration and the effect of the finite dimensions of the grains (mostly the cement grains) in the grout. Pressure infiltration will occur in the conditions tested at WCR values of 2 and higher. Pressure infiltration forms a filter cake comprising the coarser grains in the grout (normally the cement particles). The finite grain dimensions in the grout imply that there must be a minimum value of *d/s* before there can be any flow.

9.2 Further research

To improve our understanding of the technique of compensation grouting or fracture grouting, the following areas require further study.

Experimental programmes have been conducted on clay (Au, 2001) and in this study on sand. There are different mechanisms depending on the soil material used and so it would be of interest to perform some laboratory tests with a set-up comparable to this study on materials with permeabilities and grain size distributions in between sand and clay, such as silt, to determine the mechanisms that then occur.

The study has identified the mechanisms present in sand. With these results, it will be possible to establish a numerical simulation of the soil response that takes these mechanisms into account. Modelling fracturing itself in a Finite Element program is difficult, but the unloading of the soil that occurs due to pressure filtration can be modelled and will result in a better understanding of the phenomena. Finite Element calculations taking into account the phenomena revealed by field tests and analytical calculations has proved to be useful in tunnelling (Nagel et al., 2009).

The number of tests in which the installation procedure was modelled was only limited. The effect of different sand properties and densification has not yet been investigated and testing these factors would be of interest because of the impact of the installation procedure on the results. Additional tests with a set-up that takes into account the installation procedure will therefore result in a more complete "picture" of the behaviour of grout that is injected through Dämmer into soil that has been unloaded due to pressure filtration from the Dämmer.

Grout was injected twice in only 1 of the 34 tests performed. In all other tests, grout was injected only once in each test. This is quite different from the field situation: in the Vijzelgracht case, for example, up to 70 injections were made in the same hole. According to the usual theory (Kummerer, 2003), this should densify the sand and change the stress state. As described in the discussion, this study has shown that it is likely that new fractures will follow existing fractures and that the influence of the K_0 is probably less.

Since multiple injections are "standard" for compensation or corrective grouting because this approach makes it possible to inject, measure the heave and inject again, it would be worthwhile to study this factor further in subsequent tests and to measure, for example, the effect of two large grout injections compared to five smaller injections.

The impact of compensation or corrective grouting on a pile foundation needs some further study. What is the minimum distance between the pile tips and the TAM needed to prevent a decrease in tip resistance and is there an optimal distance between the pile tips and TAM that results in maximum efficiency?

The number of field tests in which the shape of the grout body has been determined after injection is rather limited. This study has shown that the installation procedure can have a significant impact. More field tests could show how this factor affects the shape of the grout body.

The tests show that grout with a higher WCR than commonly used nowadays in the field can lead to more fracture-like behaviour when used in compensation grouting in sand. It is worthwhile to investigate the stability of such high-WCR grouts over time to prevent long-term settlement problems due to the decline of the quality of the grout.

List of symbols

A	calculation constant (section 4.7.3)	[-]
A	fracture area (section 4.10)	[m^2]
A	area of the sample (chapter 5)	[m^2]
b	radius with constant pressure	[m]
B	calculation constant (section 4.7.3)	[-]
c	cohesion	[kPa]
C_1, C_2	calculation variables	[-]
C	calculation constant (section 4.7.3)	[-]
d	fracture thickness	[m]
d_{15}	diameter of particles with 15% of the particles smaller	[m]
d_{50}	diameter of particles with 50% of the particles smaller	[m]
d_{eff}	thickness of the liquid area in the fracture	[m]
D	diameter of grain (in micro mechanical calculation)	[m]
D	calculation constant (section 4.7.3)	[-]
k_c	permeability of grout filter cake	[m/s]
e	volumetric strain	[-]
e_e	void ratio of the filter cake after filtration	[-]
e_i	initial void ratio (before filtration)	[-]
E	Young's modulus	[kPa]
E_{50}	Young's modulus at 50% of the shear strength (in triaxial test)	[kPa]
E_{ref}	Young's modulus (in Plaxis calculation)	[kPa]
F_i	force on grain	[kN]
F_l	force on grain due to grout flow	[kN]
g	acceleration of gravity	[m/s^2]
G	shear modulus	[kPa]
G_B	Pressure gradient in Binham liquid	[kN/m^3]
i	hydraulic gradient	[-]
k	permeability	[m/s]
k_c	permeability grout cake	[m/s]

K_0	ratio between horizontal and vertical stress	[-]
l	length	[m]
n	porosity	[-]
n_e	porosity of the filter cake after filtration	[-]
n_i	initial porosity grout (before filtration)	[-]
$n_{c,i}$	initial porosity of the larger particles in the grout	[-]
$n_{c,e}$	final porosity of the larger particles in the grout	[-]
n_s	porosity of the sand	[-]
N_a	coefficient of active earth pressure	[-]
N_p	coefficient of passive earth pressure	[-]
p	(injection) pressure	[kPa]
p'	effective pressure	[kPa]
p_a	active pressure	[kPa]
P_d	driving pressure (Chapter 5)	[kPa]
p_d	press. in sleeve grout during retraction of model casing (Chapter 6)	[kPa]
P_{ext}	external injection pressure	[kPa]
P_f	fluid pressure	[kPa]
P'_f	the pressure in a cavity at which plastic deformation starts	[kPa]
p_p	passive pressure	[kPa]
p_r	pressure in the cavity	[kPa]
P_τ	pressure necessary to overcome the yield stress	[kPa]
q	specific discharge	[m/s]
q_s	specific discharge of the fine particle slurry	[m/s]
Q	injection rate	[m^3/s]
Q_1	coefficient in cavity expansion formula Luger and Hergarden	[-]
r	coordinate	[-]
R	radius of imaginary cavity	[m]
R_a	radius active plastic zone	[m]
R_d	relative density	[-]
R_f	flow resistance for water	[s]

R_0	original radius of the bore hole	[m]
R_p	radius passive plastic zone	[m]
R_w	radius of cavity	[m]
Rey	Reynolds number	[-]
s	fracture length	[m]
s_c	thickness of cake with larger particles	[m]
s_s	thickness of the sand layer in which the small particles invade	[m]
S_a	material parameter	[kPa]
S_p	material parameter	[kPa]
t	(injection) time	[s]
t_d	time that the sleeve grout could harden before injection	[hours]
t_{marsh}	the marsh funnel time	[s]
u	radial displacement	[m]
V	volume in fracture	[m^3]
V	volume of pore water (Chapter 5)	[m^3]
V_c	volume of cake	[m^3]
V_s	volume of slurry	[m^3]
w	width of a planar fracture	[m]
WCR	water-cement ratio (by weight)	[-]
x	coordinate	[m]
x_e	thickness of the filter cake	[m]
y	coordinate	[m]
z	coordinate	[m]
α	angle between grains	[degr]
α_t	coefficient	[-]
α_c	coefficient that describes the influence of yield stress for flow through large particles	[-]
α_s	coefficient that describes the influence of yield stress for flow through sand	[-]
β	coefficient	[-]

γ_w	volumetric weight of water	[kg/m^3]
γ_{dry}	volumetric weight dry soil	[kg/m^3]
ΔP_{dyn}	pressure drop due to dynamic forces (Chapter 7)	[kPa]
ΔP_{tot}	total pressure drop over injection system (Chapter 7)	[kPa]
ΔP_{visc}	pressure drop due to viscous forces (Chapter 7)	[kPa]
ΔP_{tot}	pressure drop due to yield strength (Chapter 7)	[kPa]
$\Delta\varphi$	pressure head difference over soil body (Equation 4.4)	[m]
$\Delta\varphi$	pressure head difference over penetration zone (Equation 4.6)	[m]
$\Delta\varphi$	pressure head difference grout-soil	[m]
ε_{ii}	principal strain in the ii direction	[-]
θ	angle of tortuostity	[degr]
φ_y	piezometric head at the boundary between grout and soil	[m]
ϕ	friction angle	[degr]
κ	part of the grain that is subjected to the hydraulic gradient	[-]
λ, μ	Lamé constants (Section 4.7)	[kPa]
μ	dynamic viscosity (Chapter 7)	[pa.s]
ν	Poisson ratio	[-]
ψ	dilatancy angle	[degr]
ρ	density of slurry	[kg/m^3]
ρ_w	density of water	[kg/m^3]
σ	stress	[kPa]
σ'	effective stress (also with subscripts ' means effective stress)	[kPa]
σ_0	initial stress around the opening	[kPa]
$\sigma_{h,initial}$	horizontal stress at beginning of experiment	[kPa]
σ_{min}	minimum stress to start fracturing	[kPa]
σ_r	radial stress	[kPa]
$\sigma_{v,initial}$	vertical effective stress at beginning of experiment	[kPa]
σ_θ	tangential stress	[kPa]

σ_{ii}	principal stress in the *i* direction	[kPa]
τ_y	yield stress	[kPa]
τ_p	peak yield strenght	[kPa]
τ_r	residual yield strength	[kPa]

References

Adel den H., (1989). "Re-analysing permeability experiments with the Forchheimer relation (in Dutch)". GeoDelft *report CO-272553/56*

ASCE Committee on grouting (1980). "Preliminary glossary of terms relating to grouting." *J. Geotech. Eng. Div. Proc. ASCE,* Vol. 106, New York, 803-815.

Au, W., Masini L., (2008). "*Compensation grouting in sandy soils: the influence of TAM installation*" Report on the Research collaboration between Deltares, University of Cambridge and "Sapienza" University of Rome.

Au, S.K.A., Soga K., Jafari, M.R., Bolton, M.D. and Komiya, K., (2003). "Factors affecting long-term efficiency of compensation grouting in clay." *Journal of Geotechnical and Geoenvironmental Engineering.* 129; 254-262.

Au, S.K.A., (2001). "Fundamental study of compensation grouting in clay." PhD Thesis, University of Cambridge

Atkinson, B.K. (ed.) (1989). *Fracture mechanics of rock.* Academic Press, geology series. ISBN 0-12-066266-3.

Baars S. van, (1996). "Discrete element analysis of granular materials." PhD thesis, Delft University of Technology.

Bezuijen. A., Sanders M.P.M., Hamer D. Den, (2009). "Parameters that influence the pressure filtration characteristics of bentonite grouts" *Géotechnique,* Vol 59, Isue 8, 717-721.

Bezuijen, A., Tol, A.F.van, Sanders M.P.M., (2008). "Mechanisms that determine between fracute grouting and compaction grouting in sand." *Proc. 6st Int. Symposium on Geotch. Aspects of Underground Construction in Soft Ground, Shanghai.261-267*

Bezuijen A. and Tol A.F. van, (2007). Compensation grouting in sand, fractures and compaction, *Proc. XIV European Conference on Soil Mechanics & Geotechnical Engineering,* Madrid. pp. 1257-1262.

Bezuijen, A., Kleinlugtenbelt, R., Tol, A.F. van, (2006). "Laboratory tests, compaction or compensation grouting." *Proc. 5th Int. Conf. on Physical Modelling, Hong Kong* 1245-1251

Bezuijen A., Talmon A.M, Kaalberg F.J. and R.Plugge, (2004). "Field measurements on grout pressures during tunnelling of the Sophia Rail Tunnel/" *Soils and Foundations*,Vol.44, no.1, pp39-48.

Bezuijen, A., Talmon, A.M., (2003). "Grout, the foundation of a bored tunnel"; *Proc. BGA. Int. Conf. Foundations,* (*ICOF) Dundee*, Thomas Telford.

Bezuijen A., (2003). "Hydraulic fractures experiments at low stresses in sand" Report Delft University of Technology *TA/TG/02-03*, GeoDelft *report CO-405400/03*. October.

Bezuijen A., Pruikma J.P. and Pater C.J., (2003). "Maximum pressures in tunnelling limited by hydraulic fractures." *Proc ITA conference Amsterdam*

Bezuijen, A. and Schrier, J.S van, (1994). "The influence of a bored tunnel on pile foundations." *Centrifuge 94*, edited by Lee and Tan, Balkema, Rottterdam, pp. 681-686.

Bohloli, B. and Pater C.J. de, (2006). "Experimental study on hydraulic fracturing of soft rocks: Influence of fluid rheology and confining stress." *Journal of Petroleum Science and Engineering* 53, 1-12.

Bosch, J.W. and Broere W., (2009). "Small incidents, big consequences. Leakage of a building pit causes major settlement of adjacent historical houses. Amsterdam north-south metro line project." *Proc. World Tunnel Congress*, Budapest. 13 pp

Cambefort, H. and Puglisi R., (1971). "Soulèvement d'un batiment par injection du sol." *Annales de l'Institut Technique du Batiment et des Traveaux Publics, No 281, Mai, Série: sols et fondations, No 80.*

Chambosse G. and Otterbein R., (2001[a]). "Central Station Antwerp; compensation grouting under high loaded foundations." *Response of buildings to excavation-induced ground movements.* Imperial College, London, July 17-18, Technical paper 61-56E.

Chambosse G. and Otterbein R., (2001[b]). State of the art of compensation grouting in Germany. *Proc.XVth Int. Conf. on Soil Mechanics & Foundation Engineering*, Turkey, Istanbul. 1511-1514

Chang, H., (2004). "*Hydraulic fractures in particulate materials*", Phd. Thesis, Georgia Institute of Technology, November.

Chin, C.Y., (1996). "*An experimental study of hydrofracture in soils*" Phd Thesis, Department of Engineering, University of Cambridge, Cambridge, UK.

Cho G.C. (2009), Private communication (Picture taken from Kaist website, removed).

Cundall, P. A., (2001). "A discontinuous future for numerical modelling in geomechanics." *Proceeding of the Institution of Civil Engineers, Geotechnical Engineering*, 149, 41-47.

Dam van, D.B., (1999). "*The influence of inelastic rock behaviour on hydraulic fracture geometry*" PhD Thesis, Delft University of Technology, ISBN 90-407-1958-6

Dong, Y. and Pater, C.J. de, (2008). "Observation and modelling of the hydraulic fracture tip in sand", *Proc. 42nd U.S. Rock Mechanics Symp.,* San Fransico.

Eisa, K., (2008). "*Compensation grouting in sand*" Phd-Thesis, University Cambridge, November.

Falk, E., (1997). "Underground works in urban environment" *Proc.XIVth Int. Conf. on Soil Mechanics & Foundation Engineering,* Germany, Hamburg. 1401-1406.

Fujisawa, T., Nakamura, A. and Yamaguchi, Y., (1996). "Development of fracture direction controlled grouting." *Proc. Int. Conf on grouting and deep mixing.* Tokyo, Balkema, Rotterdam, the Netherlands. 689-694.

Gafar, K., Soga, K., Bezuijen A., Sanders M.P.M. and Tol A.F. van, (2008). "Fracturing of sand in compensation grouting." *Proc. 6st Int. Symposium on Geotch. Aspects of Underground Construction in Soft Ground, Shanghai. 281-286*

Garnier, J. (2002). "Properties of soil samples used in centrifuge models." *Proceedings of the International Conference on Physical Modelling in Geot echnics: ICPMG '02,* St. John's, Nfld., 10–12 July (2002. *Edited by* R. Phillips, P.J. Guo, and R. Popescu, A.A. Balkema, Lisse, the Netherlands. pp. 5–19.

Gens, A., Di Mariano A., Gesto J.M. (2005)."Ground movement control in the construction of a new metro line in Barcelona" *Proc. 5th Int. Symposium Geotechnical Aspects of Underground Construction in Soft Ground,* Amsterdam, the Netherlands. 389-395

Gens, A., (2005). Presentation at 5th Int. Symposium Geotechnical Aspects of Underground Construction in Soft Ground, Amsterdam, the Netherlands.

Greenwood, D.A. and Hutchinson, M.T., (1982). "Squeeze grouting unable ground in deep tunnels." *Proceedings of Grouting in Ground Eng. Conf.,* New Orleans, 631-650.

Grotenhuis R., (2004). "*Fracture grouting in theory*" Msc. Thesis Delft University of Technology, November.

Gustin E.J.G., Karim U.F.A., Brouwers H.J.H., (2007). "Bleeding characteristics for viscous cement and cement-bentonite grouts." *Géotechnique*, **52**, No 4, 391-395.

Haasnoot, J.K., Stoel, A.E.C. van der, Kaalberg, F.J., (2002). "Fracture Grouting to mitigate settlements of wooden pile foundations" *Proc. of AITES/ITA Down under*, Sydney (Australia).

Haimoni A.M. Wright R.H., (1999). "Protection of Big Ben using compensation grouting." *Ground Engineering,* Vol. 32, No 8 August 33-37.

Harris, D. I., Menkiti, C. O., Pooley, A.J., Stephenson, J.A., (1996). "Construction of low level tunnels below Waterloo Station with compensation grouting for the Jubilee Line Extension." *Proc. of Geotechnical Aspects ofUnderground Construction in Soft Ground,* Mair & Taylor (eds):361-366.

Harris D. I., R. J. Mair, J. P. Love, R. N. Taylor, and T. O. Henderson, (1994). "Observations of ground and structure movements for compensation. grouting during tunnel construction at Waterloo Station." *Geotechnique, 44(4):* 691-713

Heidelberg, (2009). http://www.heidelbergcement.com/de/en/geotechnik /produkte /Blitzdaemmer.htm (march (2009)

Huisman M., (1998). "Theory and experiments static plastering (in Dutch)." BTL *report 34.*

Jaworski, G.W., Seed, H.B and Duncan, J.M., (1981). "Laboratory study of hydraulic fracturing." *Journal of the Geotechnical Engineering Division* 107(6): 713-732.

Kaalberg F.J., (2006). Private communication.

Kaalberg F.J., Teunissen E.A.H., Tol A.F. van, and Bosch J.W., (2005). "Dutch research on the impact of shield tunnelling on pile foundations." *Proc. 5th Int. Symposium Geotechnical Aspects of Underground Construction in Soft Ground*, Amsterdam, the Netherlands. 123-131

Keller brochures (undated reference), "*Das Soilfrac-Verfaren*" Prospekt 61-02D (in German) and "**B***ouwwerkbescherming*" Brochure 61-29 NL (in Dutch).

Keulen, B., (2001). "*Maximum allowable pressures during horizontal directional drillings focused on sand*" MSc thesis Delft University of Technology; September.

Kleinlugtenbelt R., (2006). "*Compensation grouting, Perth, Australia*" private communication, March.

Kleinlugtenbelt R., (2005). "*Compensation grouting experiments*" MSc thesis Delft University of Technology; October.

Khodaverdian M. and McElfresh P., (2000). "Hydraulic fracturing simulation in poorly consolidated sand: Mechanism and consequences." *Proc. Conf.. Soc. of Petroleum Engineers*, Dallas no. 63233.

Koenders M.A., (1985). "*Hydraulic criteria for filters*." Estuary Physics report, kew, Surrey, England

Komiya, K., Soga, K., Akagi, H., Jafari, M.R., Bolton, M.D., (2001). "Soil consolidation associated with grouting during shield tunnelling in soft clayey ground." *Géotechnique 51, No.* 10, pp 835 – 846.

Korff, M., Mair, R.J. and Tol, A.F. van, (2009). "Building damage examples due to leakage at a deep excavation in Amsterdam." *Proceedings of the 17th International Conference on Soil Mechanics and Geotechnical Engineering*, M. Hamza et al. (Eds.), © (2009 IOS Press. doi:10.3233/978-1-60750-031-5-2060, 2060-2063.

Kovacevic, N., Edmonds, H.E., Mair, R.J., Higgens. K.G. and Potts, D., (1996). "Numerical modelling of the NATM and compensation grouting trails at Redcross Way." *Proc. Int. Symp. on Geotech. Aspects of Underground Construction in Soft Ground*, (eds. by Mair and Taylor), London, 553-559.

Kummerer, C., (2003). "*Numerical modelling of displacement grouting and application to case histories*" PhD thesis, University Graz; October .

Kummerer, C., Gollegger, J., Schweiger, H.F., Conzáles, C. and Sagaseta C., (2002). "Numerical and analytical studies of the effects of compensation grouting." *Proc. NUMOG VIII*, Rome, April. 379-384.

Lefebvre, G., Bozuzuk, M., Philibert, A. and Hornych, P., (1991). "Evaluating K_0 in Champlain Clays with hydraulic fracture tests." Canadian Geotechnical Journal Vol. 28, No. 3. Pp. 365-377.

Leca, E. and Dormieux, L., (1990). "Upper bound and lower bound solutions for the face stability of shallow circular tunnels driven in frictional material." *Géotechnique, vol. 40*, n°4, p. 581-606

Littlejohn, S. (2003). "The development of practice in permeation grouting and compensation grouting, A historical review (1802 – 2002), Part 2 Compensation grouting." *Proc. 3rd. Int. Conf. on Grouting and Ground Treatment, vol. 1*. Johnsen, L.F., Bruce D.A., Byle M.J. (eds.), Februari, ACSE, pp 100-144.

Lo, K.Y. and Kaniaru, K., (1990). "Hydraulic fractures in earth and rock-fill dams." *Canadian Geotechnical Journal*, Vol. 27, No. 4, pp. 496-506.

Lombardi, G., (1985). "Some theoretical considerations on cement rock grouting". Lombardi SA. N.Rif.:102.-R-19. http://www.lombardi.ch/publications/pdfviewer.php?ID=253(Jan. 30, (2009).

Luger, H.L., Hergarden, H.J.A.M., (1988). "Directional Drilling in soft soil, influence of mud pressures." *Proc. No-Dig, Int. Soc. Trenchless Technology*, 155-161

Mair R. J., (2009). Private communication.

Mair R. J., (1992). Report on Session 4. *Proc. Grouting in the ground*, Bell. ed. 25-26 November.

Massarsch, K.R., (1978). "New aspects of soil fracturing in clay." *Journal of the geotechnical division, ASCE*, Vol. 104, No. 8, pp. 1109-1123.

McKinley J.D. and Bolton M.D., (1999). "A geotechnical description of fresh cement grout – Filtration and consolidation behaviour." *Magazine of Concrete Research* **51**, Vol. 5 October, 295-307.

McKinley, J.D., (1993). "*Grouted ground anchors and soil mechanical aspects of cement grouting*" PhD Thesis, University of Cambridge.

Mhach, H.K., (1991). "*An experimental study of hydraulic fracture and Erosion*" PhD Thesis, City University, London, UK.

Mitchell J.K., (1976). "*Fundamentals of soil behaviour*". John Wiley & Sons. ISBN: 0471611689.

Mori, A., Tamura, M. and Fukui, Y., (1990). "Fracture pressure of soil ground by viscous material." *Soils and Foundations*, Vol. 30, No. 3, pp. 129-136.

Mori, A. and Tamura, M., (1987). "Hydro-fracturing pressure of cohesive soil." *Soils and Foundations* 27(1): 14-22.

Murdoch, L.C., (1993[a]). "Hydraulic fracturing of soil during laboratory experiments, Part 1. Methods and observations" *Géotechnique* 43, No. 2, 255 – 265.

Murdoch, L.C., (1993[b]). "Hydraulic fracturing of soil during laboratory experiments, Part 2. Propagation." *Géotechnique* 43, No. 2, 267 – 276.

Nagel, F., Bezuijen, A., Stascheit, J., Meschke, G., (2009). "Measurments and simulations of fluid and grout pressures around a TBM". *Proc. 2nd Int. Conference on Computational Methods in Tunnelling*. Bochum. 61-70.

Nash K.L., (1974). "Stability of trenches filled with fluids." *Journal of the construction division, Proc. ASCE*, Vol 100, No. CO4, December. 533-542.

Paans, W.J.M., (2002). "*The influence zone and effectiveness of fracture grouting on piled foundations*" MSc thesis TU Delft. April.

Panah, A.K. and Yanagisawa, E., (1989). "Laboratory studies on hydraulic fracturing criteria in soil." *Soils and Foundations* 29(4), 14-22.

Pater. C.J. de,(2009). "*Effect of dilatancy around the borehole during polymer injection",* Private communication.

Pater, C.J. de, and Dong, Y., (2009). "Fracture containment in soft sand by permeability of strength contrast". Proc. SPE, The Woodlands, Texas.SPE 119634.

Pater, C.J. de, Beugelsdijk, L., Lhomme, T., Henry, F., Helfferich, P., Bohloli, B. and Bezuijen, A., (2003[a]). "*Geometry of hydraulic fractures III*" TU-Delft report TA/TG/02-03, October.

Pater, C.J. de, Bohloli, B., Pruiksma, J., Bezuijen, A., (2003[b]). "Experimental study of hydraulic fracturing in sand." *Proc. Soil/Rock America.* 8pp.

Pleithner M. and Bernatzik W., (1953). "Nouveau procédé de remise à niveau de bâtiments affaissés au moyen d'injections de ciment (a new method of compensating settlement of buildings by injections of cement grout)." *Proc. 3rd Int. Conf. on Soil Mech and Found. Eng*. Switzerland 16-27August. 450-453.

Poel J.T. van der, and Schenkeveld, F.M., (1998). "A preparation technique for very homogenous sand models and CPT research", *Centrifuge 98*, Vol. 1, 149-154.

Pruiksma J., (2002), "*Hydraulic fracturing with the distinct element method*" DelFrac report, GeoDelft CO386730/12 V3.0.

Raabe A.W. and Esters K., (1993). "Soil fracturing techniques for terminating settlements and restoring levels of buildings" *Ground Improvement* (Mosely ed.). Chapman and Hall, London 175-192.

Rietdijk J., Schenkeveld F.M., Schaminée P.E.L., Bezuijen A., (2010). "The drizzle method for sand sample preparation" *to be published: Proc. 6th Int. Conf. on Physical Modelling,* Zürich.

Rhee, C. van, and Bezuijen, A., (1992). "Influence of seepage on stability of sandy slope" *ASCE Journal of Geotechnical Engineering,* Vol. 8, August. 1236-1240. paper no. 26655.

Salgado R. and Randolph M.F., (2001). "Analysis of cavity expansion in Sand." *The Int. J. of Geomechanics*, Vol. 1. No 2, 175-192.

Sanders M.P.M., (2007) "*Hydraulic fracture grouting, Laboratory experiments in sand*" Msc thesis, Delft University of Technology

Schenkeveld, F.M., (1996). "*Density measurements in model container*" Delft Geotechnics internal memo.

Schlumberger (2010). "Oilfield glossary" ID:1459. http://www.glossary.oilfield.slb.com/Display.cfm?Term=leakoff (Jan. 2010)

Schweiger, H. F., Kummerer, C. Otterbein, R. and Falk, E., (2004). “Numerical Modelling of Settlement Compensation by Means of Fracture Grouting.” *Japanese Geotechnical Society* Vol. (44), No. (1), pp 71-86.

Sugiyama, T., Nomoto, T., Nomoto, M., Hagiwara, T., Mair, R.J., Bolton, M.D., Soga, K. (2000). “Compensation Grouting at the Docklands Light Railway Lewisham Extension project.” *Proc. Geotechnical aspects of Underground Construction in Soft Ground*, Tokyo. 319-324.

Stoel, A.E.C. van der, (2001). “*Grouting for pile foundation improvement*” PhD thesis Delft University of Technology; September.

Teunissen J.A.M., (2006). “*Fracture calculations (In Dutch).*” GeoDelft internal technical note, 14-02-2006.

Tremblay, B. and Oldakowski K., (2003). “Modeling of wormhole growth in cold production.” *Transport in Porous Media 53*, Kluwer Academic publishers. 197-214.

Verruijt A., (2002). “*Consolidation around a cavity*” Memo 20 January.

Vesić A.S., (1972). “Expansion of cavities in infinite soil mass.” *Soil mechanics and foundations division, proceedings ASCE, Vol. 98, No. SM3; March*. 265-290.

Wang Y. and Dussault M.B., (1994). “Stresses around a circular opening in an elastoplastic porous medium subjected to repeated Hydraulic loading.” *Int. J. Rock Mech. Min. Sci. & Geomech. Abstr. Vol 31. NO 6. 597-616.*

Watt, A., (2002). “Ruwbouw tunnel onder Antwerp-Centraal succesvol afgerond, Theorie van Compensation Grouting bewijst zich in de praktijk.” *Cement 2002 nr. 1,* 56 – 60. (in Dutch)/

Witteveen + Bos, (2008). “Final report compensation grouting Vijzelgracht 20-26 (in Dutch).” *Witteveen + Bos report (author Kaalberg F.J.) SD1185-/mads/009, November.*

Yanagisawa, E. and Ali, K.P., (1994). “Two dimensional study of hydraulic fracturing criteria in cohesive soils.” *Soils and Foundations, vol. 34, No. 1,* pp. 1-9.

Younes, M.F., (2008) Private communication, (partly published in: El-Ashaal A.A., Abdel-Fattah A., Fayed A.L. and Younes M.F. (2009 Investigation the performance and limitations of fracture grouting in sand. *Proceedings of the 17th International Conference on Soil Mechanics and Geotechnical Engineering, M. Hamza et al. (Eds.)© (2009 IOS doi:10.3233/978-1-60750-031-5-2188, pp 2188-2191.)*

Yu, H.S., (2000). “*Cavity expansion methods in Geomechanics*”, Kluwer Academic Publishers, Dordrecht, the Netherlands.

Zhai, Z. and Sharma, M.M., (2005). “A new approach to modelling hydraulic fractures in unconsolidated sands.” *Proc. SPE, Dallas, Texas*. SPE 96246. 14pp.

Appendix 1: Table of tests

The tables in the following pages present an overview of the laboratory tests performed for this study with the set-ups described in Section 6.4.1 and Section 6.4.2.
A range of parameters are presented alongside the test numbers.

Table A.1 shows the dimensions for the parameters.

Parameters			
WCR	-	p	kPa
% ben.	%	p/σ_v	-
comp.	-	σ_v	kPa
k_{grout}	m/s	σ_h	kPa
R_d	%	In.V.	ml.
rate	L/min.	Eff.	%
For 4th test series			
Har.t	hours	P_d	kPa

WCR : water-cement ratio
% ben : percentage of bentonite
comp. : composition of the grout
b = bentonite
c = cement
f = fly ash
r = retarder
s = silica flour
k_{grout} : permeability of the grout cake
R_d : relative density of the sand
rate : injection rate
p : injection volume
p/σ_v : ratio between the injection volume and the vertical confining stress
σ_v : vertical confining stress before the experiment
σ_h : horizontal confining stress before the experiment
in.V. : grout volume injected
Eff. : efficiency (volume of heave/volume of grout injected)
har.t : Dämmer hardening time before the grout injection
P_d : pressure on Dämmer during retraction of the casing

1st test series						
Test	Parameters				Picture	Remarks
1-1	WCR % ben. comp. k_{grout} R_d rate	1 5 b,c 1e-7 60 0	p p/σ_v σ_v σ_h In.V. Eff.	500 18.5 27 27 0 n.d.	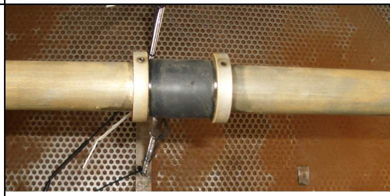	1 injection opening 5 mm Test failed, no injection. Max. press. pump too low
1-2	WCR % ben. comp. k_{grout} R_d rate	1 5 b,c 9.4e-8 60 1	p p/σ_v σ_v σ_h In.V. Eff.	n.d. n.d. 28 23 167 62	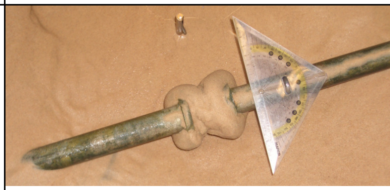	2 injection openings 7 mm. Slow injection, no fracturing. Low stress level, low injection rate
1-3	WCR % ben. comp. k_{grout} R_d rate	1 5 b,c 1.1e-7 60 10	p p/σ_v σ_v σ_h In.V. Eff.	410 17.1 24 21 333 42		2 injection openings 7 mm, Low stress level
1-4	WCR % ben. comp. k_{grout} R_d rate	1 5 b,c 1e-7 60 20	p p/σ_v σ_v σ_h In.V. Eff.	500^{pl} 20.8 24 20 667 37		2 injection openings 7 mm, Low stress level, max. pump pressure reached (^{pl} indicates pump limit)
1-5	WCR % ben. comp. k_{grout} R_d rate	1 7 b,c 5.3e-8 60 10	p p/σ_v σ_v σ_h In.V. Eff.	480 20 24 20 667 43	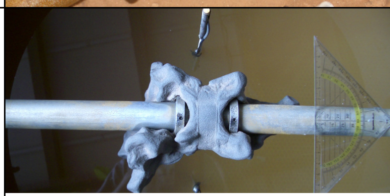	2 injection openings 7 mm, low stress level.
1-6	WCR % ben. comp. k_{grout} R_d rate	1.2 5 b,c 2.3e-8 60 10	p p/σ_v σ_v σ_h In.V. Eff.	850 17 50 35 667 34	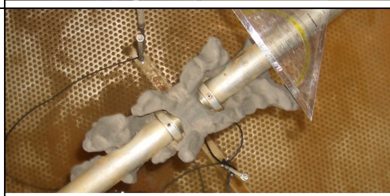	Test failed, no injection. Pump upgraded to 10 bar. Stress level 50 kPa. From here onwards, bentonite from injection fluid hydrated for 20-24 hours.
1-7	WCR % ben. comp. k_{grout} R_d rate	1.2 5 b,c 2.3e-8 60 10	p p/σ_v σ_v σ_h In.V. Eff.	1220 12.2 100 34 667 26		Pump upgraded to 15 bar. No pressure infiltration, rather thick fractures Picture gives view from below injection pipe
1-8	WCR % ben. comp. k_{grout} R_d rate	1.4 5 b,c 1.2e-8 60 10	p p/σ_v σ_v σ_h In.V. Eff.	1480 12.8 116 42 1000 20		No pressure infiltration, rather thick fractures. Injection of 1000 instead of 667 ml grout did not change the fracture shape.

1-9	WCR 1.4 % ben. 5 comp. b,c k_{grout} 4e-9 R_d 75 rate 10	p 1500 p/σ_v 62.5 σ_v 24 σ_h 35 In.V. 667 Eff. 42		Dense sand lower conf. Stress. Extreme p/σ_v Injection pressure and shape comparable to Test 1-8. Horizontal fracture
1-10	WCR 1.4 % ben. 5 comp. b,c k_{grout} 7e-9 R_d 40 rate 10	p 700 p/σ_v 7 σ_v 100 σ_h 40 In.V. 667 Eff. 6		Loose sand, low value of p/σ_v. Low efficiency. Picture shows side view of fracture.

2nd test series						
Test	Parameters				Picture	Remarks
2-1	WCR % ben. comp. k_{grout} R_d rate	3 7 b,f,r 1.5e-10 76 10	p p/σ_v σ_v σ_h In.V. Eff.	1600 12.3 130 59 670 10		No fractures, compaction grouting
2-2	WCR % ben. comp. k_{grout} R_d rate	3 7 b,r,s 1.4e-11 69 10	p p/σ_v σ_v σ_h In.V. Eff.	1200 12.6 95 53 670 16		Only bentonite, silica flour and retarder, lot of pressure infiltration, Some short fractures
2-3_1	WCR % ben. comp. k_{grout} R_d rate	3 12 b,f,r,s 6.5e-11 67 10	p p/σ_v σ_v σ_h In.V. Eff.	1200 9 134 49 670 10		Compaction grouting, no fractures.
2-3_2	WCR % ben. comp. k_{grout} R_d rate	3 7 b,f,r,s 1e-10 67 10	p p/σ_v σ_v σ_h In.V. Eff.	1060 8,9 119 41 670 10	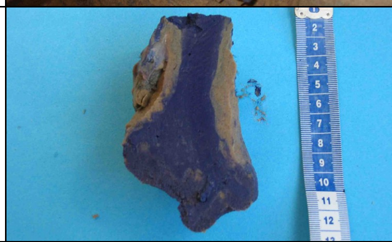	Fracture through grout of First layer. Fracture stops in sand
2-4	WCR % ben. comp. k_{grout} R_d rate	- - X-gel 1.8e-12 69 10	p p/σ_v σ_v σ_h In.V. Eff.	7500 6 126 63 670 4		Test with X-linked gel, thin fractures, low injection pressure.
2-5	WCR % ben. comp. k_{grout} R_d rate	200 6.2 b,s 6e-12 65 10	p p/σ_v σ_v σ_h In.V. Eff.	1000 7.7 130 51 670 12.5	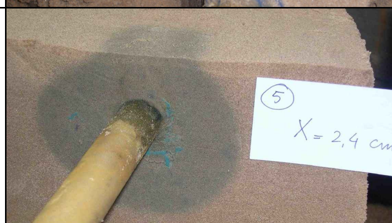	Pure bentonite, test dominated by pressure infiltration.
2-6	WCR % ben. comp. k_{grout} R_d rate	200 6.2 b,c 5e-11 65 10	p p/σ_v σ_v σ_h In.V. Eff.	1700 12.1 140 70 670 11.2		Test dominated by pressure infiltration

2-7	WCR % ben. comp. k_{grout} R_d rate	20 6.2 b,c 6e-10 65 10	p p/σ_v σ_v σ_h In.V. Eff.	1200 8.5 142 67 1000 13		Lot of pressure infiltration, some fracturing
2-8	WCR % ben. comp. k_{grout} R_d rate	10 6.2 b,c 6e-10 62 0	p p/σ_v σ_v σ_h In.V. Eff.	1900 14.8 128 53 1000 22		Pressure infiltration and fractures
2-9	WCR % ben. comp. k_{grout} R_d rate	5 6.2 b,c 7.5e-10 62 10	p p/σ_v σ_v σ_h In.V Eff.	2900 20.4 142 69 800 29		Test with highest efficiency from this series, limited pressure infiltration.
2-10	WCR % ben. comp. k_{grout} R_d rate	2 6.2 b,c 1e-9 58 10	p p/σ_v σ_v σ_h In.V. Eff.	2350 16.5 142 53 670 26.7		Fractures and compaction, still some pressure infiltration.

3rd test series						
Test	Parameters				Picture	Remarks
3-1	WCR	5	p	2724		Probably inhomogeneous soil sample. Long fracture in one direction. Thin fractures surrounded by sand 'glued' to the fracture by pressure infiltration.
	% ben.	7	p/σ_v	16.6		
	comp.	b,c	σ_v	164		
	k_{grout}	n.d	σ_h	72		
	R_d	65	In.V.	820		
	rate	10	Eff.	32		
3-2	WCR	5	p	2349		Slower injection rate, 'thicker' fractures and less pressure infiltration compared to Test 3-1.
	% ben.	7	p/σ_v	14		
	comp.	b,c	σ_v	168		
	k_{grout}	n.d	σ_h	56		
	R_d	65	In.V.	820		
	rate	2	Eff.	23		
3-3	WCR	5	p	2638		Sample height 0.6 m, fracture propagation at lower injection pressure. Same fracture pattern as Test 4-1.
	% ben.	7	p/σ_v	28		
	comp.	b,c	σ_v	95		
	k_{grout}	n.d	σ_h	70		
	R_d	67	In.V.	820		
	rate	10	Eff.	28		
3-4	WCR	5	p	1852		Sample height 0.6 m. Lower injection pressure than reference, Test 4-1. Comparable fractures.
	% ben.	7	p/σ_v	18		
	comp.	b,c	σ_v	103		
	k_{grout}	n.d	σ_h	59		
	R_d	65	In.V.	820		
	rate	10	Eff.	35		
3-5	WCR	5	p	1771		Frac.D Leighton Buzzard s. Sodium bentonite (Cam.) Sample height 0.6 m. Different materials did not influence the results.
	% ben.	4	p/σ_v	21.6		
	comp.	b,c	σ_v	82		
	k_{grout}	n.d	σ_h	69		
	R_d	65	In.V.	820		
	rate	10	Eff.	35		
3-6	WCR	1	p	1915		Frac.D Leighton Buzzard s. Sample height 0.6 m. Slow injection rate, low WCR. As expected no fracturing, no pressure infiltration.
	% ben.	4	p/σ_v	15.3		
	comp.	b,c	σ_v	125		
	k_{grout}	n.d	σ_h	76		
	R_d	65	In.V.	840		
	rate	2	Eff.	36		
3-7	WCR	1	p	1958		Frac.D Leighton Buzzard s. Sample height 0.6 m. Failure of rubber ring.
	% ben.	4	p/σ_v	18		
	comp.	b,c	σ_v	109		
	k_{grout}	n.d	σ_h	83		
	R_d	65	In.V.	840		
	rate	10	Eff.	32		
3-8	WCR	1	p	2620		Frac.D Leighton Buzzard s. Sample height 0.6 m. Dynamic injection hardly influences the results.
	% ben.	4	p/σ_v	19.7		
	comp.	b,c	σ_v	133		
	k_{grout}	n.d	σ_h	73		
	R_d	65	In.V.	830		
	rate	10±5.66	Eff.	36		

4th test series						
Test	Parameters				Picture	Remarks
4-1	WCR % ben. comp. k_{grout} R_d rate har. t	5 6.2 b,c 1.7e-9 60 10 3	p p/σ_v σ_v σ_h In.V. Eff. P_d	370 3.6 102 16 667 18 85		Grout around Dämmer and some thin fractures Sample height 0.6 m
4-2	WCR % ben. comp. k_{grout} R_d rate har. t	5 6.2 b,c 1.7e-9 60 10 24	p p/σ_v σ_v σ_h In.V. Eff. P_d	1390 13.9 100 6 667 8 85		Limited fractures. A lot of grout spread over Dämmer. Sand not always loaded after preparation. Sample height 0.6 m
4-3	WCR % ben. comp. k_{grout} R_d rate har. t	5 6.2 b,c 1.7e-9 60 10 24	p p/σ_v σ_v σ_h In.V. Eff. P_d	3400 32 105 19 667 6 85		No fractures. Grout (light blue in the picture) spread over Dämmer. Sample height 0.6 m
4-4	WCR % ben. comp. k_{grout} R_d rate har. t	1.8 6.2 b,c 6.4e-9 60 10 3	p p/σ_v σ_v σ_h In.V. Eff. P_d	600 5,8 103 4 667 21 85		Highest efficiency from series 4. Grout made fractures and spread over Dämmer and casing (see left side of the picture). Sample height 0.6 m
4-5	WCR % ben. comp. k_{grout} R_d rate har. t	1 5 b,c 6.4e-9 60 10 3	p p/σ_v σ_v σ_h In.V. Eff. P_d	370 4.7 78 6 0 19 *20*		Low Dämmer pressure during removal of the casing resulted in sand deformation before the injection. Largest fracture in all tests. Sample height 0.6 m
4-6	WCR % ben. comp. k_{grout} R_d rate har. t	1.8 62. b,c 6.4e-9 60 10 3	p p/σ_v σ_v σ_h In.V. Eff. P_d	550 5.3 103 13 667 15 *110*		Overall picture comparable to Test 4-4. Picture shows grout (blue) fracturing through Dämmer. Sample height 0.6 m

Acknowledgements

Frans Barends asked me to take up a Ph.D. study after more than 20 years of research and consultancy work at GeoDelft (under its various names). It was not the first time that the possibility of a doctorate had been raised, but it was his question that really got the ball rolling.

My promoter, Frits van Tol, and my co-promotor, Johan Bosch, kept me going thereafter, discussing why the first experiments did not deliver the expected results, what changes were needed and how the experiments related to field situations. At a later stage, we discussed the first versions of this thesis, which were improved by their comments and advice. Kenichi Soga from the University of Cambridge showed continuous interest in the results. In my discussions with him, we both furthered our ideas about the processes in place, learning a great deal along the way. The comments of other members of the "promotiecommissie" helped to improve the manuscript. I gratefully acknowledge the support of all members of the committee.

Remco Kleinlugtenbelt, Monique Sanders, Khalid Gafar Eisa, Luca Massini and Wilson Au: thank you for making the measurements and for your help with the analysis of the results. Your enthusiasm and knowledge have been a real help during this study. Our discussions about the results were very useful. We can now see that the results of the experiments went from 'searching in the dark' for Remco's results to a more or less predicted outcome during the last tests of Luca and Wilson. At the beginning of one series of experiments, it was uncertain where we were on that road, but your contributions certainly helped the journey to progress. Monique, thank you for coming back after your graduation to show Khalid, Luca and Wilson how to work with the equipment.
Dianne den Hamer taught the students how to make the grout mixtures and how to perform the necessary classification experiments. The expertise of Willem van der Zon and Dianne about the effects of the various grout components on the properties of the grout helped to find the mixtures with the required properties.

I want to thank my employer Deltares (the former GeoDelft) and the foundation Delft Cluster for giving me the opportunity for this doctorate and for their patience when it emerged that the original time schedule was too optimistic.

Paul Schaminée, thank you for your advice during the development of the experimental set-ups. This study led to an unforeseen result with respect to the sand preparation procedures for geotechnical physical modelling at Deltares. The first student (Remco) still had to dry 900 kg of sand in an oven before each test. Paul realised that this was probably quite an arduous task for a female student (Monique) and so, upon her arrival, he developed a different preparation technique in which drying was not necessary. This technique, wet raining, worked so well that it has more or less replaced the old technique at Deltares, saving a lot of work during this study and on other projects.
Ferry Schenkeveld, thank you for your help and your focus on details when it comes to sand preparation. Ruud van den Berg, Thijs van Dijk, Willem van Pernis and Jack van der Vegt, my thanks for your assistance during the experimental part of this study.

Hans de Pater was the one who first introduced me to the hydraulic fracturing of soils. In discussions with him focusing on hydraulic fracturing for enhanced oil recovery, I became convinced that this subject had enough interesting implications to merit study as part of a Ph.D.

The reviewers of the first two journal papers I wrote based on the results of this study gave me a hard time with their comments. Their contribution really improved not only the paper, but also my understanding of the results.

The CITG department at Geo- and Geo-Environmental Engineering gave me a workplace during this study. Even as a part-time student, I had all the facilities necessary to do the work. My thanks go to the staff and all the Ph.D. students, in particular Jelke Dijkstra and Nathanael Geleynse, for their hospitality and discussions of various subjects.

The data from Projectbureau Noord|Zuidlijn and Saturn X v.o.f. were essential for that part of this study where I analysed the data from the trial at Rokin and from Vijzelgracht. Their authorisation to use and publish the monitoring data is greatly appreciated. It is not very common for a project organisation to allow data about repair work after an incident to be used for an academic study. As well as supplying the data, the project organisation also performed some field tests. These tests were important for the interpretation of the data.

Pete Thomas helped a lot in improving the English of the manuscript. Arne Bezuijen made the cover and some of the nicer figures in this thesis.

Traditionally, the final paragraph in acknowledgements is reserved for the family who have had to “suffer” so much as the author has worked hard to achieve the doctorate goal. This paragraph is an exception to that rule. My eldest son Marijn was in Qatar most of the time I was working on this study. Furthermore, I want to thank the colleagues of my youngest son Arne at Deltares, TBM and his teachers at the faculty of Industrial Design, as well as Germa's colleagues and patients, for keeping them both busy so that they hardly noticed me burrowing away.

Curriculum vitae

Adam Bezuijen was born 30 September 1955 in Ouddorp in the Netherlands. In 1974 he obtained his Atheneum diploma at the Rijksscholengemeenschap Goeree-Overflakkee, Middelharnis. In 1981, he graduated from the Applied Physics Department of the TU Delft with a M.Sc. thesis titled: Measurements on small area aluminium-aluminium tunnel junctions.

After graduating, he started his professional career at Delft Soil Mechanics Laboratory, which later changed its name to Delft Geotechnics and then GeoDelft before becoming part of Deltares.

He is now a senior consultant with Deltares and a member of the Scientific Board of the unit Geo-Engineering. He was and is mainly involved in research projects. He performed research on wave impact on saturated sands, placed block revetments, dredging, geosystems, tunnelling and compensation grouting. He is the author or co-author of 11 international journal papers and of more than 100 conference and other publications.

Since 2000, he has been the chairman of the European normalisation technical committee CEN/TC189 “Geosynthetics”. He is a core member of the ISSMGE TC28 “Geotechnical aspects of underground construction in soft ground”, a member of ISSMGE TC2 “Physical modelling” and a member of ITA working group 2 “Research”.

He was a member of the organisation committee and the scientific board, and one of the editors of the proceedings for the 2005 Amsterdam conference of the ISSMGE TC28 committee “Geotechical aspects on underground construction in soft ground” and a keynote speaker at the 2008 conference of the same committee.

For his contribution to fact-finding after Hurricane Katrina, he received a certificate of appreciation for “patriotic civilian service” from the U.S. Army Corps of Engineers.

Adam has been married to Germa Joppe since 1981. They have 2 sons, Marijn en Arne, born in 1982 and 1985.